Enzyme Responsive Surfaces – Towards a Smart Cell-Material Interface

Anne Canning

Sept 2017

Thesis submitted to The University of Nottingham for the degree of Doctor of Philosophy

Abstract

Enzymes are promising stimuli for the development of responsive biomaterials for biomedical applications. Enzymes are inherently present in the biological environment thus cleverly designed materials for biomedical applications may require no external stimuli to ellicit the required material response. They have been targeted as stimuli in self assembly of bulk materials owing to the material changes in chemical composition afforded by the enzyme interaction. The first examples of autonomous self-regulated drug delivery systems have been reported via the development of reversible enzyme responsive materials that undergo a material change regulated by the enzymes in their environment. Although enzyme responsive surfaces have been reported there are no examples of reversible enzyme response surfaces.

The surface is the first point of contact between the biological environment and a biomedical device/implant. Improving this interaction will improve the integration of these biomaterials in biological systems and it has been proposed that biomimetic surfaces are a promising method for full biomaterial integration in the biological environment. The body strives towards homeostasis and this is frequently achieved by enzymatic activating and deactivation of proteins in the body. This process is repeatable and reversible. Herein we address the absence of reversible and repeatable synthetic enzyme responsive surfaces towards the improvement of biomaterial integration. We aim to develop a truly autonomous system wherein enzymes present in the environment can interact with the modified surface to mediate a reversible material response.

This goal was achieved by modifying surfaces with copolymers that contain the recognition sequence for Casein kinase II and Alkaline phosphatase to undergo enzymatic phosphorylation and dephosphorylation. Co and homo polymers of serine and glutamic acid were synthesised in solution and conformation/composition relationship was determined by analysis with NMR, GPC and FTIR. Polymerisation from the surface with NCA-Glu and NCA-Ser was achieved as characterised by FTIR, ToF SIMS, XPS and WCA. Enzymatic mediated phosphorylation (CKII) and dephosphorylation (AP) was monitored by surface analysis (ToF SIMS), by monitoring ATP to ADP conversion and phosphate cleavage from the surface using luminescence and colorimetric assays. Conformational changes mediated by enzymatic interactions with the surface was monitored indirectly using a FRET system incorporated in the surface modification. The modified surfaces were able to support cell culture and osteogenesis.

This project has made advances in several fields, 1) The use of NCA-ROP as a method to modify surfaces with copolymers, in particular for a random/ alternating amino acid sequence. 2) The use of NCA-ROP as a method to develop stimuli responsive surfaces, specifically, this is the first report of an enzyme responsive surface prepared from NCA-amino acid derivatives. 3) The use of enzymes as stimuli, specifically, this is the first report of a reversible enzymatic responsive surface.

In this system reversible phosphorlyation and dephosphorylation was monitored via changes in fluorescence output indicative of induced conformational changes.

Contents

Abstract i
List of Tables ix
List of Figures xvii
Publications xviii
Acknowledgements xix

1 Introduction **1**
1.1 Regenerative medicine 1
1.2 Biointerfaces 1
1.3 The extracellular environment 2
1.3.1 Mechanical cues 2
1.3.2 Biochemical cues 3
1.4 Biomaterials 4
1.4.1 Dynamic materials 5
1.4.2 Autonomous biomaterials 6
1.5 Introduction to Enzymes 6
1.5.1 Enzyme responsive materials (ERM)'s 8
1.5.2 Kinases and Phosphatases 9
1.5.3 ERM's response to cell secreted phosphatases 9
1.6 Importance of conformation 10
1.7 Synthetic polypeptides 11
1.7.1 Solid peptide phase synthesis (SPPS) 12
1.7.2 Recombinant peptides 12
1.8 N-carboxy anhydride Ring opening polymerisation (NCA-ROP) 12
1.8.1 Mechanism of NCA ROP 12
1.8.2 Side reactions 14
1.8.3 Use of initiators 14
1.9 Copolymers 14
1.9.1 Block copolymers 15
1.9.2 Random copolymers 15
1.9.3 Conformational studies of polymers synthesised by NCA ROP . . . 16
1.10 Biological applications – functional materials using NCA ROP 17

1.11 Surface modification . . . 17
1.11.1 Responsive surfaces . . . 18
1.11.2 Surface grafting of polypeptides by NCA-ROP . . . 19
1.11.3 Grafting "to" a planar surface . . . 20
1.11.4 Grafting "from" a planar surface with NCA-ROP . . . 20
1.12 Surface analysis techniques . . . 22
1.12.1 Förster Resonance energy transfer (FRET) technique to monitor conformational changes . . . 25
1.13 Challenges in the field . . . 26
1.14 Aims of thesis . . . 27

2 N-Carboxyanhydride ring opening polymerisation in solution: A study of serine and glutamic acid 30
2.1 Introduction . . . 30
2.1.1 Polyglutamic acid synthesised by NCA ROP . . . 30
2.1.2 Poly-serine synthesised by NCA ROP . . . 31
2.1.3 Aims . . . 32
2.2 Methods . . . 33
2.2.1 NCA-Serine (Bn) . . . 33
2.2.2 NCA-Glutamic acid (Bn) . . . 34
2.2.3 NCA polymerisation . . . 34
2.2.4 Copolymerisation kinetics . . . 34
2.2.5 Characterization FTIR . . . 34
2.2.6 ^{1}H NMR . . . 35
2.2.7 Gel Permeation Chromatography (GPC) . . . 35
2.2.8 Circular Dichroism (CD) . . . 35
2.3 Results and Discussion . . . 36
2.3.1 Synthesis and characterisation of copolypeptides with systematically changing composition . . . 36
2.3.2 Copolymerisation kinetics . . . 39
2.3.3 Copolymer conformation . . . 43
2.4 Conclusions . . . 45

3 N-Carboxy anhydride ring opening polymerisation from the surface 47
3.1 Introduction . . . 47
3.1.1 Co-polymerisations from the surface by NCA ROP . . . 47
3.1.2 Aims . . . 48
3.2 Methods . . . 49
3.2.1 Surface silanisation . . . 49
3.2.2 Addition of FMOC-Pentafluoro- L-phenylalanine on the surface . . . 49

3.2.3 Addition of PEG-diamine . . . 49
3.2.4 Coupling of N(ϵ)-BHQ-1 FMOC Lys OH . . . 49
3.2.5 NCA ROP from the surface . . . 50
3.2.6 Benzyl deprotection . . . 50
3.2.7 Coupling of NHS-Fluorescein . . . 50
3.2.8 Characterisation . . . 50
3.2.9 Analysis software . . . 51
3.3 Results and Discussion . . . 53
3.3.1 NCA-ROP from amine functionalised surfaces . . . 53
3.3.2 NCA ROP initiated from PEG-amine functionalised surface . . . 56
3.3.3 Comparison of surfaces within and between batches of samples . . . 62
3.3.4 Incorporation of FRET pair (fluorophore and quencher) on the surface . . . 73
3.3.5 XPS analysis . . . 79
3.4 Conclusions . . . 85

4 Enzyme interactions with polypeptide modified surfaces 86
4.1 Introduction . . . 86
4.1.1 Introduction to target enzymes for surface interactions: Casein Kinase II (CKII) and Alkaline Phosphatase (AP) . . . 86
4.1.2 Mechanism of Alkaline phosphatase . . . 88
4.1.3 Reversible enzyme responsive surfaces . . . 90
4.1.4 Aims . . . 90
4.2 Methods . . . 91
4.2.1 Surface preparation . . . 91
4.2.2 ToF SIMS . . . 91
4.2.3 Surface treatment with CKII . . . 91
4.2.4 Surface treatment with AP . . . 91
4.2.5 ADP-Glo assay . . . 91
4.2.6 AP calibration . . . 92
4.2.7 Phosphate assay . . . 92
4.2.8 FRET measurements . . . 92
4.3 Results and Discussion . . . 92
4.3.1 Enzyme interactions with APTMS initiated polypeptide coated substrates . . . 93
4.3.2 Enzyme interactions with PEG-NH_2 initiated polypeptide coated surfaces . . . 99
4.3.3 Reversible phosphorylation/ dephosphorylation . . . 103
4.3.4 Enzyme interactions with BHQ-1-Lysine and fluorophor containing substrates . . . 103

4.3.5 Reversibility on the same sample monitored by ToF SIMS 107
4.3.6 Change in surface fluorescence with enzyme interactions with the polypeptide surfaces 108
4.4 Conclusions 111

5 Cell interactions with enzyme responsive materials 113
5.1 Introduction 113
5.1.1 Aims 113
5.2 Methods 114
5.2.1 General Mouse primary calvarial (MPC) cell culture 114
5.2.2 Seeding 115
5.2.3 Cell Titer blue assay 115
5.2.4 RUNX2 staining 115
5.2.5 AP assay 116
5.2.6 Cytotoxicity assay 116
5.2.7 Microscopy 117
5.2.8 Analysis software 117
5.2.9 Graphpad 117
5.3 Results and discussion 117
5.3.1 Adhesion and proliferation 117
5.3.2 Cell proliferation assay 121
5.3.3 Osteogenic markers 122
5.3.4 Cell viability in the presence of CKII 124
5.4 Conclusion 127

6 Conclusions and Outlook 129
6.1 Future work 131

A 133
A.1 Chapter 2 133
A.1.1 Kinetic studies 134
A.2 Chapter 3 136
A.3 Chapter 4 139
A.4 Chapter 5 140

Bibliography 146

List of Tables

2.1 Characteristics of copolymers prepared from Ser(Bn)-NCA (S) and Glu(Bn)-NCA (E) at different monomer ratios as determined by NMR. Average over three repeats. Feed Ratio (S:E) 37

2.2 Number (Mn) and weight (Mw) average molecular weight and polydispersity index (PDI) of copolymers prepared from Ser (Bn)-NCA and Glu (Bn)-NCA at different ratios as determined by NMR and GPC Feed Ratio 40

3.1 Position constraints (binding energy shifts with respect to the C-C / C-H component) imposed when fitting components to the C1s high resolution spectra for PEG NH_2 initiated polymers. 52

3.2 Position constraints (binding energy shifts with respect to the C-C / C-H component) imposed when fitting components to the C1s high resolution spectra for BHQ-1-Lysine initiated polymers. 52

3.3 Water contact angle values (n=5) of modified substrates. One Way ANOVA between protected and deprotected surfaces of the same type shown. . . . 53

3.4 Water contact angle values (n=5) of modified substrates initiated from PEG diamine. One way ANOVA multiple comparison. Significant values reported for benzyl protected S(Bn):E(Bn) vs. deprotected S:E of the same surface type 59

3.5 Average ion count for the assigned ion fragments as determined by ToF SIMS (n=4) 1.5 x 1.5 mm areas, normalised to total ion count for PEG diamine initiated surfaces with NCA ROP of 1:1 S:E monomer feed ratio. 62

3.6 Average ion count for the assigned ion fragments, 1.5 x 1.5 mm areas, normalised to total ion count for PEG diamine initiated surfaces with NCA ROP with serine and glutamic acid in a 1 to 1 ratio. Samples within and between batches were analysed. (n=4) 68

3.7 Elemental composition of modified surfaces as determined by XPS. 70

3.8 Chain length of polymer on the surface as calculated using the ratio of elemental count of N1s to F1s for the protected and deprotected polymers as determined by XPS (n=3). The ion count is data under the curve and they have been normalised to sensitivity factors 72

3.9 Experimental percentage contributions of the different C environments at each modification step as determined by XPS (n=3) 73

3.10 Water contact angle values (n=5) of modified substrates with BHQ and fluorophor. One way ANOVA multiple comparison. 75

3.11 Chain length of co and homopolymers as calculated using the ration of elemental counts of N1s to F1s for the protected and deprotected polymers. three measurement positions on one sample of each type 80

3.12 Experimental percentage contributions of the different C environments at each modification step for samples initiated from BHQ-1-Lysine as determined by deconvolution of C1s peaks on XPS spectra. 81

3.13 Elemental composition of modified surfaces functionalised with BHQ-1-Lysine as determined by XPS. 84

4.1 Table of ion intensities attributed to phosphate normalised to total ion count. Each 3 x 3 mm area was split into four 1.5 x 1.5 mm areas and the ion intensities determined by the software, normalised and averaged (n=4). One way ANOVA with multiple comparison was used for the statistics. 94

4.2 Table of ion intensities attributed to phosphate for copolymer S:E (1:1) samples incubated with CKII and ATP at 1, 4 and 12 hours. Each 3 x 3 mm area was split into four 1.5 x 1.5 mm areas and the ion intensities determined by the software, normalised to total ion count and averaged (n=4). One way ANOVA with multiple comparison was used for the statistics. 98

4.3 Table of ion intensities attributed to phosphate normalised to total ion count for samples incubated with AP for 1, 2 and 12 hours. Each 3 x 3 mm area was split into four 1.5 x 1.5 mm areas and the ion intensities determined by the software, normalised and averaged (n=4). One way ANOVA with multiple comparison was used for the statistics. 98

4.4 Table of ion intensities attributed to phosphate normalised to total ion count for samples incubated with CKII and ATP, followed by incubation with AP for 1 and 4 hours. Each 3 x 3 mm area was split into four 1.5 x 1.5 mm areas and the ion intensities determined by the software, normalised and averaged (n=4). One way ANOVA with multiple comparison was used for the statistics. Significant values shown are comparisons with 1:1 S:E (ATP + CKII). 99

4.5 Table of ion intensities attributed to phosphate normalised to total ion count for samples incubated with three cycles of CKII then ATP. Each 3 x 3 mm area was split into four 1.5 x 1.5 mm areas and the ion intensities determined by the software, normalised and averaged (n=4). One way ANOVA with multiple comparison was used for the statistics. Significant values shown are comparisons between themselves and the previous step. . 104

4.6 Amount of phosphate bound on the surface after CKII incubation and the amount of phosphate cleaved from the surface. Determined by ADP-Glo and Phosphate assay, respectively, for copolymer S:E (1:1) modified substrates. (n=4) 106

5.1 The number of MPC's adhered to control (fibronectin, glass and TCP) and polypeptide surface of varying composition after 1 and 2 hours incubation after seeding (n=5) 119

A.1 ToF SIMS ion count for fragments of interest normalised to total ion count for samples initiated from BHQ. n=4 for 1.5 x1.5mm areas 138

List of Figures

1.1 Evolution of biomaterials from bioinert: a material that exhibits no interaction with the biological envrionment, bioactive: a material that has bioactive or biophysical cues to interact with the biological environment, biodynamic: a material that undergoes a response on action of a stimulus and autonomous: a material that undergoes reversible physical/chemical changes on action of stimulus present in the biological environment . . . 4

1.2 Representation of one directional biomaterial response to common stimuli, including light, pH, electricity and temperature, which causes an irreversible material response . . . 5

1.3 Representation of autonomous biomaterial drug delivery systems with feedback loops, whereby the stimuli is released by the biological cell, this causes a material response and a release of a payload which deactivates the stimuli that was released by the cell, thus stops any further material response. . . . 7

1.4 NCA-polymerisation via the normal amine mechanism . . . 13

1.5 NCA-ROP polymerisation via the activated monomer mechanism . . . 13

1.6 Scheme of grafting 'from' (with amino acids) and grafting 'to' (with a synthesised polypeptide) a surface. . . . 19

1.7 Schematic of photoelectron emission in XPS . . . 23

1.8 Illustration of ToF SIMS instrument set up . . . 24

1.9 Illustration of the collision cascade on a solid sample (red) initiated by a primary ion beam (black) . . . 25

1.10 Jablonski diagram illustrating Forster resonance energy transfer . . . 27

1.11 Summary figure of the experimental chapters included in this thesis . . . 29

2.1 Structure of amino acids glutamic acid and serine . . . 30

2.2 Schematic of chapter 2. Illustration of synthesis in solution of serine and glutamic acid in different monomer feeds and the analysis of the resultant polymers by FTIR (conformation) and GPC and NMR (composition) . . . 33

2.3 Scheme of preparation of copolypeptides of Glu(Bn) and Ser(Bn) via NCA polymerization. . . . 36

2.4 ^{1}H NMR of NCA-Serine(Bn) . . . 36

2.5 ^{1}H NMR of NCA-Glutamic acid(Bn) 37
2.6 ^{1}H NMR of NCA-Glutamic acid (Bn): NCA-Serine (Bn) 1:1 copolymer . 38
2.7 Fittings to the backbone CH signals in the H NMR spectrum to determine the experimental ratios of Ser (Bn) to Glutamic (Bn) after copolymerisation (ratios displayed as S (Bn) to E (Bn) 39
2.8 ^{1}H NMR of NCA-Glutamic acid(Bn): NCA-Serine(Bn) 1:1 copolymer isolated after treatment with TFA: HBr. 40
2.9 Chromatogram of Ser(Bn) and Glu(Bn) polymers at ratios of Ser(Bn):Glu(Bn) = 2:1, 1:1, 1:2, 0:1 (in descending order) as determined from GPC. Data normalized to the peak with the highest intensity. 41
2.10 Schematic illustrating the determination of copolymer composition based on calculated monomer reactivity ratios 42
2.11 Linear regression of monomer ratios as determined by Finemann Ross (a) and Kelen-Tüdös (b) methods 42
2.12 NMR peak fitting data of shift peaks assigned to the α-CH from polymerisations with different monomer feed compositions (S:E) and parameters calculated from the NMR data for the determination of the reaction kinetics 43
2.13 Change of the mole fraction in the feed and in the polymer as determined by NMR. The line represents the theoretical behaviour of an ideal random or alternating copolymerisation. 44
2.14 Copolymerisation parameters for serine (rSer) and glutamic acid (rGlu) . 44
2.15 Percent of secondary structure motifs measured in solid benzyl protected polypeptides of different composition determined by FTIR. 45
2.16 Peak fits of the amide I region in the IR spectra of the copolypeptides with varying Ser(Bn) and Glu(Bn) (S:E) content. Fitted components are β-sheets (Blue), α-helices (green) and unordered structures (orange). Measured data: black; envelope of sum of components: red. 46

3.1 Illustration of the work carried out in this chapter; the modification of a glass surface via grafting from method with NCA-Glu and NCA-Ser and subsequent surface characterisation. 48
3.2 ToF SIMS spectra of fragment intensities inidicative of APTMS:light blue (CH_4N^+), Serine: dark blue ($C_3H_3O_3^+$, $C_2H_6NO^+$), Glutamic acid: green ($C_4H_6NO^+$, $C_4H_8NO_2^+$) and Benzyl protecting group ($C_7H_6^+$, $C_7H_7^+$)normalised to total ion count 54
3.3 ToF SIMS Raster images of fragment intensities inidicative of APTMS:light blue (CH_4N^+), Serine: dark blue ($C_3H_3O_3^+$, $C_2H_6NO^+$), Glutamic acid: green ($C_4H_6NO^+$, $C_4H_8NO_2^+$) and Benzyl protecting group ($C_7H_6^+$, $C_7H_7^+$) normalised to total ion count in a 3x3 mm area. 55

3.4 Monitoring of NCA consumption with FTIR looking at the reduction in the carbonyl peak 1750 cm^{-1} over time (0 to 16 hours) of the NCA-ROP of S(Bn):E(Bn) 1:1 from a PEG-amine functionalised surface 57

3.5 Scheme of surface modification to include PEG_18 linker chain between the surface and the polypeptide chain 58

3.6 ToF SIMS spectra of fragment intensities inidicative of PEG: purple (CH_3O^+, $C_2H_5O^+$), Serine: dark blue ($C_3H_3O_3^+$, $C_2H_6NO^+$), Glutamic acid: green ($C_4H_6NO^+$, $C_4H_8NO_2^+$) and Benzyl protecting group ($C_7H_7^+$)normalised to total ion count. 60

3.7 ToF SIMS Raster images of assigned fragments indicative of PEG: (CH_3O^+, $C_2H_5O^+$), Serine:($C_3H_3O_3^+$, $C_2H_6NO^+$), Glutamic acid:($C_4H_6NO^+$, $C_4H_8NO_2^+$) and Benzyl protecting group ($C_7H_7^+$) normalised to total ion count. . . . 61

3.8 ToF SIMS spectra of fragment intensities inidicative of Sodium: dark purple (Na^+), Silicon: pink (Si^+), PEG: purple (CH_3O^+, $C_2H_5O^+$), Serine: dark blue ($C_3H_3O_3^+$, $C_2H_6NO^+$), Glutamic acid: green ($C_4H_6NO^+$, $C_4H_8NO_2^+$) and Benzyl protecting group ($C_7H_7^+$)normalised to total ion count of four samples made in the same batch. 63

3.9 ToF SIMS Raster images of assigned fragments inidicative of sodium (Na^+), silicon (Si^+), PEG: (CH_3O^+, $C_2H_5O^+$), Serine:($C_3H_3O_3^+$, $C_2H_6NO^+$), Glutamic acid:($C_4H_6NO^+$, $C_4H_8NO_2^+$) and Benzyl protecting group ($C_7H_7^+$) normalised to total ion count of four samples made in the same batch. . . 64

3.10 ToF SIMS spectra of fragment intensities inidicative of Sodium: dark purple (Na^+), Silicon: pink (Si^+), PEG: purple (CH_3O^+, $C_2H_5O^+$), Serine: dark blue ($C_3H_3O_3^+$, $C_2H_6NO^+$), Glutamic acid: green ($C_4H_6NO^+$, $C_4H_8NO_2^+$) and Benzyl protecting group ($C_7H_7^+$)normalised to total ion count of four samples made in four different batches. 66

3.11 ToF SIMS Raster images of assigned fragments inidicative of sodium (Na^+), silicon (Si^+), PEG: (CH_3O^+, $C_2H_5O^+$), Serine:($C_3H_3O_3^+$, $C_2H_6NO^+$), Glutamic acid:($C_4H_6NO^+$, $C_4H_8NO_2^+$) and Benzyl protecting group ($C_7H_7^+$) normalised to total ion count of four samples made in four different batches. 67

3.12 XPS spectra of surfaces modified with GOPTS, PEG diamine, Pentafluoro-L-phenylalanine to which NCA ROP was initiated with a theoretical feed ration of S:E 1:1 Left: Wide scan with fitted peaks and envelope (grey), fit (black dash) and Right: narrow scan of C1s of samples at each modification step 69

3.13 Scheme of surface modification with Fmoc-pentafluoro-L-phenylalanine coupled to the PEG_{18} linker chain. 71

3.14 Chemical structure of a) Black hole quencher-1-Lysine and b) Fluorescein covalently bound to the base and end of the polypeptide chain 73

3.15 Scheme of surface modification with Black hole quencher-1-lysine coupled to the PEG_{18} linker chain and a fluorophore coupled to the terminal amine 74

3.16 Monitoring NCA consumption in a 1:1 S:E feed ratio polymerised by NCA ROP from the surface by FTIR over time by the carbonyl peak 1790cm(^{1}) 75

3.17 ToF SIMS spectra of fragment intensities indicative of PEG: purple (CH_3O^+), ($C_2H_5O^+$) Serine: dark blue ($C_3H_3O_3^+$, $C_2H_6NO^+$), Glutamic acid: green ($C_4H_6NO^+$, $C_4H_8NO_2^+$), Benzyl protecting group: orange ($C_7H_6^+$, $C_7H_7^+$) and Fmoc: dark purple $C_14H_10^+$normalised to total ion count 77

3.18 ToF SIMS ROI images of fragment intensities indicative of PEG: (CH_3O^+), ($C_2H_5O^+$) Serine: ($C_3H_3O_3^+$, $C_2H_6NO^+$), Glutamic acid: ($C_4H_6NO^+$, $C_4H_8NO_2^+$), Benzyl protecting group ($C_7H_6^+$, $C_7H_7^+$) and Fmoc $C_14H_10^+$ normalised to total ion count 78

3.19 XPS spectra of surfaces modified with GOPTS, PEG diamine, BHQ-1-Lysine and Pentafluoro-L-phenylalanine Left: Wide scan with fitted peaks and envelope (grey), fit (black dash) and Right: narrow scan of C1s of samples at each modification step 82

3.20 XPS spectra of surfaces coated in polymer initiated from BHQ-1-Lysine for homo and copolymers. Left: Wide scan with fitted peaks and envelope (grey), fit (black dash) and Right: narrow scan of C1s of samples at each modification step 83

4.1 Mechanism of phosphorylation and dephosphorylation for a copolymer with sequence S-x-x-E mediated by the enzymes AP and CKII 87

4.2 Motifs required for each group of casein kinases, casein kinase I (CKI), caseine kinase II (CKII) and genuine-casein inase (G-CK) with shorter motifs, phosphorylate residues (orange) and specificity determinants (green). X can be any amino acid, in the case of CKII acidic amino acids are preferable. 88

4.3 Kinetic scheme for enzymatic hydrolysis of phosphate monoesters by AP . 88

4.4 Illustration of predicted conformational change of co-polypeptide modified surface as a result of interactions with the enzymes AP and CKII. The fluorescent probes, a flurophor and a BHQ are present on the surface. Quenching of fluorescence is illustrated with the conformational change caused by dephosphorylation of the serines. 90

4.5 ToF SIMS spectra of surfaces (co and homopolymer) incubated with CKII and ATP to monitor for changes in phosphate on the surface. Samples: Glutamic acid homopolymer with ATP and CKII (control A), copolymer with ATP and without CKII (Control B), co polymer without ATP and with CKII (Control C) and copolymer with ATP and CKII. Indicative ion fragments shown for glutamic acid, serine and phosphate. Intensities normalised to total ion count. Area 3 x 3 mm. 93

4.6 ToF SIMS Raster images for samples: Glutamic acid homopolymer with ATP and CKII (control A), Copolymer with ATP and without CKII (Control B) Co polymer without ATP and with CKII (Control C) and copolymer with ATP and CKII normalised to total ion count. Area 3 x 3 mm. . 96

4.7 ToF SIMS spectra of fragment intensities assigned to phosphate ions PO−2 and PO−3 of S:E (1:1) copolymer modified surfaces by NCA ROP. The surfaces were incubated with ATP (10 µM) and CKII (10 U/mL) and analysed at time 1, 4 and 12 hours. Normalised to total ion count. 3 x 3 mm area was measured. 97

4.8 ToF SIMS spectra of fragment intensities assigned to phosphate ions PO−2 and PO−3 of S:E (1:1) copolymer modified surfaces by NCA ROP. The surfaces were incubated with AP (12 U/mL) and analysed at time 1, 4 and 12 hours. Normalised to total ion count. 3 x 3 mm area was measured. 98

4.9 ToF SIMS raster images (left) and spectra (right) of fragment intensities of S:E (1:1) copolymer modified surfaces: control A (incubated with ATP no CKII), control B (incubated without ATP with CKII), substrate incubated with CKII/ATP, phosphorylated substrate incubated with AP at time 1 and 4 hours. Normalised to total ion count. 3 x 3 mm measured area. . . 100

4.10 Copolymer samples of S:E (1:1) incubated with CKII (10 U/mL) and ATP (1 µM and 10 µM). Supernatant was removed at each time point and incubated with ADP-Glo assay reagents and measured by luminescence to determine ATP to ADP conversion (n=4) 102

4.11 Copolymer modified surfaces S:E (1:1) incubated firstly with CKII/ATP, were then incubated in AP. The amount of phosphate present in the supernatant was determined using a colorimetric assay and absorbance measured at 650 nm before and after exposure to AP for different amounts of time (n=4). 102

4.12 ToF SIMS spectra of surfaces modified with S:E (1:1) that have undergone three subsequent incubations with the enzymes CKII/ATP and AP, normalised to total ion count (top), ADP-Glo assay performed after incubation of samples with CKII and ATP(bottom left) and Phosphate assay performed after incubation of samples with AP(bottom right) 104

4.13 Monitoring of CKII/ATP and ATP induced phosphorylation and dephosphorylation of copolypeptide modified surfaces (S:E„ 1:1) using ToF-SIMS and spectroscopic assays. ToF SIMS spectra of ions attributed to amino acids and phosphate, normalised to total ion count (a) ADP-Glo assay (b) and Phosphate assay (c) after three cycles of incubation with CKII/ATP and AP for BHQ-Lysine initiated polypeptides. 106

4.14 Assay data corresponding to ToF SIMS spectra for the same slides exposed to two cycles of enzyme incubation (CKII/ATP followed by AP) Left: Phosphate detected in supernatant. Right: Conversion of ATP to ADP. . 108

4.15 ToF SIMS of BHQ-1-Lysine initiated copolymers of S:E (1:1) incubated with enzymes CKII/ATP and AP for 2 cycles, presence of ion intensity attributed to phosphate was measured. The same slide was analysed at each step. Left: spectra normalised to total ion count. Right: Raster image 3 x 3 mm. 109

4.16 Excitation spectrum (left) and Emission spectrum (right) of fluorophore labelled surfaces modified with S:E (1:1) copolymer with BHQ-1-Lysine at the base of the polymer chain and fluorescein bound to the end of the chain. Fluorescence measured on the surface using z-scan to determine optimal Z-value. 110

4.17 Change in fluorescence of a modified surface with copolymer S:E (1:1), with a BHQ-1-Lysine and fluorescein present. Fluorescence was measured on a plate reader at Exc_{480nm} and Em_{527nm} over multiple cycles of CKII/ATP and AP treatment for controls (black) and three batches of copolymer surfaces (n=4). 111

5.1 Illustration of the culture of MPC cells on the modified surfaces and their subsequent attachment, spreading and secretion of AP which will be monitored and measured in this chapter 114

5.2 Brightfield images of MPC cells seeded on fibronectin coated surfaces as well as co and homopolymer modified surfaces of serine and glutamic acid at 10 X magnification, scale bar 100 µm (n=5) 118

5.3 Brightfield images of MPC cells seeded on control substrates as well as co and homopolymer modified surfaces of serine and glutamic acid at 10 X magnification, scale bar 100 µm (n=5) at day 1, 7 and 14. 120

5.4 Cell number as determined using resazurin assay on different controls and polypeptide substrates at time 1, 3 and 7 days. One way ANOVA carried out to determine significance compared to the fibronectin control sample (*<0.05, ****<0.00005) error bar=SD (n=5) 121

5.5 Images of cells stained with Hoechst (nucleus stain) and Goat anti-rat secondary antibody-Alexafluor546 (RUNX2 stain) seeded on copolypeptide of serine and glutamic acid in a 1:1 ratio and control surface at 10 x magnification (n=5) at day 3. scale bar = 100µm 123

5.6 AP activity detected in supernatant after 60 minutes incubation with pnpp (0.5 mM) normalised to cell number (as determined with Cell Titer blue assay). One Way ANOVA compared to Fibronectin substrate with error bars=SD. A/V/T U = amount of enzyme to generate 1 µM of pnp in 1 min in 1 mL (n=4) 124

5.7 Brightfield images of cells incubated with different amounts of CKII for 2 days on copolymer modified surfaces and controls of fibronectin and glass (n=4). Scale bar = 100µm 125

5.8 Cell number as determined using resazurin assay on different substrates after 2 days incubation with CKII in different concentrations. One way ANOVA test carried out to determine significance compared to control, 1:1 no enzyme. (n=5) 126

5.9 Live cell detected at Excitation 400 nm/ Emission 505 nm for detection of AFC fluorescence for MPCs seeded onto copolymer substrates incubated with different amounts of CKII. Statistics used: One way ANOVA, multiple comparison to 1:1 (S:E) error bars=SD of n=4 126

5.10 Dead cells detected atExcitation 400 nm/ Emission 505 nm for detection of R11O fluorescence for MPC's seeded onto copolymer substrates incubated with different amounts of CKII. Statistics used: One way ANOVA, multiple comparison to 1:1 (S:E) error bars=SD of n=4 127

A.1 Mass spectra for NCA-Ser (Bn) 133

A.2 Mass spectra for NCA-Glu (Bn) 133

A.3 Molar ellipticity of the copolypeptides at different ratios as determined by CD in HFIP. 135

A.4 Full ion spectra for substrates silanised with APTMS and polymerised with Serine and Glutamic acid in homo and copolymers. Most prominent ions have been labelled. 136

A.5 Full ion spectra for substrates silanised with GOPTS, and polymerised with serine and glutamic acid from the BHQ-Lysine. Most prominent ions have been labelled. 137

A.6 Full ion spectra for substrates silanised with GOPTS, and polymerised with serine and glutamic acid from the PEG-diamine. Most prominent ions have been labelled. 137
A.7 Calibration curve for 1 (left)and 10 (right) µM ATP concentration 139
A.8 Phosphate calibration curve 139
A.9 AP calibration curve 139
A.10 ToF SIMS of samples initiated from PEG-NH_2 of three incubation cycles with CKII/ATP followed by AP. Left:Raster images of 3 x 3mm areas, Right: Spectra with peaks attributed to phosphate normalised to total ion count 140
A.11 ToF SIMS of samples initiated from BHQ-1-Lysine of three incubation cycles with CKII/ATP followed by AP. Left:Raster images of 3 x 3mm areas, Right: Spectra with peaks attributed to phosphate normalised to total ion count 140
A.12 Full mass spectra for negative polarity ToF SIMS. Surfaces polymerised from APTMS exposed to CKII/ATP and AP 141
A.13 Full mass spectra for negative polarity ToF SIMS. Surfaces polymerised from PEG diamine exposed to CKII/ATP and AP 141
A.14 Full mass spectra for negative polarity ToF SIMS. Surfaces polymerised from BHQ-1-Lysine exposed to CKII/ATP and AP 141
A.15 CellTiter blue calibration curve 142
A.16 Live cell calibration curve Excitation 400 nm/ Emission 505 nm for detection of AFC fluorescence 142
A.17 Dead cell calibration curve Excitation 485 nm/ Emission 520 nm for detection of R11O fluorescence 143
A.18 Cell Titer calibration curve with known number of cells at different incubation times: 1 hour(R^2 = 0.9900), 2 hours (R^2 = 0.9967) and 3 hours (R^2 = 0.9802). Excitation 560nm/ emission 590 nm 143
A.19 Images of MPC cells cultured on controls glass and fibronectin after 1 and 2 hours incubation. Scale bar = 100µm 144
A.20 Brightfield images of MPC cells seeded on control substrates glass and TCP at 10 X magnification, scale bar 100 µm (n=5) at day 1, 7 and 14. . 144
A.21 Images of cells stained with Hoechst (nucleus stain) and Goat anti-rat secondary antibody-Alexafluor546 (RUNX2 stain) seeded on control surfaces at 10 x magnification (n=5) at day 3. scale bar = 100µm 145

Publications

Publications arising from this PhD research:

Canning, A., Pasquazi, A., Fijten, M., Rajput, S., Buttery, L., Aylott, J. W. and Zelzer, M. (2016), Tuning the conformation of synthetic co-polypeptides of serine and glutamic acid through control over polymer composition. J. Polym. Sci. Part A: Polym. Chem., 54: 2331-2336. doi:0.1002/pola.28104

Acknowledgements

Firstly I would like to thank EPSRC for funding my PhD on grant (EP/F500491/1) I thank my supervisors Dr Buttery, Dr Aylott and Dr Zelzer for their expertise, guidance and support throughout my PhD. In particular Dr. Zelzer for his training, scientific discussions, patience and group socials. I couldn't have imagined a better primary supervisor to guide me through my PhD.

I would like to thank Glen Kirkwood for training in cell culture and Matthew Hollingworth for assistance with immunohistochemical staining and advice on MPC cell culture.

I would like to thank the members of the functional biointerfaces group, for making working in the lab full of laughter and for their helpful scientific discussions. I'd like to thank all those who have worked in lab C24 alongside me for their encouraging attitudes, laughter and kindness. I want to particularly thank Sunil Rajput for his assistance in the lab, input and ideas throughout. I thank Arianna Pasquazi for her help at the beginning of my PhD in the lab and her contributions. I am also very grateful for all the assistance from the technicians in Boots building in particular Paul Cooling and Tom Booth.

Thanks to Floor Ruiter, Jacqueline Melisande Hicks and Ivana Staka for laughter, guidance and support and for maintaining my sanity.

I'd like to particularly thank my desk buddy Jacqui for providing me with charging cables and importantly pens throughout my PhD. I'd like to thank those who made it possible for me to work in the Netherlands in Enschede as part of Horizon2020 Futform scheme. I thank those in Hy2care and the University of Twente for their support and friendship during the placement. Thank you to Benjamin Davies for introducing me to Latex and importantly, teaching me how to use it. I thank my family for their support throughout the past four years, in particular my sister Dr. Clare Canning.

Abbreviations

AMM	Activated monomer mechanism
ADP	Adenine Diphosphate
ATP	Adenine triphosphate
AP	Alkaline phosphatase
APTES	Amino triethoxy silane
APTMS	Amino trimethoxy silane
ANOVA	Analysis of variance
ATR	Atenuated transmission reflection
AFM	Atomic force microscopy
Bn	Benzyl
BHQ	Black hole quencher
BSA	Bovine serum albumin
CKI	Casein kinase I
CKII	Casein kinase II
$CDCl_3$	Chloroform
CD	Circular Dichroism
CNS	Central nervous system
DIC	N,N'-Diisopropylcarbodiimide
Dp	Degree of polymerisation
DSC	Differential scanning colorimetry
DMF	Dimethyl formamide
E	Glutamic acid
ECM	Extra cellular matrix
EHICA	Ethyl(hydroxy-imino)cyanoacetate
EDTA	Ethylenediamine tetra acetic acid
ERM	Enzyme responsive material
FBS	Foetal bovine serum
FMOC	Fluo-renylmethoxycarbonyl (Fmoc)

FR	Finemann Ross
FRET	Förster resonance energy transfer
FTIR	Fourier transform infra red
GPC	Gel permeation chromatography
G-CK	Genuine casein kinase
GOPTS	3-(glycidyloxypropyl)trimethoxysilane
Glu	Glutamic acid
HFIP	Hexafluoro isopropanol
HBr	Hydrobromic acid
IPSC	Induced pluripotent stem cells
$\mathbf{K}_{cat}$	First order rate constant
KT	Kelen Tödüs
kDa	KiloDalton
$\mathbf{K}_M$	Substrate concentration that leads to half-maximal velocity
LCST	Lower critical solution temperature
LN	Laminin
µM	micromolar
µL	microlitre
µm	micrometre
µg	microgram
MAPK	Mitogen activate protein kinase
MMP	Metal metalloproteinase
MPC	Mouse primary calvarial
$\mathbf{M}_w$	Molecular weight
$\mathbf{M}_n$	Number average molecular weight
MS	Mass spectroscopy
MSC	Mesenchymal stem cell
NCA-ROP	N-carboxyanhydride ring opening polymerisation
NEB	New England Biolabs
NAM	Normal amine mechanism
NMR	Nuclear magnetic resonance
p-npp	Para-nitrophenolphosphate
PBLG	Poly(γ-benzyl l-glutamate)
PBS	Phosphate buffered silane
PMLG	Poly(γ-methyl l-glutamate)
PCPLG	Poly (γ-chloropropyl-L-glutamate)

PDMS-co-APMS	Poly (dimethylsiloxane)-co-(3-aminopropyl)methylsiloxane
PDI	Poly dispersity index
PEG	Poly (ethylene glycol)
PG	Poly-glutamic acid
PLL	Poly-L-Lysine
RAFT	Reversible addition -fragmentation chain transfer
RGD	Arginine-glycine-aspartic acid
RUNX2	Runt related transcription factor
ROI	Region of interest
rpm	Rotations per minute
S	Serine
SAM	Self assembled monolayer
Ser	Serine
SPPS	Solid peptide phase synthesis
TCP	Tissue culture plastic
ToF SIMS	Time of Flight Secondary Ion mass spectrometry
TIS	Triisopropylsilane
Tris-HCl	Tris(hydroxymethyl)aminomethane-hydrochloride salt
θ	Water contact angle
WCA	Water contact angle
XPS	X-ray photoelectron spectroscopy
TFA	Trifluoroacetic acid

Chapter 1

Introduction

1.1 Regenerative medicine

The restoration of damaged tissue and organs to their original function is known as the field of regenerative medicine. It works towards harnessing the healing capabilities of the body, sometimes with help from artificial biological material. It has become interchangeable with tissue engineering, which aims to maintain, restore or rebuild damaged tissue or organs [2]. This field has grown into four main stems:

- Medical devices and artificial organs
- Cellular therapy
- Biomaterials
- Clinical translation

These areas all interlink and the field has seen some incredible advances in recent years thanks to the introduction of techniques such as 3D printing, advances in gene editing, for example CRISP-R [3] and T-Cell therapies [4], the discovery of induced pluripotent stem cells (IPSC's) [5], advances in the sophistication of biomaterials and imparting biological function to those biomaterials. It is this aspect that will be addressed in this work. Specifically this is an investigation at the biointerface to enhance understanding and function between the synthetic biomaterial and the biological environment.

1.2 Biointerfaces

The implantation of a material/device in a biological system is followed by immediate interactions of cells, fluids and tissues with the surface of the implant. These interactions are critical for obtaining the desired functionality and to determine the success of the procedure [6]. This communication occurs at the biointerface, and it is the surface properties that dictate the success of this interaction. For instance, formation of avascular fibrous/collagenous shell around implants is a common reaction to implanted materials/devices. This prevents further interactions between the implant and the body which

can be detrimental for the implant requiring revision surgeries [7–9]. By enhancing the interactions between the biological environment and the implant through the introduction of biological recognition sites, which can be achieved via topography, mechanical and chemical cues, the success of the implant could be improved. Further understanding of the interactions at the biointerface can aid the development of materials with improved function and longevity.

1.3 The extracellular environment

The extracellular environment is constantly delivering information to the cell via signalling pathways which dictate cell activities. The environment outside the cell is communicated inside the cell via transmembrane receptors that fall into three main categories: G-protein (via protein interactions), ion channel reporters (via channel opening) and enzyme linked receptors (via enzyme interactions) [10].

Integrins that are mechanosensitive membrane spanning receptors that link the extra cellular matrix (ECM) to the cytoskeleton thus transmit information from outside the cell into the nucleus affecting gene transcription [11]. Once the receptor protein receives a signal it alters conformation which in turn induces a series of biochemical reactions in the cell. Integrins respond to recognition motifs detected on the material. The most commonly found integrins are $\alpha_5\beta_1$ and $\alpha_v\beta_3$ for fibronection and vitronectin respectively. Fibronectin contains the recognition sequence arginine-glycine-aspartic acid (RGD) which is a highly specific motif recognised by many integrins [12].

Even with the required motif present in the protein (for example RGD in fibronectin) for cell-material interactions, the conformation of the integrins has to be so, that the binding site is available. This conformational change can be instigated by soluble factors or the surface itself [13, 14]. Both biochemical and mechanical cues in the ECM affect cell behaviour. These cues have been explored in the synthesis of synthetic materials in understanding how they interact with the biological environment and what responses they can elicit.

1.3.1 Mechanical cues

Mechanical cues such as material topography and stiffness can influence cell behaviour. Mechanotransduction is the mechanism whereby cells convert mechanical stimuli into electrical or chemical activity. It has been investigated in the field of stem cell research to encourage stem cells down a particular lineage. Nanotopographical influence has been demonstrated as an effective method in influencing stem cell behaviour [15]. Dalby et al. reported mesenchymal stem cell's (MSC) multipotent phenotype can be retained through using square lattice symmetry [16]. Directed osteogenesis of MSCs has been demonstrated with micro-patterned features on biomaterials [15, 17, 18]. Furthermore,

Engler et al. cultured MSCs on materials with varying degrees of stiffness with all other conditions remaining consistent. Stiffness was shown to directly affect stem cell differentiation, with lower stiffness directing cells to a neuronal phenotype and higher stiffness directing cells down an osteogenic lineage. [19]. Surface effects on absorbed fibrinogens and their subsequent effect of cell attachment was investigated. Polyurethane surfaces were modified with different concentrations of silica nanocages. This affected the conformation of absorbed fibrinogens and the availabilty of the RGD sequence which in turn affected cell adhesion [20].

1.3.2 Biochemical cues

Biochemical cues have long been accepted as effective ways in which to influence cell behaviour and interactions with materials [21–23]. An important milestone in regenerative medicine was achieved in the discovery of Induced Pluripotent stem cells, where the addition of 4 factors Oct3/4, Sox2, c-Myc, and Klf4 to the culture medium of somatic mouse cells lead to the induction of pluripotency akin to embryonic stem cells [5]. VEGF, BMP-2 IGF-2, IGF-2 are examples of growth factors that have been found to influence the induction of osteogenesis and bone formation from various stem cell types [24–26]. Optimising the availability of these cues, in terms of concentration and frequency, remains a challenging hurdle [27].

The introduction of biochemical cues on the surface is an essential way to improve the functionality of a material in a biological environment. Roach et al. investigated the effect of surface coating with Poly-L-Lysine and Laminin (PLL-LN) to support primary central nervous system (CNS) neurones alongside topographical cues. Neuronal adhesion was enhanced compared to non coated material. This enhancement was explained by the positive charge generated on the substrates from PLL-LN creating electrostatic interactions with the negatively charged membranes of the neurites [28].

Surface wettability and its effect on cell adhesion has been systematically investigated by seeding osteosarcoma cells on a surface with a range of water contact angles from 12° to 155°. Optimal cell adhesion was observed at around 64° on the siloxane substrates [29].

The effect of surface chemistry on protein absorption and subsequent cell attachment was investigated by modifying gold surfaces with different functional molecules and measuring protein and cell adhesion via an antibody based assay. It was found that different chemistries affected the exposure of binding sites in the absorbed proteins (Fibronectin), which inturn affected cell adhesion with the trend of chemical functionalities $OH > COOH = NH_2 > CH_3$ for integrin binding and cell adhesion, with OH exhibiting highest binding [30].

When designing biomaterials it is important to consider how both mechanical and chemical cues can interact with the biological environment. The introduction of these cues has the potential to enhance the function of the biomaterial. This will be discussed

in the following section.

1.4 Biomaterials

A biomaterial is defined as a natural or synthetic material (such as a polymer or a metal) that is suitable for introduction into living tissue especially as part of a medical device [31].

The field of biomaterials was established in the 1960s leading to many advances including pacemakers, hip replacements, knee replacements and stents [32]. The materials chosen for these devices were so, due to their inert properties, ie. they had little interaction with the biological environment which was beneficial in avoiding any adverse effects. With the advancement of new materials such as Larry Hench's bioglass and hydrogels, which influenced cell behaviour, research began to move in the direction of materials that could provide interactions through biological cues in the biological environment to further enhance their function (Figure 1.1) [33, 34].

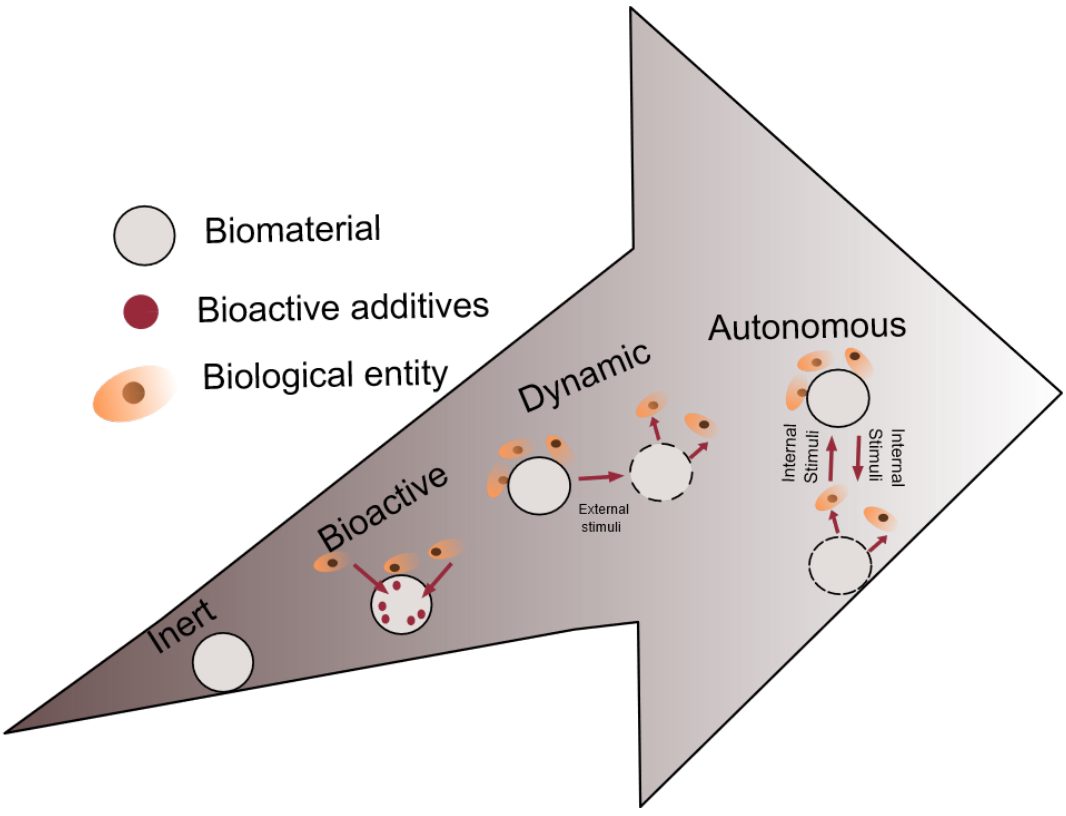


Figure 1.1: Evolution of biomaterials from bioinert: a material that exhibits no interaction with the biological envrionment, bioactive: a material that has bioactive or biophysical cues to interact with the biological environment, biodynamic: a material that undergoes a response on action of a stimulus and autonomous: a material that undergoes reversible physical/chemical changes on action of stimulus present in the biological environment

1.4.1 Dynamic materials

Tissue engineering was a field born in the 1990s creating actual biological materials that can be used for repairs and replacements in the body [35]. There was a shift to more sophisticated material design including the exploration into stimuli response or smart materials. In the present context, smart materials shall be defined as materials that undergo a physical/chemical change on exposure to a stimulus [36,37]. Advances in polymer chemistry aided the synthesis of polymers and hydrogels that undergo responsive behaviour whilst being biocompatible. Applications include biosensors, drug delivery and biomedical implants [38–40]. Thermo-responisve polymers have found applications in drug delivery, enzyme free cell passaging and controlling cell behaviour. Polymers can be tuned to have a lower critical solution temperature (LCST) of around body temperature which stimulates a morpholigical change in the polymer [41] [42]. Thermo responsive behaviour has also been investigated for injectable hydrogels that gel at 37°C, avoiding the need for surgical implantation of the biomaterial. pH changes throughout the body, and is therefore an effective stimulus particularly in drug delivery for a target area of the body. The biomaterial can be designed to undergo changes at a specific pH to release a payload in the desired location [43]. Photoresponsive materials can be beneficial with the introduction of light labile linkers into the material enabling cleavage that could release/ alter chemistry read by the biological environment, resulting in a biological response [44].

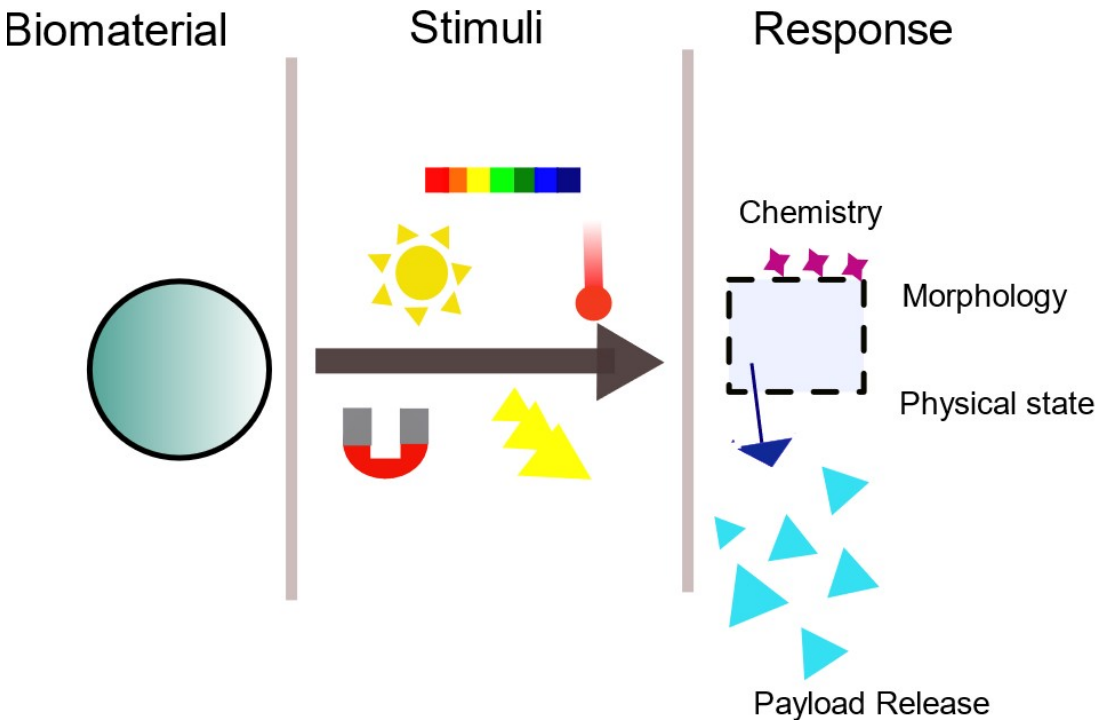


Figure 1.2: Representation of one directional biomaterial response to common stimuli, including light, pH, electricity and temperature, which causes an irreversible material response

All the above examples share a common theme in that the material responds to a

stimulus that causes a physical or chemical change. This is a one directional change that causes the desired change in material properties (Figure 1.2). The biological environment does not function in such a sequential (one stimulus eliciting one material change) and unidirectional manner, but is a truly dynamic environment continuously striving towards homeostasis, whereby conditions are maintained for optimal function. Therefore, autonomous materials could better mimic and interact with the biological environment through a reversible, self-regulating material responsive system.

1.4.2 Autonomous biomaterials

Autonomous biomaterials can be defined as materials that undergo a repeatable and reversible response on action of two stimuli within a self-regulated system (Figure 1.3). Autonomous feedback loops have been investigated for applications in self regulated drug release systems, whereby the drug release is controlled by a stimulus present in the system. An example of which is an insulin delivery vehicle. Cheng et al. developed an insulin loaded hydrogel composed of a glucose responsive material that forms a gel at low concentrations and a solution at high concentrations. Therefore unlike a passive release system, this dynamic system releases insulin when it is needed (high concentrations of glucose) and then returns to a gel at low concentrations stopping insulin release through this feedback loop [45].

In another hydrogel based system aimed at regulating blood coagulation, heparin is bonded to a thrombin sensitive moiety. In the presence of thrombin, heparin is mobilised and reacts with thrombin to render it inactive, thus reducing thrombin in the environment, preventing further heparin release [46]. Drug overdose can lead to increased CO_2 concentration in the blood. Researchers developed a feedback loop system whereby carbonic anhydrase is released from a hydrogel triggered by CO_2 which reversibly hydrates CO_2 and simultaneously releases an antidote naloxone [47].

These systems are cleverly designed for drug release, and follow a similar pathways whereby a hydrogel undergoes dynamic changes to release a payload which interacts with a biological substance to cause a reversal in the dynamic change of the hydrogel preventing further release. This paves the way for self regulating drug release systems. To date, there are no examples of autonomous systems with reversible self regulating interactions with a surface. As exploited in some of these examples dynamic processes in the biological system are almost exclusively controlled by enzymes.

1.5 Introduction to Enzymes

Enzymes are biological catalysts. They are proteins that drive chemical reactions in living organisms for a specific action or nutrient by instigating or speeding up the reaction rate. The chemicals that react with enzymes are called substrates and they react at the

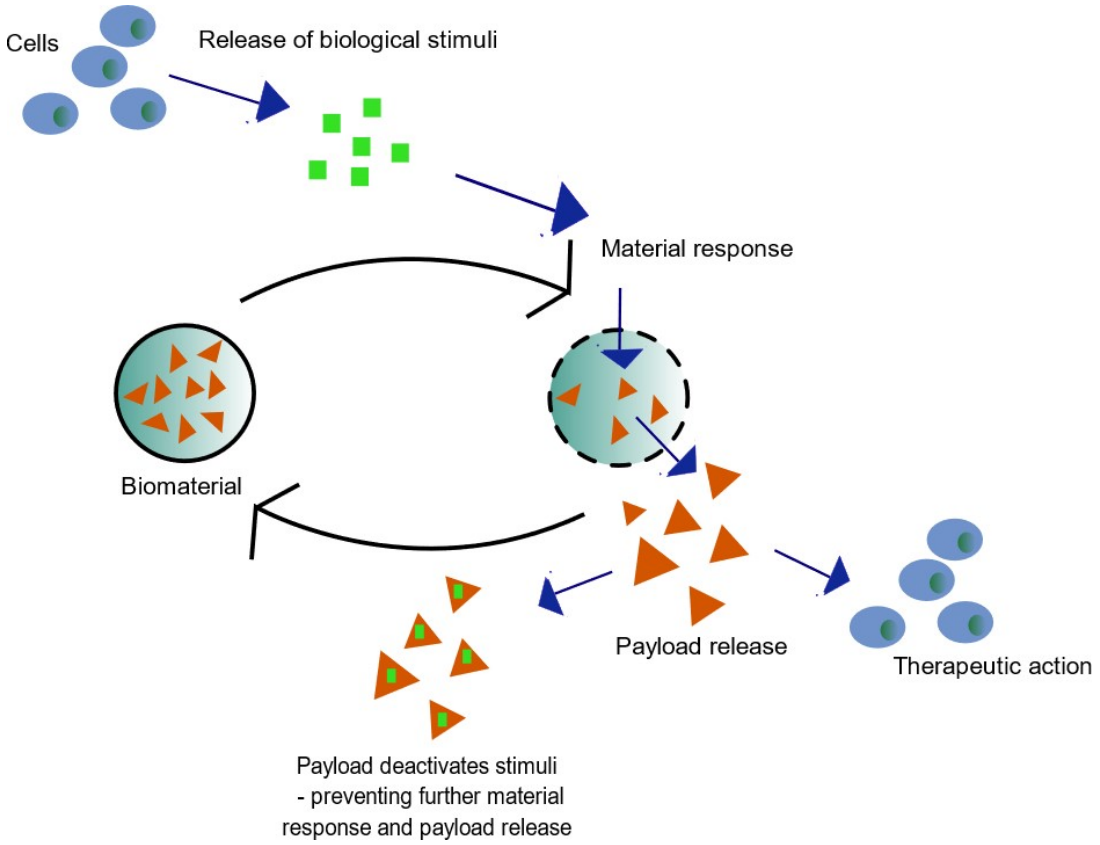


Figure 1.3: Representation of autonomous biomaterial drug delivery systems with feedback loops, whereby the stimuli is released by the biological cell, this causes a material response and a release of a payload which deactivates the stimuli that was released by the cell, thus stops any further material response.

active site of an enzyme. The active site of the enzyme recognises protein sequences. Enzymes have non-specific recognition sites whereas others are highly specific requiring a particular amino acid sequence to activate the enzyme. Once they have released the substrate after a reaction the enzyme is free to react with another substrate. Enzymes can catalyse the formation or the destruction of chemical bonds. As the body is striving for homeostasis there is frequently an enzyme for a certain bond formation and another enzyme that is able to break this bond. This balance is often disturbed in diseased states, notably cancer. The absence of even one enzyme can cause fatal diseases in humans. They have been a target for many life saving drugs, including penicillin which inhibits enzymes in bacteria, destroying their ability to survive [48].

Enzymes typically operate in reversible systems inherent to their function to regulate the presence of certain chemicals. Some enzymes are linked to specific areas of the body whereas others are ubiquitous throughout the body. Certain environmental conditions can cause the upregulation of certain enzymes including stressed and diseased states.

1.5.1 Enzyme responsive materials (ERM)'s

The essential role enzymes play in homeostasis makes them an advantageous target for stimuli in responsive biomaterials. They are inherently present in the body, therefore are an advantageous target stimulus in responsive systems as they do not require an external stimuli to illicit a material response and can be extremely specific to their substrate. As they are involved in homeostasis and reversible reactions, they are a sensible target for the development of an autonomous biomaterial.

Enzyme-responsive materials are a young class of materials and have been defined as materials that change their functionality on action of an enzyme on the material [49]. In diseased states the cell niche environment changes, this includes changes in the concentrations and types of enzymes which are secreted; efforts have been made towards developing a system where the response of the biomaterial is a result of action of up-regulated enzymes in the diseased states. Chien et al. developed a system for more targeted drug delivery of cisplatin, via a hydrogel which underwent supramolecular self-assembly in environments with high Alkaline phosphatase (AP) enzyme, associated with certain tumour environments [50]. Additionally, Gianneschi et al. developed an animal model test using fluorescently labelled amphiphilic micelles composed of nanoparticles [51]. Their retention was monitored in xenograft tumours, the mechanism of retention proposed being that enzyme action of Matrix metalloproteinases (MMP) secreted by tumour cells, resulted in the formation of micron scale aggregates, kinetically trapping the micelles in the tumour site. Controlling conformation and inducing conformational changes in biomaterials has been accomplished through enzymatic action. Chien et al synthesised shape shifting micelles which on the action of DNAzyme altered their physical properties leading to a change in micelle conformation and shape [52]. Enzyme

responsive surfaces have been synthesised for drug release on action of targeted Cathepsin D, a protease involved in cancer pathology and apoptosis [53].

Based on these studies it is clear ERMs are forecast as having promising applications as alternative drug delivery methods. The potential specificity achievable makes ERMs a promising class of materials for this function. Enzyme responsive surfaces will be discussed in detail in subsequent sections.

1.5.2 Kinases and Phosphatases

Phosphatases partake in approximately 30% of intra and extracellular activities, they form an antagonistic relationship with kinases to regulate many cellular functions via the phosphorylation and dephosphorylation of their substrates. Phosphatases are overexpressed in several cancer cell lines suggesting the development of ERMs which respond to phosphatase activity have applications in disease diagnostics and in targeted therapeutic drug delivery [54]. Phosphatases have been targeted as the stimuli for ERMs primarily in self-assembly, owing to the large differences in amphiphilicity and hydrophobicity of the polymer chain with or without the phosphate group, which can lead to morphological changes [55].

A cleverly designed material can exhibit phosphate groups on amino acids, threonine, serine and tyrosine. Dephosphorylation leads to an increase in hydrophobicity, which when designed well leads to self-assembly into gels and nanofibers. Uljin et al. reported micelle to fibre formation in a Fluorenylmethylcarbonyl chloride (Fmoc)-short peptide system triggered by an alkaline phosphatase [56]. Xu et al reported the use of nucleopeptides as hydrogelators made by the dephosphorylation of a tyrosine phosphate, providing a method to explore the potential applications of nucleopeptides as biomaterials [57]. Yang. Z et al. reported an efficient short peptide gelator system driven by the dephosphorylation of a conjugated phospho-tyrosine [58]. These examples are good demonstrations of rational material design to elicit a physical property change of the material in response to a phosphatase. However, in these studies the function is not controlled by the cells directly, rather by enzymes added by an operator.

1.5.3 ERM's response to cell secreted phosphatases

The first example of cell-secreted phosphatases successfully stimulating a material response *in vivo* was reported by Yang et al. who developed hydrogelators that are enzymatically and reversibly controlled by phosphatases and kinases [59]. They synthesised a pentapeptide, with a terminal tyrosine, which underwent one sol-gel-sol transition cycle in vitro, however no further cycles could be achieved due to varying activities between the two enzymes used. On in vivo subcutaneous injection of the phosphorylated peptide solution in mice a hydrogel was formed, strongly implying cell secreted phosphatases drove the dephosphorylation, thus triggering gel formation. An *in vivo* study suggested tumour

cell overexpression of AP leads to the targeted dephosphorylation and supramolecular self-assembly of cisplatin loaded micelles. However due to suggested particle size formation it is likely there was another mechanism driving the cisplatin release [50].

The first example of a modified surface which responded to native phosphatases provided by cells, altering the phosphorylation state, was reported by Zelzer et al. in 2012 [60]. They conjugated RGDS and YRGDS to a surface, where the tyrosine and serine residues were phosphorylated. Dephosphorylation of these residues was achieved via the action of MSC secreted AP, as determined by phosphate released from the surface into solution. Building upon this, forming a reversibly enzymatic responsive surface would be beneficial to create a dynamic interaction between cells and the surface interface for cell-induced or cell-controlled interaction or remodelling of an artificial surface. This has potential to improve material integration (eg. for implants) or provide new tools to engineer tissue. Thus the next logical step being to create a surface which has a peptide sequence containing the motif for non-specific phosphatases as well as specific kinases.

There are a large number of different kinases which have different specificities for peptide sequences and motifs. Ser/Thr Kinases represent around 80% of kinase specificity, thus making it a more applicable target system. In most cases kinases interact with 4 amino acids either side of the residue that can undergo phosphorylation, requiring a recognition sequence of eight amino acids [61,62]. In the case of casein kinase II the required motif is Ser/Thr-X-X-Glu/Thr [63]. When designing a material with the purpose of interacting with this kinase, it is integral that the system contains this specific sequence. This phosphorylation is reversible and the Ser/Thr residue can be dephosphorylated by AP, a non-specific enzyme. This system has been extensively explored in the literature to establish the mechanism and specificity requirements of different kinases. AP has been explored as a trigger in ERMs for applications in drug delivery, however there are no published examples of work exploring this as a reversible enzyme system for applications in tissue engineering and in control of cell behaviour.

1.6 Importance of conformation

The conformation of proteins in the biological environment is subject to change depending on the local environment. This can be induced by change in pH, temperature, ionic strength binding with receptors or substrates [64–66]. The conformation of the protein dictates how and what they can interact with dependent on the exposure of certain motifs within the structure. This in turn can dictate cell behaviour through the activation or deactivation of signalling pathways [13,14].

Phosphorylation by kinases is a prevalent example in living organisms which induces conformational changes whereby a phosphate group is bound to specific amino acids in the protein. This can be reversed with a second set of enzymes, phosphatases that remove the phosphate from the protein. This action can turn “on” or “off” proteins en-

abling or disabling their interaction with other proteins. This is an important regulatory mechanism [67–69]. The addition of a PO_4^- to a polar R group on the amino acid can render a hydrophobic portion of the protein more polar and hydrophilic which can induce a conformational change based on protein dynamics.

The phosphate is provided by adenine triphosphate (ATP) which is present intracellularly at concentrations of 1 to 10 mM. It is produced by a number of cellular processes: 1) Glycolysis 2) Oxidative phosphorylation and 3) beta-oxidation [70].

Courtesy of the abundance of phosphorylation mediated pathways in the biological environment, it has been investigated as a drug target. The activation of mitogen activate protein kinase (MAPK) by growth factors is required for the proliferation and differentiation of certain cells. The uncontrolled activation of this pathway is one pathology of certain cancers and targeting this pathway and inhibiting MAPK activation is a promising treatment for these types of cancers [71].

1.7 Synthetic polypeptides

Biomaterials derived from synthetic peptides have potential to contribute greatly to the synthetic polypeptides arena. Considerable efforts have been made to replicate the structure and function of natural proteins in synthetic systems to improve biocompatibility [72]. Using amino acids as building blocks for biomaterials offers great promise for applications in drug delivery, cell culture materials, biosensing and tissue engineering due to their functional versatility, potential biocompatibility and their ability to integrate with, or exploit, natural processes such as enzyme activity or targeted binding events [73–75]. Compositional and conformational diversity of peptide based materials can be readily achieved using amino acids as building blocks which directly contributes to their functional versatility as material building blocks. In addition to the diverse combination of natural amino acids possible, pre and post side chain modifications further expand the possibilities and capabilities of synthetic polypeptides. They have found applications as responsive materials, e.g. for pH dependent sustained drug release [76], photo responsive antibacterial devices [77, 78] and enzyme responsive scaffolds in tissue engineering [79].

The properties of natural and synthetic peptides (e.g. enzyme recognition or binding affinity) are related to the peptide's conformation, which in turn depends on the type, amount and distribution of amino acids in the peptide sequence. Understanding and manipulating these variables thus provides an attractive route to access peptide materials with a range of different properties and tailored functionalities. Control over peptide structure is important to modulate properties of the materials and different synthetic procedures are used to do this. There are three main routes to polypeptide synthesis; solid peptide phase synthesis (SPPS), recombinant peptide and N-carboxy anhydride ring opening polymerisation (NCA ROP).

1.7.1 Solid peptide phase synthesis (SPPS)

SPPS enables a high degree of control over the amino acid sequence through systematically growing the peptide by coupling each amino acid step by step to the peptide chain. This allows generation of peptides with desired chain length and sequence. Although highly controlled, high cost and time are a hindrance, particularly when synthesising long chain polypeptides (>30 amino acids) [80]. Moreover, incomplete de-protection, folding and side reactions can also hinder the synthesis. Problems such as back folding and chain to chain interactions can seriously affect preparation of high molecular weight polypeptides via SPPS [81].

1.7.2 Recombinant peptides

Overexpression from *E. coli* is a popular method to form peptides which are categorised as natural proteins [82]. Plasmids undergo a transformation which encourages the uptake of the cloned DNA sequence which encodes for the protein of interest. Replication occurs in the host (or via polymerise chain reaction (PCR) prior to the transformation). On addition of specific expression genes, expression of the peptide will be induced. This peptide is often purified using a column chromatography method. The recombinant peptide synthesis approach is economically favourable, however peptide folding and insolubility can frequently lead to significant challenges in the purification and subsequent uses [82].

1.8 N-carboxy anhydride Ring opening polymerisation (NCA-ROP)

An alternative approach that has seen an increase in attention during the past decade due to rapid technical advances is NCA ROP. Polymerisations of α-amino acid N-carboxyanhydrides (NCAs) was reported for the first time in 1906 by Herman Leuchs [83, 84]. It has found most success in industrial applications of large scale synthesis of long chain polymers. It presents an opportunity to synthesise long chain peptide based copolymers in a facile one batch process making it the most straightforward and practical approach for large scale synthesis of high molecular weight polymers composed of amino acids and their derivatives.

1.8.1 Mechanism of NCA ROP

An NCA is a carbon activated α-amino acid derivative that provides high electrophilic reactivity at the carbonyl group of the α-amino acid, providing it with its high reactivity with various nucleophiles. NCAs are most often synthesised using phosgene (or triphosgene as a safer alternative) [85]. Side reactions between the generated HCl by-product and synthesised NCAs forming α-amino acid acyl chloride and others have been

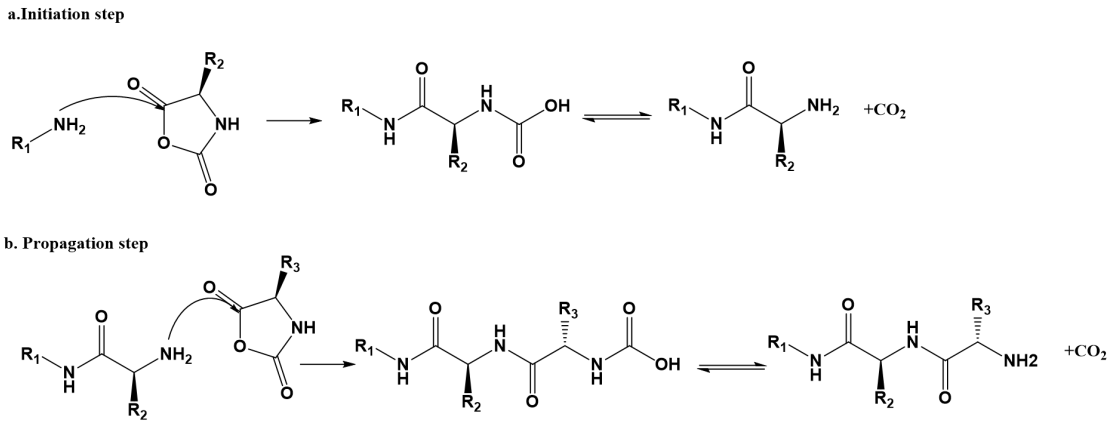


Figure 1.4: NCA-polymerisation via the normal amine mechanism

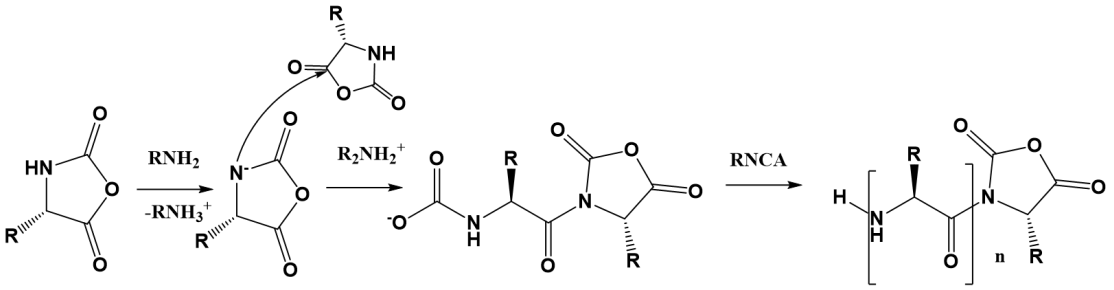


Figure 1.5: NCA-ROP polymerisation via the activated monomer mechanism

eliminated by the introduction of a HCl scavenger e.g. α-pinene [86]. Yields of NCAs can vary and are highly dependent on the type of amino acid, the side chain protecting group and synthesis route. The NCA reaction with nucleophiles is generally clean, with a co-product of CO_2. NCAs have a high sensitivity to moisture, therefore have low storage stability. Care must be taken to avoid contact with air (moisture) and synthesis must be carried out in dry conditions, using dry solvents and under nitrogen gas. NCA ROP can be initiated by a nucleophile or a base, each follows a different reaction mechanism. Primary amines (nucleophiles) have been shown to have the fastest initiation rate. In the nucleophilic attack on the carbonyl of the NCA, the ring is opened and the transfer of the proton results in the formation of the carbamic acid, which in turn is converted to a primary amine with the elimination of CO_2. The final step is reversible. The formed primary amine can continue polymer chain propagation (Figure 1.4). This is known as normal amine mechanism (NAM).

In the second mechanism, a base deprotonates the nitrogen on the NCA forming an anion which undergoes nucleophilic addition at the carbonyl on the NCA (Figure 1.5). The reaction continues to propagate in this manner, eliminating CO_2 as before at each addition step. This mechanism is known as Activated monomer mechanism (AMM) [87]

1.8.2 Side reactions

It has been proposed that limited control over NCA polymerisation is a result of the two mechanisms stated above occurring in one polymerisation, increasing polydispersity and explaining experimental results which are often very different than those predicted [88]. It has been suggested that impurities (water or ions) are the main contributing factors to the formation of side reactions, thus their elimination from the synthesis results in better controlled polymerisations. Aliferis et al. and later Messiman et al., reported using high vacuum and glove box techniques conditions [89, 90]. Under high vacuum techniques polymerisation followed exclusively NAM, whereas under glove box it was a mix of AMM and NAM with several termination products being present.

1.8.3 Use of initiators

Different initiators have been investigated to determine the optimum initiator to suppress side reactions and for a well-defined polymer. Denning introduced the use of organometal catalysts to suppress chain transfer and termination side reactions using organo-nickel and cobalt [91]. The authors proposed the following mechanism; the metals undergo oxidative addition across the anhydride bonds of the NCAs, causing metallcycle ring formation and contraction on the release of CO_2 mediated by NCA addition. The metal can then migrate along the growing chain [91].

More recently a new approach, the "accelerated amine mechanism through monomer activation" (AAMAA), has been investigated. A series of initiators that contained both secondary and tertiary amines act cooperatively to trigger living polymerisation of NCA-Glu and block copolymer of NCA-Lys/ NCA-Glu at 25°C. They reported a controlled PDI and molecular weights all within a 3 hour reaction time [92,93]. Secondary amines have been widely adopted as initiators [94–96]. When coupled with a decrease in temperature to 0 °C a reduction in side reactions and polydispersity with chain lengths close to the monomer feed ratio has been observed [96]. It has been suggested that at lower temperatures the activation energy for side reactions is not reached unlike in higher temperatures where these conditions readily enable the reactions to occur. The use of high vacuum has been proposed to shift the reaction equilibrium forward by removing the product, CO_2 [89]. Low temperatures and primary amines (with or without vacuum) is the most commonly used combination of reaction conditions, in the literature in the past 5 years, and has been successful in controlled synthesis of a variety of peptide based block co-polymers. Therefore these reaction conditions were used in this research.

1.9 Copolymers

The living polymerisation technique of ROP NCA presents the possibilities of creating homo-polymers, block and co-polymers. These can, however, often lack the specificity

and sophistication of natural proteins. The main limitation of this method is the lack of control over the amino acid sequence, causing variability in the folding and structure of the resulting polypeptides which are therefore not classified as proteins. Although sequence control may not be achieved via traditional methods, it can certainly be controlled to some degree through increased knowledge and understanding of the kinetics of NCA-monomer coupling, thus enabling control through monomer feed [49].

1.9.1 Block copolymers

NCA-ROP has been a successful method to synthesise di- and tri-block polymers, controlled simply by the addition of NCA amino acids in the desired sequential order into the reaction [91,97–99]. Block co-polymerisations have been primarily investigated for their ability to form micelles owing to ease of introduction of a hydrophobic and hydrophilic blocks. Such micelles can be drug loaded and can be designed to contain a crosslinker of a responsive moiety (commonly pH or redox) and have thus found applications in targeted drug delivery [97]. An example in phase III clinical trials (Japan-Asia) is a nanocarrier system, whereby a drug is encapsulated in nanoparticles that targets breast cancerous tissue. The carriers are composed of a hydrophilic PEG and a hydrophobic poly aspartic acid core, synthesised from NCA-aspartic acid [100,101]. Cameron et Hehir review 2014 discussed the advances in NCA-ROP for block co-polymerisations for responsive drug delivery vehicles [102].

1.9.2 Random copolymers

Thus far, we have discussed the advances and improvements made in NCA ROP over the past 20 years. This has been exclusively for homo polymers and in the synthesis of block copolymers. A principal challenge remains with NCA ROP of copolymer that is the synthesis of more sophisticated polymer sequences. There are however some success stories. For example, glatiramer acetate is the first example of a copolymer drug composed of a random copolymer of 4 amino acids, glutamic acid, alanine, tyrosine and lysine, first developed in the late 1960s. It is effective at suppressing EAE (the animal version of MS) [103].

NCA ROP presents an opportunity to synthesise long chain copolymers in a facile one batch process. Although sequence control may not be achieved via traditional methods, it can certainly be controlled through increased knowledge and understanding of the kinetics of NCA-monomer coupling, thus enabling control through monomer feed. While full control of the amino acid sequence is currently not possible in NCA ROPs, recent work has seen the establishment of tools to monitor NCA monomer consumption in copolymerisations, and thus provided the means to exert enhanced compositional control over polypeptides by controlling the monomer feed [104]. Understanding how monomer feed composition affects the composition of the resulting polypeptides is a first step

towards enhanced control over NCA ROP derived polypeptides, and several reports have used this approach to understand the underlying polymerization kinetics [49, 104].

1.9.3 Conformational studies of polymers synthesised by NCA ROP

Polymers synthesised by NCA ROP are a subject of interest in conformational studies, in particular how the conformation affects and can be manipulated for a specific application. Secondary structure formation during ROP can affect the polymerization progress. Notably β-sheet adopting oligopeptides can stop chain growth completely due to steric hindrance blocking the end of the chain [105]. An enhanced understanding over composition/conformation relationships in such systems will enable optimization of synthesis of well defined polymers for subsequent applications.

Iatrou et al. investigated the effects of pH and temperature on the secondary structure conformation of poly histidine synthesised from Trt-His-NCA and the impact these secondary structures have on polymer aggregation. Secondary structure conformation was a key parameter that defined the aggregation behaviour of the poly histidine with controllable pH and temperature mediated random coil to β-sheet transitions [106]. This demonstrates the tuneablity of such materials and potential as drug delivery vehicles.

Thermo responsive polymers have been synthesised through a novel NCA ROP and Reversible addition-fragmentation chain transfer (RAFT) copolymer block synthesised from MES -Glu-NCA, at low temperatures without the use of metal, which is normally required to mediate RAFT polymerisation. The polymers adopted α-helical structures and exhibited increased α-helical stability with increasing chain length, consistent with other reports in the literature. They achieved tuneable LCST, low polydispersities and controllable chain lengths. This is an approach to develop tuneable polypeptides without the use of metal that exhibit responsive behaviour [107].

Chain length can affect secondary structure composition as shown with the NCA-ROP of TFA and carboxylbenzyl protected Lysine. A bimodal distribution was absent in α-helical adopting long chain (DP 65>) polymers but it was observed in polymers with a (DP $<$ 20). The CD data shows these polymers adopt α-helical and random coil conformation. The authors conclude the bimodal distribution is attributed to the differing hydrodynamic radius of the two conformation types rather than differing chain length populations. It is to be noted that on deprotection of the lysine side chain this effect is no longer observed with all polymers exhibiting a unimodal distribution and α-helical conformation.

1.10 Biological applications – functional materials using NCA ROP

Ring opening polymerisation from NCA-amino acid monomers provides an attractive route to the synthesis of functional polypeptides.

A high proportion of literature focuses on the application of drug delivery vehicles as release systems that respond to stimuli present in targeted enviroments (e.g. change in pH/temperature). Frequent stimuli investigated include pH, temperature, light and electric field. There are detailed reviews on NCA ROP to synthesise functional peptides responsive to different stimuli: pH, temperature and light and the associated conformational changes. They focus on biodegradable polymers and routes to side chain modification for desired functionalities [108, 109]. Although biomolecules are discussed in the reviews, the focus remains on glycopolypeptides and discussion of enzyme-responsive polypeptides synthesised via NCA ROP is not discussed. In fact, there is little focus on NCA ROP to synthesise polymers that can interact with enzymes in the literature. The challenges in achieving specific amino acid sequences is likely the highest contributing factor, however there are many non-specific enzymes that could be targeted as well as enzymes that require a less sophisticated amino acid motif to be active. Therefore there is a wealth of possibilities yet to be explored of the use of NCA ROP in the synthesis of enzyme responsive polymers.

A few notable examples are the work by Thornton et al. who have developed drug delivery micelles focusing on enzymes as a release stimulus [110–112]. A detailed study into the tuneability of such systems to target specific enzymes was performed. Dopamine loaded micelles Dop-(Ala)-(Sar) and Dop-(Phe)-(Sar) have been synthesised by Thornton et al for targeted drug release on action of proteases [113]. They have demonstrated the ability to preferentially target Chymotrypsin, Thermolysin or Elastase by tuning the amino acid component on the first block (i.e. elastase favour alanine cleavage and Chymotrypsin favour Phenylalanine).

1.11 Surface modification

Surface modification is the act of modifying the surface of a material by bringing physical, chemical or biological characteristics different from the ones originally found on the surface of a material. The modification can be done by different methods with a view to altering a wide range of characteristics of the surface, such as: roughness, hydrophilicity, surface charge, surface energy and biocompatibility [114–116].

Surfaces are modified to impart function, herein the focus of this function will be biological. Appropriate modification can enhance biocompatibility and cell-material interactions. Furthermore, the introduction of polypeptides onto the surfaces can introduce biological cues that interact with the biological environment and stimuli that can further

improve the development of highly functioning biomaterials [117].

1.11.1 Responsive surfaces

Responsive surfaces is a growing field and has received considerable attention in recent years owing to their biomimetic nature and broad potential applications. Stimuli responsive surfaces can deliver a function in response to a stimuli and a broad range of stimuli have been investigated including; electric, pH, temperature, enzyme and photo [18], [118]. There are different methodologies to modify surfaces, which will be discussed below, in order to contain the desired chemistries to interact with the target stimuli to undergo the desired response. Electrically switchable surfaces have been developed by the Mendes group. This includes the design of two component SAMs whereby one acts as a linker to the surface and the other as the functional switchable entity. They developed a system whereby on application of an electric potential negatively charged/ hydrophobic entities were exposed which in turn affected early stage surface bacterial adhesion. Cell adhesion was controlled by synthesising a SAM on a gold substrate containing the cell recognition sequence, RGD, at the terminus linked to the surface by three lysine residues. Application of a negative potential drove a conformational change that concealed the RGD sequence which effectively and reversibly controlled adhesion of macrophage cells onto the surface [119]. Exploitation of the LCST of poly(N-isopropylacrylamide) has been effectively used to control cell attachment on a surface. Different thicknesses of PNIPAAM was grafted to tissue culture polystyrene and changing the temperature from 37 °C to 20°C (LCST) resulted in a change in hydrophobic/hydrophilic surface properties and detachment of endothelial cell sheets for the lower thickness modified surfaces [120]. A block co-polymer containing pH sensitive poly(L-glutamic acid) polypeptide was derived, pH was switched between pH 1 and pH 8.3 over a number of cycles and Rhodamine B immobilisation on the surface was reversibly controlled, with greater immobilisation at basic pH [121]. UV and visible light have been explored as a reversible trigger for surface modifications, chemical exposure can drive conformational switching of photochromic compounds such as spiropyran and azo-benzene. Silicon substrates were modified with a surface linker molecule covalently bound to an azobenzene-GRGDS, on exposure to UV light trans-azobenzene is transformed to cis-azobenzene on subsequent visible light exposure this was reversed. This was demonstrated by change in surface wettability, XPS and reversible cell attachment/detachment of Hela cells [122].

A huge variety of surface modifications and chemistries have been explored to undergo a functional change on action of a target stimuli. Furthermore different stimuli have been effective and have benefits fitting to the end application. Reversibly responsive modified surfaces have been demonstrated for a number of stimuli; electrochemical, light and thermo, however this has not been achieved for enzyme responsive surfaces, likely due to the enhanced complexity in developing and demonstrating such a system. Most of

the published research focuses on demonstrating the desired surface chemistry can be achieved for the desired material response to the stimuli, as it stands there is limited focus on specific and demonstrable applications of the technology. It is a field anticipated to grow and greatly contribute to biomedical research.

1.11.2 Surface grafting of polypeptides by NCA-ROP

Common surfaces that have been used as bases from which to build a functionalised surface in the literature include silica nano-particles, germanium and gold coated materials, glass surfaces and silicon wafers. The method of surface attachment must be compatible with the materials involved and produce a stable final material under the conditions of the expected application, and the responsive material must retain its responsive properties after immobilisation. Also, control over orientation and density of material can be essential to the function and for reproducibility. Synthesis of self-assembled monolayers (SAMs) notably using functionalised silanes on glass and thiols on gold surfaces has frequently been employed to varying degrees of success. Thiols on gold surfaces benefit from the ease at which they form self assembled monolayers with a high degree of control achievable owing to the mechanism of attachment. Whereas silanisation onto glass surfaces has potential to form self assembled monolayers, however the silanisation conditions are required to be optimised in order to achieve this owing to the possibility of the siloxane bonds being formed with silane already bound to the surface leading to multi-layered surfaces. This can effect the surface properties and any subsequent modifications. Therefore have been a subject of investigation for many researchers, this will be discussed in more detail below [123].

The grafting to and grafting from approach are common, versatile techniques for surface modification whereby one part of a molecule is covalently tethered to the surface, which provides stability under different environmental conditions (Figure 1.6). In both scenarios, it is usually necessary to introduce functionality onto the surface to attach the preformed polypeptide to the surface (grafting to), or to initiate the polymerisation from the surface (grafting from). There are different approaches available to introduce a functionality to the surface and the optimum approach is dependent on the material

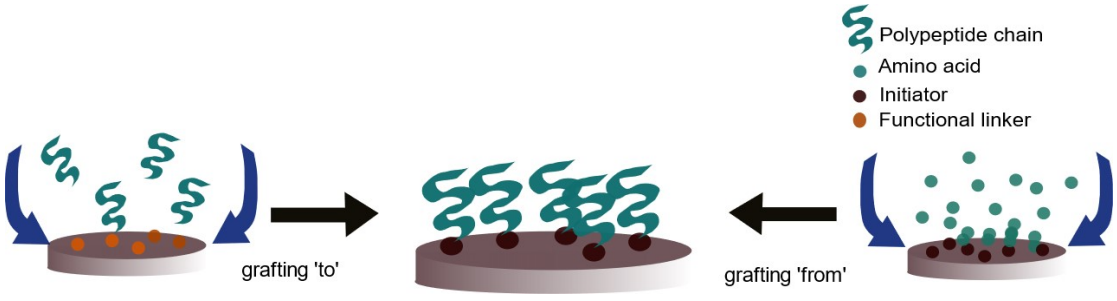


Figure 1.6: Scheme of grafting 'from' (with amino acids) and grafting 'to' (with a synthesised polypeptide) a surface.

to be modified.

In the case of this work we aim to modify borosilicate glass coverslips, chosen because they are able to transmit fluorescence from the surface. The most convenient method to introduce functionality on glass is to use the process of silanisation. Silanes exist with different terminal functional groups therefore offer a versatile way to functionalise the surface. The SiOH groups condense to form covalent bonds with the surface hydroxy groups to form O-Si-O covalent bonds. There are different techniques to silanise such as vapour deposition and solution deposition. Different factors affect the success of forming a homogenous monolayer namely: concentration, solvent type, temperature and incubation time [124]. There is little consensus within the literature of the optimum system to achieve a monolayer of silane with many researchers adopting different protocols. One study looked into the effects of different conditions with amino terminated silane amino propyl triethoxy silane (APTES). They concluded that at low concentrations (1 %) 1 hour was an optimal incubation time and increasing times resulted in the formation of thicker layers which were no longer monolayer. Concentration and temperature dictated surface roughness, with higher concentrations and temperatures increasing roughness, however they had a minimal effect on film thickness [125].

NCA ROP has been previously shown as an effective method to functionalise a surface with a polymer thin film and has been used to functionalise surfaces by the grafting to and grafting from method [126]. This will be discussed in more detail in the following sections.

1.11.3 Grafting "to" a planar surface

Grafting "to" offers the benefits of solution polymerisation including low polydispersities and high degrees of control often achieved. Facile and complete characterisation of the polymer through conventional methods such as NMR, mass spectrometry and IR can be performed before attachment of the polymer to the surface. However, inhomogenous and low density coverage on the surface has been reported due to limiting factors such as steric hindrance and diffusion of poly peptide chains onto the surface [127–129].

1.11.4 Grafting "from" a planar surface with NCA-ROP

The Grafting "from" method is not self-limiting as the polymerisation is both initiated and propagated from the surface. Hence, higher grafting densities can be achieved which is expected to impart enhanced function and properties to the films. Challenges do exist in controlling the initiation and polymerisation rate from the surface which can lead to broad molecular weight distributions [130,131]. It has been suggested that this drawback is offset by the high grafting density and high density of functional groups on the surface as a result [132]. In this work, we have focused on the grafting from method, which requires an initiator immobilized on the surface. For NCA polymerisation this is usually

an amine.

Functionalisation of the surface with an initiator can be achieved via methods mentioned above ie. organosulphide/thiol and alkyl/alkoxy silane compounds onto gold and silicon surfaces respectively. These methods usually lead to densely packed initiator, often more so than the space occupied by growing polypeptides. The effect of packing density of surface initiator was investigated by NCA ROP of NCA-phenylalanine from a modified gold surface. Firstly, when a monolayer of aminotrithiol was immobilised on the surface and samples were incubated with NCA-phenylalanine polymerisation did not proceed. However when a second layer of aminotrithiol was bound to the surface, reulting in a lower density of free amine groups NCA ROP polymerisation was successful. This was attributed to the difference in spacing between the amino groups. In the first case, the spacing between the amino groups was smaller than that required for an α-helical conformation to grow, whereas in the double layered initiator the spacing increased to 15 Å. Thus, the polymer had sufficient space to grow and adopt to the required conformation without steric hindrance effects from neighbouring groups [133].

It is generally accepted that improved grafting density of polypeptides can be achieved via grafting "from" method, however, an early study found the contrary [134]. Duran et al. investigated three different attachment techniques of poly-benzyl-L-glutamate (PBLG) to a surface; grafting to by condensation, grafting to by deposition and grafting from a surface immobilised initiator, APS. They found that grafting from achieved a lower surface thickness with ellipsometry measurements than grafting to methods, to which they concluded a lower surface grafting density was achieved. However thickness does not directly provide information on grafting density. This study does agree with the idea that grafting from a planar surface can suffer from low degree of polymerisation courtesy of chain transfer and terminating side reactions. In a more recent study into NCA-ROP of PBLG from soft substrates a high grafting density was achieved as determined by AFM, XPS and FTIR [134].

As discussed earlier in this introduction NCA ROP has two mechanistic routes. The normal amine mechanism, whereby a nucleophilic attack occurs from the surface bound amine to an NCA ring which creates a free amine group to undergo subsequent nucleophillic attacks. This mechanism has a fast initiation rate, good control over end group fidelity and molecular weight and is dependent on NCA purity, solvent purity, temperature and pressure. In the alternative mechanism, activated monomer mechanism (AMM) the NH proton is abstracted from the NCA ring under basic condition to form an NCA anion which can initiate the polymerisation [91, 95, 96]. This leads to a polymer in solution, not tethered to the surface, as well as poor molecular weight distribution, lower initiation rates and is regarded as uncontrolled. It is possible for both mechanisms to occur simultaneously [128, 135].

The suppression of AMM is integral to reduce the synthesis of polypeptides in so-

lution, not grafted to the surface, thus to further improve control within the system. Wibowo et al. published an extensive review on NCA ROP grafting to and from the surface in 2014 [136]. The kinetic profile of polymerisation provides information on the polymerisation mechanism, with fast initial NCA consumption followed by a slow consumption indicative of normal amine mechanism. There are a number of examples of homopolymerisations from the surface however there are few examples of successful surface initiated copolymerisations by NCA-ROP. In one such study from planar surfaces blocked combinations of poly(N-carbobenzyloxy-L-lysine), poly(g-benzyl-L-glutamate) and poly(S-tert-butylmercapto-L-cysteine) brushes from respective NCA monomers were successfully prepared from a nickel mediated surface initiated polymerisation. Analysis by XPS indicated a controlled polymerisation was achieved with the retention of the Ni end group [137]. To date, there are no reports of alternating co polymer sequences obtained via surface initiated NCA ROP.

1.12 Surface analysis techniques

Water contact angle (WCA)

Water contact angle provides information on the wettability of the surface, which is among other parametres, related to surface chemistry. Surfaces with a high WCA $>80°$ are considered hydrophobic and this is attributed to the presence of apolar groups such as hydrocarbons. Surfaces with a low WCA $<30°$ are considered to be hydrophilic and this is attributed to surface with polar groups, such as hydroxyl groups [138].

The principle behind water contact angle measurements is based upon surface tension. Surface tension occurs at the interface between two materials and is dependent on the properties of both materials [139]. If a liquid is placed on a solid material, the liquid will form a droplet with a defined contact angle θ based on the surface tension between the three interfaces. This can be explained by the Young equation:

$$\sigma_{sg} = \sigma_{sl} + \sigma_{lg}.cos\theta \tag{1.1}$$

The Young equation describes the relationship between the contact angle θ, the surface tension of the liquid σ_{lg}, the interfacial tension σ_{sl} between liquid and solid and the surface free energy of the solid σ_{sg}.

WCA is very surface sensitive (1 nm) thus can detect the very top layer of the surface [140].

X-ray photo electron spectroscopy (XPS)

XPS is a quantitative surface analysis technique that provides information on elemental and chemical composition of the surface enabling the precise determination of chemical surface changes due to surface modifications. XPS was used here to follow subsequent

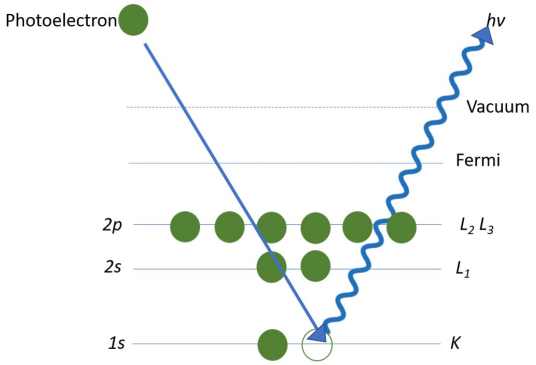


Figure 1.7: Schematic of photoelectron emission in XPS

surface modification steps via the changes in elemental composition and chemical functionalities and to determine the chain length of the polymers grafted from the surface.

XPS uses photons of a specific energy (determined by the anode material of the X-ray source) used to remove electrons from the core shells of the atoms, known as photoelectron emission. This occurs at high vacuum. To be able to stimulate the emission of a photoelectron, the energy of the X-rays (hν) has to be greater than the binding energy (E_B) – the energy difference between the ground state and the Fermi level – of the electron. In addition, to separate the photoelectron from the bulk material, a small and constant amount of energy is needed, which is referred to as work function (Φ). The remaining X-ray energy is transferred to the photoelectron as kinetic energy (E_K) and can be measured. Thus, the binding energy of the photoelectron can be calculated according to the Einstein equation 1.2.

$$E_B = h\nu - EK - \Phi \tag{1.2}$$

Electrons that are ejected from the surface are energy filtered by a hemispherical analyser before the intensity for a defined energy is recorded by the detector. The resultant energy spectra exhibit peaks characteristic for the electronic structure for the atoms at the surface. The escape depth of electrons to leave the surface is approximately 10 nm (this is material dependent) and the sensitivity is 0.1 to 1 atomic % (0.1 - 1000 ppm). The resultant peaks are well defined as the electron binding energies of the electronic state of the atoms. Further, the chemical environment of the atom at the surface results in shifts of the binding energies based on their electron withdrawing effects. The number of electrons recorded is proportional to the number of atoms at the surface (Figure 1.7) [141].

Quantitative accuracy under optimum conditions is around 90 % for major peaks, however this is reduced for weaker peaks to 10 to 20 % that of major peaks ie. 60 to 80 %. Wide scan spectra record binding energies (0 - 1300 eV) are low energy resolution spectra and narrow scan are high resolution, normally of binding energies of known interest.

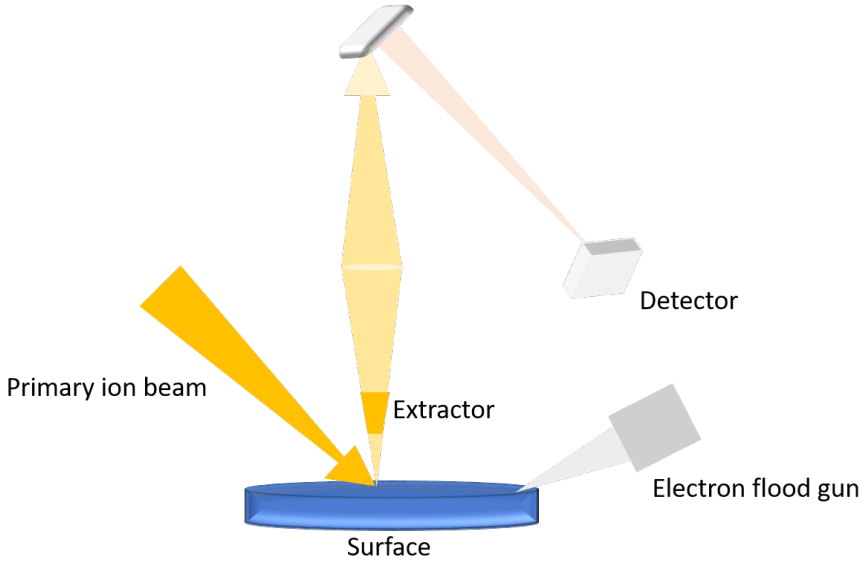


Figure 1.8: Illustration of ToF SIMS instrument set up

Time of flight secondary ion mass spectrometry (ToF SIMS)

ToF SIMS is a semi quantitative ultra high vacuum mass spectrometry technique that enables the chemistry on a surface to be determined. This can be achieved at a single point or across a certain area enabling a chemical map to be built of the surface. The instrumental set up can be see in Figure 1.8.

A primary ion beam is generated from a low boiling metal (Bi_n^+, Cs^+, Ar^+...) is heated under a nozzle in a high extraction field and field ionisation produces primary ions that are directed onto the sample. During this bombardment of the surface with the primary ions, not only secondary ions are emitted from the surface but an excess of electrons which can cause positive charging. This is compensated for by a stream of low energy electrons during mass separation. In static SIMS the ion dose of the primary beam is kept low ($<10^{-13}$ ions cm^{-2}) to minimise surface damage caused by the sputtering of ions.

When a sample is bombarded with primary ions, the primary ion energy is transferred to target atoms via atomic collisions and a collision cascade is generated (Figure 1.9). A part of the energy is transported back to the surface where its amount is just about sufficient for the respective atomic and molecular compounds to overcome the surface binding energy. ToF SIMS is a very sensitive surface technique as the emitted particles are generated from the uppermost monolayers, making it more sensitive than XPS (ppm to pbb) but with lower depth penetration. The charged state of the sputtered particles depends largely on the chemical environment which effects the emission probability of any secondary ion making full quantification of data complicated, known as the matrix effect.

Fragments up to 10 000 u can be emitted intact. Fragmentation leads to smaller

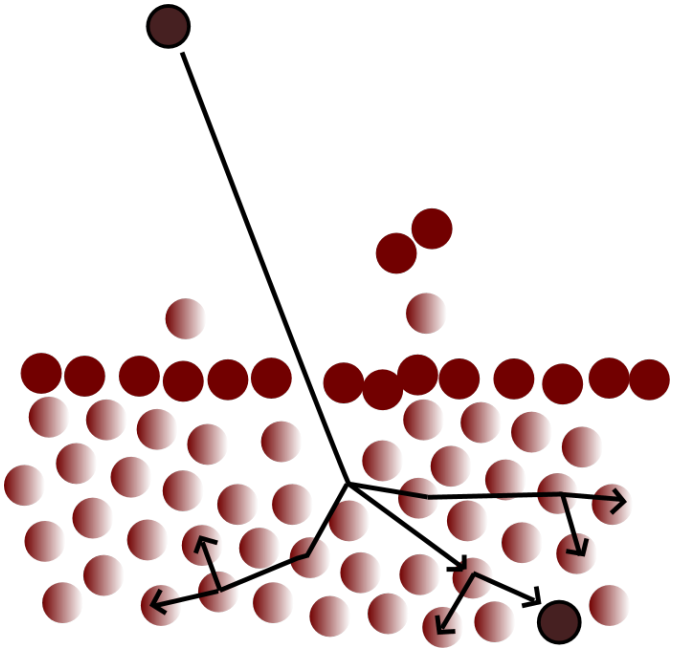


Figure 1.9: Illustration of the collision cascade on a solid sample (red) initiated by a primary ion beam (black)

charged ions that can be indicative of the parent molecule. These fragments are accelerated into a flight tube and the mass is determined by the exact time that they hit a detector based on their time of flight which is proportional to their mass and charge (m/z). Mass resolution of 0.00X atomic mass units (one part in a thousand of the mass of a proton) can be achieved [141].

In this work, ToF SIMS has been used as a semi-quantitative technique to determine successful surface modifcation and presence of amino acids glutamic acid and serine.

1.12.1 Förster Resonance energy transfer (FRET) technique to monitor conformational changes

Förster resonance transfer is a technique used to determine changes in distance between two molecules by monitoring fluorescence. The two molecules typically consist of a fluorophore, that emits fluorescence when excited at a certain wavelength and a molecule that can be simultaneously excited by the energy release, known as a quencher. The ability for the quencher to be excited by the energy released is highly dependent on the distance between the two molecules, therefore by monitoring fluorescence intensities, changes in conformation can be inferred. Specifically, a donor group is excited by a photon, which then relaxes to the lowest energy excited state. When the energy returns to the ground state if the acceptor is within a certain distance, typically 10 to 100 Angstroms, non-radiative energy transfer will occur to excite the acceptor group, which will return to the ground state or be quenched (Figure 1.10). If the acceptor is a black hole quencher, the energy does not cause photon emission but dissipation of the energy

in the form of heat as it relaxes to the ground state [142].

Static quenching mechanisms can also operate whereby the fluorophore and the quencher physically interact to form a dimer which is non-fluorescent, as fluorophores and quenchers are often planar hydrophobic molecules they can interact in aqueous solutions.

When choosing a FRET pair it is important the quencher has optimal absorbance overlap with the fluorophore emission energy. Efficient FRET [143] requires:

1) Proximity: the donor and acceptor molecules must be close to one another (within 10 to 100 Å). The equation below describes the relationship on the dependence on fluorescent quenching on the distance between the FRET pair.

$$E = \frac{R_6^o}{R_6^o + r^6} \tag{1.3}$$

Where E is the efficiency of FRET, R^o is the Forster distance where the donor acceptor distance is 50 % and r is the distance between the donor and acceptor.

2) Spectral overlap: Acceptor absorption needs to be in the spectral range of the donor emission.

3) Relative donor/acceptor orientation

Quenchers have typically been a second fluorescent dye to the fluorophore, however this can increase background noise due to overlap in fluorescence signal between the donor and acceptor. Dark quenchers are molecules that absorb excitation energy from a donor and dissipitate this energy as heat rather than light [144]. In this work a black hole quencher-1 was chosen as the acceptor. The BHQ-1 absorbs wavelengths of 480 to 580 nm. Fluorescein emits at 535 nm, therefore is a complementary fluorophore for the BHQ-1 with good spectral overlap. A lysine amino acid was coupled to the BHQ-1 via the amine group on the side chain thus providing a primary amine (from amino acid NH_2) to initiate NCA-Polymerisation.

1.13 Challenges in the field

As previously discussed, reversible enzyme responsive hydrogels as autonomous drug delivery systems have been explored, however this has not been achieved on a surface. Enzyme responsive surfaces have been reported, however these respond to a stimulus to undergo a material change and this change is not reversible [49]. To date no reversible enzyme responsive surface has been reported. A smartly designed surface that behaves biomimetically is advantageous and an autonomous material better mimics the biological environment than a static or dynamic material. The stem cell niche is a tightly regulated environment that we have not yet been able to replicate in synthetic biomaterials. A reversible enzyme responsive surface could present a way to create a more advanced artificial stem cell niche that allows improved control over stem cell fate by enabling expansion and differentiation of a whole population when and to the extent that is required by the biological unit rather than an external operator.

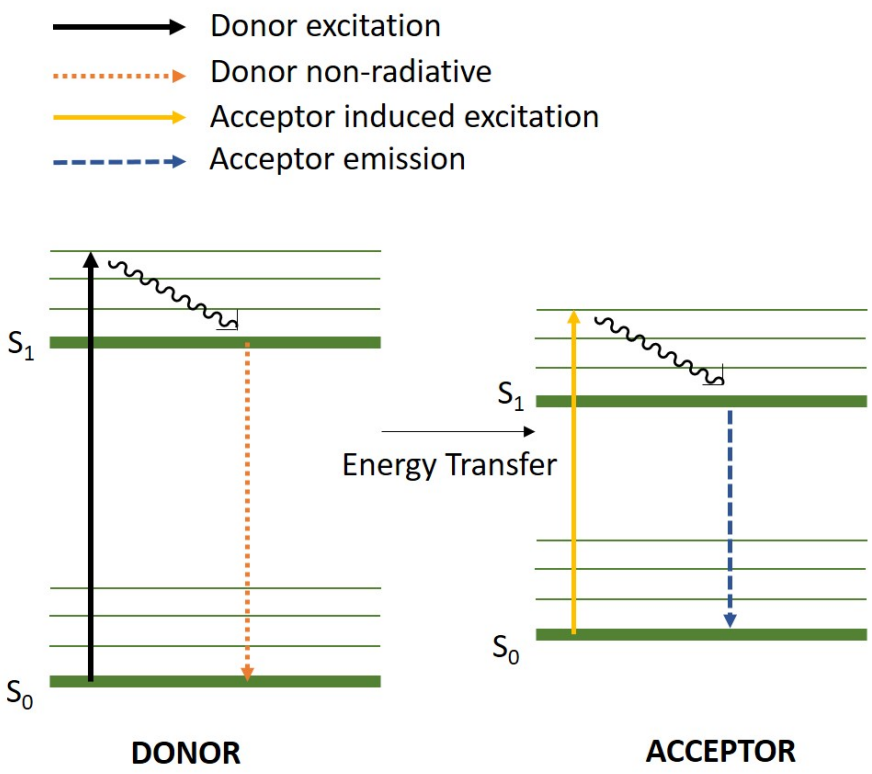


Figure 1.10: Jablonski diagram illustrating Forster resonance energy transfer [145]

1.14 Aims of thesis

The overall aim of this work is the development of a peptide modified surface by NCA ROP that can respond reversibly in the presence of enzymes. The aim of this thesis can be split up into four questions that will form each chapter:

- Can a relationship between polypeptide structure and polypeptide composition be determined of a co and homopolymer system composed of serine and glutamic acid synthesised by NCA ROP in solution?

As previously stated, control of co-polymer sequence via NCA-ROP is not possible, however the kinetic relationships between amino acids can be determined to gain information on the preferred sequencing. This will be investigated for serine and glutamic acid copolymers. The relationship between monomer feed and polymer secondary conformation will be determined to elicit control over NCA-ROP and to determine if there is a direct correlation.

- Can surfaces be modified with glutamic acid and serine by NCA ROP from a surface? Can a fluorophore and quencher be incorporated into the surface modification?

Surface modification by NCA-ROP will be explored to determine if it's possible to modify surfaces with copolymers. The modified surfaces will be analysed using surface analytical techniques to determine the presence of the polymer. One of the goals of

this work is to monitor any surface conformational changes as a result of enzymatic interactions with CKII and AP, therefore the incorporation of a fluorophore and quencher onto the surface will be investigated.

• Can these surfaces be modified with casein kinase II (phosphorylation) and Alkaline phosphatase (dephosphorlyation)? Can these interactions be monitored optically by fluorescence?

If the polymer is present on the surface we will then determine whether the serine in the polymer chain can be phosphorylated with CKII, this will be monitored via surface analytical techniques such as ToF SIMS to determine whether phosphate is present. Dephosphorylation will be attempted in the presence of AP. If we can show that the surfaces reversibly interact with the two enzymes we will then determine if this interaction is repeat-ably reversible and if so over how many cycles. With successful incoporation of a fluorophore and quencher into the surface we aim to monitor phosphorylation/ dephosphorylation indirectly via change in fluorescent output attributed to the predicted change in polymer conformation on interaction with the enzymes.

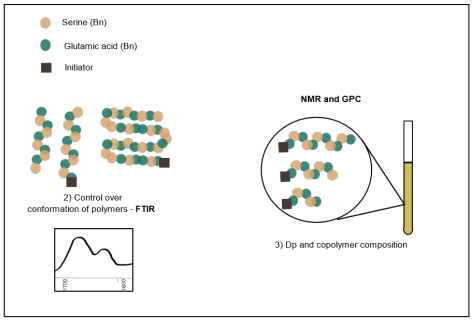
• Can these surfaces support cell culture in the presence of Casein Kinase II? Can enzyme interactions be monitored in the presence of cells by fluorescence?

The aim of this work is to develop a system whereby conformational changes induced by enzyme interactions on the surface can be detected in a non destructive method (optically via change in fluorescence) in situ in the presence of cells. It is therefore important to establish whether the modified surfaces can support cell culture. Furthermore, to monitor conformational changes on the surface as a result of cell secreted AP in the presence of CKII would be advantageous towards a truly autonomous system. It is therefore important the cell type supported by the surface secretes AP in sufficient amounts, this will also be monitored.

This is illustrated in Figure 1.11.

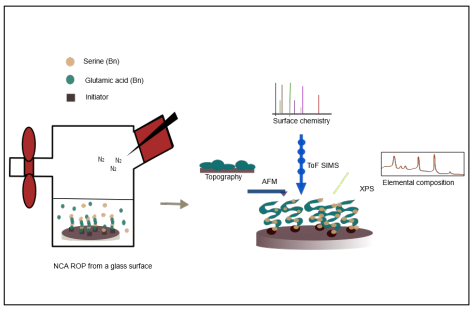
Chapter 2

Can composition structure relationship be determined of a co and homopolymer system composed of serine and glutamic acid synthesised by NCA ROP in solution?



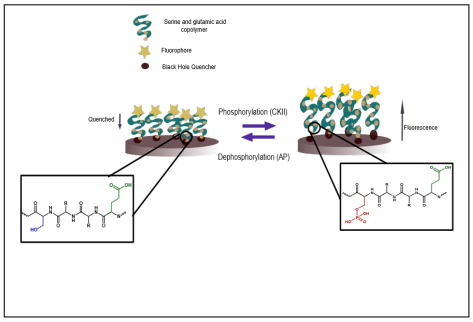
Chapter 3

Can surfaces be modified with glutamic acid and serine by NCA ROP from a surface? Can a fluorophore and quencher be incorporated into the surface modification?



Chapter 4

Can these surfaces interact with casein kinase II (phosphorylation) and Alkaline phosphatase (dephosphorlyation)? Can these interactions be monitored optically by fluorescence?



Chapter 5

Can these surfaces support cell culture in the presence of Casein Kinase II? Can enzyme interactions be monitored in the presence of cells by fluorescence?

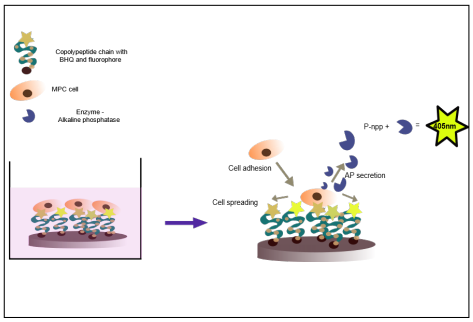


Figure 1.11: Summary figure of the experimental chapters included in this thesis

Chapter 2

N-Carboxyanhydride ring opening polymerisation in solution: A study of serine and glutamic acid

2.1 Introduction

As outlined in the previous chapter, to develop this enzyme responsive system it is necessary to synthesise a polypeptide that contains the amino acid sequence S-x-x-E for the CKII recognition motif. In this chapter we will explore NCA-ROP as a method to develop polymers that contain serine and glutamic acid.

2.1.1 Polyglutamic acid synthesised by NCA ROP

Glutamic acid (E) is an α amino acid with a carboxylic acid side chain (Figure 2.1). It has been studied and successfully used in a range of applications owing to its biodegradability and non-immunogenic properties, for example in waste water management, medicine

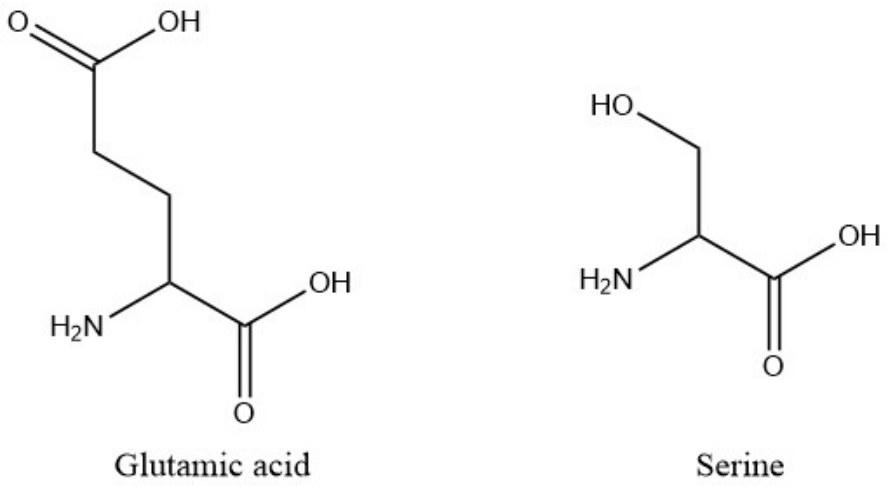


Figure 2.1: Structure of amino acids glutamic acid and serine

and in the food industry [146]. Poly glutamic acid (PGA) has been used in biomedical applications. PGA has unique biocompatibility, the N-terminal promoting cellular uptake of γ-PGA containing material, making it attractive in drug delivery [147,148]. The carboxylic acid side group can be readily modified with bio/chemical factors adding to its versatility in potential applications. It has been studied for applications in wound dressings, as a drug carrier and in tissue engineering [149,150].

Poly(glutamic) acid has been successfully synthesised by NCA ROP. Thornton et al. reported the synthesis of NCA-glutamic-benzyl polymerisation initiated from poly [dimethylsiloxane-co-(3-aminopropyl)methylsiloxane] (PDMS-co-APMS), which contains a secondary amine [151]. Solubility issues of the resultant product prevented full characterisation, however they were able to confirm full benzyl deprotection with TFA:HBr treatment (NMR) and infer some control over polypeptide grafting by monomer feed composition (DSC). Poly(γ-chloropropyl-L-glutamate) (PCPLG) polymers were synthesised from NCA- γ-chloropropyl-L-glutamic acid with controlled molecular weight and PDI that adopted α-helical conformation. Modifications with sugar derivatives did not change the conformation as determined by circular dichroism (CD) [152].

There are reports whereby NCA-BLG has been incorporated into copolymer systems synthesised by NCA-ROP. Chen et al. synthesised PEG-poly(l-glutamic acid) (PEG-PGlu) diblock copolymer by ROP to which cinnamyl alcohol was conjugated via the carboxyl groups (after benzyl deprotection) to afford copolymer mPEG-poly(l-glutamic acid-co-cinnamyl-l-glutamate) (mPEG-b-P(Glu/CGlu)) that were capable of forming photolabile micelles [153]. NCA-BLG has been used in NCA-ROP combined with ATRP to form pH and thermo-responsive poly(lglutamicacid-co-(l-glutamate-g-oligo(2-(2-(2-methoxyethoxy)ethoxy)ethyl methacrylate))) (P(Glu-co-(Glug-OMEO3MA))) graft copolymers [154].

These examples explore the use of NCA modified glutamic acid in block copolymer systems leading to self assembly and micelle formation. There are no examples whereby NCA-Glutamic acid has been incorporated in a copolymer with one other NCA modified amino acid to form a random or alternating copolymer.

2.1.2 Poly-serine synthesised by NCA ROP

Serine (S) is an α amino acid with a side chain hydroxyl group, classifying it as a polar amino acid (Figure 2.1). Studies reporting homo serine polymers are rare and typically use serine derivatives (e.g. phosphorylcholine side groups) instead, to improve water solubility and control chain length distribution [155], with the exception of one group that has found an interesting application for serine polymer synthesised from NCA-Ser. Thornton et al. synthesised a graft copolymer that consisted of a Poly(L-serine) backbone that was synthesised by NCA-ROP from O-benzyl-L-serine - NCA for applications in drug delivery of therapeutic agents within acidic environments [111]. ^{1}H

NMR analysis showed full benzyl deprotection was achieved with TFA:HBr treatment and the resulting polymer has low polydispersity (DI=1.05). A serine polymer backbone was also used in the development of self assembling nanoparticles for the release of chemotherapeutic agents. The serine poly backbone was synthesised from O-benzyl-L-serine-NCA then modified with phenylalanine to drive the self assembly of nanoparticles with narrow polydispersities [156].

As observed in the literature for glutamic acid, there are few examples of serine used in copolymer systems and none that explore the relationship between NCA-Ser and a second amino acid with respect to control and conformation achieved in polymerisations.

While there are no examples in the literature of copolymers of glutamic acid and serine synthesised by ROP, a similar system, a random copolymer of L-serine and N-(4-hydroxybutyl)-glutamine, was reported to undergo a thermally induced helix-coil transition. Using circular dichroism, it was shown that serine acts as an α-helical breaker and participates in β-turns, but the effect of copolymer composition was not explored [157].

The interplay between peptide composition and conformation has been extensively explored in disease modelling and drug optimization [158–162], for example to understand amyloid fibre formation [163]. The focus of these studies generally lies on the effect of changing specific amino acid residues in an existing natural peptide sequence. The connection between the polypeptide sequence afforded by this approach and the conformation of the resulting polypeptides has not been explored in detail. Serine has been shown to stabilize secondary structures (α-helix/β-sheet) and is dependant on the position of the amino acid in the sequence. Several studies showed that PGA forms an α-helical structure under aqueous conditions at ambient temperatures [149, 164]. In the design of our system, it is important we consider the polypeptide conformation, how this is affected and controlled by different monomer feed compositions and ideally to determine if or how conformation is affected by serine phosphorylation. This key information will enable greater understanding and informed design of the system when used in a biological setting.

2.1.3 Aims

The aims of this chapter are as follows:

- To synthesise homo and copolymers of NCA derivatives of side chain protected serine and glutamic acid by NCA ROP.
- To determine the control afforded by NCA ROP in terms of DI and chain length with respect to initial monomer feed.
- To explore the effect of different monor feed compositions on the conformation of copolymers by systemically altering the ratio in the monomer feed of glutamic acid and serine.
- To determine the kinetic reactivity of the amino acids.

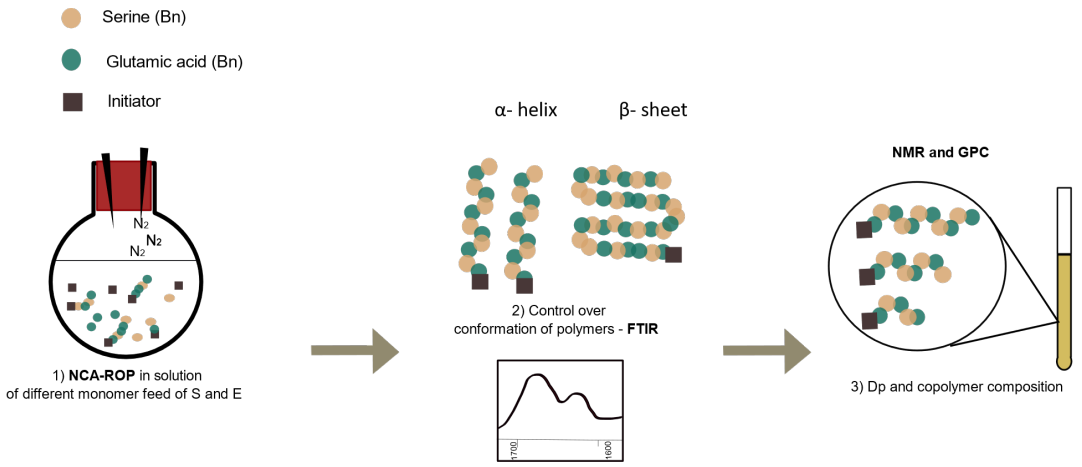


Figure 2.2: Schematic of chapter 2. Illustration of synthesis in solution of serine and glutamic acid in different monomer feeds and the analysis of the resultant polymers by FTIR (conformation) and GPC and NMR (composition)

We aim to establish whether the polymerisations are well controlled in order to determine if it is a viable route to develop the polymers required for our enzymatic system. Furthermore, we aim to establish whether a random copolymer is possible and whether it is a sensible copolymer combination for applications as enzyme responsive material for CKII and AP.

2.2 Methods

2.2.1 NCA-Serine (Bn)

H-Ser(Bn)-OH (0.05 moles, 11.275 g) was dissolved in ethyl acetate (dry, 90 ml) and α-pinene (0.17 moles, 27.5 mL), heated at 90 °C. The resulting suspension was placed under N_2 and stirred under reflux. After 15 minutes a solution of triphosgene (0.04 moles, 11.128 g) and dry ethyl acetate (37.5 mL) was added drop wise. The final suspension was stirred for 2 hours under reflux and N_2 at 90 °C (the reaction was considered complete when the suspension converted to a clear yellow solution). The solvent was removed to approximately 30 % of its original volume via rotary evaporation. Product was precipitated with petroleum ether (200 mL) and isolated by vacuum filtration. The crystallization process was repeated twice using ethyl acetate (50 mL) and petroleum ether (150 mL). The final product was dried at 50 °C in a vacuum oven overnight and analysed by NMR and MS. ^{1}H NMR (400 MHz, $CDCl_3$) δ 7.41 - 7.22 (m, 5H, Ar-H), 6.24 (s, 1H, N-H), 4.66 - 4.46 (m, 2H, CH_2), 4.43 (t, J = 4.1 Hz, 1H, CH), 3.96 - 3.50 (m, 2H, CH_2). MS ; EIMS (m/z (%)): $[MH]^+$ cald calc for $C_4H_5NO_4$, 132.6897, $[2M]^+$ cald calc for C_7H_8O, 216.6966.

2.2.2 NCA-Glutamic acid (Bn)

The same procedure was followed for H-Glu(Bn)-OH except the following masses and volumes were used: H-Glu(Bn)-OH (0.05 moles, 11,425 g) ethyl acetate (dry; 90 mL), α-pinene (0.14 moles, 22 mL), triphosgene (0.02 moles, 7,050 g) in ethyl acetate (dry; 45 mL). The product was analysed by NMR and MS. ^{1}H NMR (400 MHz, $CDCl_3$) δ 7.43 - 7.31 (m, 5H, Ar-H), 6.07 (s, 1H, NH), 5.15 (s, 2H, Ar-CH2), 4.39 - 4.32 (m, 1H, CH), 2.61 (td, J = 6.1, 1.3 Hz, 2H, γCH_2), 2.35 - 2.03 (m, 2H, βCH_2). EIMS (m/z (%)):$[2M^+Na]^+$, calc for $C_{13}H_{13}NO_5$, 548.7929, $[M^+Na]^+$ calc for $C_{13}H_{13}NO_5$, 238.1617.

2.2.3 NCA polymerisation

The procedure was adapted from the literature [49]. Random copolypeptides of NCA-Glu(Bn) (E) and NCA-Ser(Bn) (S) were prepared with monomer molar feed ratios (S:E) of 0:1, 1:2, 1.5:2.5, 1:1, 2:1.3, 2:1, 4:1 and 1:0. A total monomer concentration of 0.5 M (in dry DMF) and 0.1 mmol heptylamine (2 mol-%) were used in all polymerisations to obtain a theoretical chain length of 50 amino acids in each experiment. Polymerizations were performed under nitrogen and kept at 1 - 3 °C using a metal cooling block whose temperature was regulated by a cryostat. Completion of the polymerization was confirmed by FTIR by following the reduction of the C=O signal of the NCA at 1760 to 1800 cm^{-1}. On completion of the reaction, products were precipitated and washed (20 mL $\times$3) using diethyl ether and isolated by vacuum filtration. Resultant product was dried in a vacuum oven overnight at 40 °C.

2.2.4 Copolymerisation kinetics

The copolymerization parameters for the copolymerization of E and S were determined following a previously established procedure [49]. 5 mmole solutions of NCA-Glu(Bn) and NCA-Ser(Bn) were prepared at ratios (S:E) 1.5:1, 2.5:1, 3:1, 4:1, 4.5:1 and 6.5:1 were prepared in 500 µL of DMF, placed under N_2 and polymerisations were initiated with heptylamine (2 %). Reactions were stopped after 20 minutes ($\sim$10 % monomer conversion) and reaction mixture was added into a quenching solution (1 mL) of composition; CH_3CN:H_2O:HCl (1 M), (40:40:15) to deactivate unreacted NCA monomers. The polymers were precipitated and washed in diethyl ether (2 mL and 10 mL respectively). Isolation was performed by vacuum filtration and the polymers were dried in a vacuum oven at 50 °C overnight.

2.2.5 Characterization FTIR

An IR Agilent technologies Cary 630 FTIR instrument equipped with an attenuated transmission reflection (ATR) was used for FTIR analysis. 32 scans were taken for each sample. Peak areas for signals at 1787 cm^{-1} (COO stretching of NCA) [75] were

obtained to monitor reaction progression. For conformational studies spectra of solid samples (n=3) were taken using 128 scans, peak areas for Amide I (1600-1700 cm^{-1}), were used for component peak fitting with Casa XPS software. Spectra were normalised and peaks fitted using linear base until sum of peak areas followed total peak area (new components < 5 % of peak area, and residual error of peaks fitted <0.01). Peak fittings are shown in 2.16 for the polymers with different feed ratios.

2.2.6 ^{1}H NMR

^{1}H NMR spectra were obtained with a Bruker 400 MHz NMR spectrometer. NCA-amino acids and Glu(Bn) homopolymer were prepared in chloroform ($CDCl_3$), all other polymers were prepared in Trifluoroacetic acid (TFA-d). Peak fitting for kinetic analysis was achieved using Mestrenova software version 6.0.2. Spectra were baseline corrected using Whittaker smoother. Peaks were fitted to the CH regions using manual peak fitter and the software automatically fit the added peaks to the spectrum, until an optimal fit was achieved.

2.2.7 Gel Permeation Chromatography (GPC)

Relative molecular weights and polydispersities of the polymers were determined using GPC. The instrument was equipped with a Waters 1515 Isocratic HPLC pump, a Waters 2414 refractive index detector (40 °C), a Waters 2707 autosampler, a PSS PFG guard column and subsequently with two PFG-linear-XL columns (8 x 300 mm, 7 micron) in series (at 40 °C). The eluent (flow rate: 0.8 mL min^{-1}) used was HFIP (Biosolve) containing potassium trifluoro acetate (3 g L^{-1}). Polymethyl methacrylate standards with MP of 580 Da up to 7100 kDa were used as a reference (Polymer Laboratories).

2.2.8 Circular Dichroism (CD)

Measurements were taken on a JASCO J8108 spectrometer. Samples were prepared at 0.2 mg/mL in HFIP and transferred into a 250 µL quartz cuvette. Spectra were taken from 260 to 195 nm, CD and absorbance were measured. Spectral bandwidth used was 1 nm, response time 4 seconds and 2 scans were accumulated per sample. Data was normalized and molar ellipticity was calculated using the following equation: $[\theta] = 100x\theta/(Cxl)$ Concentration was calculated using polymer molecular weights as determined from NMR spectra.

2.3 Results and Discussion

2.3.1 Synthesis and characterisation of copolypeptides with systematically changing composition

To prepare a series of serine and glutamic acid copolymers with a systematic change in amino acid composition via NCA polymersation (Figure 2.3), polymerisations were carried out with varying monomer feed ratios (Table 2.1) but constant total monomer (0.5 M) and initiator concentrations (2 mol-%). NCAs of the benzyl protected amino acids, glutamic acid and serine, were synthesised according to literature procedures and characterised by NMR and mass spectrometry [96](Figures 2.4 and 2.5).

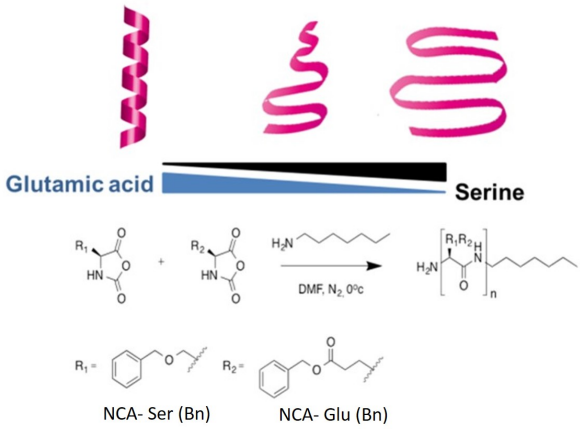


Figure 2.3: Scheme of preparation of copolypeptides of Glu(Bn) and Ser(Bn) via NCA polymerization.

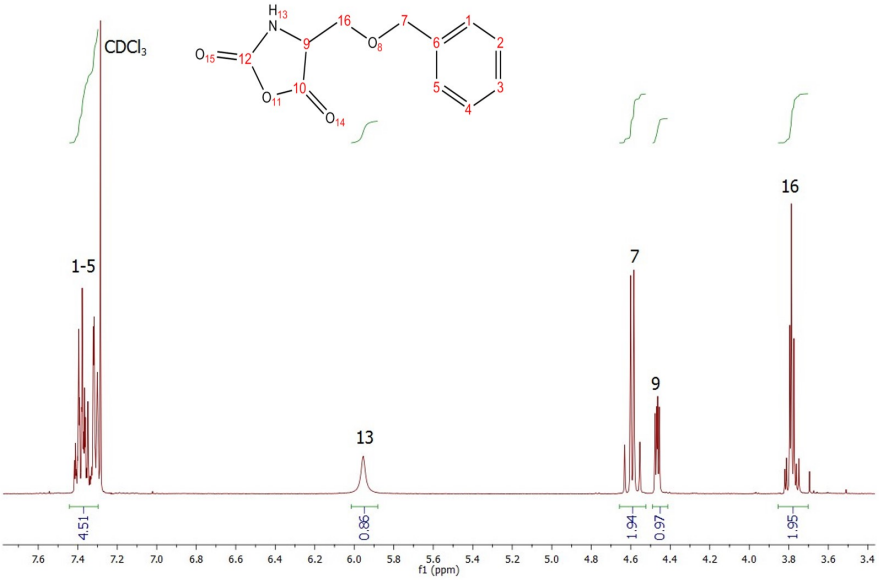


Figure 2.4: ^{1}H NMR of NCA-Serine(Bn)

The co-polypeptides obtained after polymerisation were characterised to determine

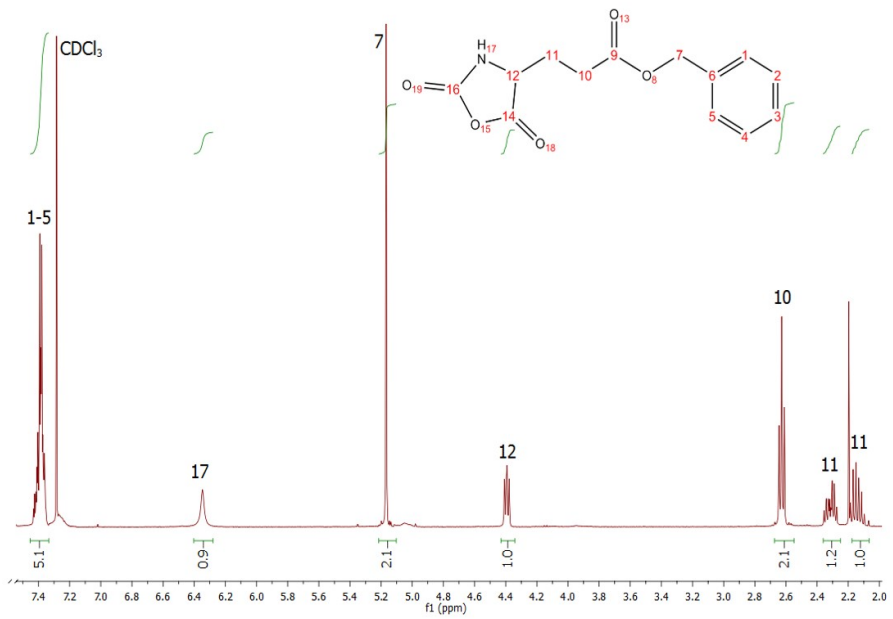


Figure 2.5: ^{1}H NMR of NCA-Glutamic acid(Bn)

Table 2.1: Characteristics of copolymers prepared from Ser(Bn)-NCA (S) and Glu(Bn)-NCA (E) at different monomer ratios as determined by NMR. Average over three repeats. Feed Ratio (S:E)

Feed ratio (S:E)	initiator: monomer ratio	Dp (experimental)	Final conversion (%)	mole fraction (theoretical)	mole fraction (experimental n=3)
0:1	50:1	34 ±1	68 ±2	0	0
1:2	50:1	48 ±1	98 ±2	0.33	0.32 ±0.01
1:1	50:1	47 ±2	94 ±4	0.5	0.47 ±0.02
2:1	50:1	42 ±7	84 ±14	0.67	0.61 ±0.03
1:0	50:1	33 ±4	66 ±8	1	0

polymer composition, molecular weight and dispersity. The NMR spectra showed that polymerisation was successful as indicated by the loss of the peak corresponding to the NH adjacent to the anhydride (6.4 ppm) and the appearance of the peaks at 4.75 and 5.1 ppm corresponding to the proton on the α carbon. Integration of the peaks was achieved using the CH_3 on the initiator heptylamine as a reference to obtain experimental chain lengths and ratios (Table 2.1). The copolymers achieved up to 90 % conversion of monomers into polymer.

In contrast, homopolymers did not reach full conversion. In the case of the serine homopolymerisation, this can be rationalised by the poor solubility of the Serine-NCA in DMF, which could account for the lower chain length, in the homopolymer as well in the copolymer 2:1, which obtained lower chain length than the other copolymers. The

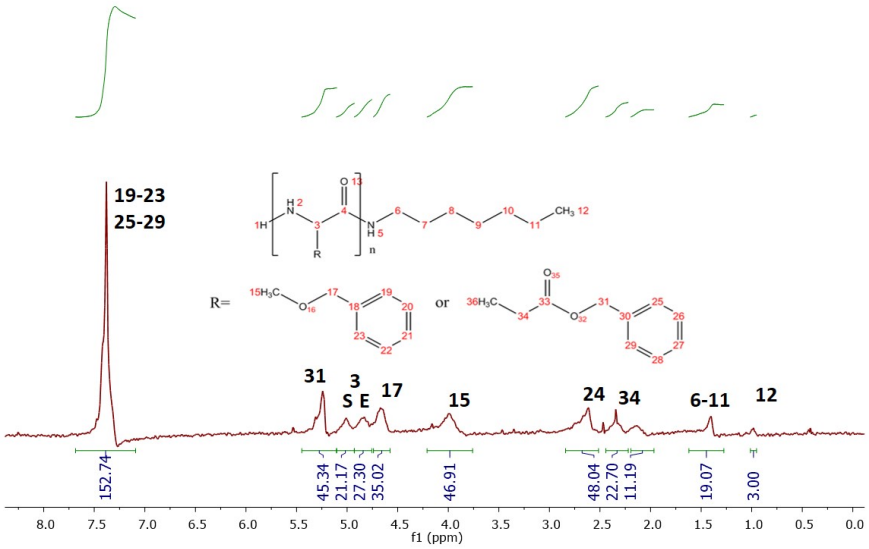


Figure 2.6: ^{1}H NMR of NCA-Glutamic acid (Bn): NCA-Serine (Bn) 1:1 copolymer

low degree of polymerisation for the Glu(Bn) NCA obtained here was repeatable and consistent for three separate reactions but stands in contrast to the literature which reported between 80% and 100% conversion [165]. Different reaction conditions and analysis methods (NMR vs GPC) may account for the discrepancy between our results and the literature. The ratio of the two monomers was determined by integrating the peaks at 4.75 ppm and 5.1 ppm using MestreNova peak fitting software, this can be seen in Figure 2.7 for the three copolymers. The copolymer ratios were close to the initial monomer feed, with slightly lower amounts of serine than predicted for the 1:1 and 2:1 (S:E) copolymers. Further indicating low solubility of serine could be influencing the composition of the resultant copolymer.

To investigate the unprotected polypeptides alongside the protected materials, we attempted deprotection of the polypeptides in TFA/HBr (3:1) for 16 h and Triisopropylsilane (TIS)/H_2O/TFA (95:2.5:2.5). Signals of the aromatic compounds of the protection groups in the NMR spectrum indicated that the deprotection did not proceed to completion (Figure 2.8). Hydrogenation was also attempted with Pd/C catalyst, however this was also unsuccessful, likely due to the length of polymer chain preventing complete access to the catalyst as has been previously reported for other polypeptides [166, 167]. Thus subsequent analysis was carried out on benzyl protected polymers only.

The Dispersity (DI) of the homo- and copolypeptides was determined by GPC (Table 2.2). No data could be obtained for the serine homopolymer due to the low solubility of the polypeptide. The DI of the polymers increased with increasing Ser(Bn) content, indicating that Ser(Bn)-NCA has a negative effect on chain length homogeneity. The GPC chromatograms show that high relative amounts of Ser(Bn) causes a bimodal distribution of the polymer (Figure 2.9).

It is possible that the low solubility of poly(Ser(Bn)) and copolymers with high

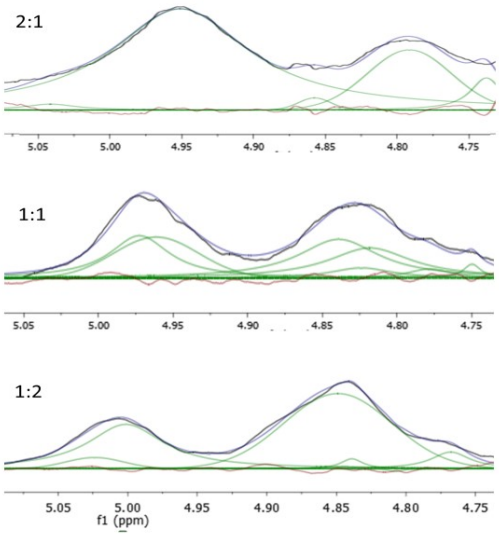


Figure 2.7: Fittings to the backbone CH signals in the H NMR spectrum to determine the experimental ratios of Ser (Bn) to Glutamic (Bn) after copolymerisation (ratios displayed as S (Bn) to E (Bn)

Ser(Bn) content causes these polymers to precipitate from the reaction mixture. This is supported by the observation of precipitation early during the polymerisation which would reduce the likelihood of chain propagation for these materials. More soluble copolymers with higher Glu(Bn) content subsequently grow faster, giving rise to the unimodal distribution observed in the GPC. Consequently, our data suggests that greater control over polymerization can be achieved with co-polymers where glutamic acid predominates in the initial monomer feed. As GPC measures the hydrodynamic radius of the polypeptides, the variations in the chemical composition of the different polypeptides can be expected to affect the GPC derived molecular weights, preventing any further comparison between the polymers. This may also explain the higher than expected molecular weight for GPC derived measurements. Molecular weights derived from the NMR spectra were calculated based on the number of amino acid residues present in each polymer. While reaction mixtures with low S:E feed ratios result in significantly higher molecular weights, the molecular weights do not consistently increase with increasing Glu(Bn) content and the trends observed for the GPC and the NMR based data are consistent. Attempts to further characterize the polymers with MALDI TOF MS were unsuccessful, due to poor solubility of the polymers.

2.3.2 Copolymerisation kinetics

Polymerisation kinetics can provide insight into the probable distribution of the monomers in the polymer chain. This is achieved by determining whether the monomers preferentially react with themselves (block copolymer), each other (alternating co polymer) or no preference (random copolymer). This was achieved by monitoring the initial rate of

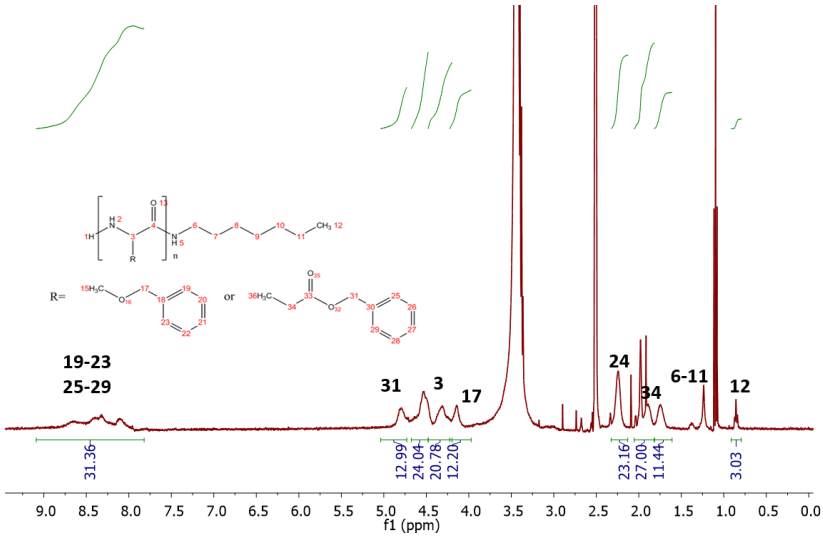


Figure 2.8: ^{1}H NMR of NCA-Glutamic acid(Bn): NCA-Serine(Bn) 1:1 copolymer isolated after treatment with TFA: HBr.

Table 2.2: Number (Mn) and weight (Mw) average molecular weight and polydispersity index (PDI) of copolymers prepared from Ser (Bn)-NCA and Glu (Bn)-NCA at different ratios as determined by NMR and GPC Feed Ratio

S:E	Mn/ g mol^{-1a} (n=3)	Mw/ g mol^{-1b}	Mn/ gmol^{-1b}	PDI^{b}
0:1	7554 ± 200	8000	7000	1.1
1:2	9993 ± 180	14 000	10 000	1.36
1:1	10820 ± 1100	17 000	11 000	1.5
2:1	8297 ± 1200	12 000	7000	1.79
1:0	7585 ± 400	-	-	-

^{a} as determined by NMR

^{b} as determined by GPC

consumption of the amino acid NCAs to determine the copolymerization parameters for Glu(Bn)-NCA and Ser(Bn)-NCA (rSer and rGlu). Reaction kinetics for the copolymerisation were determined from polymer samples isolated at low conversion (approximately 10 %) to eliminate the effects of compositional drift. Six different monomer feed ratios were used, and the copolymer composition was determined via NMR analysis (Table 2.12).

Through determination of the molar ratio of Ser to Glu in the copolymer chain by NMR and by knowing the monomer feed ratio the reactivity ratios of each monomer can be calculated via linear regression. The value of the reactivity parametres of the amino acids provides insight as to whether the coploymers will preferentially form a random, alternating or block copolymer Figure 2.10. Two different methods, the Finemann-Ross (FR) [168] and the Kelen-Tüdös (KT) [169] method (see below), were used to calculate

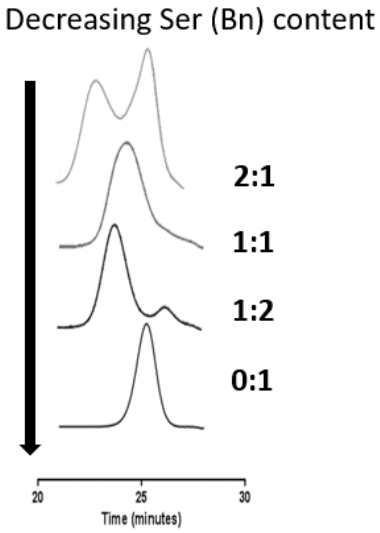


Figure 2.9: Chromatogram of Ser(Bn) and Glu(Bn) polymers at ratios of Ser(Bn):Glu(Bn) = 2:1, 1:1, 1:2, 0:1 (in descending order) as determined from GPC. Data normalized to the peak with the highest intensity.

the copolymerization parameters rSer and rGlu (Table 2.14) defined in Equation 2.1 and 2.2.

$$r_{Ser} = \frac{r_{Ser}r_{Ser}}{r_{Ser}r_{Glu}} \tag{2.1}$$

$$r_{Glu} = \frac{r_{Glu}r_{Glu}}{r_{Glu}r_{Ser}} \tag{2.2}$$

A one way ANOVA test was used to determine that there is no significant difference between rSer and rGlu for the two methods, suggesting that the values are good approximations of the monomer reactivities. Both rSer and rGlu are closer to 0 than 1, indicating that Ser(Bn) and Glu(Bn) preferentially forms alternating copolymers. This is visually demonstrated in Figure 2.13, which shows that the feed and monomer compositions closely match each other. Only a small drift is observed when the feed concentrations of the two NCAs approach equimolarity. We can therefore conclude that polymerisations kinetics dictate a mostly uniform polymer composition and prefers alternating copolymers. Hence, only copolymers with significantly different monomer starting concentrations will be expected to display a compositional drift towards the end of the polymer chain.

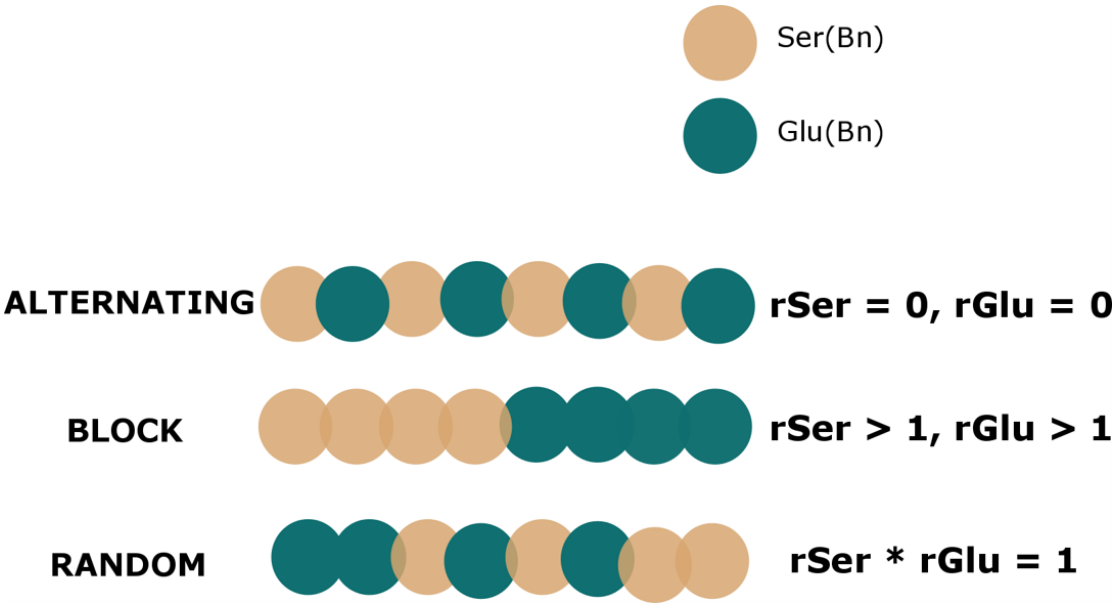


Figure 2.10: Schematic illustrating the determination of copolymer composition based on calculated monomer reactivity ratios

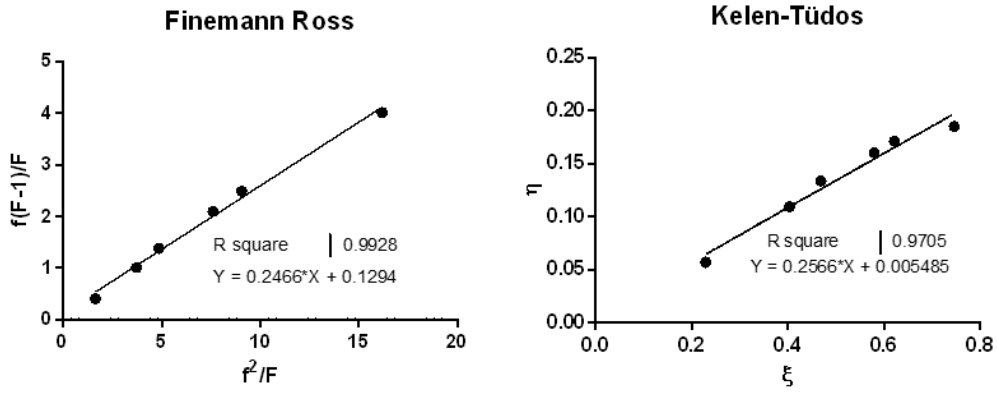


Figure 2.11: Linear regression of monomer ratios as determined by Finemann Ross (a) and Kelen-Tüdös (b) methods

Figure 2.12: NMR peak fitting data of shift peaks assigned to the α-CH from polymerisations with different monomer feed compositions (S:E) and parameters calculated from the NMR data for the determination of the reaction kinetics

Experimental composition					Calculated values			
Feed composition (S:E)	Feed ratio (f)	Peak area (S)	Peak area (E)	Ratio (F)	f^2/F	f(F-1)/F	ɛ	η
1.5:1	1.5	1456	1061	1.37	1.64	0.41	0.23	0.0
2.5:1	2.5	6532	3896	1.68	3.73	1.01	0.40	0.1
3:1	3	6418	3463	1.85	4.86	1.38	0.47	0.1
4:1	4	1334	634	2.10	7.60	2.10	0.58	0.1
4.5:1	4.5	4156	1856	2.24	9.05	2.49	0.62	0.1
6.5:1	6.5	3550	1360	2.61	16.19	4.01	0.75	0.1

2.3.3 Copolymer conformation

The prevalence of secondary structure motifs in the copolypeptides was measured to study the effect of changing polymer composition on polypeptide conformation. The presence of secondary structures in five polymers at ratios (S:E) 0:1, 1:2, 1:1, 2:1 and 1:0 was measured with CD for solutions and FTIR for solid samples. As applications of the polypeptide materials are likely to be in a solvated environment, we started by investigating the conformation of the polymers in solution. All samples follow a similar trace with negative bands at $\theta(222)$ and $\theta(208)$ characteristic of α-helical secondary structures (Figure A.3). Due to poor solubility of the polymers, HFIP was the only suitable solvent; it is, however, known as a strong α-helical inducer, and the presence of α-helices are therefore not necessarily indicative of the native peptide conformation [170]. We therefore also studied the secondary structure of the copolypeptides in their solid state using FTIR.

The amide I band (1600 - 1700 cm^{-1}) is indicative of C=O stretching and composed of overlapping bands corresponding to different secondary structure types (i.e. α-helices, β-sheets, unordered and random), enabling quantification of the prevalence of specific secondary structure motifs [171]. The deconvoluted spectra of the amide I band can be found in (Figure 2.16).

It was found that the polymers formed predominantly α-helical and β-sheet structures. The change of the relative amount of these two secondary structural motifs with changing Ser(Bn) content in the polypeptides is plotted in Figure 2.15.

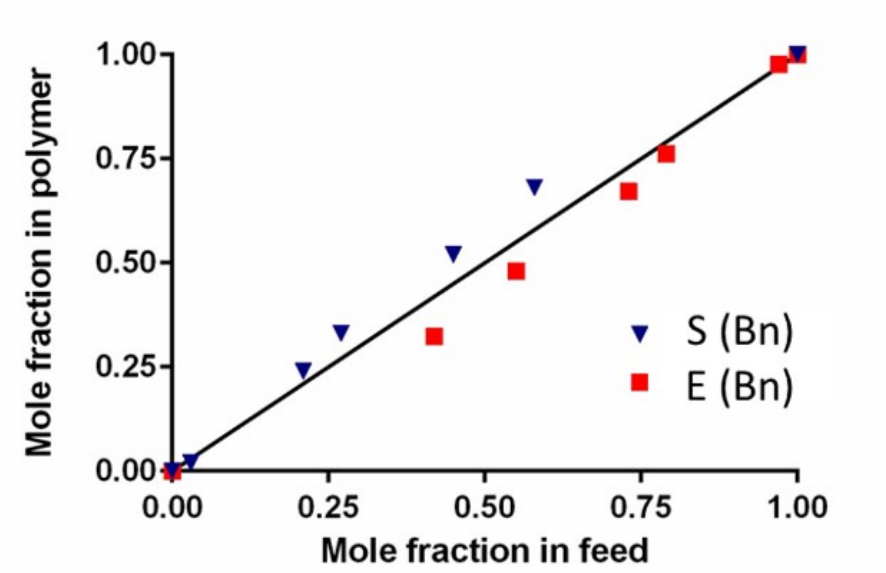


Figure 2.13: Change of the mole fraction in the feed and in the polymer as determined by NMR. The line represents the theoretical behaviour of an ideal random or alternating copolymerisation.

Figure 2.14: Copolymerisation parameters for serine (rSer) and glutamic acid (rGlu)

Method	rSer	rGlu	rSer*rGlu
Finemann-Ross	0.25 ±0.01	0.13 ±0.09	0.03±0.02
Kelen-Tüdös	0.26 ±0.01	0.01 ± 0.03	0.003 ± 0.02

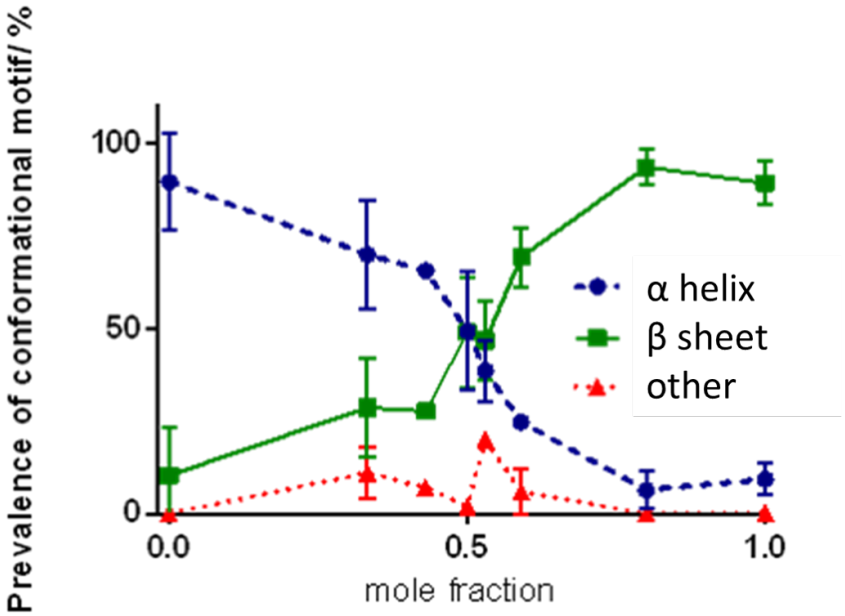


Figure 2.15: Percent of secondary structure motifs measured in solid benzyl protected polypeptides of different composition determined by FTIR.

2.4 Conclusions

Homopolymers of glutamic acid adopted α-helical conformations and (in contrast to the CD results) serine homopolymers showed β-sheet structures. Conformations adopted by both homopolymers are consistent with previous studies in the literature [81, 98]. By altering the monomer ratio in a systematic manner, we have highlighted that an increase in the serine content of a Glu(Bn)/Ser(Bn) copolypeptide directly correlates with an increasing presence of β-sheet motifs and a decrease in the α-helix content in the polymer. The latter is consistent with previous reports identifying serine as an α-helix breaker [157] Serine forms hydrogen bonds with the backbone of the α-helix, disrupting the helical structure. Here we have shown that this effect is tuneable by altering the composition of the copolypeptides which can be readily accomplished through controlling the monomer feed ratio. The preference for NCA-Ser(Bn) and NCA-Glu(Bn) to react with each other rather than themselves makes this a viable system for synthesising copolymers with the sequence S-x-x-E (the required motif for interactions with CKII).

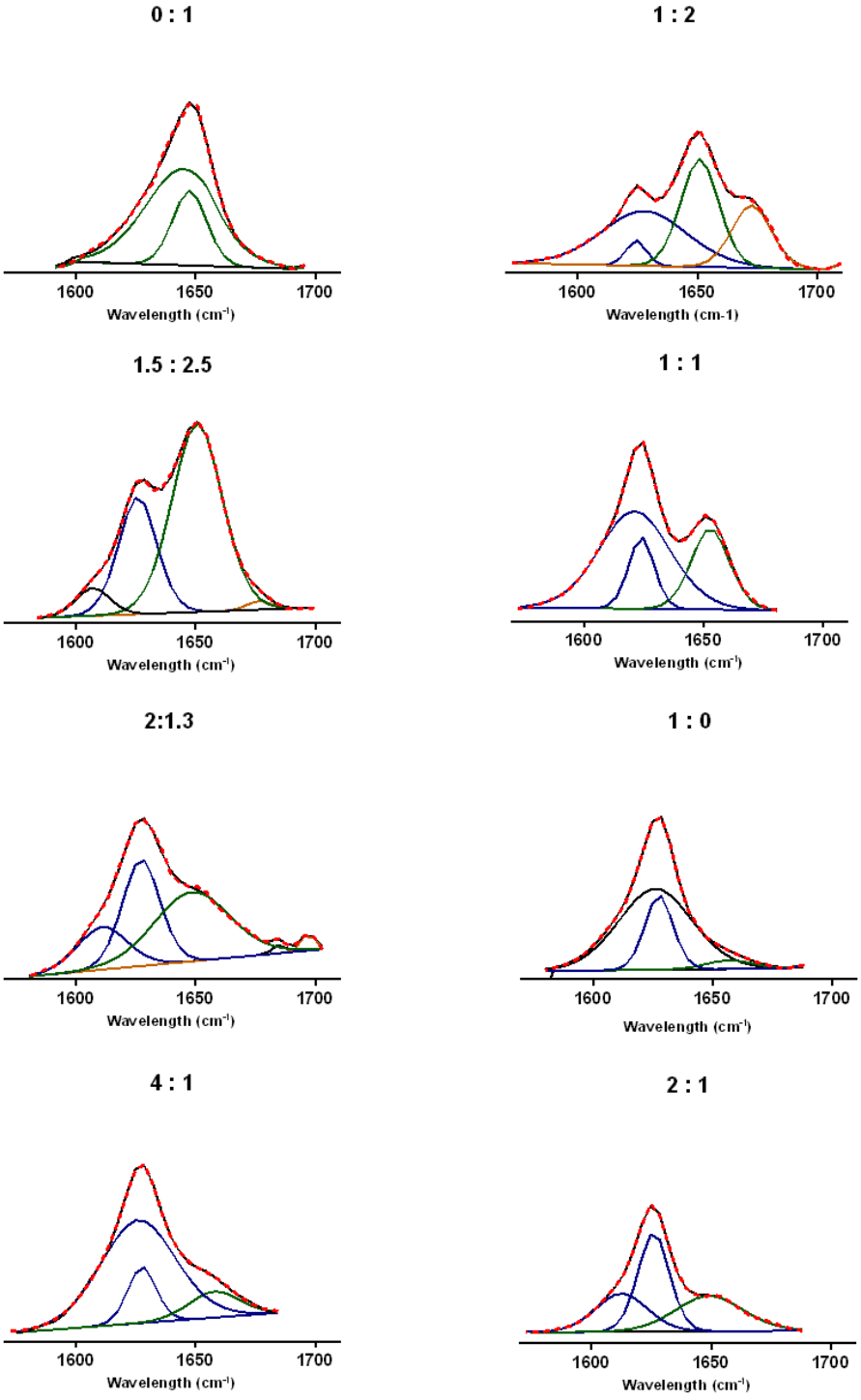


Figure 2.16: Peak fits of the amide I region in the IR spectra of the copolypeptides with varying Ser(Bn) and Glu(Bn) (S:E) content. Fitted components are β-sheets (Blue), α-helices (green) and unordered structures (orange). Measured data: black; envelope of sum of components: red.

Chapter 3

N-Carboxy anhydride ring opening polymerisation from the surface

3.1 Introduction

In the previous chapter it was established that NCA-ROP with glutamic acid and serine was well controlled by monomer feed. Furthermore, the polymerisation kinetics suggest it is likely the copolymers will have an alternating sequence, and thus have the recognition motif for CKII within. In this chapter we will discuss the translation of the solution polymerisations onto a surface and their subsequent characterisations.

3.1.1 Co-polymerisations from the surface by NCA ROP

As discussed in the opening chapter, surfaces can be modified with polypeptides via grafting from and grafting to approaches. The grafting from approach has been predominately investigated for the formation of homopolymer brushes on the surface. Examples of copolymer modified surfaces by this method are less prevalent [172]. The first block copolymer was reported by Wienger et al. from primary amine functionalised substrates in solution. They developed an AB block copolymer consisting of poly(γ-benzyl L-glutamate) (PBLG) as the A-block and poly(γ-methyl L-glutamate) (PMLG) as the B-block [173]. The brush thickness increased from 45 to 100 Å(block A) to 140-270 Å(block AB). Elemental analysis by XPS further confirmed the presence of both blocks. Patton et al. functionalised a surface with a Nickel catalyst to be used as the initiator in the synthesis of poly(N-carbobenzyloxy-L-lysine), poly(g-benzyl-L-glutamate) and poly(S-tert-butylmercapto-L-cysteine) homo and block copolymer brushes [137]. They measured low film thicknesses ($<$5 nm) for the homopolymers and on subsequent treatments with NCA-S-tert-butylmercapto-L-cysteine the thickness increased by 4.4 nm, indicating further chain growth. This was confirmed with XPS analysis and the presence of sulphur on the surface.

To our knowledge there is no polymer brush grown from the surface from NCA-Ser,

nor in the literature is there a study exploring the surface initiated polymerisation of NCA amino acids to form a random or alternating copolymer. Furthermore, the surface initiated copolymerisation of NCA-Glu and NCA-Ser has not been explored. There is a clear need to explore the area of NCA ROP from the surface to develop copolymers. This will enhance our current understanding of NCA ROP behaviour of different NCA-amino acids to form both homo and copolymers. This could have significant implications for the use of NCA ROP as a technique to modify surfaces and develop polypeptide brushes for biomedical applications.

3.1.2 Aims

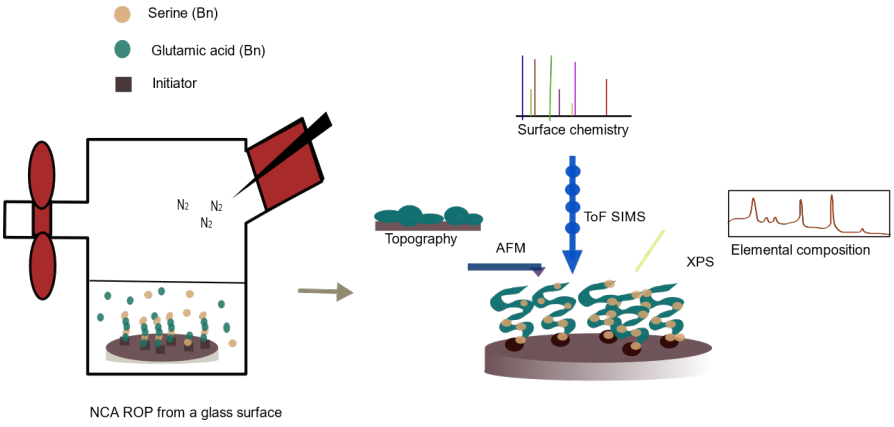


Figure 3.1: Illustration of the work carried out in this chapter; the modification of a glass surface via grafting from method with NCA-Glu and NCA-Ser and subsequent surface characterisation.

The aims of this chapter are:

• To modify planar surfaces using NCA ROP to make homo and copolymers of glutamic acid and serine tethered to the surface.

• To characterise the surface modifications using WCA (to determine wettability of the surface), ToF SIMS (to determine surface ion fragments and the homogeneity of their distribution), XPS (for surface elemental analysis) and AFM (to determine surface topography) (Figure 3.1).

Three different surface modification routes will be investigated, all using an amine as the initiator. This information is essential to determine whether the surface modification steps can effectively form copolypeptide brushes from the surface containing serine and glutamic acid. This data will be important in explaining any enzymatic interactions and any resultant surface changes in the later chapters in this work.

3.2 Methods

3.2.1 Surface silanisation

Glass surfaces were modified using aminopropyltrimethoxysilane (APTMS). 13 mm diametre glass coverslips were immersed in acetone, propan-2-ol and DMF and sonicated for 5 minutes in each solvent. Coverslips were dried with compressed air and immersed in piranha solution (1:3, hydrogen peroxide: sulphuric acid), for 30 minutes. Coverslips were washed with MilliQ water, dried and immediately incubated in a 1 % APTMS solution in toluene at room temperature for 60 minutes. Coverslips were then washed in acetone and MilliQ water, dried and stored in a vacuum desiccator for analysis and further modifications.

3.2.2 Addition of FMOC-Pentafluoro- L-phenylalanine on the surface

APTMS and PEG diamine modified surfaces were incubated in FMOC-pentafluoro-L-phenylalanine (20 mM), DIC and EHICA (2 eq.) in DMF on an orbital shaker at 20 rpm for 2 hours. The samples were washed respectively in DMF, isopropanol, methanol and DMF for 15 minutes each. This reaction was repeated and left overnight to maximise surface reactions. Samples were washed in DMF, isopropanol, methanol and DMF for 15 minutes each. A 20 % piperidine solution was prepared in dry DMF on the substrates and left for 2 hours to cleave the Fmoc group. The samples were washed respectively in DMF, isopropanol, methanol and DMF for 15 minutes each, then dried with N_2.

3.2.3 Addition of PEG-diamine

13 mm glass coverslips were cleaned in piranha solution as before. The dried coverslips were immersed in 100 % GOPTS solution and incubated for 1 hour at 37 °C. The coverslips were washed in acetone 3 times followed by the melt of PEG_{18}-diamine onto the surface at 75 °C for 2 days. The samples were washed in MilliQ water three times and blow dried under N_2.

3.2.4 Coupling of N(ϵ)-BHQ-1 FMOC Lys OH

The pegylated slides were immersed in a solution of N(ϵ)-BHQ-1 FMOC Lys OH (20 mM) with EHICA (40 mM) and DIC (40 mM) (10 mL/ 15 slides) in DMF and incubated overnight at room temperature on an orbital shaker (20 rpm). The samples were sonicated in DMF, Methanol, isopropanol and DMF (10 mins each) then dried with compressed air. Samples were FMOC deprotected using 20 % piperidine solution in DMF for 2 hours.

3.2.5 NCA ROP from the surface

Modified APTMS, pentafluoro-L-phenylalanine, PEG diamine or N-1-BHQ-Lysine functionalised surfaces were placed in an oven dried glass planar vessel (modified with a gas inlet and outlet) flushed with nitrogen, a constant flow of nitrogen was used throughout the reaction. Ratios of S:E, 0:1, 1:1 and 1:0 (0.25 mM) were dissolved in dry DMF and added into the reaction vessel on the orbital shaker (50 rpm). The reaction was monitored by periodically taking samples and monitoring the NCA carbonyl peak by FTIR. On completion, the samples were washed in DMF, acetone, and then dried, the samples were then washed overnight in HFIP to ensure complete removal of any monomer or polymer not reacted from the surface.

3.2.6 Benzyl deprotection

Coverslips with polymer on the surface were immersed in a solution of TFA:HBr (33 % in acetic acid) in a 1:3 ratio. The reaction was agitated on an orbital shaker for 4 hours at 20 rpm. Samples were removed, washed and sonicated for 15 minutes in diethyl ether, acetone and water, dried and stored in a vacuum dessicator.

3.2.7 Coupling of NHS-Fluorescein

Polymerised slides were immersed in a solution of DMF (10 mL), EHICA (20 mM), DIC (20 mM) NHS-Fluorescein (10 mM) protected from the light and allowed to react overnight at room temperature on an orbital shaker (20 rpm). Samples were washed in DMF, methanol, isopropanol and water (15 mins each), then dried and stored in a vacuum dessicator protected from light.

3.2.8 Characterisation

Attenuated transmission reflection Fourier transform infra red (ATR) (FTIR)

An IR Agilent technologies Cary 630 FTIR instrument equipped with an (ATR) was used for FTIR analysis. 32 scans were taken for each sample. Peak areas for signals at 1787 cm^{-1} (COO stretching of NCA) were obtained to monitor NCA consumption. SpectraGryph spectroscopy software was used to analyse the data.

Time of flight secondary ion spectroscopy (ToF SIMS)

An ION TOF, ToF SIMS IV instrument equipped with a Bi liquid metal ion gun (LMIG) was used to investigate the modified surfaces. A Bi_3^+ primary ion source and 25 kV were used. The beam was directed at a 45 ° angle to the sample with a beam spot of 1-2 µm in the high current bunched mode. 500 µ x 500 µm images were taken with 256 x 256 pixels, 15 scans (1 shot per pixel) as well as larger images 3 mm x 3 mm with 256 x 256 pixels, 1 scan. Positive spectra were calibrated with m/z=1 (H^+), 15 ($CH_3{}^+$) 29

($C_2H_5^+$) 43 ($C_3H_7^+$) 57 ($C_4H_9^+$). Negative spectra were calibrated with m/z=1 (H^-), 17 (OH^-) 18 (OH_2^-) 35 (Cl^-) 26 (CN^-). Spectra were normalised to total ion count and analysed using Surface lab6 software.

X-ray Photoelectron spectroscopy (XPS)

An AXIS Nova, Kratos Analytical, was used to investigate the modified surface. A Monochromatic AlK α with X-ray energy of 1486.6 eV, voltage:15 kV, current: 15 mA and power 225 W was used. 700 x 300 pm areas were analysed at zero degrees emission angle, using a pass energy of 160 eV for survey spectra with 3 sweeps and a pass 4 energy of 20 eV for high resolution regions with 10 sweeps, at 60 seconds/sweep at 3 positions per sample. XPS casa software was used to analyse the data.

Water contact angle (WCA)

A CAM200 instrument was used to measure the static water contact angle of the surfaces. Measurements were taken at room temperature, using MilliQ water 18 Ω, The instrument was set to begin recording images based on a trigger function (the trigger was a change in background colour induced by release of the droplet) were taken of the droplet with 20 frames with 1 second intervals, circle fitting was applied to the images to determine the angle of the left and right side of the droplet in relation to the perpendicular surface. The first three data points were omitted and linear regression was used to determine the WCA at time = 0. For each condition, four measurements were taken on each sample.

Atomic force microscopy (AFM)

Topography on the surfaces was determined using AFM. The modified cover glass were imaged using a Bruker Dimension Icon atomic force microscope in tapping mode (75 kHz, spring constant 3 N/m, scan rate: 1 Hz). Images were analysed using NanoScope Analysis 1.5. Four images of 1 x 1 µm were taken per sample. Data found in Appendix B (Figure **??**).

3.2.9 Analysis software

Spectraglyph

FTIR spectra were imported into Spectraglyph software version 1.0.2. The spectra were baseline corrected and normalised to the peak at 1730 cm^{-1}.

XPS casa

XPS casa software version 2318PR1-0 was used to analyse all XPS data. CasaXPS.lib file was imported for sensitivity factors. Survey scan spectra were normalised to C1s peak at 284.8 eV. Narrow scan were normalised to the following: N1s - 400 eV , C1s -

284.8 eV and O1s - 532 eV. Peak fitting was used on narrow scan spectrum and peak restrictions found in Table 3.1 and Table 3.2.

Table 3.1: Position constraints (binding energy shifts with respect to the C-C / C-H component) imposed when fitting components to the C1s high resolution spectra for PEG NH_2 initiated polymers.

Sample	(C=O)N	(C=O)O
PEG-NH_2	+ 3.5	-
Pentafluoro-L-phenylalanine	+ 3.5	-
S(Bn):E(Bn) 1:1	+ 3.22	+ 4
S:E 1:1	+ 3.22	+ 4

Table 3.2: Position constraints (binding energy shifts with respect to the C-C / C-H component) imposed when fitting components to the C1s high resolution spectra for BHQ-1-Lysine initiated polymers.

Sample	(C=O)N	(C=O)O
PEG-NH_2	+ 3.5	-
Pentafluoro-L-phenylalanine	+ 3.5	-
BHQ-Lysine	-	-
S(Bn):E(Bn) 1:1	+ 2.91	+ 3.99
S:E 1:1	-	+ 4.11
S(Bn):E(Bn) 0:1	-	+ 4.11
S:E 0:1	-	+ 4.11
S(Bn):E(Bn) 0:1	-	-
S:E 0:1	-	+ 3.99

Nanoscope analysis

Nanoscope analysis version 1.5 software was used to analyse all AFM images. Images were flattened, and scale bar set to zero. Both Rq and Ra values were calculated by the software.

ToF SIMS software

Instrument analysis software was used to assign peaks in the mass spectrum to a maximum standard deviation of fit 100 ppm. Region of interest images were generated by the software and the scale was optimised for each ion assignment. All spectra were normalised to total ion count. The 3 x 3 mm areas were split into four and each quadrant

Table 3.3: Water contact angle values (n=5) of modified substrates. One Way ANOVA between protected and deprotected surfaces of the same type shown.

	WCA/ degree
APTMS	65.3 ±1.5
1:1 S(Bn):E(Bn)	82.4 ±1.5
1:1 S:E	75.4 ±1.3 [a]

[a] P<0.005 **

was analysed to obtain an average and standard deviation for the distribution of the assigned mass fragments.

3.3 Results and Discussion

3.3.1 NCA-ROP from amine functionalised surfaces

The grafting from method was adopted to modify the surfaces with the copolymer of serine and glutamic acid, therefore it was necessary to introduce an amine onto the surface to initiate the polymerisation. This can be achieved by silanisation which facilely enables the introduction of different functionalities onto the surface dependent on the choice of silane. Amino propyl trimethoxy silane (APTMS) has a terminal amine group and a short hydrocarbon connecting the amine to the trimethyl silane. Firstly glass coverslips were treated with piranha solution to remove organic material on the surface, followed by APTMS. Subsequently the surfaces were incubated with a 1:1 ratio of glutamic acid to serine to make copolymer modified surfaces.

Water contact angle measured 24 hours after silanisation to ensure surface was completely dry. WCA's increased significantly and consistently from <15 ° for piranha cleaned slides to 65.3 ° for silanised slides (Table 3.3). The WCA of the surface had increased significantly (P<0.00005 ****) after incubation with S and E for the copolymer surfaces indicating a change in the surface chemistry. The hydrophobic benzyl side chain protecting group is likely a big contributor to this increase. The copolymer modified surfaces underwent a significant reduction in WCAs after incubation in TFA: HBr indicating the benzyl protecting group had been successfully hydrolysed from the substrate.

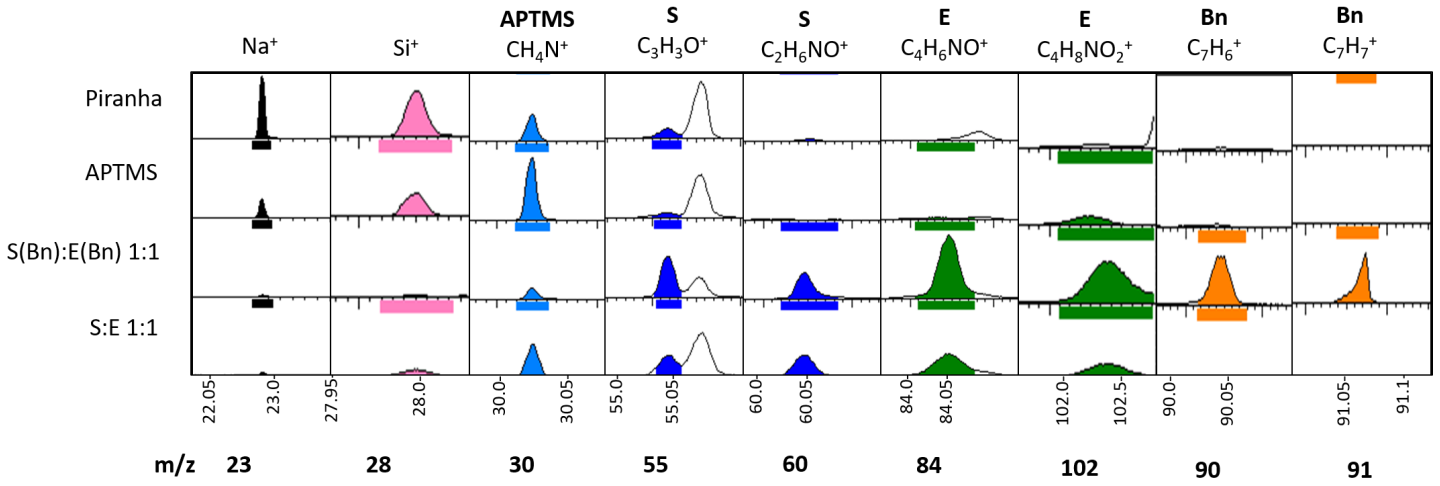


Figure 3.2: ToF SIMS spectra of fragment intensities inidicative of APTMS:light blue (CH_4N^+), Serine: dark blue ($C_3H_3O_3^+$, $C_2H_6NO^+$), Glutamic acid: green ($C_4H_6NO^+$, $C_4H_8NO_2^+$) and Benzyl protecting group ($C_7H_6^+$, $C_7H_7^+$)normalised to total ion count

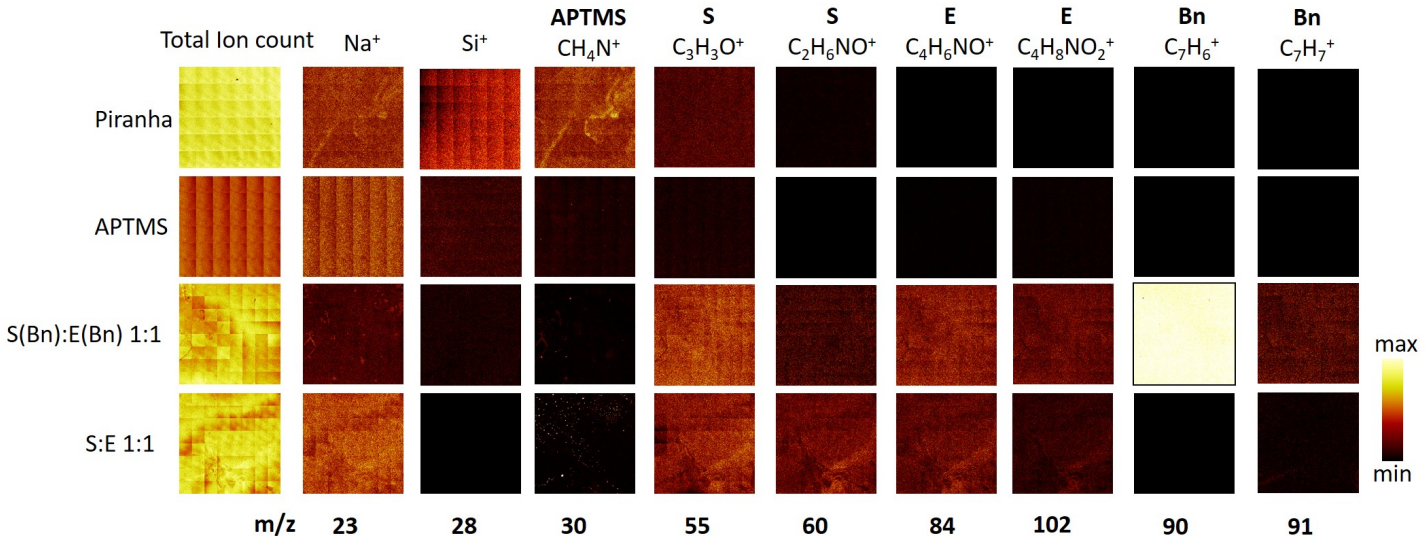


Figure 3.3: ToF SIMS Raster images of fragment intensities inidicative of APTMS:light blue (CH_4N^+), Serine: dark blue ($C_3H_3O_3^+$, $C_2H_6NO^+$), Glutamic acid: green ($C_4H_6NO^+$, $C_4H_8NO_2^+$) and Benzyl protecting group ($C_7H_6^+$, $C_7H_7^+$) normalised to total ion count in a 3x3 mm area.

ToF SIMS analysis

Surfaces were analysed by ToF SIMS at each modification step to provide information on the chemical structures present on the surface. The spectra is found in Figure 3.2. ToF SIMS spectra for the piranha cleaned slide has strong Si^+ and Na^+ ion peaks which are components of the glass coverslips. There is a reduction in intensity of these peaks after silanisation with APTMS, this is coupled with an increase in the intensity of $CH_4{}^+$ ion. This indicates the glass is being covered limiting the exposure to the primary ion beam.

Different amino acids have different chemical structures therefore can be detected with ToF SIMS by their signature ion fragments that can be detected when present on a surface. This enables the assignment of signature fragments to certain amino acids [174]. Incubation with Serine NCA and Glutamic acid-NCA has resulted in samples with ion fragments indicative of the amino acids on the surface that weren't present on the silanised sample. Firstly, fragments attributed to serine are present on the surface; m/z 55 and 60. Indicative fragments for glutamic acid are present on the samples at m/z 84 and 102. The Copolymer presents strong peaks at m/z 90 and 91, highly indicative of a benzyl group, which further proves the presence of the protected amino acids on the surface.

After treatment with TFA:HBr there is an almost complete loss of the ions assigned to the benzyl protecting groups m/z 90 and 91 (ion counts insignificantly different to the piranha cleaned sample) indicating that full deprotection has occured on top of the copolymer sample surface. The ions for the amino acids are still present after deprotection, indicating the harsh conditions have not cleaved the peptide from the surface. There is however an observable reduction in the ion intensity of Glutamic acid in the case of the copolymer. This reduction could be explained by sample to sample variation, however it is important to be cautious with such conclusions with a non quantitative technique.

The Raster images (Figure 3.3) provide information on the homogeneity of the ion distribution across the surface. Distribution of the fragments corresponding to serine and glutamic acid are predominantly homogenous indicating an even polymerisation across the sample area of 3×3 mm. Therefore we can conclude that grafting from is an effective method to modify the surface using NCA ROP with NCA glutamic acid and NCA serine to make chemically homogenous surfaces.

Polymerising from APTMS functionalised slides was effective method to prepare slides that contain both serine and glutamic acid by NCA-ROP from the surface.

3.3.2 NCA ROP initiated from PEG-amine functionalised surface

The overall aim of this work is to have interactions between enzymes and the polymers modified on the substrates. It is necessary for the polypeptide motif to be available

for the enzyme to have access to modify the polypeptide. Steric hindrance effects from the polymer being tethered close in proximity to the surface could hinder the enzymes ability to reach the polymer. It is also possible the density of amines was too high on the surface for either successful polymerisation or this high density of initiator resulted in high density of polypeptides restricting enzyme access to the polypeptide [175]. Enzymatic phosphorylation and dephosphorylation was attempted and was unsuccessful on the APTMS initiated samples this will be discussed in detail in the next chapter. Therefore an alternate grafting from sequence was adopted whereby a chain linker was built into the surface which ensures the polymer is positioned further away from the surface thus reducing steric hindrance effects to the enzyme. Samples were prepared with the insertion of an 18 chain PEG molecule before the polymerisation.

The original surface modification scheme was adapted to enable the introduction of the PEG linker molecule (Figure 3.5). After piranha cleaning the samples were silanised in GOPTS to introduce an epoxy group to react with an amine at the terminus of the PEG chain at 75 °C. The second amine will be available to initiate the polymerisation. Polymerisation was followed by FTIR and the polymerisation was completed by 16 hours corresponding to the consumption of NCA's by the reduction of C=O at 1750 cm^{-1} (Figure 3.4). Not all NCA-monomer is consumed in the reaction, comparable to the APTMS initiated polymerisations, indicating there is a limitation to the polypeptide chain length that can be achieved. This could be attributed to the formation of chemically or 'physically' dead chain ends or due to steric hindrance preventing the subsequent addition of NCA monomers. When both AMM and NAM are contributing to the reaction progress, it has been reported that any unbound polymer prevents further growth as observed in the study of poly-L-glutamate synthesised from the respective NCA. After no more NCA consumption was observed the substrates were thoroughly washed and submerged in a fresh monomer solution, a further increase was observed in polymer film thickness, indicating the end groups were still active [176].

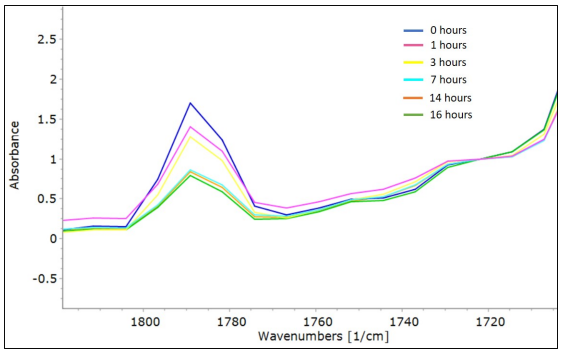


Figure 3.4: Monitoring of NCA consumption with FTIR looking at the reduction in the carbonyl peak 1750 cm^{-1} over time (0 to 16 hours) of the NCA-ROP of S(Bn):E(Bn) 1:1 from a PEG-amine functionalised surface

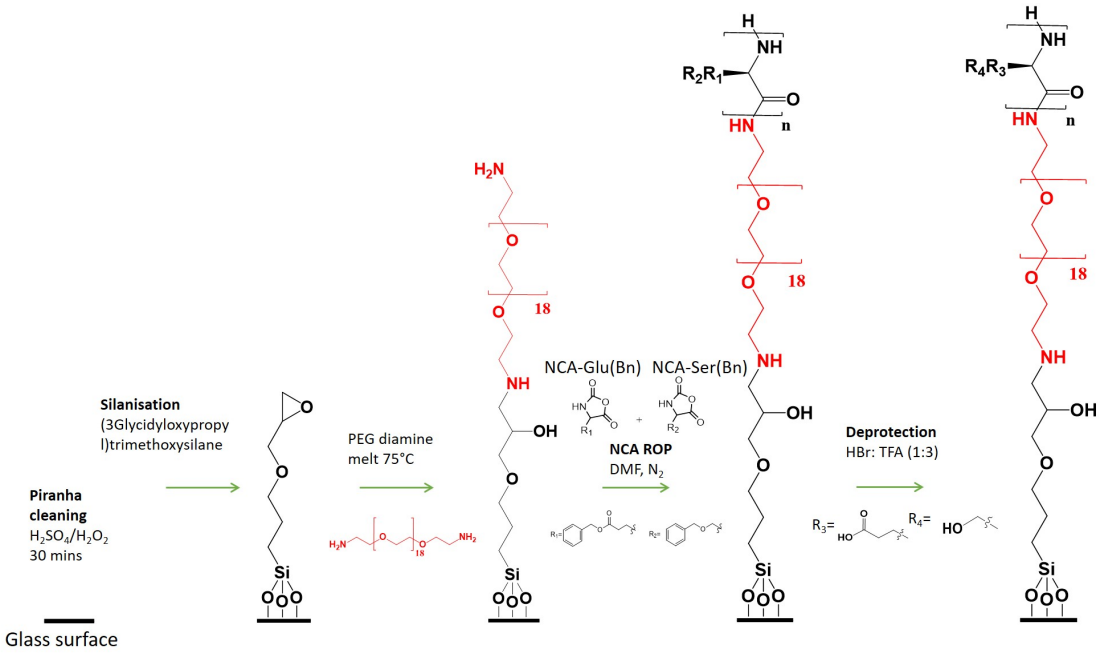


Figure 3.5: Scheme of surface modification to include PEG_18 linker chain between the surface and the polypeptide chain

The reaction steps were followed with Water contact angle analysis (Table 3.4).

Table 3.4: Water contact angle values (n=5) of modified substrates initiated from PEG diamine. One way ANOVA multiple comparison. Significant values reported for benzyl protected S(Bn):E(Bn) vs. deprotected S:E of the same surface type

	WCA/ degree
Piranha	<15
GOPTS	43.1 ±1.2
PEG-NH_2	28.3 ±2.2
1:1 S(Bn):E(Bn)	82.4 ±1.3
1:1 S:E	65.0 ±3.8 [a]

[a] P<0.0005 ***

There was an increase in hydrophobicity on the surface after silanisation followed by a significant drop on the introduction of the highly hydrophillic PEG linker chain. A significant WCA increase was observed as a result of the polymerisation indicating the presence of the polymer chain on the surface with hydrophobic benzyl protecting groups comparable to APTMS polymerised samples. As the TFA:HBr deprotection step was successful previously on the surface it was adopted for these substrates. A significant reduction in the WCA was observed after acid hydrolysis.

ToF SIMS was used to analyse the substrates to obtain further information of the chemistry on the surface. No ions specific for GOPTS were detected and therefore it has not been included in this characterisation. The success of PEG diamine melt is clear from the presence of the fragments $C_2H_5O^+$ and CH_3O^+. There is a reduction in the intensity of these ions after NCA ROP with S(Bn) and E(Bn) indicating the PEG has been coated with polymer.

Ion intensities allocated to fragments $C_2H_6NO^+$ and $C_3H_3O_2^+$ indicative of serine and ion fragments $C_4H_2NO_2^+$ and $C_4H_8NO_2{}^+$ indicative of Glutamic acid are present on the surface. The ion fragment at m/z 91 has high intensity for the protected samples, as observed for the APTMS polymerised samples this peak is absent after treatment with TFA: HBr confirming full benzyl deprotection of the polymers. Contrary to APTMS polymerised substrates the intensity of the fragments for S and E after deprotection are similar or increase compared to before acid hydrolysis.

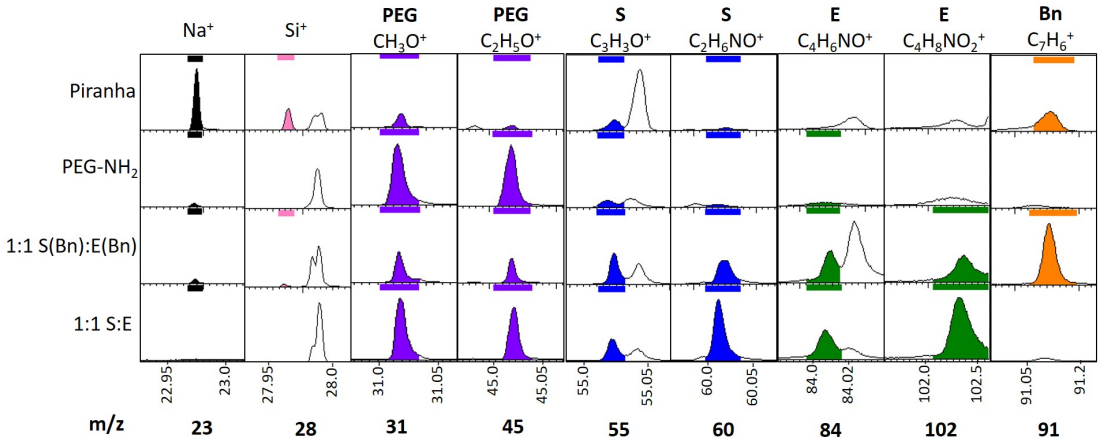


Figure 3.6: ToF SIMS spectra of fragment intensities inidicative of PEG: purple (CH_3O^+, $C_2H_5O^+$), Serine: dark blue ($C_3H_3O_3^+$, $C_2H_6NO^+$), Glutamic acid: green ($C_4H_6NO^+$, $C_4H_8NO_2^+$) and Benzyl protecting group ($C_7H_7^+$)normalised to total ion count.

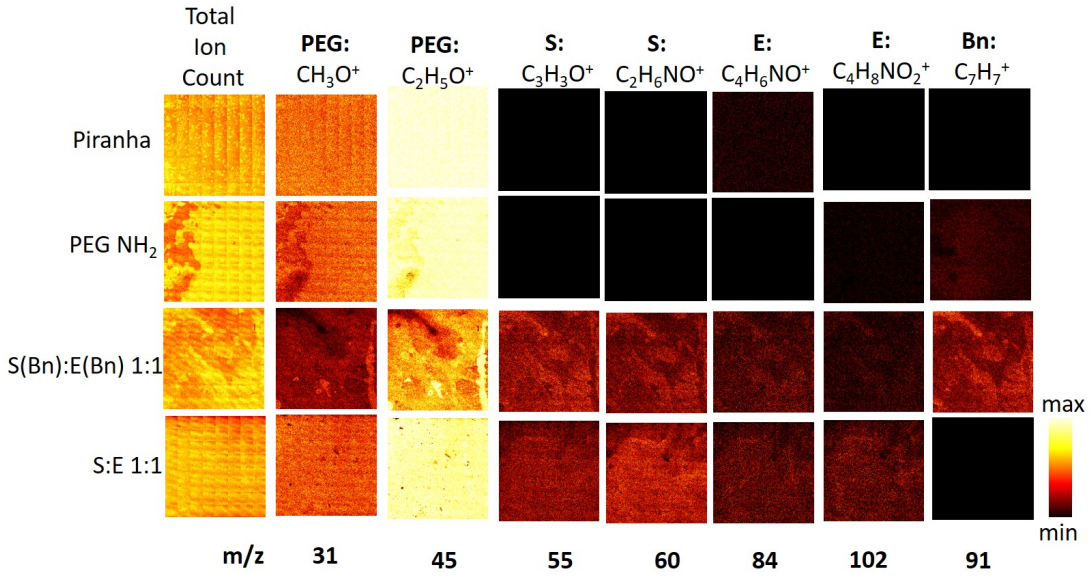


Figure 3.7: ToF SIMS Raster images of assigned fragments indicative of PEG: (CH_3O^+, $C_2H_5O^+$), Serine:($C_3H_3O_3^+$, $C_2H_6NO^+$), Glutamic acid:($C_4H_6NO^+$, $C_4H_8NO_2^+$) and Benzyl protecting group ($C_7H_7^+$) normalised to total ion count.

Table 3.5 contains the ion intensities normalised to total ion count attributed to spectra in Figure 3.6. Each 3 × 3 mm image has been split in four and the average ion count in each quadrant calculated. It is also worth noting that the ion count of ion fragments assigned to PEG reduce greatly after polymerisation then increase to values close to those of the Pegylated samples after deprotection. The increase in PEG ions is not coupled with a decrease in the ion count of fragments associated with serine and glutamic acid, so cannot be explained by loss of polymer on the surface. ToF SIMS data does not provide information on the orientation or conformation of the polymers it is likely that loss of the deprotecting group infers a conformational change which in turn may effect the orientation of the polymer chains on the surface exposing the underlying PEG.

Table 3.5: Average ion count for the assigned ion fragments as determined by ToF SIMS (n=4) 1.5 x 1.5 mm areas, normalised to total ion count for PEG diamine initiated surfaces with NCA ROP of 1:1 S:E monomer feed ratio.

Ion fragment	PEG-NH_2	S(Bn):E(Bn)	S:E
CH_3O^+	$4.63*10^{-2}$ $\pm 1.00*10^{-3}$	$1.94*10^{-2}$ $\pm 7.00*10^{-3}$	$4.33*10^{-2}$ $\pm 8.00*10^{-4}$
$C_2H_5O^+$	$2.65*10^{-1}$ $\pm 1.00*10^{-2}$	$8.89*10^{-2}$ $\pm 18.00*10^{-4}$	$2.13*10^{-1}$ $\pm 3.00*10^{-3}$
$C_3H_3O^+$	0	$1.45*10^{-2}$ $\pm 6.00*10^{-3}$	$1.03*10^{-2}$ $\pm 5.00*10^{-3}$
$C_2H_6NO^+$	0	$1.14*10^{-2}$ $\pm 6.00*10^{-3}$	$1.83*10^{-2}$ $\pm 4.00*10^{-3}$
$C_4H_6NO^+$	$1.15*10^{-3}$ $\pm 4.00*10^{-3}$	$4.49*10^{-2}$ $\pm 6.00*10^{-4}$	$4.18*10^{-3}$ $\pm 8.00*10^{-4}$
$C_4H_8NO_2^+$	0	$2.43*10^{-3}$ $\pm 8.00*10^{-4}$	$4.29*10^{-3}$ $\pm 8.00*10^{-4}$
$C_7H_7^+$	$2.83*10^{-4}$ $\pm 3.40*10^{-5}$	$1.64*10^{-2}$ $\pm 8.00*10^{-4}$	$6.83*10^{-4}$ $\pm 8.42*10^{-5}$

The Raster images of ion distribution on the surface of the PEG coated and copolymer coated surfaces indicate they are inhomogeneous. In this case inhomogeneities are introduced by the PEG linker chain this in turn introduces inhomogeneities on subsequent samples, leading to non-homogenous polymer distribution. This can introduce topographical features as well as areas of high and low polypeptide density both of which have been shown in other systems to affect cell behaviour. This is less apparent on the deprotected samples (Figure 3.7).

3.3.3 Comparison of surfaces within and between batches of samples

To determine the reproducibility of NCA ROP from the pegylated surface samples within the same batch are compared with each other aswell as between batches. Firstly the samples within the same batch are compared using ToF SIMS. The spectra in Figure 3.8 show the ion intensities of the ion fragments on the surface, the ions attributed to PEG, serine and glutamic acid are present on all samples. The distribution of those ions is even across the surface as seen in Figure 3.9.

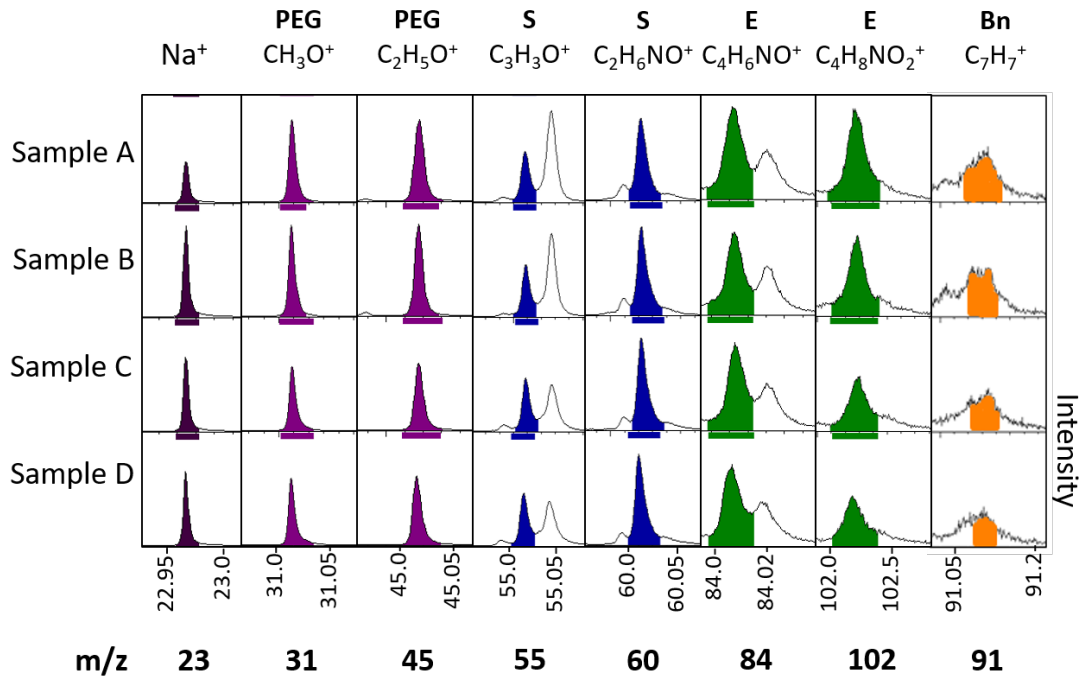


Figure 3.8: ToF SIMS spectra of fragment intensities inidicative of Sodium: dark purple (Na^+), Silicon: pink (Si^+), PEG: purple (CH_3O^+, $C_2H_5O^+$), Serine: dark blue ($C_3H_3O_3^+$, $C_2H_6NO^+$), Glutamic acid: green ($C_4H_6NO^+$, $C_4H_8NO_2^+$) and Benzyl protecting group ($C_7H_7^+$)normalised to total ion count of four samples made in the same batch.

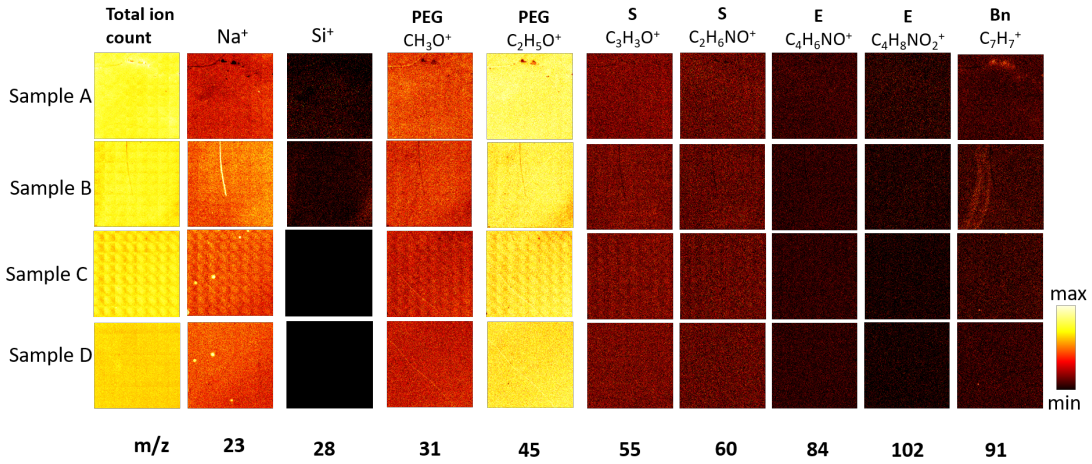


Figure 3.9: ToF SIMS Raster images of assigned fragments inidicative of sodium (Na^+), silicon (Si^+), PEG: (CH_3O^+, $C_2H_5O^+$), Serine:($C_3H_3O_3^+$, $C_2H_6NO^+$), Glutamic acid:($C_4H_6NO^+$, $C_4H_8NO_2^+$) and Benzyl protecting group ($C_7H_7^+$) normalised to total ion count of four samples made in the same batch.

Samples were prepared and analysed from 4 different batches. The relative ion distributions can be found in figure 3.10. Ions attributed to PEG, glutamic acid and serine are present on all four surfaces. The intensity of the ions does vary between samples, notably the amount of $C_2H_6NO^+$ ion is different between the samples, this is also apparent for the two ions attributed to glutamic acid. The distribution of the ions attributed to serine and glutamic acid is predominantly homogeneous in three of the four samples with the fourth sample displaying some inhomogeneities and hot spots. Furthermore the silicon and PEG distribution is not homogenous across all samples as shown in figure 3.11. The ion intensity values can be found in Table 3.6, the differences in the average ion counts between samples in the same batch vs different batches is not significant, however the samples prepared in different batches do have larger errors associated with them indicating greater variance between these samples.

Therefore the samples prepared within the same batch can be expected to be homogenous with respect to intensity and ion distribution across the surface. It can be deemed based on the variations seen between the samples prepared in different batches with respect to ion intensity and surface distribution that the surface modification process does not produce fully reproducible samples. However, it does enable the modification of all samples with the two amino acids of interest, serine and glutamic acid. These results are an important consideration in future work when looking at enzyme interactions with the surfaces.

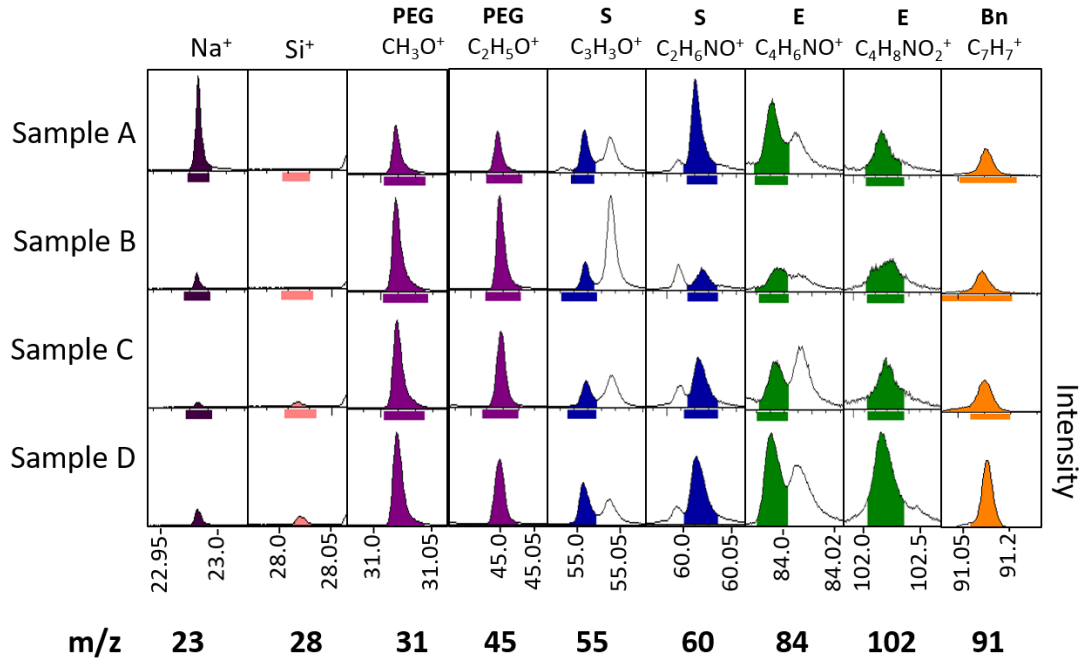


Figure 3.10: ToF SIMS spectra of fragment intensities inidicative of Sodium: dark purple (Na^+), Silicon: pink (Si^+), PEG: purple (CH_3O^+, $C_2H_5O^+$), Serine: dark blue ($C_3H_3O_3^+$, $C_2H_6NO^+$), Glutamic acid: green ($C_4H_6NO^+$, $C_4H_8NO_2^+$) and Benzyl protecting group ($C_7H_7^+$)normalised to total ion count of four samples made in four different batches.

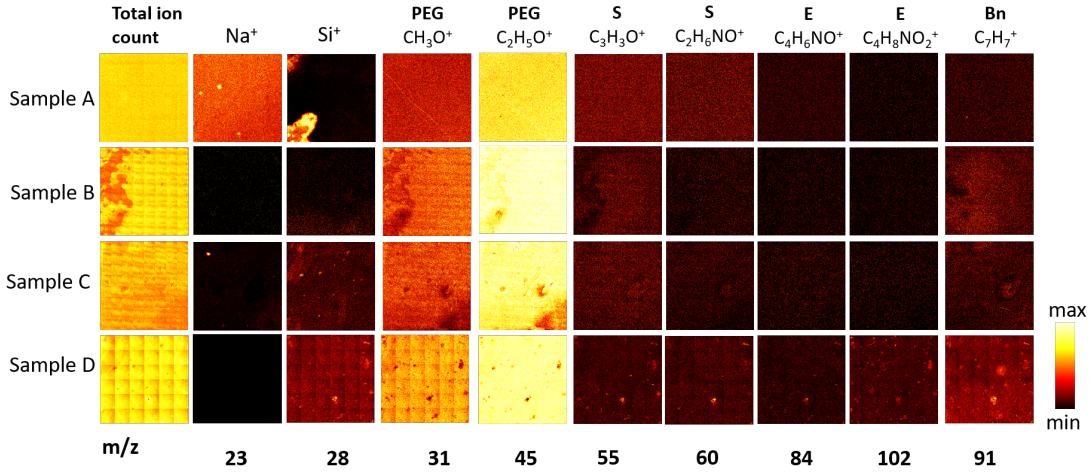


Figure 3.11: ToF SIMS Raster images of assigned fragments inidicative of sodium (Na^+), silicon (Si^+), PEG: (CH_3O^+, $C_2H_5O^+$), Serine:($C_3H_3O_3^+$, $C_2H_6NO^+$), Glutamic acid:($C_4H_6NO^+$, $C_4H_8NO_2^+$) and Benzyl protecting group ($C_7H_7^+$) normalised to total ion count of four samples made in four different batches.

Table 3.6: Average ion count for the assigned ion fragments, 1.5 x 1.5 mm areas, normalised to total ion count for PEG diamine initiated surfaces with NCA ROP with serine and glutamic acid in a 1 to 1 ratio. Samples within and between batches were analysed. (n=4)

Ion fragment	Same batch	Between batches
Na^+	$4.13*10^{-2}$ $\pm 9.62*10^{-3}$	$6.29*10^{-3}$ $\pm 2.28*10^{-3}$
Si^+	$7.63*10^{-4}$ $\pm 3.06*10^{-4}$	$1.23*10^{-3}$ $\pm 7.46*10^{-4}$
CH_3O^+	$2.40*10^{-2}$ $\pm 2.18*10^{-3}$	$4.08*10^{-2}$ $\pm 7.97*10^{-4}$
$C_2H_5O^+$	$1.13*10^{-1}$ $\pm 1.06*10^{-2}$	$1.93*10^{-1}$ $\pm 1.92*10^{-2}$
$C_3H_3O^+$	$7.52*10^{-3}$ $\pm 2.61*10^{-4}$	$6.12*10^{-3}$ $\pm 1.68*10^{-3}$
$C_2H_6NO^+$	$4.40*10^{-3}$ $\pm 2.06*10^{-4}$	$2.86*10^{-3}$ $\pm 1.13*10^{-3}$
$C_4H_6NO^+$	$2.39*10^{-3}$ $\pm 1.14*10^{-4}$	$1.90*10^{-3}$ $\pm 8.55*10^{-4}$
$C_4H_8NO_2^+$	$8.56*10^{-4}$ $\pm 1.84*10^{-4}$	$1.06*10^{-3}$ $\pm 3.84*10^{-4}$
$C_7H_7^+$	$2.48*10^{-3}$ $\pm 3.02*10^{-4}$	$4.76*10^{-3}$ $\pm 3.84*10^{-4}$

The information obtained from ToF SIMS analysis informs us of the presence and distribution of the ions on the surface however it does not give an indication of any quantitative data, including chain length and ration of amino acids on the surface, therefore a more quantitative method is required to compliment ToF SIMS information. For this the samples have been analysed by XPS.

In solution polymer chain length can be determined using GPC and NMR, however those methods are not possible whilst the polymers are tethered to the surface. Therefore we developed a method to determine our polymer chain length using XPS. XPS provides individual elemental information relative to the other elements present. The introduction of an element not present in the polymer chain, in a known quantity (relative to the number of polymerisation initiating amine groups on the surface) enables the amount of the elements in the polymer chain to be determined in reference to the known element. In this case the unique marker element will be Fluorine and it will be introduced by the inclusion of a Fmoc-Pentafluoro-L-phenylalanine onto the surface (Figure 3.13).

Wide and narrow scan spectra were obtained for the modified substrates at each modification step.

XPS characterisation of the modified substrates shown in Figure 3.12, wide scan spectra show contributions from C1s, N1s and O1s in all samples. The relative intensities of the elements varies between samples. Notably, there is an increase in contribution from C1s observed from GOPTS to PEG modification attributed to the repeat unit (C_2H_4O) in the 18 chain PEG. The N1s contribution increases for the polymerised samples attributed to the presence of amides in the polypeptide backbone. A more detailed breakdown of the ratios of contributions of the elements can be found in table 3.7

F1s is present on the surface after the DIC coupling modification step indicating it is present because of this modification step and it is not inherently present on the substrates so can be used for subsequent determination of polymer chain length. It is possible the

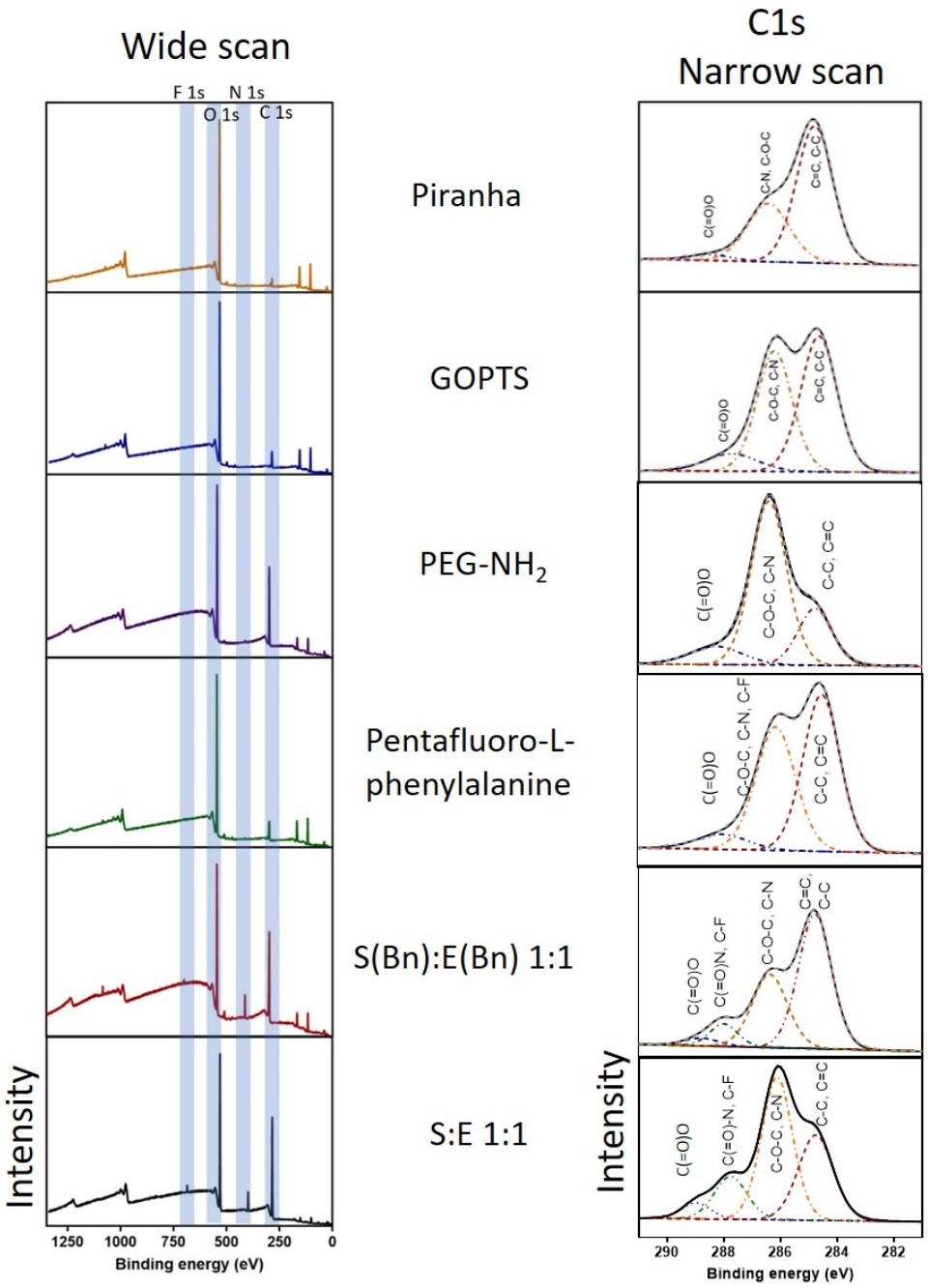


Figure 3.12: XPS spectra of surfaces modified with GOPTS, PEG diamine, Pentafluoro-L-phenylalanine to which NCA ROP was initiated with a theoretical feed ration of S:E 1:1 Left: Wide scan with fitted peaks and envelope (grey), fit (black dash) and Right: narrow scan of C1s of samples at each modification step

Table 3.7: Elemental composition of modified surfaces as determined by XPS.

	% C	N	O	Si	F	Sum of rest*
GOPTS	16.5 ±3.6	0.3 ±0.0	52.0 ±3.5	25.7 ±2.1	0.0 ±0.0	5.5 ±2.0
PEG-NH_2	40.0 ±8.2	1.2 ±0.2	41.8 ±3.7	15.0 ±3.5	0.0 ±0.0	2.0 ±0.9
Pentafluoro-L-phenylalanine	23.9 ±6.2	0.8 ±0.1	47.4 ±3.6	24.0 ±2.6	0.4 ±0.2	3.4 ±0.7
1:1 S(Bn):E(Bn)	43.8 ±3.7	4.1 ±0.2	27.0 ±2.0	10.3 ±1.5	0.2 ±0.1	14.6 ±1.8
1:1 S:E	52.8 ±9.4	4.5 ±1.7	34.3 ±5.7	7.5 ±5.2	0.5 ±0.2	0.3 ±0.3

* Mg, Zn, Ti, K, Na

TFA:HBr deprotection step can introduce fluorine on the surface if the samples were not effectively washed. A CF_3 signal is very distinguishable at 291 eV in a high resolution C1s spectra. This signal is not observed in these samples therefore the F signal can be attributed to the pentafluoro-L-phenylalanine coupled to the surface.

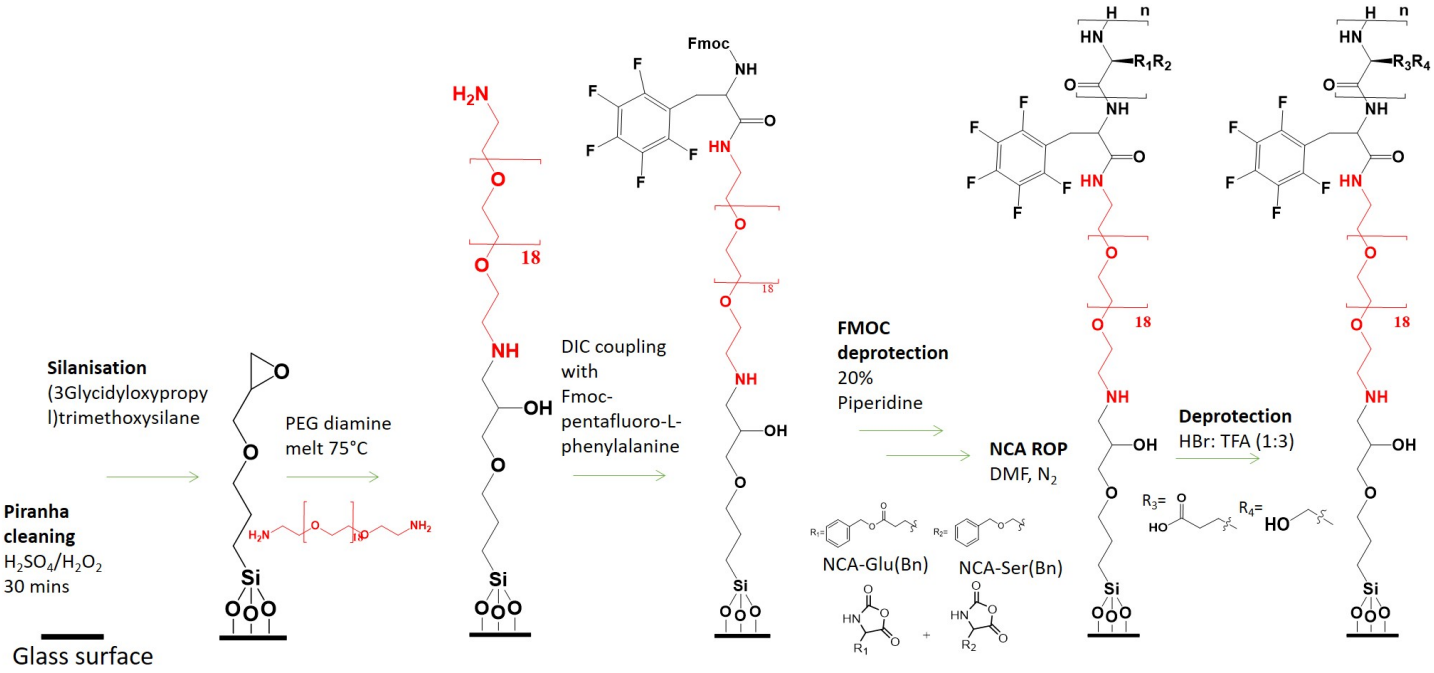


Figure 3.13: Scheme of surface modification with Fmoc-pentafluoro-L-phenylalanine coupled to the PEG_{18} linker chain.

Table 3.8: Chain length of polymer on the surface as calculated using the ratio of elemental count of N1s to F1s for the protected and deprotected polymers as determined by XPS (n=3). The ion count is data under the curve and they have been normalised to sensitivity factors

S(Bn):E(Bn) 1:1 (N/(F/5))-3	S:E 1:1 (N/(F/5))-3
81.0 ±14.0	43.7 ± 13.6

The ion intensities for F1s was divided by the number of fluorines present per polymer chain, in this case five contributed from the pentafluoro-L-phenylalanine. The contribution of N1s per amino acid is one (from the amide). The ratio of the intensity of F1s/5 to N1s, with the subtraction of the three nitrogen's present externally of the polymer chain, enables the average polymer chain length on the surface to be determined Table 3.8. The chain length for the protected polymers is 81.0 ± 14.0 this is reduced by almost half for the deprotected samples to 43.7 ± 13.6. This could indicate a loss in chain length as a result of the TFA:HBr treatment. However the contribution of carbon and nitrogen does not decrease therefore this can't be the case. Sampling depth is limited by the attenuation of the emerging photoelectrons from the surface, meaning the intensity of the photoelectrons is dampened as a function of the depth into the solid. The orientation or conformation of the polymer chain on the surface therefore can alter the depth of penetration to the surface. The loss of the benzyl protecting group in other systems has been shown to alter polypetide conformation, due to the change in hydrophobicity thus may effect the depth. This is consistent with the ToF SIMS data whereby the PEG signal increases after benzyl deprotection. To investigate the change in conformation the modifications were carried out of silicon wafers and ATR-FTIR was ran however the signal was not sufficient of the amide peak to obtain any reliable data and to make any reasonable conclusions.

The narrow scan spectra for the C1s peak can be deconvoluted using XPS casa software to determine the environment of the C1s electrons, which provides information on their neighbouring atoms. The assignments are in Figure 3.12. The GOPTS substrate has an increase in the bond contribution of C-O-C/C-N, attributed to the epoxy functionality. The PEG linker substrate has a decrease in C=C/C-C and an increase in C-N/C-O-C bond contribution, attributed to the amine and the PEG repeating unit. The addition of Pentafluoro-L-phenylalanine molecule increases the contribution of C(=O)N/C(=O)O/C-F as well as C=C/C-C. The increase in the carbonyl groups indicates there is remaining Fmoc on the surface after deprotection. S(Bn):E(Bn) 1:1 substrate has an increase in the contribution of C=C/C-C bond attributed to the introduction of the benzyl protecting group. There is also a distinguishable peak at 288 eV attributed to the amide bonds on the polymer backbone. After treatment with TFA:HBr there is a reduction in the contribution of C=C/C-C bond attributed to the loss in the

Table 3.9: Experimental percentage contributions of the different C environments at each modification step as determined by XPS (n=3)

%	C-C/C=C	C-N/C-O-C	C(=O)N / C-F	C(=O)O
GOPTS	55.6 ± 5.8	36.6 ± 6.6	0.0	7.6 ± 1.1
PEG NH_2	29.2 ± 6.7	64.8 ± 5.9	0.0	2.9 ± 2.5
Pentafluoro-L-phenylalanine	47.7 ± 8.0	47.0 ± 9.8	0.0	4.1 ± 1.9
1:1 S(Bn):E(Bn)	53.5 ±1.9	34.4 ± 1.5	7.5 ± 2.4	4.6 ± 2.5
1:1 S:E	29.7 ± 3.9	53.9 ± 4.8	10.9 ± 0.7	5.4 ± 5.4

benzyl protecting group indicating successful deprotection. Detailed contributions can be seen in Table 3.9.

3.3.4 Incorporation of FRET pair (fluorophore and quencher) on the surface

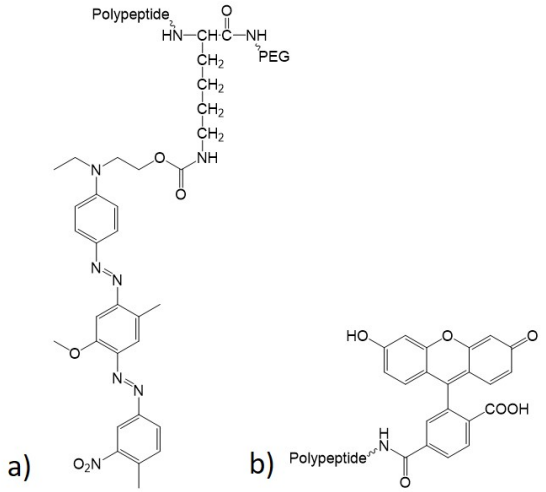


Figure 3.14: Chemical structure of a) Black hole quencher-1-Lysine and b) Fluorescein covalently bound to the base and end of the polypeptide chain

The aim of this work was to be able to monitor conformational changes on the polypeptide indirectly but in situ with a non destructive optical approach. To achieve this a FRET system was adopted whereby a Fluorophor quencher pair is used within the system 3.14. The FRET system will be further discussed in chapter 3, herein the modification and characterisation of the surface will be discussed. The quencher will be covalently attached to the free amine on the terminus of the PEG and the Fluorophor coupled to the free amine at the terminus of the polypeptide chain (Figure 3.15). Homopolymers of glutamic acid and serine have also been prepared as they will be used as controls in future experiments with cells and enzymes. Consumption of NCA monomers followed a similar profile to the PEG NH_2 initiated polymerisation (Figure 3.16).

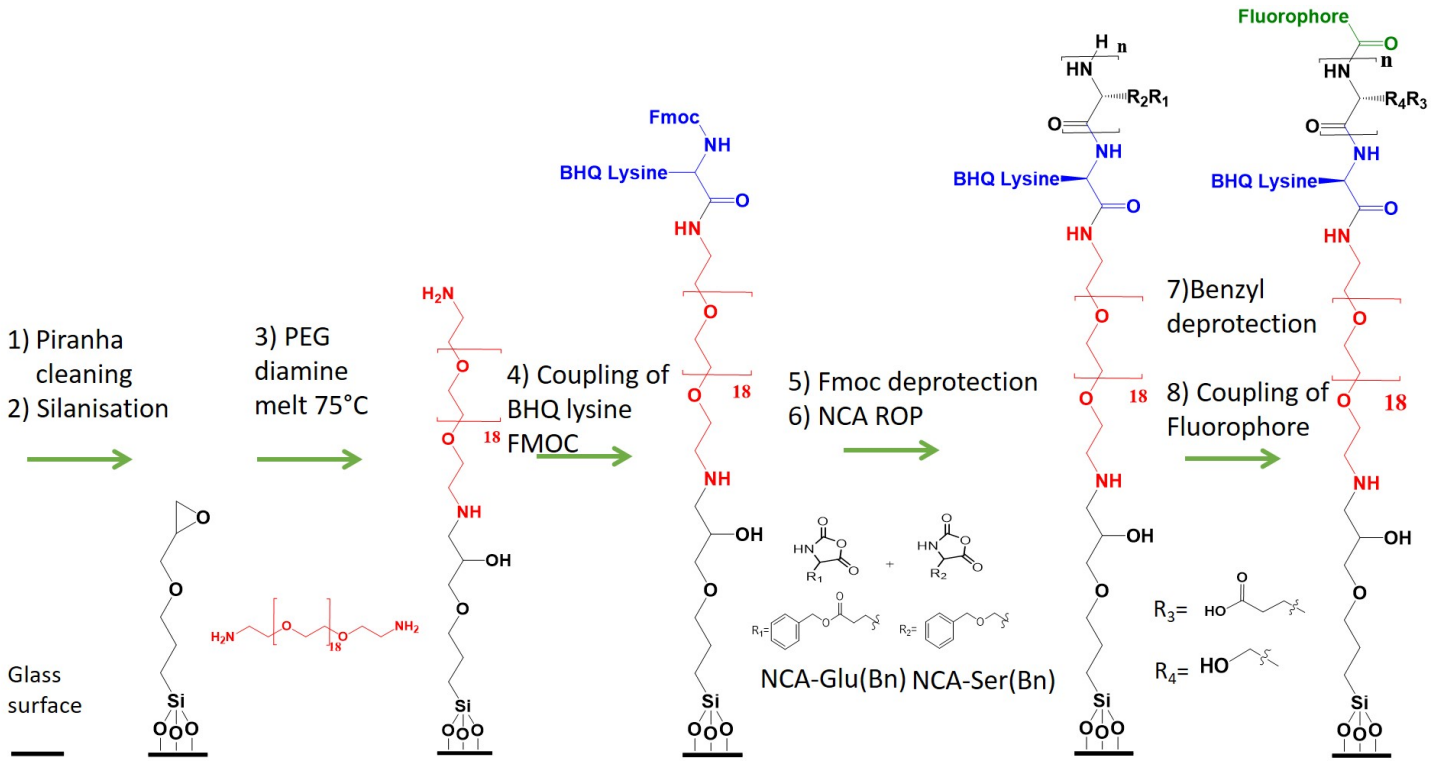


Figure 3.15: Scheme of surface modification with Black hole quencher-1-lysine coupled to the PEG_{18} linker chain and a fluorophore coupled to the terminal amine

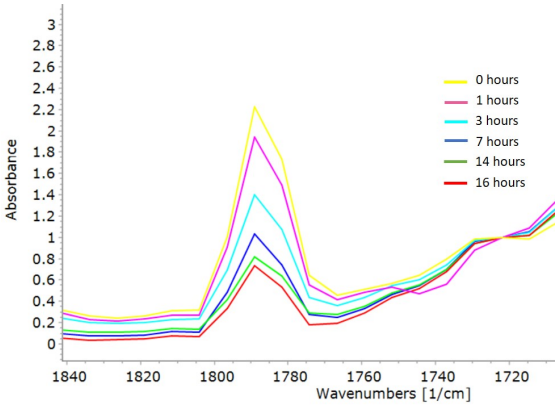


Figure 3.16: Monitoring NCA consumption in a 1:1 S:E feed ratio polymerised by NCA ROP from the surface by FTIR over time by the carbonyl peak 1790cm(^{1})

Table 3.10: Water contact angle values (n=5) of modified substrates with BHQ and fluorophor. One way ANOVA multiple comparison.

	WCA/ degree
Pianha	< 15
GOPTS	43.4 ± 1.8
PEG-NH_2	29.6 ± 2.8
BHQ-1-Lysine-Fmoc	45.0 ± 2.2
BHQ-1-Lysine	47.4 ± 2.5
1:1 S(Bn):E(Bn)	72.4 ± 1.6
1:1 S:E	53.6 ± 1.7
1:1 S:E-F	58.3 ± 2.5
E(Bn)	68.6 ± 4.6
E	55.6 ± 1.5
E-F	57.8 ± 3.8
S(Bn)	72.4 ± 1.1
S	50.1 ± 1.8
S-F	49.8 ± 2.1

As previously water contact angle was used to measure the surface changes at each modification step as shown in Table 3.10.

The GOPTS and PEG terminated substrates are in agreement with the previous measurements. On addition of the BHQ, there is a significant increase in the WCA with the introduction of hydrophobic residue of the Fmoc protecting group. However there is no decrease in the WCA on deprotection. The WCA for the substrates after polymerisation increase as anticipated, however to a lower value measured for the PEG NH_2 samples, the reduction after deprotection is of a similar magnitude as the previous samples. The addition of the fluorphore on the surface does not significantly change the

WCA.

Subsequently ToF SIMS was used to analyse the surface chemistry of the modified substrates (Figure 3.17). PEG diamine melt was successful as shown by the presence of the fragments CH_3^+ and $C_2H_5O^+$. After DIC coupling with the BHQ-1-FMOC Lysine a typical peak for the Fmoc protecting group is present, indicating successful coupling onto the surface. After deprotection with piperidine, the signal is completely lost, indicating the Fmoc has been fully cleaved from the surface. The polymerisation was successful with the presence of serine and glutamic acid typical ion fragments on the surface. However it is possible that polymers grew from the free amine on the PEG as well as from the deprotected Lysine. Ion intensity values can be found in the appendix (Table A.1). There is loss of the benzyl protecting group after deprotection, there are still ion fragments present on the surface of $C_7H_7^+$ however these can be attributed to the aromatic functionalities in the BHQ structure. There is an increase in the presence of the fragment $C_{10}H_{14}^+$ for the fluorophore terminated sample. The fluorophor contains similar structure to Fmoc therefore it is likely this is an indicator of successful coupling to the surface of the fluorescein. The raster images show predominantly a homogenous distribution of the ions presented with the exception of the BHQ-1-FMOC Lysine where there is a ion black spot where there is a high amount of Na^+ present, indicating in this area the underlying glass is exposed, the sample may have been contaminated in this area eg. a small droplet of water that dried in this area (Figure 3.18). The fluorophore terminated samples indicate inhomogeneities in the distribution of the Serine and Glutamic acid with visible hotspots of corresponding fragments, which correspond to dark spots in the PEG and Fmoc terminated samples. This could indicate there was no fluorophore bound in these areas, so the serine and glutamic acid fragments present more strongly.

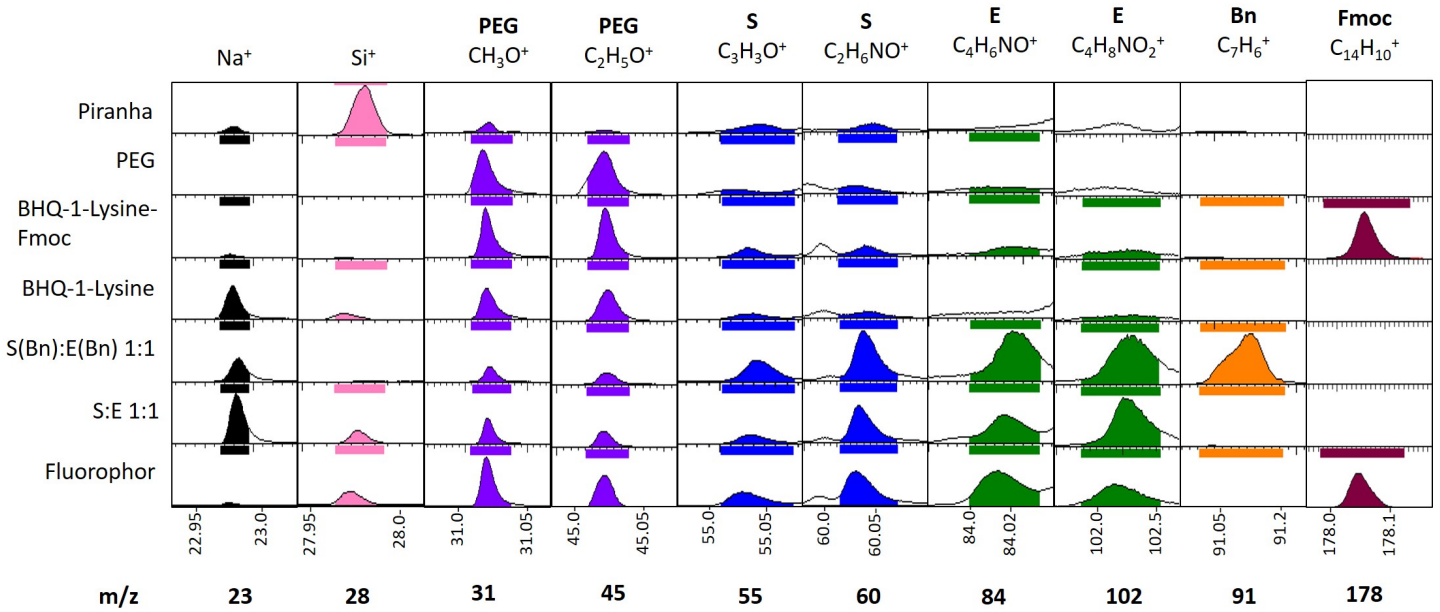


Figure 3.17: ToF SIMS spectra of fragment intensities indicative of PEG: purple (CH_3O^+), ($C_2H_5O^+$) Serine: dark blue ($C_3H_3O_3^+$, $C_2H_6NO^+$), Glutamic acid: green ($C_4H_6NO^+$, $C_4H_8NO_2^+$), Benzyl protecting group: orange ($C_7H_6^+$, $C_7H_7^+$) and Fmoc: dark purple $C_14H_10^+$normalised to total ion count

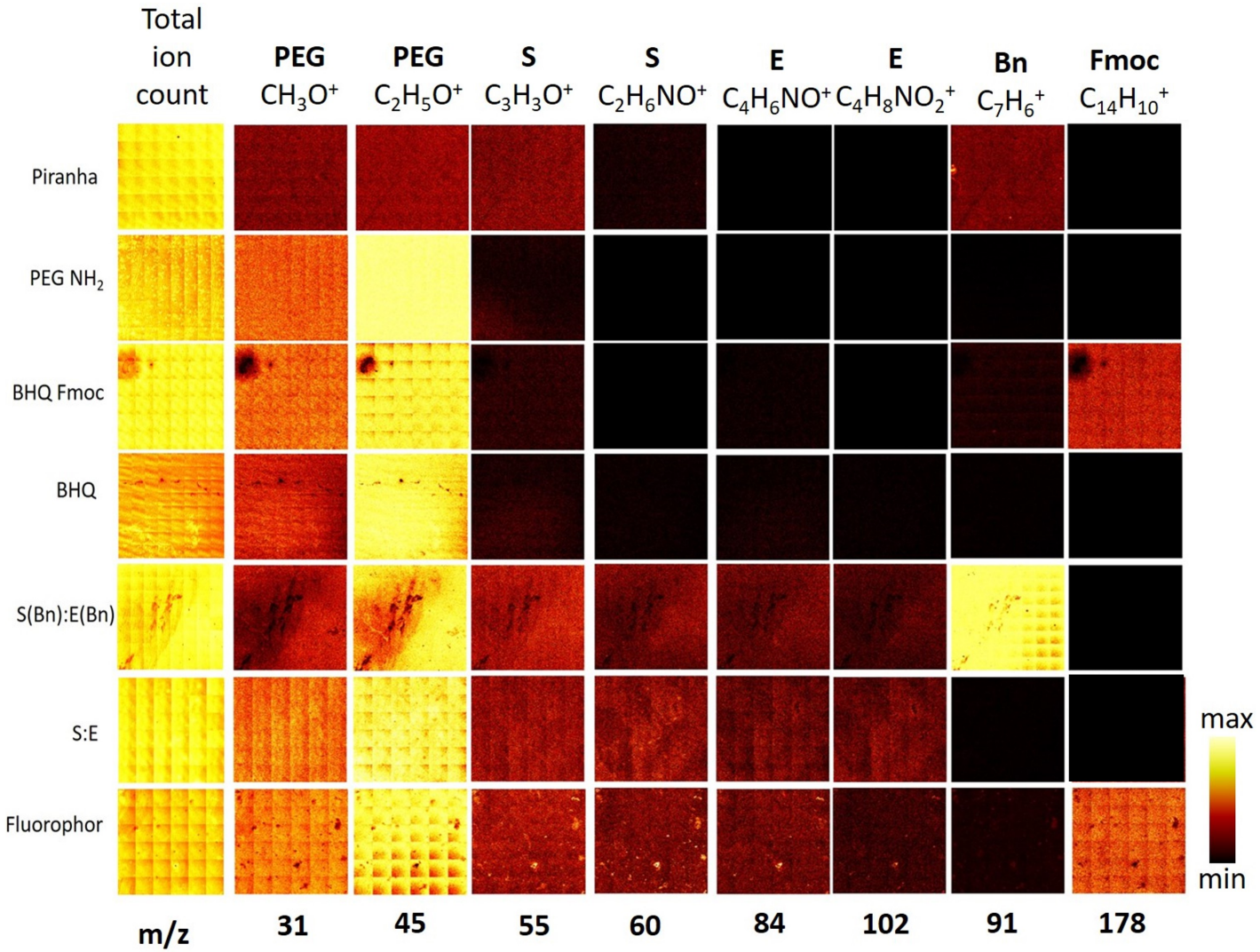


Figure 3.18: ToF SIMS ROI images of fragment intensities indicative of PEG: (CH_3O^+), ($C_2H_5O^+$) Serine: ($C_3H_3O_3^+$, $C_2H_6NO^+$), Glutamic acid: ($C_4H_6NO^+$, $C_4H_8NO_2^+$), Benzyl protecting group ($C_7H_6^+$, $C_7H_7^+$) and Fmoc $C_14H_10^+$ normalised to total ion count

3.3.5 XPS analysis

The surfaces were modified with a pentafluoro-L-phenylalanine coupled to the PEG diamine, to which the BHQ-1-FMOC Lysine was coupled to initiate the polymerisation. This sequence enabled the introduction of a marker element, the fluorine as explained in the previous section (NCA ROP from PEG amine functionalised surface). As before the samples were analysed at each modification step and the spectra can be seen in Figure 3.19 and Figure 3.20. Wide scan spectra show contributions from O1s, N1s and C1s in all samples. Oxygen is one of the main constituents of the glass coverslip and is present in high amounts in all samples. As previously observed in the samples without the BHQ-1-FMOC Lysine an increase in contribution of carbon is observed after silanisation and pegylation. A further increase in carbon occurs after the coupling of BHQ-1-FMOC Lysine coupled with an increase in the nitrogen contribution from the azides in the structure. The % of Nitrogen contribution decreases after polymerisation for the co and homopolymers, this can be attributed to large increase in carbon contribution. The % of contribution of nitrogen and oxygen are similar to the samples described earlier (without the BHQ present). Silica contribution decreases after BHQ-1-FMOC Lysine coupling step and stays relatively low after co and homoserine polymerisation. The contribution increases with the homoglutamic acid coupling step, indicating the underlying glass coverslip is more accessible in these samples. Table 3.13 gives a detailed breakdown of the contributions of each element.

The narrow scan spectra for C1s are shown in Figure 3.19 and Figure 3.20 which shows the different chemical environments of the carbon electrons on the surface. The GOPTS, PEG NH_2 and Pentafluoro-L-phenylalanine coated surfaces show similar contributions of C-O-C/C-N as the previous set of samples analysed as discussed in the previous section. The main difference is the C-O-C/C-N contribution from GOPTS is 11% lower in these samples, with a higher contribution of C-C/C=C, this could be attributed to hydrocarbon contaminants on the surface. The introduction of the BHQ-1-FMOC Lysine increases the C-N/C-O-C contribution which can be attributed to the the azides in the structure and the amide bond formed. The polymer surfaces (co and homopolymers) have contributions from C(=O)N attributed to the amide on the backbone of the polypeptide. The C-F contribution was indistinguishable from the amide, therefore have been grouped together. There is a decrease in the contribution of C-C/C=C for the copolymer after HBr/TFA treatment attributed to deprotection of the benzyl group similar to the previous samples. This is not however observed for the homopolymers nor is there a reduction in the total carbon contribution (wide scan) indicating the deprotection was not completed for these samples. The serine homopolymer does not have a contribution from C(=O)O which would be expected as the serine side chain does not contribute any carboxylic acids. After treatment with TFA/HBr there is a carboxylic acid contribution, this could arise from the underlying BHQ which does contain a car-

boxylic acid. It is also possible the TFA/HBr treatment is sufficient to cause cleavage of amide bonds, or of the carbonate linker in the BHQ structure, thus creating C(=O)O environments. However this is not coupled with a change in the contribution of the other electron environments, nor with the elemental contribution so this is unlikely.

As with the previous set of samples, the chain length was calculated from the ratio of the N1s to F1s elemental counts (Table 3.11). Firstly looking at the copolymer, the AD is high indicating inhomogeneities across the sample. The chain length almost halves after treatment with TFA/HBr, this observation was also apparent in the samples not containing the BHQ-1-Lysine, however the polymer chain lengths for both protected and deprotected are around half what was calculated for the previous samples. On the contrary the homopolymers serine and glutamic acid show an increase in chain length after TFA/HBr treatment. This data was derived from one repeat sample, therefore only conclusions on homogeneity across the sample can be confidently drawn any differences may be accounted for by sample to sample variability.

Table 3.11: Chain length of co and homopolymers as calculated using the ration of elemental counts of N1s to F1s for the protected and deprotected polymers. three measurement positions on one sample of each type

Surface	Bn protected	Bn deprotected
S:E 1:1	43 ± 20	23 ± 5
S:E 0:1	13 ± 7	35 ± 10
S:E 1:0	5 ± 1	11 ± 3

To ascertain information on the conformation and orientation FTIR has been used as an effective technique. the glass substrates had too strong a reflection masking any signal, therefore the modification procedures were performed on silicon wafers. Unfortunately there was also not a strong enough signal from the modified silicon wafers to obtain any conclusive information on conformation and orientation.

Table 3.12: Experimental percentage contributions of the different C environments at each modification step for samples initiated from BHQ-1-Lysine as determined by deconvolution of C1s peaks on XPS spectra.

%	C-C/C=C	C-N/C-O-C	C(=O)N / C-F	C(=O)O
GOPTS	70.0 ± 0.7	25.6 ± 0.7	0.0	4.1 ± 1.3
PEG NH_2	28.2 ± 0.3	61.6 ± 2.8	12.4 ± 6.1	0.0
Pentafluoro-L-phenylalanine	47.7 ± 8.0	47.0 ± 9.8	0.0	4.1 ± 1.9
BHQ-1-Lysine	31.5 ± 1.6	60.0 ± 1.8	8.1 ± 0.1	0.0
1:1 S(Bn):E(Bn)	48.9 ± 0.8	42.1 ± 0.4	6.8 ± 0.2	2.1 ± 0.7
1:1 S:E	25.4 ± 2.1	63.3 ± 3.1	9.0 ± 0.3	2.2 ± 0.9
0:1 S(Bn):E(Bn)	25.3 ± 1.5	62.6 ± 1.8	9.7 ± 1.4	2.3 ± 0.8
0:1 S:E	26.3 ± 3.5	61.6 ± 4.9	9.9 ± 1.3	2.1 ± 1.6
1:0 S(Bn):E(Bn)	28.0 ± 1.2	61.8 ± 1.3	10.7 ± 0.1	0.0
1:0 S:E	25.6 ± 2.3	58.9 ± 1.2	12.5 ± 1.5	2.8 ± 0.4

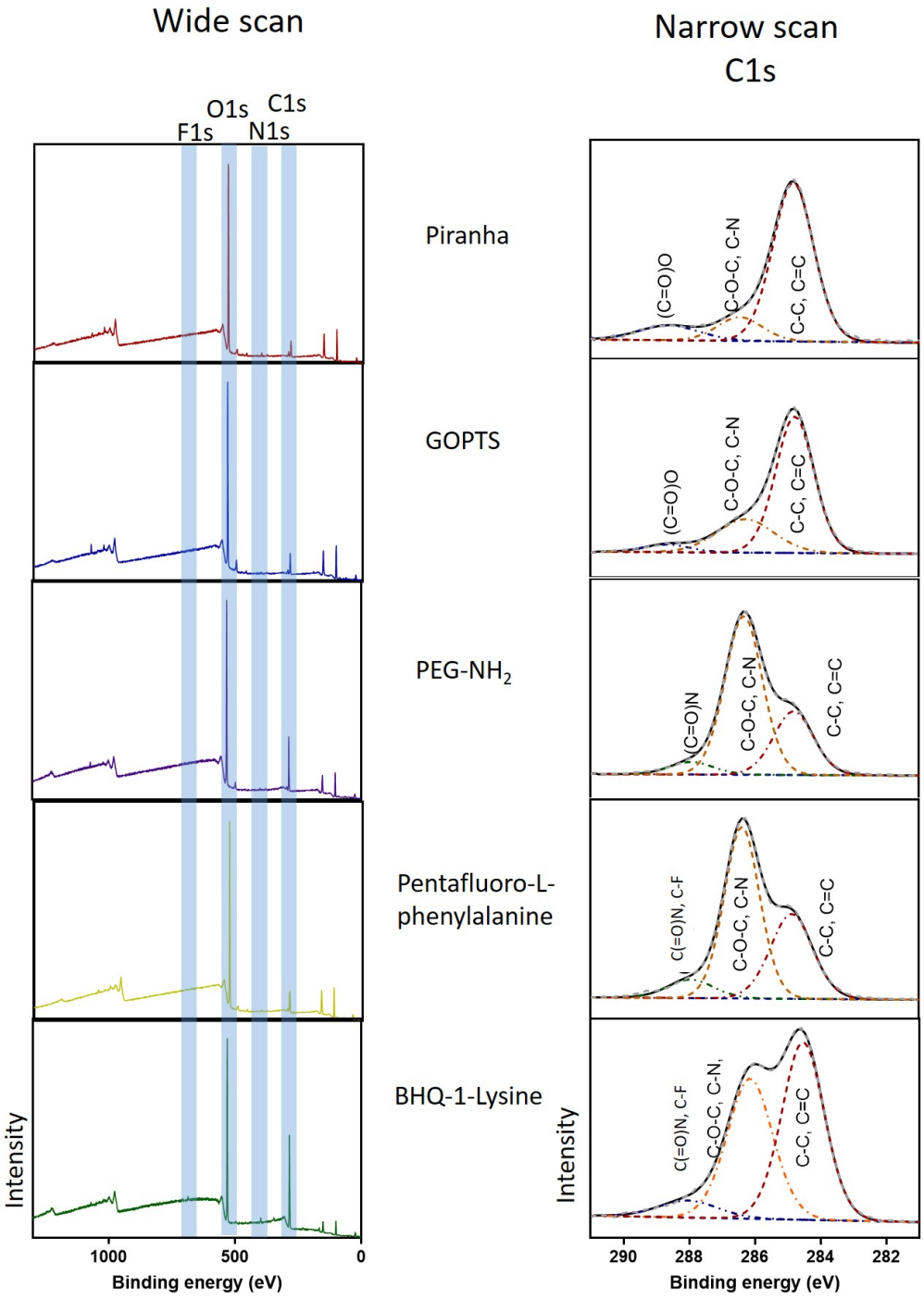


Figure 3.19: XPS spectra of surfaces modified with GOPTS, PEG diamine, BHQ-1-Lysine and Pentafluoro-L-phenylalanine Left: Wide scan with fitted peaks and envelope (grey), fit (black dash) and Right: narrow scan of C1s of samples at each modification step

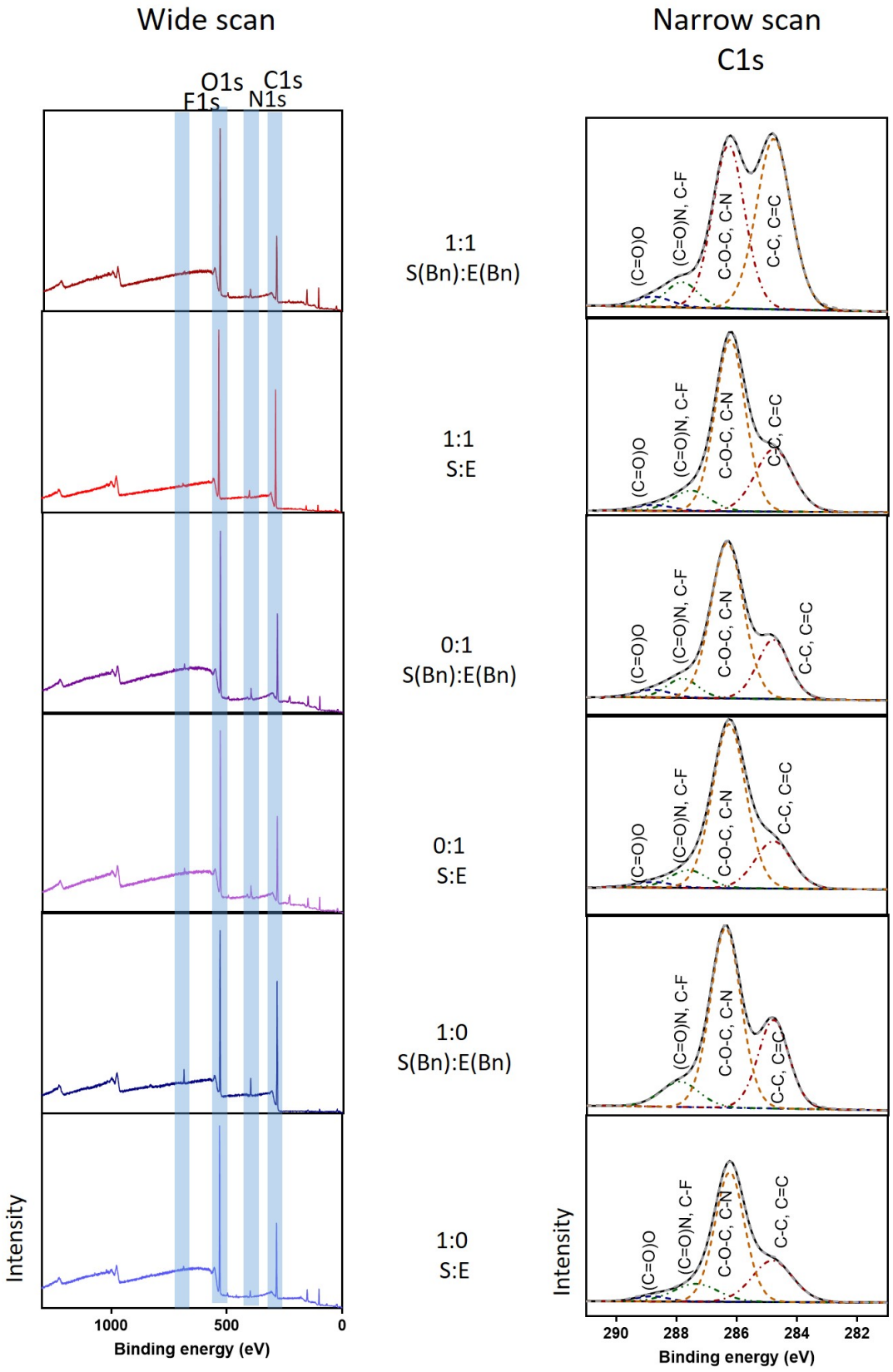


Figure 3.20: XPS spectra of surfaces coated in polymer initiated from BHQ-1-Lysine for homo and copolymers. Left: Wide scan with fitted peaks and envelope (grey), fit (black dash) and Right: narrow scan of C1s of samples at each modification step

Table 3.13: Elemental composition of modified surfaces functionalised with BHQ-1-Lysine as determined by XPS.

%	C	N	O	Si	F	Sum of rest*
GOPTS	16 ± 1.2	0.6 ± 0.2	36.7 ± 25.0	19.2 ± 11.2	0.0	28.0 ± 3.7
PEG NH_2	32.1 ± 0.8	0.7 ± 0.1	46.0 ± 0.28	17.96 ± 0.46	0.0	3.35 ± 0.63
Pentafluoro-L-phenylalanine	23.9 ± 6.2	0.8 ± 0.1	47.4 ±3.6	24.0 ±2.6	0.4 ± 0.2	3.4 ± 0.7
BHQ-1-Lysine	46.6 ± 12.25	13.8 ±8.3	22.7 ± 16.0	0.9 ± 0.4	5.7 ± 6.5	10.1 ± 0.8
1:1 S(Bn):E(Bn)	59.22 ± 7.8	4.4 ± 0.9	27.9 ± 4.6	7.6 ± 3.6	0.4 ± 0.1	0.9 ± 0.4
1:1 S:E	62.2 ± 0.3	3.0 ± 0.3	30.4 ± 0.2	3.4 ± 0.2	0.9 ± 0.6	0.1 ± 0.2
0:1 S(Bn):E(Bn)	36.4 ±2.22	5.8 ± 8.5	38.3 ± 11.3	12.0 ± 1.3	0.7 ± 0.5	7.6 ± 6.2
0:1 S:E	36.7 ± 9.0	4.3 ± 0.8	42.0 ± 4.6	14.5 ± 4.3	0.5 ±0.2	2.0 ± 1.1
1:0 S(Bn):E(Bn)	66.4 ± 2.1	3.5 ± 0.3	26.3 ± 1.1	2.5 ± 1.5	1.1 ± 0.2	0.2 ± 0.2
1:0 S:E	54.1 ± 8.0	2.8 ± 0.6	33.9 ± 4.0	7.5 ± 4.1	0.7 ± 0.2	1.07 ± 0.7

* Mg, Zn, Ti, K, Na

3.4 Conclusions

Surface initiated NCA-ROP is an effective method to modify glass surfaces from free amino groups available at the terminus of three different surface tethered molecules. Water contact angle was used to measure changes in surface wettability; treatment with NCA-Glu and NCA-Ser increased the hydrophobicity of the co and homopolymer surfaces and a significant drop was observed after benzyl deprotection. Glutamic acid and serine were both present on the surface as indicated by ToF SIMS analysis. Distribution of amino acids on the surface were predominantly homogenous, with some inhomogeneities introduced with PEG-NH_2. XPS analysis was an effective way to measure the relative change in elements on the surface, of particular interest carbon and nitrogen. The deconvolution of the narrow scan spectra of carbon showed the presence of amide bonds on the surface after polymerisation. Average chain length was also estimated by XPS. For both the BHQ-1-Lysine and PEG-NH_2 initiated samples the chain length almost halved after deprotection however this effect was not observed for the homopolymers. ToF SIMS analysis showed that samples prepared in the same batch had serine and glutamic acid present on the surface in similar amounts (based on ion intensities) and that these ions are evenly distributed. However, when analysing samples that were prepared in different batches, although the amino acids were present on all samples, the distribution and intensity of these ions varied between samples.

This data indicates that when determining if enzymes can interact with the surfaces, as in the next chapter, ideally the samples should only be compared within the same batch to minimise variability introduced in the surface preparation which may have implications on any variability observed in enzyme interactions.

It can be concluded that although there is some variability within the system, within batches the evidence suggests that samples are the same and are therefore suitable to determine if they are able to interact with enzymes. This was tested in the next chapter. If the samples show a positive or negative interaction with the enzymes, this will determine any subsequent steps to further optimise NCA ROP from the surface in this system. This could be achieved by using different techniques to gain a more detailed picture of the surface eg. investigating the orientation and density of the polymers on the surface.

Chapter 4

Enzyme interactions with polypeptide modified surfaces

4.1 Introduction

As stated in the introductory chapter to this work, the goal is to develop an enzyme responsive surface. To do this a target enzymatic system has been chosen; the phosphorylation and dephosphorylation of serine/phosphoserine mediated by Casein Kinase II (CKII) and alkaline phosphatase (AP) Figure 4.1. The materials have been synthesised by NCA ROP and characterised as described in Chapter three. Herein their ability to present the enzyme recognition motif S-x-x-E and undergo an enzyme mediated modification will be explored. Firstly the two target enzymes will be discussed in detail.

4.1.1 Introduction to target enzymes for surface interactions: Casein Kinase II (CKII) and Alkaline Phosphatase (AP)

In this work, the enzymes targeted to interact with the prepared and characterised surfaces are CKII and AP. They mediate a plethora of phosphorylation and dephosphorylation reactions to switch on and off proteins [177]. This switching on and off of proteins is inherent to maintaining homeostasis within the body and an imbalance of enzymes is often associated with disease pathology and as a result enzymes have been the target of some disease therapies. Protein kinase genes constitute 2% of the genome in most eukaryotes however they phosphorylate around 30% of cellular proteins. CKII is an intracellular enzyme and is part of the family of protein kinases, including Casein kinase I (CKI) and genuine casein kinase (G-CK). Phosphorylation regulates protein function by inducing conformational change or by disruption/ creation of protein-protein interactions. Conformational changes are driven by the creation of a network of hydrogen bonds with specific amino acids nearby, this is dependent of the three-dimensional structure of the phosphorylated protein [67, 177]. In order to phosphorylate proteins, the kinases require a specific sequence of amino acids in their target, known as a motif which differs

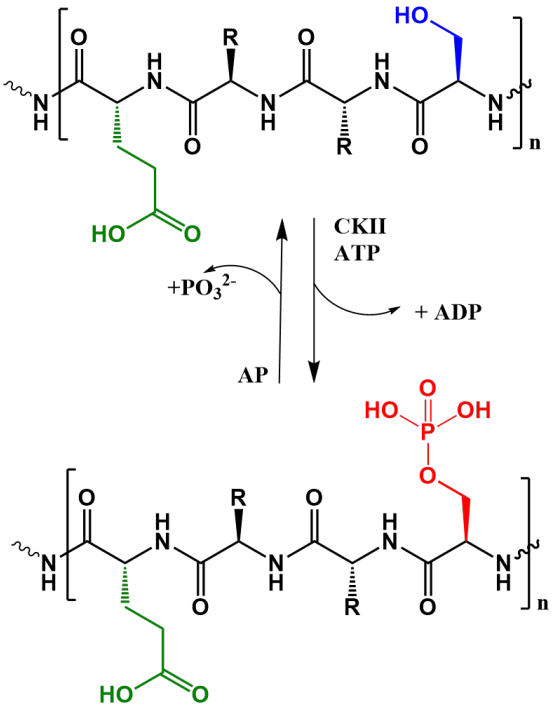


Figure 4.1: Mechanism of phosphorylation and dephosphorylation for a copolymer with sequence S-x-x-E mediated by the enzymes AP and CKII

between kinases as seen in Figure 4.2 [178–180].

In Chapter two, where the solution polymerisation of serine and glutamic acid NCAs was explored, the kinetic data indicated that the serine and glutamic acid amino acids preferentially react with each other rather than themselves. It was, therefore, highly probable the motif for CKII would be present in a co-polymer synthesised from a 1:1 serine and glutamic acid monomer feed. Moreover, approximately 50 % of the residues in the chain will be acidic, as is preferred by CKII [181].

CKII is a heterotetramic holoenzyme composed of two 44 kDa catalytic α subunits and two regulatory 26 kDa β subunits $\alpha_2\beta_2$ [182]. It has been found to have a major role in phosphorylating proteins enabling them to promote cell proliferation and/or counteract apoptosis, thus implying that the enzyme is involved in cell survival and death. CKII is consequently more prevalent in tumour cells then healthy cells and has therefore been investigated as a target in cancer therapy [183, 184].

CKII phosphorylates an extraordinary high number of proteins in the body, mostly fulfilling the motif outlined in Figure 4.2.

Casein Kinase II mechanism

The recognition sequence has been systematically determined by altering individual amino acids in the sequence and measuring the V_{max} and K_m. RRREEESEEE sequence had a 10 fold higher V_{max}/K_M over RRREEETEEE therefore CKII has a preference for serine over threonine. They determined that having an acidic residue in n+3 was essential

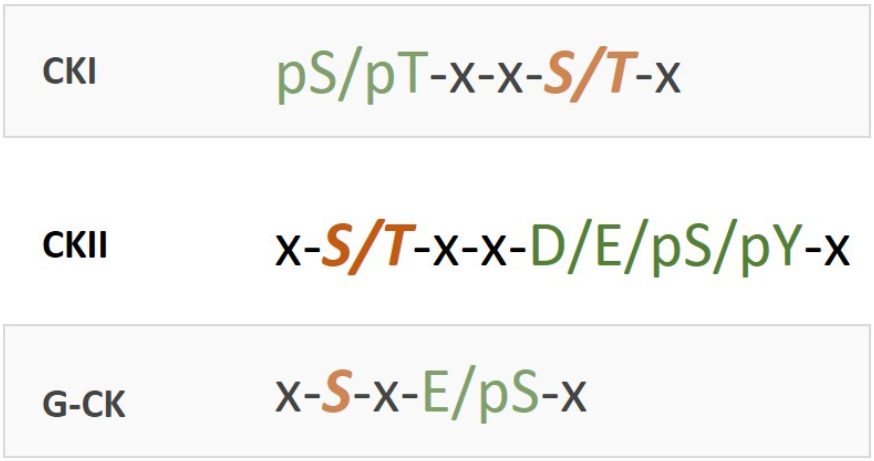


Figure 4.2: Motifs required for each group of casein kinases, casein kinase I (CKI), caseine kinase II (CKII) and genuine-casein inase (G-CK) with shorter motifs, phosphorylate residues (orange) and specificity determinants (green). X can be any amino acid, in the case of CKII acidic amino acids are preferable.

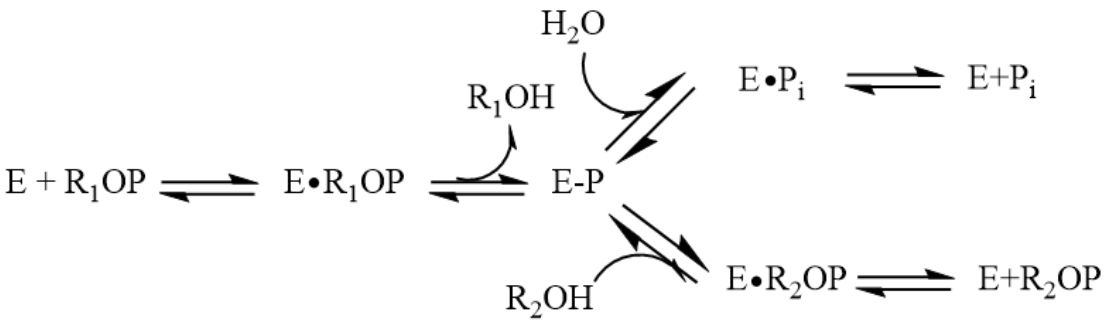


Figure 4.3: Kinetic scheme for enzymatic hydrolysis of phosphate monoesters by AP [1]

for CKII activity, whereas n+2, n+4 and n+5 had little effect on the kinetics [185].

There is an ATP binding domain and a substrate binding domain (serine/ threonine). Stereochemical arguments indicate that phosphate is transferred from the hydroxyl group via direct nucleophillic attack [186]. The chemical step is fast and the rate limiting step is the dissociation of ADP. Metal ions are seen to stabilise the orientation of the phosphate group and negative charges during catalysis [187]. It is proposed the base accepts the proton from the hydroxly group on the serine, catalysing nucleophilic attack on the γO of the phosphate [181].

4.1.2 Mechanism of Alkaline phosphatase

Alkaline phosphatase is a homodimeric enzyme that catalyses the hydrolysis of phosphate monoesters releasing phosphate and alcohol [188]. Two Zinc ions bound to AP are essential to its function, alongside one Mg^{+2} as a cofactor [189, 190]. They are non specific enzymes meaning they do not require a particular motif in the substrate. AP is

present in all tissues throughout the body, but is more prevalent in liver, bone, bile duct kidney and placenta. Humans contain three types: placental, non-specific (liver/bone and kidney) and intestinal [191].

In bone AP is involved in mineralisation and anti inflammatory effects in the intestines [192]. Elevated levels of AP have been associated with bone conditions; osteperosis, osteomalacia, various cancers; Lymphoma, Leukaemia and liver disease [193]. AP level testing is a common test for patients in healthcare institutions. It is also a common laboratory test in biological research.

In AP phosphate hydrolysis/transphosphorication the nucleophilic Ser-102 is transiently phosphorylated to give an E-P intermediate complex. The covalent E-P complex is subsequently hydrolysed to give a non-covalent enzyme phosphate complex EP_i [194], as shown in Figure 4.3. The E-P $\rightleftharpoons$ EP_i equilibrium has been studied. Under alkaline conditions the hydrolysis of EP_i complex is the rate limiting step (phosphate dissociation $\sim 30\ ^{-s}$) which is approximately equal to enzyme turnover rate (K_{cat}) [1, 195]. Below pH 6 dephosphorylation becomes rate limiting. X-ray crystallography studies provide information on the role of metal ions in the mechanism. Based on geometry of the metal binding sites Zn_2 is positioned to coordinate the Ser-102 hydroxyl group to activate its γO for nucleophilic attack of the substrates phosphorous atom [189, 196]. The Zn_1 ion coordinates the negatively charged leaving group of the substrate (alkoxide) ion, followed by activating a solvent water molecule in the second step. Magnesium has also been shown as being essential to structurally stabilise the enzyme in it's most active conformation [188].

Both enzymes have been targeted as stimuli in responsive systems, for static, reversible and dynamic induced changes [197–200]. Enzymatic mediated bond formation, or cleavage, has been the driving force behind enzyme induced self assembly of synthetic molecules to form micelles, nanofibres, macro and hydro gels for applications in drug delivery, anti bacterial systems and in imaging [49, 56, 201]. As this system in this work is focussed on enzyme surface interactions, these bulk enzymatic responsive materials will not be discussed in detail, with the exception of reversible enzyme induced changes.

Gianneschi et al. reported the first example of switchable micellar nanoparticles composed of a polymer-peptide amphiphile that contained a kinase substrate that were able to undergo reversible kinase induced aggregation after subsequent disaggregation with phosphatase treatment [51]. Xu et al. observed that a supramolecular hydrogel formation was regulated by a tyrosine kinase, which caused the Nap-FFGEY to phosphorylate into Nap-FFGEpY causing an increase in hydrophilicty of the peptide that results in a gel-sol transition. On incubation with alkali protein tyrosine phosphatase the phosphate groups were cleaved and a sol-gel transition was observed. This effect was also observed *in vivo* by injecting Nap-FFGEpY into rats and observing the formation of a gel subcutaneously on action of native enzymes [202].

4.1.3 Reversible enzyme responsive surfaces

Enzyme responsive surfaces were discussed in the introductory chapter. The reported systems are dynamic systems whereby the material is stimulated by the action of the enzyme which causes a material response. To our knowledge there are no reported reversible enzyme responsive surfaces, whereby the material response can be reversed by a second enzyme. Furthermore, there are no reported enzyme responsive surfaces whereby the substrate has been synthesised via NCA-ROP from the surface.

4.1.4 Aims

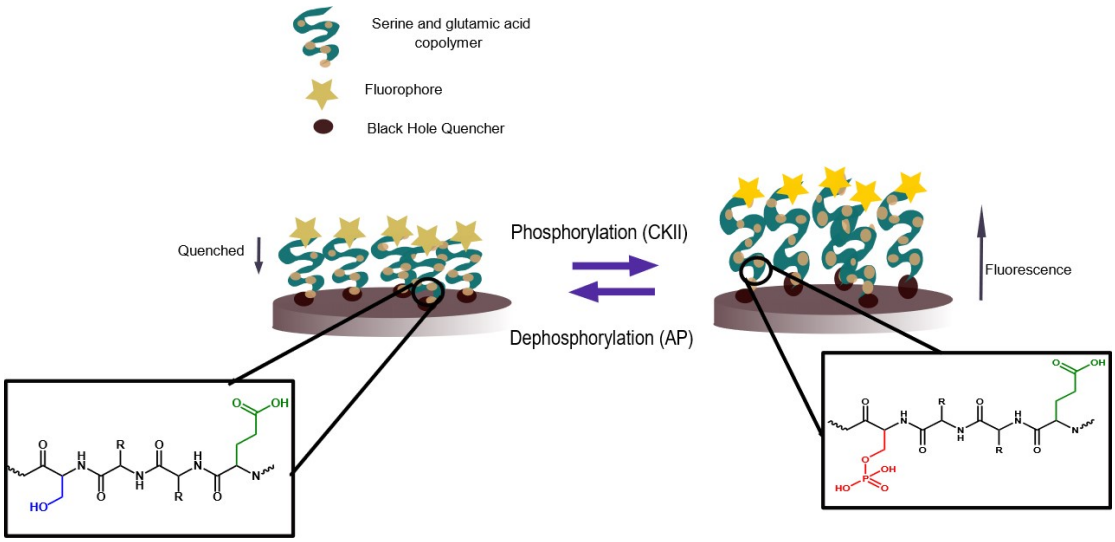


Figure 4.4: Illustration of predicted conformational change of co-polypeptide modified surface as a result of interactions with the enzymes AP and CKII. The fluorescent probes, a fluorophore and a BHQ are present on the surface. Quenching of fluorescence is illustrated with the conformational change caused by dephosphorylation of the serines.

This chapter will explore:

• The ability of CKII to recognise the polypeptide characterised in chapter three as a substrate.

• The ability of CKII and AP to phosphorylate and dephosphorylate the substrates.

• The ability of the system to undergo repeated and reversible phosphorylation and dephosphorylation cycles.

• The ability to follow these changes optically (with fluorescence) (Figure 4.4).

This work will address the lack of reported reversible enzyme responsive surfaces and further enhance the application of NCA ROP in responsive materials, in particular for copolymer systems.

4.2 Methods

4.2.1 Surface preparation

NCA's were synthesised as outlined in chapter two and surfaces were modified as outlined in chapter three.

4.2.2 ToF SIMS

ToF SIMS was used to characterise the surfaces, the same procedure was followed as outlined in chapter three.

4.2.3 Surface treatment with CKII

Deprotected coverslips were incubated in 500 µL of buffer containing Tris-HCl (50 mM), $MgCl_2$ (10 mM), EDTA (0.1 mM) at pH 8.2. Caesin kinase II (New England Biolabs, isolated from *E. coli*) was used according to manufacturers outlined activity. CKII (10 U/mL), ATP (10 µM and 1 µM) at 37 °C, stirred at 20 rpm on an orbital shaker for 1, 4 and 12 hours. Controls were prepared of homo glutamic acid with enzyme and ATP, 1:1 (S:E) with ATP, without enzyme and vice versa. Coverslips were washed overnight in ethanol then rinsed with water and dried before analysis.

4.2.4 Surface treatment with AP

Phosphorylated coverslips were incubated with calf intestinal AP (New England Biolabs). Activity was measured on site using para-nitrophenolphosphate (p-npp) (10 or 24 U/ mL) in buffer containing NaCl (100 mM), Tris-HCl (50 mM) and $MgCl_2$ (10 mM), pH 8.0 at 37 °C, stirred at 20 rpm on an orbital shaker for 1, 4 and 12 hours. Coverslips were washed overnight in ethanol then rinsed with water and dried before analysis.

4.2.5 ADP-Glo assay

ADP-Glo (Promega) bioluminescent kit was used to monitor the consumption of ATP. Modified coverslips were placed in a 24 well plate, 1 coverslip per well. Casein Kinase buffer was prepared and CKII (10 units/mL) and ATP (1 µM or 10 µM) were added to 500 µL of buffer per coverslip. Control samples were prepared with only ATP or only CKII as well as homo glutamic acid substrates. All samples were incubated at 37 °C on an orbital shaker (20 rpm). 25 µL of the reactant solution was removed after 0, 1, 3, 5, 8 and 22 hours, to which 25 µL of ADP-Glo reagent was added in a 96 white well plate. Samples were incubated for 30 minutes before the addition of kinase reagent (50 µL). Samples were incubated for 45 minutes and the luminescence was measured. A standard curve was prepared with solutions of ultra pure ADP and ATP total concentration 1 and

10 µM in the following ratios; 100:0, 80:20, 60:40, 40:60, 20:80, 10:90, 5:95, 98:2, 99:2 and 0:100 (ADP:ATP respectfully).

4.2.6 AP calibration

Para nitrophenol phosphate (p-npp) was used as a reagent to determine AP activity. P-npp is cleaved to p-nitrophenol on action of AP, to yield a yellow compound that can be measured colorimetrically at $\lambda = 405$ nm. Known concentrations of p-npp were incubated with 1 µL of AP in AP buffer in a clear 96 well plate for 60 minutes. Absorbance was read on a Tecan plate reader at $\lambda = 405$ nm.

4.2.7 Phosphate assay

Phosphate colorimetric assay (Biovision) was used to measure phosphate release after treatment of the surfaces with AP. After 24 hours incubation with CKII the supernatant was removed and samples were washed in buffer (2 mL x 4) after which AP buffer 500 µL was added to samples with AP (10 and 24 units/mL). 200 µL of supernatant was mixed with 30 µL of phosphate reagent and incubated at room temperature for 30 minutes. The absorbance was read at 605 nm on a Tecan Spark plate reader.

4.2.8 FRET measurements

A Tecan Spark plate reader was used to measure fluorescence on the surface of the substrates and any associated changes after enzyme treatment. A black coated, clear bottom 24 well plate was used. A 3D scan, which measures a range of combinations of emission and excitation wavelengths, was used to determine the optimum wavelengths of excitation and emission. This was verified with emission and excitation scans. The Z scan function was used to determine the optimum height to take the measurement. Fluorophors susceptibility to photobleaching was determined by exposing the surface to cycles of fluorescence until a reduction was observed. Optimum gain was determined by the instrument, which was kept constant within each set of experiments, but varied between different batches of samples. Five areas were measured per sample at 0 and 4 hours incubation at each treatment step.

4.3 Results and Discussion

As discussed in chapter three, glass coverslips have been modified with polypeptides using surfaces with three different functionalities; NCA ROP from APTMS, NCA ROP from PEG diamine and NCA ROP from a BHQ-1-Lysine with a fluorophor attached on the terminus.

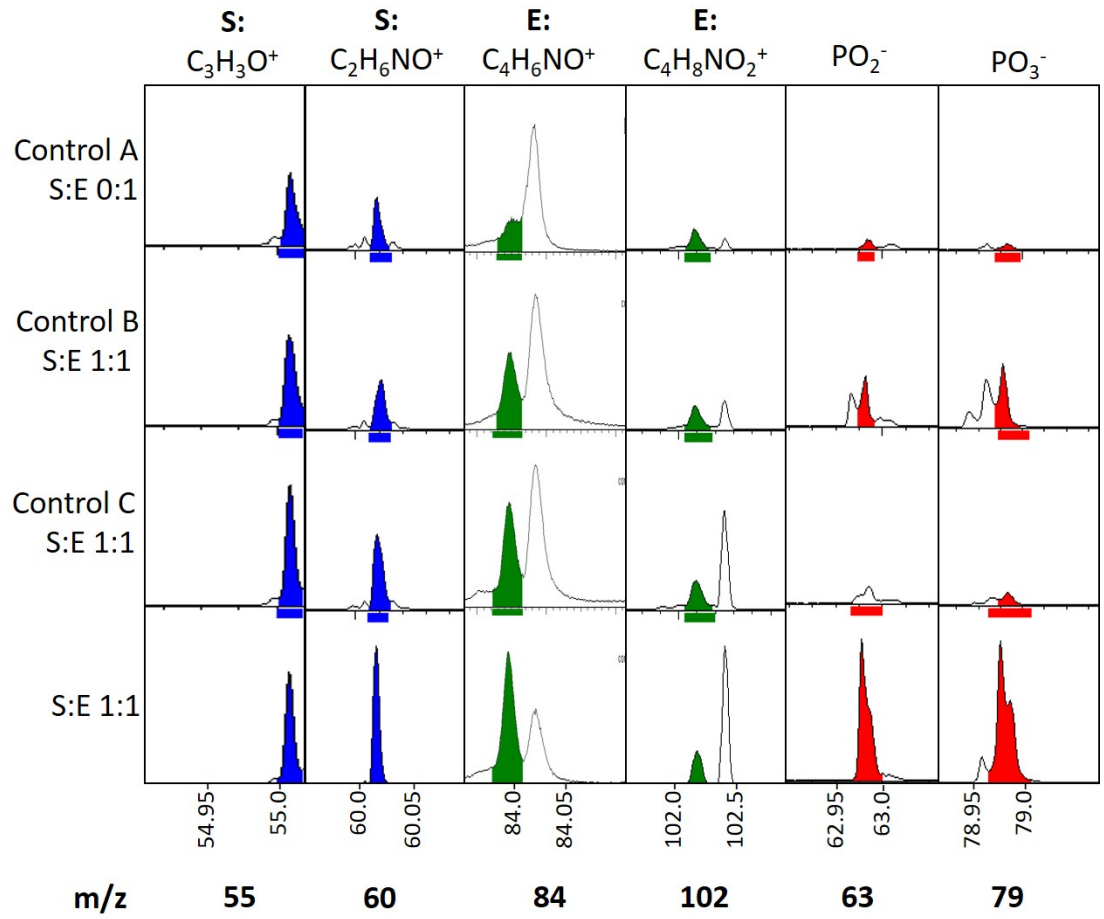


Figure 4.5: ToF SIMS spectra of surfaces (co and homopolymer) incubated with CKII and ATP to monitor for changes in phosphate on the surface. Samples: Glutamic acid homopolymer with ATP and CKII (control A), copolymer with ATP and without CKII (Control B), co polymer without ATP and with CKII (Control C) and copolymer with ATP and CKII. Indicative ion fragments shown for glutamic acid, serine and phosphate. Intensities normalised to total ion count. Area 3 x 3 mm.

4.3.1 Enzyme interactions with APTMS initiated polypeptide coated substrates

CKII/ATP interactions with the modified substrates

Firstly, the APTMS initiated polymer coated surfaces and their interactions with the enzymes CKII and AP will be discussed.

Substrates were incubated with ATP (10 µM) and CKII (10 U/mL) at 37 °C and then analysed to determine whether any phosphorylation had occured on the surface. The samples were incubated in buffer for 24 hours. Three controls were used: glutamic acid homopolymer with ATP and CKII, copolymer without ATP and with CKII and co polymer with ATP and without CKII.

The samples were analysed by ToF SIMS to determine whether a phosphate peak was present after incubation (Figure 4.5). Both positive and negative polarity was used.

Table 4.1: Table of ion intensities attributed to phosphate normalised to total ion count. Each 3 x 3 mm area was split into four 1.5 x 1.5 mm areas and the ion intensities determined by the software, normalised and averaged (n=4). One way ANOVA with multiple comparison was used for the statistics.

	Ion count	
Sample	PO_2^-	PO_3^-
Control A S:E O:1 (ATP + CKII)	$9.9*10^{-4} \pm 2.02*10^{-5a}$	$2.73*10^{-3} \pm 1.53*10^{-4a}$
Control B S:E 1:1 (ATP)	$6.43*10^{-3} \pm 4.60*10^{-3b}$	$2.05*10^{-2} \pm 2.12*10^{-2}$
Control C S:E 1:1 (CKII)	$2.41*10^{-3} \pm 2.74*10^{-5a}$	$7.09*10^{-3} \pm 1.24*10^{-3a}$
S:E 1:1 (ATP + CKII)	$1.42*10^{-2} \pm 5.23*10^{-3}$	$6.37*10^{-2} \pm 2.38*10^{-2}$

^{a} = p<0.005 **

^{b} = p<0.05 *

Firstly, the amino acids serine and glutamic acid were present on the surface of all samples as indicated by the signature ion fragments of m/z 55 and 60 (serine) 84 and 102 (glutamic acid). The intensities of phosphate PO_2^- (m/z = 63) and PO_3^- (m/z = 79) is greater on the S:E 1:1 polypeptide samples after exposure to CKII and ATP compared to the controls. Table 4.1 contains averaged ion intensities. All three control samples have significantly lower PO_2^- ion intensities ($p < 0.005$ and $p < 0.05$) and control A and C have significantly lower PO_3^- ion intensities ($p < 0.005$), however control B is not significantly lower. This could be due to trace ATP remaining on the substrate after wash steps. Nonetheless, the difference in phosphate intensities between this control and the S:E 1:1 incubated with both ATP and CKII is great enough to clearly indicate that phosphorylation has occurred on the surface as a result of the enzymatic action.

This infers the required sequence S-x-x-E must be present in the polypeptide chain for the CKII to have successfully interacted with the surface. This is in agreement with the prediction from the kinetics data obtained in solution from chapter two, whereby each monomer preferentially reacts with each other rather than themselves to form an alternating copolypeptide.

Homogeneous ion distribution for the amino acids is shown in the raster images in Figure 4.6. The negatively charged samples have areas of strong phosphate presence and areas with less, indicating a non-homogenous phosphorylation has occured. Given the distribution of the amino acids is relatively homogenous this could indicate inhomogeneities between polypeptide chains on the surface with respect to the presence and/or availability of the required motif. Given the number of manipulations these samples have undergone, there are small scratches visible on the surface.

It was then of interest to know how the phosphorylation changed over time, so samples were incubated in CKII and ATP for 1, 4 and 12 hours and analysed by ToF SIMS (Figure 4.7). There is an increase in intensity between 1 and 4 hours, with no further increase

after this time. Table 4.2 containing the ion intensities shows there is no significant difference between the ion intensities between any time point. After 4 hours, either the enzyme has lost activity or all available sites have been phosphorylated. It is necessary to perform a quantitative assay to determine the real kinetics for the interactions, which is of particular interest in future work when monitoring any conformational changes using the FRET system as a result of the action of the enzymes on the substrate.

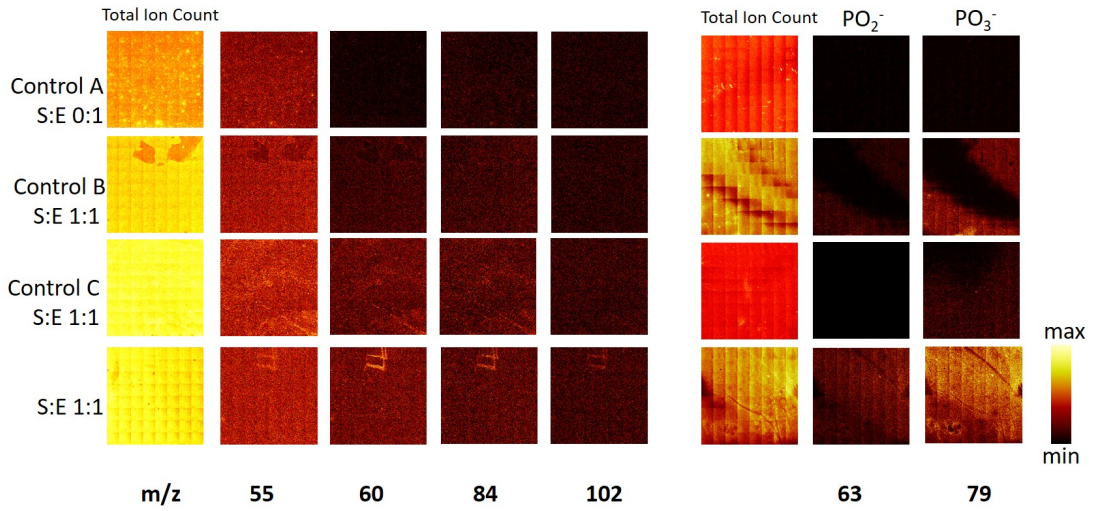


Figure 4.6: ToF SIMS Raster images for samples: Glutamic acid homopolymer with ATP and CKII (control A), Copolymer with ATP and without CKII (Control B) Co polymer without ATP and with CKII (Control C) and copolymer with ATP and CKII normalised to total ion count. Area 3 x 3 mm.

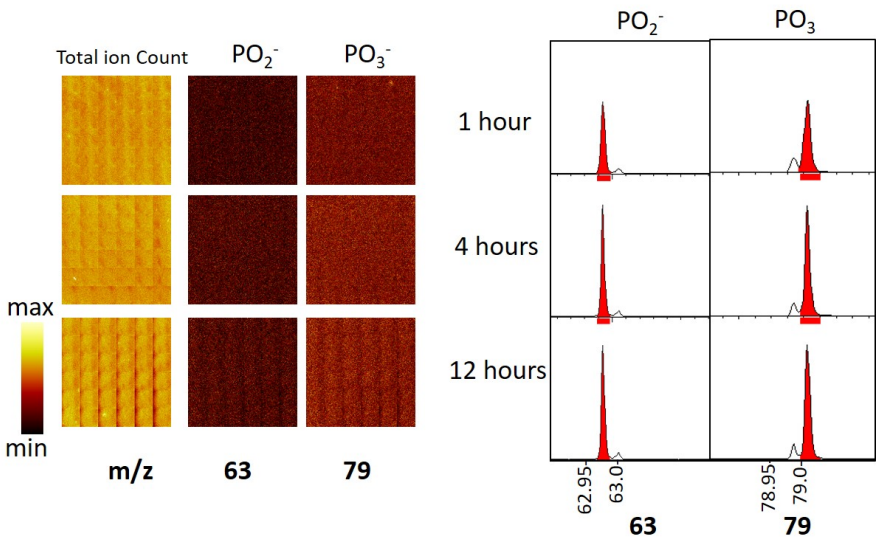


Figure 4.7: ToF SIMS spectra of fragment intensities assigned to phosphate ions PO−2 and PO−3 of S:E (1:1) copolymer modified surfaces by NCA ROP. The surfaces were incubated with ATP (10 µM) and CKII (10 U/mL) and analysed at time 1, 4 and 12 hours. Normalised to total ion count. 3 x 3 mm area was measured.

AP interactions with the phosphorylated substrates

Knowing that phosphorylation was possible on the surface, dephosphorylation with AP (12 U/mL) was attempted. Again they were analysed using ToF SIMS (Figure 4.8). If AP interacted with the substrate it would cleave the phosposerine, thus remove the phosphate from the surface. We would therefore expect to observe a loss in the phosphate peak. There is no difference in intensity of peaks after incubation at any time point, indicating the samples have not been dephosphorylated (Table 4.3). The amount of enzyme used was increased to 24 U/mL however this made no measurable difference.

It has been observed in the literature that incorporating the enzyme motif close to a surface can reduce enzyme access via steric hindrance effects. It was anticipated that on a polymer brush coated surface there would be a degree of flexibilty that would minimse surface steric hindrance effects and enable enzyme access. However as dephosphorylation was not possible with AP it is possible the chain is not flexible enough; the introduction of a linker molecule may overcome this challenge. Previous work has been successful with the introduction of a PEG diamine linker molecule in an enzyme responsive system consisting of short peptide chains to move the peptides away from the surface [203]. Therefore this method was adopted in this system. A PEG linker can be introduced on the surface by firstly silanising the glass coverslips with GOPTS to introduce an epoxy group that can be readily opened with an amine.

Table 4.2: Table of ion intensities attributed to phosphate for copolymer S:E (1:1) samples incubated with CKII and ATP at 1, 4 and 12 hours. Each 3 x 3 mm area was split into four 1.5 x 1.5 mm areas and the ion intensities determined by the software, normalised to total ion count and averaged (n=4). One way ANOVA with multiple comparison was used for the statistics.

Time (hour)	Ion count	
	m/z=63 PO_2^-	m/z=79 PO_3^-
1	$6.21*10^{-3} \pm 2.02*10^{-4}$	$4.73*10^{-3} \pm 1.18*10^{-4}$
4	$9.34*10^{-3} \pm 8.30*10^{-4}$	$1.01*10^{-2} \pm 8.12*10^{-3}$
12	$1.42*10^{-2} \pm 5.23*10^{-3}$	$6.37*10^{-2} \pm 6.71*10^{-3}$

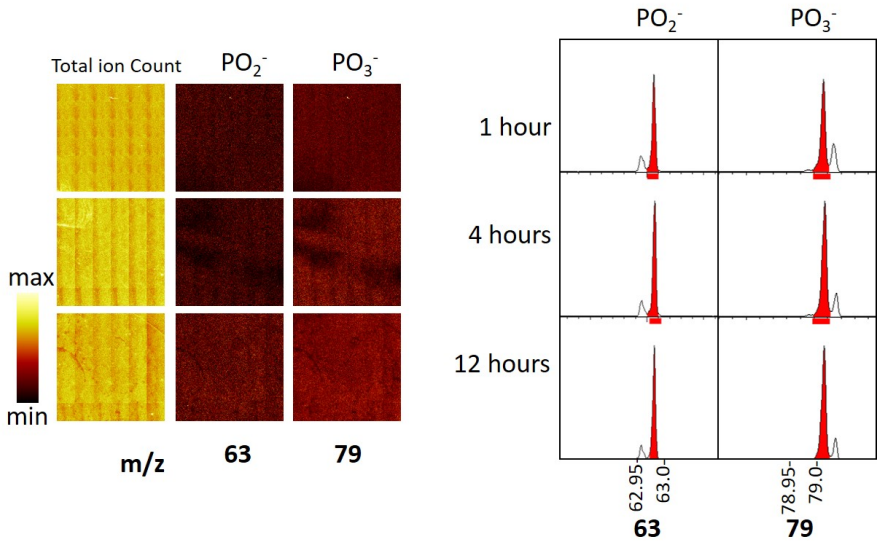


Figure 4.8: ToF SIMS spectra of fragment intensities assigned to phosphate ions PO−2 and PO−3 of S:E (1:1) copolymer modified surfaces by NCA ROP. The surfaces were incubated with AP (12 U/mL) and analysed at time 1, 4 and 12 hours. Normalised to total ion count. 3 x 3 mm area was measured.

Table 4.3: Table of ion intensities attributed to phosphate normalised to total ion count for samples incubated with AP for 1, 2 and 12 hours. Each 3 x 3 mm area was split into four 1.5 x 1.5 mm areas and the ion intensities determined by the software, normalised and averaged (n=4). One way ANOVA with multiple comparison was used for the statistics.

Time (hour)	Ion count	
	m/z=63 PO_2^-	m/z=79 PO_3^-
1	$5.71*10^{-3} \pm 1.03*10^{-4}$	$5.53*10^{-3} \pm 3.32*10^{-4}$
4	$6.43*10^{-3} \pm 1.08*10^{-3}$	$6.56*10^{-3} \pm 1.38*10^{-2}$
12	$5.42*10^{-3} \pm 7.32*10^{-3}$	$6.37*10^{-3} \pm 1.80*10^{-4}$

Table 4.4: Table of ion intensities attributed to phosphate normalised to total ion count for samples incubated with CKII and ATP, followed by incubation with AP for 1 and 4 hours. Each 3 x 3 mm area was split into four 1.5 x 1.5 mm areas and the ion intensities determined by the software, normalised and averaged (n=4). One way ANOVA with multiple comparison was used for the statistics. Significant values shown are comparisons with 1:1 S:E (ATP + CKII).

	Ion count	
Time (hour)	PO_2^-	PO_3^-
1:1 S:E (CKII)	0.00 ± 0.00 ^{c}	0.00 ±0.00 ^{c}
1:1 S:E (ATP)	$1.56*10^{-3}$ $\pm 2.78*10^{-4}$ ^{b}	$3.16*10^{-3}$ $\pm 5.40*10^{-4}$ ^{a}
1:1 S:E (ATP + CKII)	$7.64*10^{-3}$ $\pm 1.06*10^{-3}$	$2.61*10^{-2}$ $\pm 1.23*10^{-2}$
AP 1 hour	$5.56*10^{-3}$ $\pm 2.12*10^{-3}$	$2.59*10^{-2}$ $\pm 1.32*10^{-2}$
AP 4 hours	$4.73*10^{-3}$ $\pm 2.42*10^{-3}$	$2.11*10^{-2}$ $\pm 1.31*10^{-2}$

^{a}p<0.005 **

^{b}p<0.0005 ***

^{c}p<0.00005 ****

4.3.2 Enzyme interactions with PEG-NH_2 initiated polypeptide coated surfaces

The PEG-NH_2 initiated polymer surfaces were characterised as discussed in chapter three. The substrates were incubated with CKII/ATP and AP successively. Phosphorylation occured as observed for the APTMS initiated polypeptide samples and there was a significant difference in ion intensity as shown in Table 4.4. A reduction in the phosphate intensity after incubation with AP was observed, however this was not statistically significant (Figure 4.9). This was a promising result, however the peak was still present indicating dephosphorylation was incomplete. Increasing incubation time with AP had no further effect on the phosphate intensity. It would be expected that the two phosphate peaks correspond to one another however, here we observe a greater reduction in the PO_2^- peak intensity contrary to the PO_3^- peak intensity. As before the raster images indicate a non homogenous distribution of phosphate on the surface with notable 'hot spots'. The peak at 78.9 is attributed to Br^-, likely introduced in the benzyl deprotection step. Despite extensive washing and incubation steps it continues to be present on the surface.

To determine enzyme induced changes on the surface with a second method, ADP-Glo assay was used to determine the amount of phosphorylation that had occurred on the surface, the kinetics and the optimal ATP concentration. It is possible to monitor the conversion of ATP to ADP using a bioluminescence assay that depletes remaining ATP in the reaction mixture before converting the ADP to ATP. This can react with luciferase/luciferin to generate light that is measured and quantified with an ATP-ADP

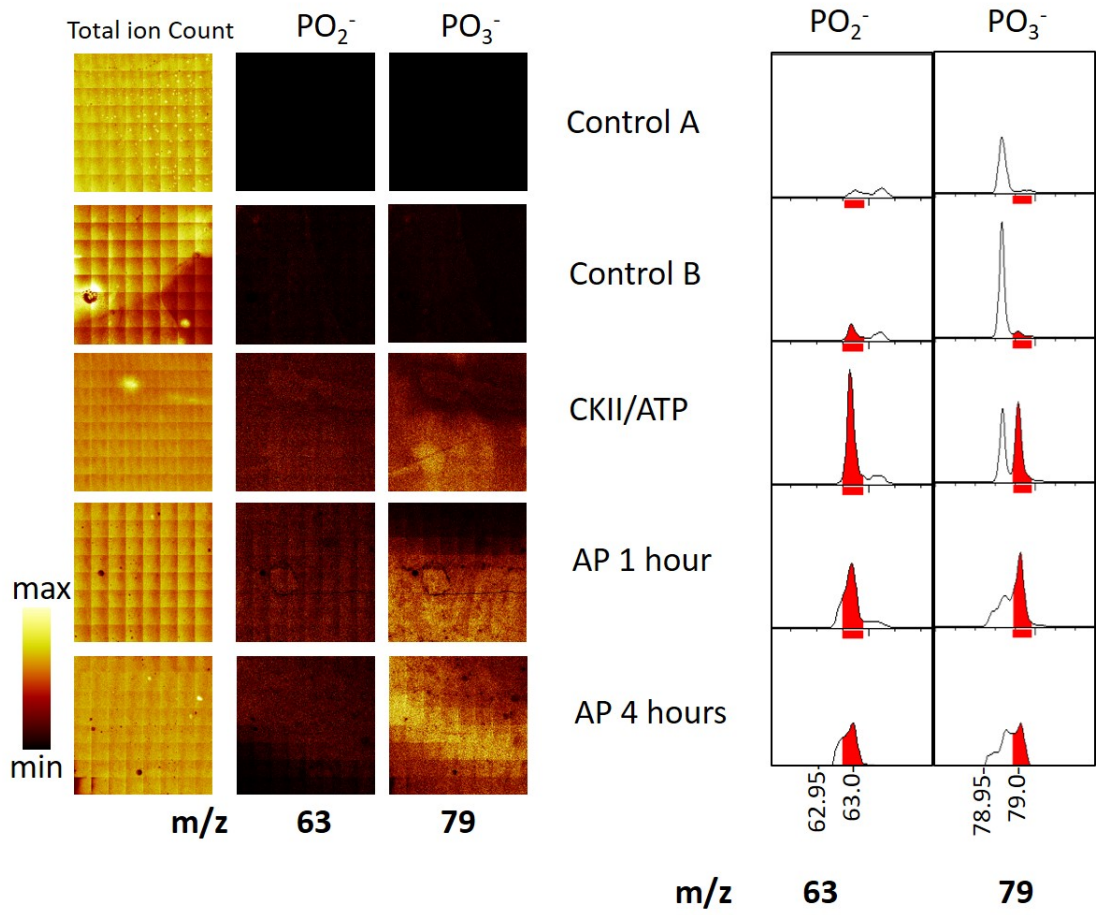


Figure 4.9: ToF SIMS raster images (left) and spectra (right) of fragment intensities of S:E (1:1) copolymer modified surfaces: control A (incubated with ATP no CKII), control B (incubated without ATP with CKII), substrate incubated with CKII/ATP, phosphorylated substrate incubated with AP at time 1 and 4 hours. Normalised to total ion count. 3 x 3 mm measured area.

calibration curve (Figure A.7). Two concentrations of ATP were used, 1 µ M and 10 µ M. Calibration curves for the two concentrations were obtained. Substrates were incubated with ATP 1 µM and 10 µM for 24 hours. At set time points the supernatant was removed from the reaction and ATP to ADP conversion was measured as seen in Figure 4.10. ATP is converted to ADP at both concentrations, indicating that phosphorylation of the substrate has occured mediated by CKII. ATP gets consumed at an equal rate until 4 hours incubation, no more conversion is observed for the 10 µM samples, whereas the 1 µM samples continues to show conversion up to 5 hours incubation. This is consistent with the SIMS data whereby no significant increase in phosphate ion intensity is observed after 4 hours. 10 % of ATP conversion occurs in the first hour with 60 % occurring between 1 and 5 hours. Similar to SIMS data, the phosphate ion intensity continues to increase after 1 hour, however the magnitude of this change does not correlate between the two techniques. This could be due to batch to batch variations as well as differences in the analysis principals of the two techniques. A concentration of 1 µM ATP was continued to be used in the subsequent work as it was able to be monitored using the luminescence method and it did not reach 100 % conversion. This is important to account for any batch to batch variations, to prevent availablility of ATP being a limiting factor. The number of moles of phosphate on the surface can be extrapolated from this data. Knowing that 70 % (0.35 nmol) of a 1 µM solution of ATP was converted to ADP, 0.35 nmol of phosphate are present on each sample.

A colorimetric assay was used to measure the amount of phosphate cleaved from phosphorylated substrates by AP treatment to complement the SIMS data. Phosphorylated substrates were incubated with AP and supernatant was removed at time 0, 4 and 24 hours (Figure 4.11) and incubated in a formulation of malachite green and ammonuium molybdate which forms a chromogenic compound with phosphate. Absorbance was read and phosphate amount determined from a calibration curve of known concentrations (Figure A.8).

There is some phosphate detected in all samples which could be residual traces from the incubation with ATP and CKII or an impurity arising from handling (phosphates common lab contaminants). A significant difference was measured between controls (no AP) and samples with AP at time 4 h (< 0.003) and time 24 h (< 0.0002) indicating that phosphate ions are present in the supernatant as a result of cleavage from serine on the substrate by AP. There is no difference after 4 hours indicating no more dephosphorylation occurs after this time. The amount of phosphate detected in the supernatant is greater than the amount measured on the surface (by the ADP-glo assay) 0.35 nmol on the surface vs 3.75 nmol in the supernatant after AP treatment. This discrepancy could have originated from the surface in the form of residual ATP/ ADP from the phosphorylation step, as observed in the controls. However this does not fully account for the difference observed in these samples.

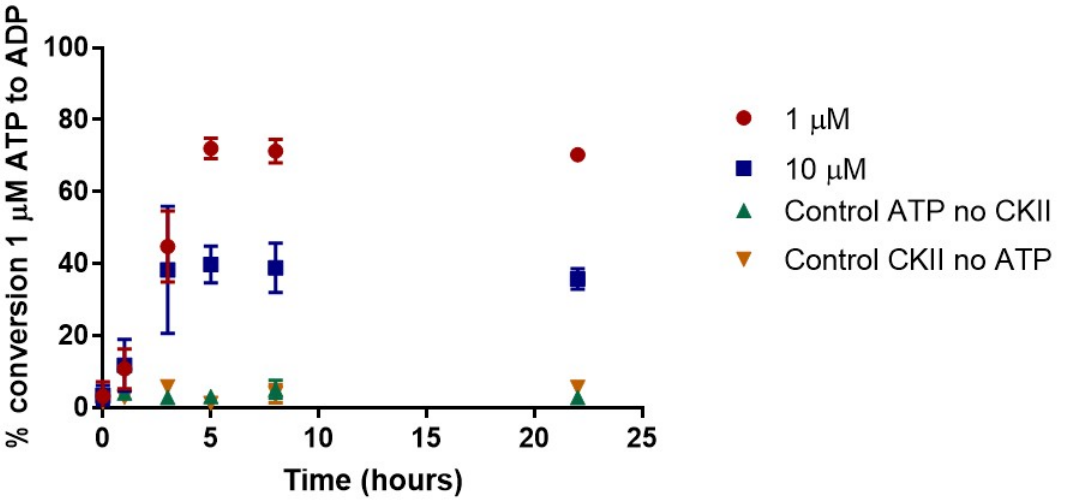


Figure 4.10: Copolymer samples of S:E (1:1) incubated with CKII (10 U/mL) and ATP (1 µM and 10 µM). Supernatant was removed at each time point and incubated with ADP-Glo assay reagents and measured by luminescence to determine ATP to ADP conversion (n=4)

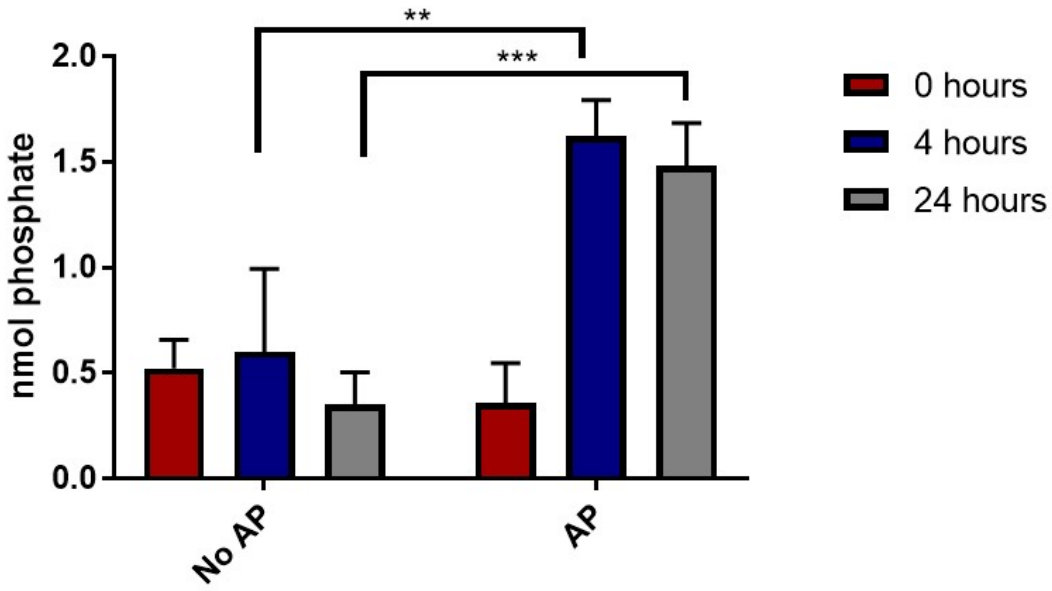


Figure 4.11: Copolymer modified surfaces S:E (1:1) incubated firstly with CKII/ATP, were then incubated in AP. The amount of phosphate present in the supernatant was determined using a colorimetric assay and absorbance measured at 650 nm before and after exposure to AP for different amounts of time (n=4).

4.3.3 Reversible phosphorylation/ dephosphorylation

The aim of this work is to develop a repeatably reversible enzyme system, so the logical next step was to investigate as to whether the phosphorylation/ dephosphorylation was reversible through a number of cycles. PEG initiated polymerised substrates were monitored at each step of three cycles of incubation with CKII/ATP followed by AP to monitor phosphorylation and dephosphorylation. ToF SIMS, ADP Glo and Phosphate assays were used to monitor any changes (Figure 4.12).

Firstly, although the ToF SIMS ion fragments corresponding to serine and glutamic acid are present on all 6 substrates, they vary in amounts, indicating sample to sample variations. There is no obvious correlation between the intensity of these fragments with the intensity of the phosphate fragments, excluding this as a contributing factor in the changes of intensity that are observed for the phosphate ions. The first enzyme incubation cycle exhibits little or no phosphorylation as indicated by the lack of ion peaks for PO_2^- and PO_3^- which correlates with the lack of conversion of ATP to ADP. In the second and third cycle phosphorylation occurs with 30 then 40 % ATP conversion and phosphate ions are present on the surface. Amount of phosphate on the substrates at cycle 2 is 0.14 nmol which correlates in order of magnitude with the 0.5 nmol detected in the supernatant. Full dephosphorylation can be observed at cycle two and cycle three indicated by the loss of the phosphate peaks. Some phosphate is measured for cycle two and three however the lower detection limit of this assay is 0.1 nmol, therefore the results are inconclusive.

CKII was able to interact with the polypeptides initiated from the PEG coated samples, as indicated by phosphate present on the surface and the consumption of ATP in the supernatant. A decrease in phosphate on the surface was observed after subsequent incubation with AP. This indicates the introduction of the PEG linker chain was beneficial in improving the availability of the polypeptide to AP. Furthermore the enzyme interactions were reversible and repeatable for up to two cycles. Having established that the enzymes could reversibly phosphorylate and dephosphorylate the polypeptides we wanted to determine whether this was accompanied with conformational changes that we could measure in real time.

4.3.4 Enzyme interactions with BHQ-1-Lysine and fluorophor containing substrates

The aim of this work is to measure enzyme interactions with the polypeptide coated surfaces in situ and, as discussed in chapter two, this can be achieved with a FRET system. Substrates with a black hole quencher at the base of the polypeptide chain and a fluorophore at the terminus have been characterised (chapter three). The introduction of the BHQ on the surface changes the initiator for the polymerisation. The BHQ is much bulkier than the PEG NH_2 with different electron density which

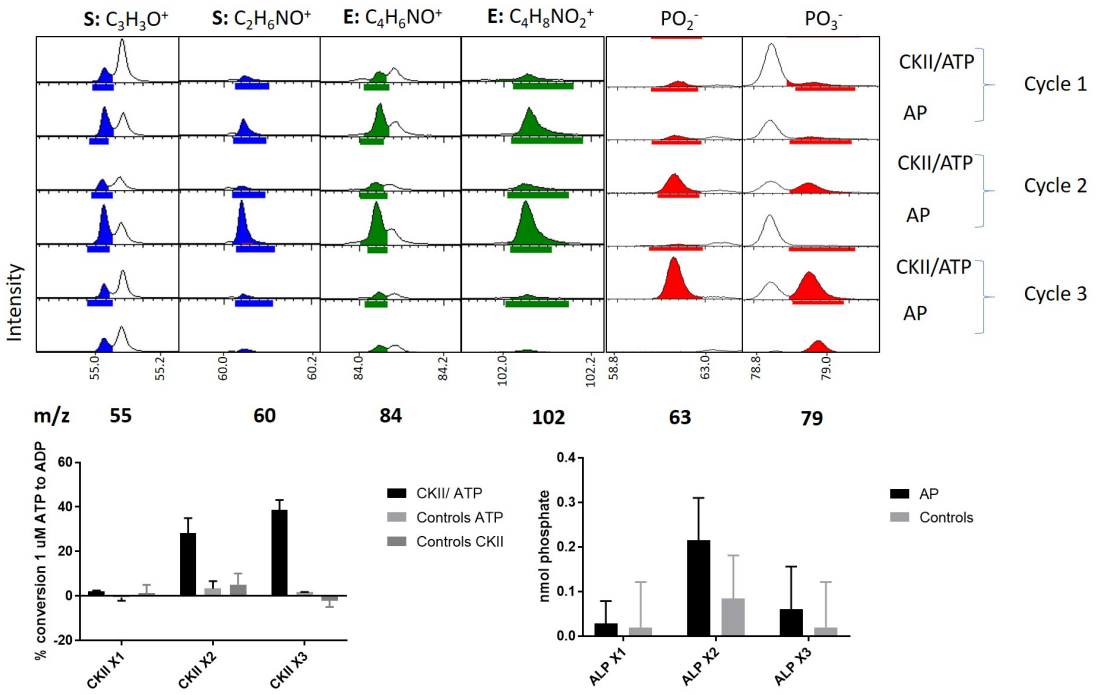


Figure 4.12: ToF SIMS spectra of surfaces modified with S:E (1:1) that have undergone three subsequent incubations with the enzymes CKII/ATP and AP, normalised to total ion count (top), ADP-Glo assay performed after incubation of samples with CKII and ATP(bottom left) and Phosphate assay performed after incubation of samples with AP(bottom right)

Table 4.5: Table of ion intensities attributed to phosphate normalised to total ion count for samples incubated with three cycles of CKII then ATP. Each 3 x 3 mm area was split into four 1.5 x 1.5 mm areas and the ion intensities determined by the software, normalised and averaged (n=4). One way ANOVA with multiple comparison was used for the statistics. Significant values shown are comparisons between themselves and the previous step.

Cycle	Ion count	
	PO_2^-	PO_3^-
CKII X1	$1.85*10^{-2}$ ± 0.0070	$1.31*10^{-2}$ ± 0.0057
AP X1	$1.71*10^{-3}$ ± 0.00050 ^{d}	$2.54*10^{-3}$ ± 0.00060 ^{a}
CKII X2	$6.23*10^{-3}$ ± 0.0025	$1.17*10^{-2}$ $\pm$ 0.0045 ^{a}
AP X2	$8.08*10^{-4}$ ± 0.00016	$1.38*10^{-3}$ $\pm$ 0.00031 ^{a}
CKII X3	$1.07*10^{-2}$ ± 0.0018 ^{a}	$2.16*10^{-2}$ $\pm$ 0.0038 ^{d}
AP X3	$4.73*10^{-4}$ $\pm$ 0.00016 ^{b}	$9.36*10^{-4}$ $\pm$ $9.55468*10^{-5}$ ^{d}

^{a}p<0.05 *

^{b}p<0.005 **

^{c}p<0.0005 ***

^{d}p<0.00005 ****

could affect the density of the polypeptide brushes on the surface which may effect the ability of the enzymes to interact with the polypeptides. It was necessary to determine if the enzymes CKII and AP could reversibly phosphorylate/dephosphorylate these substrates. The interactions were followed with Tof SIMS, ATP conversion and phosphate release (Figure 4.13). Unlike previously, phosphorylation occurs after the first incubation step with CKII/ATP with two phosphate ion peaks which are significantly reduced after treatment with AP. This is repeated for three cycles indicating that the present system is indeed a reversible enzyme responsive system. The cycles shown on the Tof SIMS data correlate to the assay data, with phosphate release measured well above the assay detection limit and for the first two cycles ATP conversion of 50 %. As observed in previous samples the amount of phosphate measured on the surface is lower than that detected in the supernatant after AP treatment.

Repeats of substrates with and without the FRET system have been carried out. Different batches of samples show different behaviour, with some phosphorylation/ dehosphosphorylation detected, however this is inconsistent and although reversible, is not always repeatable. There is no correlation between successful repeats and the different substrates (PEG vs BHQ initiated polymerisations) excluding this as a cause for the differences in behaviour. Variability could be introduced in the polymerisation step. In Chapter three, samples prepared from different batches were analysed by ToF SIMS and although serine and glutamic acid was present on all samples, the intensity and distribution varied. This indicates that there is variability introduced between batches of samples. This variability could affect three main factors that inturn may influence the ability of the enzymes to interact with the polypeptudes: polypeptide surface density, orientation and amino acid sequence. Diffusion of the enzyme to the polypeptide may be hindered if the polypeptides chains are closely packed on the surface, a change in orientation from the surface may inturn influence the NCA ROP chain growth during polymerisation and limit enzyme diffusion to the polypeptides. Given that all samples show phosphorylation, it is unlikely that amino acid sequence in the polypeptide chain is the main factor and it is likely due to limitations in accessibility to the polypeptide chains by the enzymes. As at least one cycle of phosphorlyation and dephosphorlyation always occurs, this suggests something has changed in the second cycle to prevent further enzyme interactions, for example the polypeptide does not return to it's original chemical or physical state where it had previously been shown to be able to interact with the enzymes. Furthermore the variability could arise from biological sources ie. the activity of the enzymes.

Table 4.6: Amount of phosphate bound on the surface after CKII incubation and the amount of phosphate cleaved from the surface. Determined by ADP-Glo and Phosphate assay, respectively, for copolymer S:E (1:1) modified substrates. (n=4)

Cycle	Phosphate on the substrate (ADP-Glo assay) (nmol)	Phosphate in supernatant (phosphate assay) (nmol)
1	0.14 ± 0.05	1.23 ± 0.09
2	0.26 ± 0.22	1.03 ± 0.10
3	0.03 ± 0.06	1.23 ± 0.09

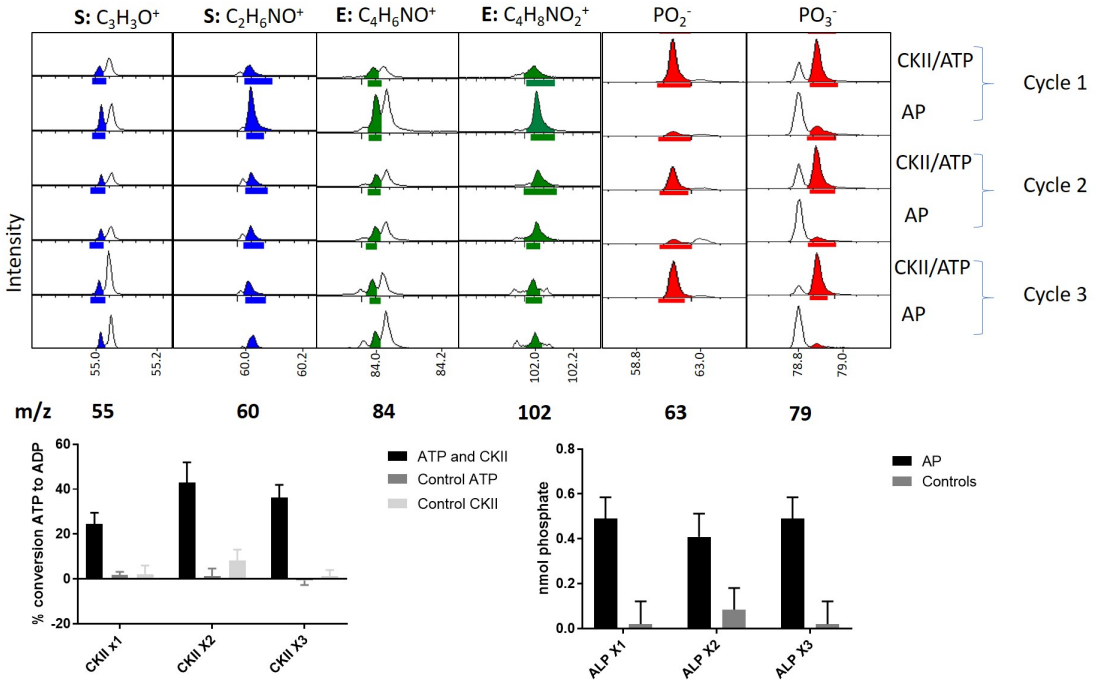


Figure 4.13: Monitoring of CKII/ATP and ATP induced phosphorylation and dephosphorylation of copolypeptide modified surfaces (S:E„ 1:1) using ToF-SIMS and spectroscopic assays. ToF SIMS spectra of ions attributed to amino acids and phosphate, normalised to total ion count (a) ADP-Glo assay (b) and Phosphate assay (c) after three cycles of incubation with CKII/ATP and AP for BHQ-Lysine initiated polypeptides.

4.3.5 Reversibility on the same sample monitored by ToF SIMS

The previous ToF SIMS data had been obtained by measuring six different slides that had been treated identically. It is assumed that each slide underwent a phosphorylation and dephosphorylation. To further support the phosphate and ADP-Glo assay, the same slides were measured with SIMS to monitor the presence/ absence of the phosphate peak. Three samples were analysed prepared in the same polymerisation batch and the most representative of the three spectra are shown in Figure 4.15. All three samples achieved one full cycle. In the second cycle they were able to be phosphorylated but dephosphorylation was not achieved. ADP-Glo and phosphate assay was also conducted at each cycle for the three samples (average for the 3 samples). AP activity was verified in solution with p-npp assay and the experimental units used were 24 U/mL. The assay data also correlates with no phosphate detected in the supernatant after the second AP incubation (Figure 4.14).

As previously observed, reversibility is not always achieved over multiple cycles. One full cycle is always achieved but multiple cycles vary with consistency between batches. A possible reason for this observation could be changing AP activities for different batches but frequent measurements of AP activity and adjustment of the AP dilution to obtain comparable enzyme activity for each experiment make this an unlikely explanation. Another explanation for the observed variability could be inhomogeneities in the composition of the polypeptides on the surfaces. Information on the sequencing of the amino acids in the polypeptide chain has not been obtained however, as all samples have been phosphorylated at least once and must therefore contain the required sequence. The frequency of available motifs in the chain does change between samples as indicated by the range of ATP to ADP conversion from 30 to 75 % between different batches, however there is no obvious correlation between ATP % conversion at cycle 1 with subsequent phosphorylation/ dephosphorylations. Surfaces have been characterised within the same batch of samples. Surfaces generated from different batches have not been directly compared, therefore it is possible that there are variations between batches. Variations such as chain length and packing density could affect enzyme access to motifs as well as available space for the polypeptide chain to alter conformation after enzymatic action. It is possible the reversibility is self limiting, meaning that after multiple cycles, the inter and intra molecular interactions prevent any further enzymatic action. More frequently it is the dephosphorylation step that is unsuccessful after two or three cycles. It is possible any residual ATP in the sample could be inhibiting the AP action. There are some early reports that glutamic acid can act as an AP inhibitor as a chelating agent of Zn^{2+} and Mg^{2+} which are cofactors, however the concentration of metal ions in the buffer solution should be sufficient to prevent this.

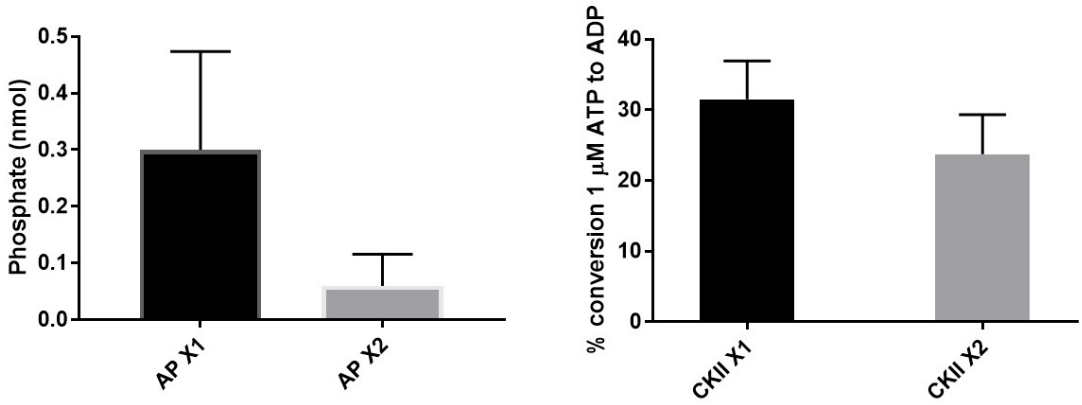


Figure 4.14: Assay data corresponding to ToF SIMS spectra for the same slides exposed to two cycles of enzyme incubation (CKII/ATP followed by AP) Left: Phosphate detected in supernatant. Right: Conversion of ATP to ADP.

4.3.6 Change in surface fluorescence with enzyme interactions with the polypeptide surfaces

Knowing that the modified substrates could be phosphorylated and dephosphorylated reversibly for at least one cycle is sufficient to proceed with the next step and to determine whether the enzyme induced changes could be monitored using the FRET system.

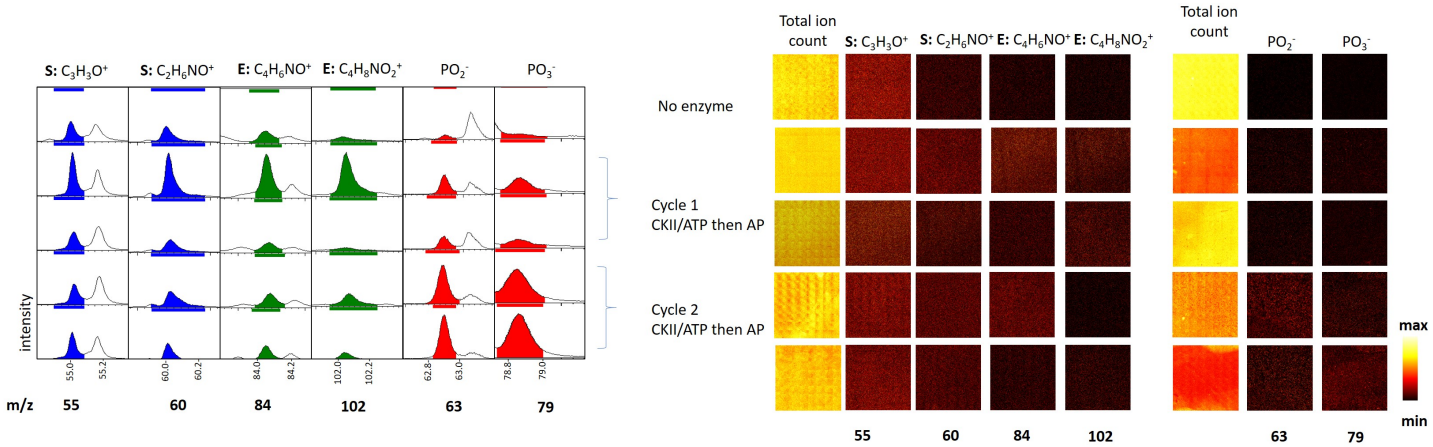


Figure 4.15: ToF SIMS of BHQ-1-Lysine initiated copolymers of S:E (1:1) incubated with enzymes CKII/ATP and AP for 2 cycles, presence of ion intensity attributed to phosphate was measured. The same slide was analysed at each step. Left: spectra normalised to total ion count. Right: Raster image 3 x 3 mm.

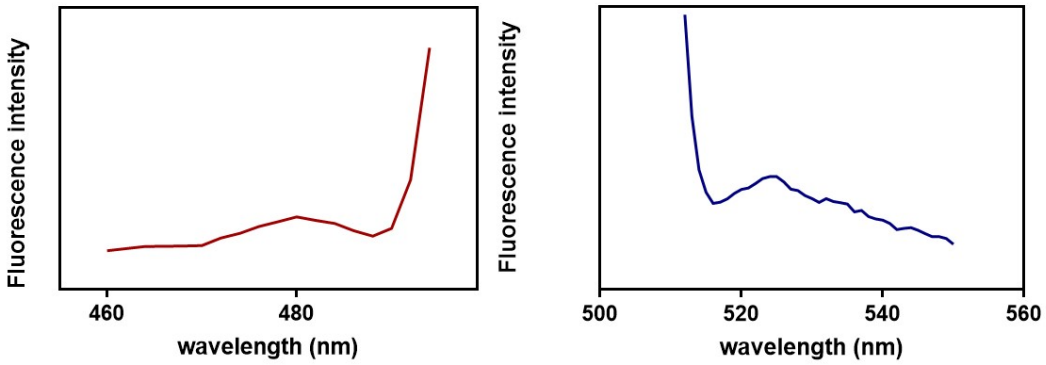


Figure 4.16: Excitation spectrum (left) and Emission spectrum (right) of fluorophore labelled surfaces modified with S:E (1:1) copolymer with BHQ-1-Lysine at the base of the polymer chain and fluorescein bound to the end of the chain. Fluorescence measured on the surface using z-scan to determine optimal Z-value.

Firstly it was necessary to verify that a fluorescent signal could be detected from the substrate and the optimal wavelengths need to be determined. A fluorescent plate reader was used for this. In solution fluorescein excitation and emission wavelengths are 485 and 535 nm, however it is possible this changes when the fluorophore is bound to the surface. A 3D scan was performed to determine at what wavelengths optimal signal was achieved. The optimal excitation wavelength was 480 nm and emission 527 nm, as can be seen in Figure 4.16. These wavelengths will be used for subsequent measurements.

Figure 4.17 illustrates the % change in fluorescence with three incubation cycles with the enzymes. It is clear the changes observed are not consistent between batches, with set A and B following a similar trend whereas C continually decreases. Focussing on A and B, there is an initial increase in fluorescence after ATP/CKII treatment, this would be as expected, as an increase in hydrophilicty on the chain may cause lengthening in aqueous environment increasing the distance between the quencher and the fluorophore thus reducing the quenching effects. On treatment with AP, the fluorescence decreases with removal of the phosphate group, thus increasing hydrophobicity which causes the chain to retract. A similar effect is seen in the second cycle, however on the third cycle the fluorescence continues to decrease after CKII/ATP treatment in both cases. This is consistent with the ToF SIMS data in a number of cases whereby after one or two cycles the reversibility is no longer apparent. Moreover with different batches as in the case of set C, there is only a decrease in fluorescence observed between treatments. For FRET to be effective the change in proximity of fluorofore to qencher has to be within a narrow distance range (10 to 100 Å). It is possible that after multiple switches the proximity between the BHQ and F no longer falls within this range, however as this observation is consistent with previous ToF SIMS data it is unlikely to be a specific issue relating to the fluorescence. As previously discussed, the absence of phosphorylation could be

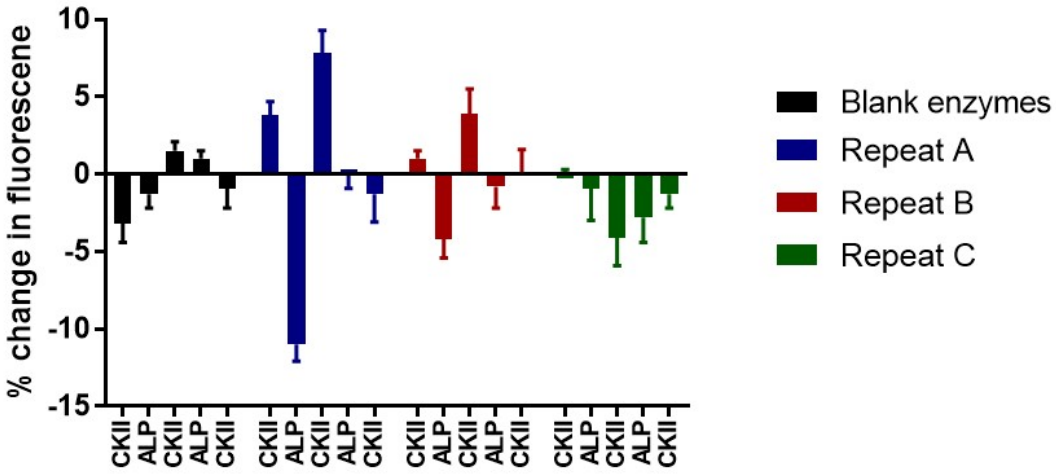


Figure 4.17: Change in fluorescence of a modified surface with copolymer S:E (1:1), with a BHQ-1-Lysine and fluorescein present. Fluorescence was measured on a plate reader at Exc_{480nm} and Em_{527nm} over multiple cycles of CKII/ATP and AP treatment for controls (black) and three batches of copolymer surfaces (n=4).

attributed to the loss of the availability of the active site to the enzymes after repeated phosphorylation/dephosphorylation.

4.4 Conclusions

The substrates prepared and characterised in chapter three have been treated with two enzymes, Casein Kinase II and Alkaline phosphatase. The substrates whereby the polypeptides were grown from the amine on the silane (APTMS) successfully underwent phosphorylation on treatment with CKII and ATP, as determined by ToF SIMS analysis. Subsequent treatment with AP did not change the amount of phosphate detected on the surfaces, even with prolonged inucbation, therefore AP was unable to dephosphorylate phosphoserines. It had been proposed as the polypeptide chain was in close proximity to the surface, that the enzyme was sterically hindered from accessing the motif, therefore no dephosphorylation was possible. An 18 chain PEG linker was introduced between the surface and the polypeptide; when these substrates were treated with CKII and ATP, phosphate was again observed on the surface and on AP treatment there was some reduction in phosphate detected but this was incomplete. Longer incubation had no further effect. The amount of AP was increased in future treatments to push the dephosporylation to completion. The phosphorylation/dephosphorylation was further confirmed using an ADP-Glo assay, to measure ATP to ADP conversion, and a phosphate colorimetric assay to measure cleaved phosphate in the supernatant.

We had successfully developed a system which underwent a reversible change on action of stimuli by the two enzymes. To be a repeatable reversible system, it was of interest

to see if the substrate could undergo multiple cycles of phosphorylation and dephosphorylation. This was investigated for the PEG initiated samples as well as those with a BHQ-1-Lysine incorporated onto the surface as the initiator. Both surfaces demonstrated some repeated reversibility on cyclic enzyme treatments and this was confirmed with ToF SIMS, ADP-Glo and Phosphate assay. The substrates always underwent at least one cycle, often two or three, however this wasn't consistent between batches. AP treatment was always the limiting step. The FRET system detected changes in fluorescence on action of the two enzymes. A similar trend was observed from the ToF SIMS data whereby a change in intensity of fluorescence was observed in the first and sometimes second cycles.

Chapter 5

Cell interactions with enzyme responsive materials

5.1 Introduction

In previous chapters we have determined that we can synthesise enzyme responsive surfaces that respond reversibly to treatment with Casein Kinase (CKII) and Alkaline phosphatase (AP). The aim of this work is to be able to monitor conformational changes on the action of cell secreted AP in the presence of CKII. Therefore, when choosing a cell type to culture on the surfaces it was important that they are capable of secreting AP. Cells that undergo osteogenesis were therefore a sensible choice as AP is involved in bone formation [204].

Mouse primary calvarial cells (MPCs)

Mouse primary calvarial cells are neonatal osteoblasts that undergo osteogenesis to differentiate into mature osteoblasts. This maturation is accompanied by the expression of certain markers; RUNX2, osteocalcin, osteopontin and AP [205,206]. As these cells proliferate, they synthesise a mineralized collagen matrix, and are an excellent experimental model to test how specific factors (biochemical and biomechanical cues) may affect this process [207].

They have not been reported as being cultured on enzyme responsive surfaces, nor have they been investigated to provide AP (via cell secretions) to interact with enzyme responsive substrates.

5.1.1 Aims

In order to be able to monitor any conformational changes on action of enzymes in the presence of cells, it is important to assess whether the substrates can support cell culture, whether these cells undergo osteogenesis and if they secret AP (the target enzyme). The aims of this chapter are as follows and summarised in Figure 5.1:

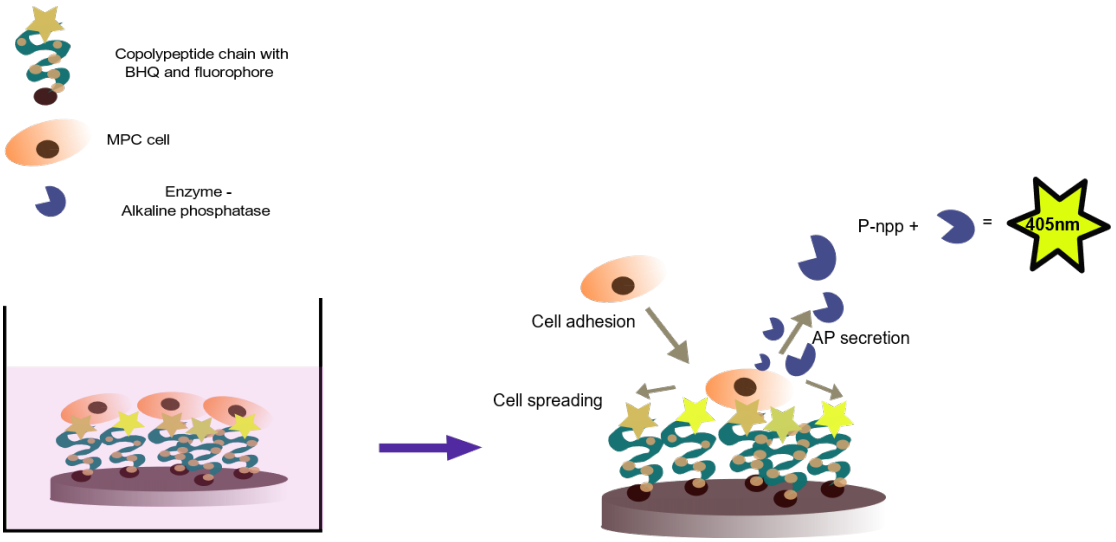


Figure 5.1: Illustration of the culture of MPC cells on the modified surfaces and their subsequent attachment, spreading and secretion of AP which will be monitored and measured in this chapter

• MPC's will be cultured on homopolymer and copolymer surfaces with and without the FRET system to test for adherence, proliferation and cell survival compared to controls of tissue culture plastic, glass and Fibronectin coated coverslips.

• Osteogenic markers RUNX2 and AP will be monitored of MPC's cultured on the surfaces, to determine whether cells undergo osteogenesis on the modified surfaces and secrete the target enzyme AP.

• MPC survival in the presence of CKII will be studied as CKII is an intracellular enzyme.

This preliminary cell work will be a basis to determine whether the surface and cell type are compatible to investigate cell secreted enzyme (AP) surface interactions in the presence of CKII.

5.2 Methods

5.2.1 General Mouse primary calvarial (MPC) cell culture

MPC cells were isolated in the lab (passage 3) (1 mL) and stored in the cryostore. the cells were were reanimated in 10 mL of warmed α MEM culture and expansion media; α MEM (440 mL), Foetal bovine serum (FBS) (50 mL), Penicillin/Streptomycin (5 mL) L-Glutamine (5 mL). The solution was centrifuged at 300g for 5 minutes, after which the supernatant was removed and the cells were reanimated in fresh media and transferred to a T75cm^3 and incubated at 37 °C. Cells were incubated until they reached 80-90% confluency (3 - 4 days).

5.2.2 Seeding

Glass substrates were placed in a 24 well plate and covered in 500 µL of ethanol for 30 minutes after which the samples were washed in PBS three times. Depending on the experiment a number of glass coverslips were incubated with 100 µL (5 µg /mL) of fibronectin for 20 minutes and then washed with PBS three times.

Media was removed from confluent flasks and cells washed with phosphate buffered saline (PBS). This was then removed, trypsin/EDTA (2 mL) was added and the flasks were incubated at 37 °C for 4 minutes. Trypsin was deactivated with the addition of media (3 mL) and the sample was then transferred to a centrifuge tube and centrifuged at 300 g for 5 minutes. After which the supernatant was removed and the remaining pellet was resuspended in 1 mL of primary bone media (Culture and expansion media with the addition of L-ascorbic acid, 50 µg / mL, β-glycerophosphate, 50 mM and dexamethasone, 10 µM). A heamocytometer was used to determine the number of cells. Substrates were placed in wells and 20 000 cells / well were seeded followed by the addition of 500 µL of primary bone media to each well. The plates were slowly oscillated by hand to ensure even distribution and then incubated at 37 °C and 5 % CO_2.

5.2.3 Cell Titer blue assay

Cell Titer blue assay (Promega) was used to follow MPC proliferation. A Calibration curve was developed by adding a known number of MPC cells (150 000, 100 000, 50 000, 25 000, 12 500, 7 250, 3 625, 0) in each well. Each condition was performed in triplicates. Cells were incubated for 4 hours at 37 °C before being incubated with Resazurin reagent and media in a ratio of 1:5. Fluorescence intensity was measured at Excitation 560 nm/ Emission 590 nm at 1, 2 and 3 hours. Linear regressions were performed for each concentration / fluorescence intensity dataset. The dataset with the best linear relationship was used in future work for the incubation time (2 hours) (Figure A.18).

The cells seeded on the substrates were incubated with 1:5 ratio of resazurin to media at day 1, 3 and 7. Each incubation step was 2 hours after which 100 µL were removed and added to a 96 black well plate and fluorescence intensity was measured on the plate reader (Tecan Spark). After which the remaining reagent on the cells was removed, the cells were washed with PBS and 500 µL of media was added. The same samples were monitored at each time point.

5.2.4 RUNX2 staining

At day 3 media was removed and samples were washed in 2 mL of PBS/well. Samples were incubated in 200 µL of fixative solution (3.7 % paraformaldehyde in PBS) for 20 minutes. The samples were washed in 3 x 2 mL PBS and stored at 4 °C.

Samples were permeabilised in 100 µL permeabilisation solution (0.1 % v/v Triton X-100 in PBS). Samples were washed 3 x 5 min in PBS (1 mL/sample/wash). Samples were then incubated with 200 µL of blocking solution (3 % in goat serum diluted in 1 % BSA/PBS) for 30 minutes. This was removed and washed in 1 % BSA/PBS 3 x 5 min wash (1 mL/ sample/wash). Rat anti human RUNX2 CBFA1 monoclonal antibody solution was prepared in BSA/PBS 1 % (1:200 dilution) was added to all wells but secondary antibody controls to which just BSA/PBS 1 % solution was added. They were incubated overnight at 4 °C.

The following day the primary antibody solution was removed and samples were washed in 3 x 5min in 1% BSA/PBS (1 mL/sample/wash). Goat anti-rat secondary antibody (Alexafluor546) was diluted 200:1 in 1% BSA/PBS. Samples were incubated for 2 hours at room temperature then washed in 3 x 5min wash (1 mL/ sample/wash).

Samples were then incubated in Hoechst solution (1:200 dilution in PBS) for 15 minutes then washed 3 x 5 min in PBS. Samples were then stored in PBS (500 µL) and imaged under a microscope (see section 2.27 Microscopy below for details).

5.2.5 AP assay

At time points 1, 7 and 14 days of culture, media was removed from wells, cells were washed with PBS and replaced with media (400 µL) containing paranitrophenolphosphate (pnpp) (0.5mM). Samples were incubated for 60 minutes at 37 °C and absorbance was read at 405 nm. A pnpp calibration curve was used to determine the amount of enzyme present after one hour (Figure A.9). Blank measurements from media with pnpp was subtracted from all samples. One way ANOVA was used to determine any significant differences between samples.

5.2.6 Cytotoxicity assay

Multiflox cytotoxicity assay (Promega) was used to determine the effects of the addition of CKII into the culture media on cell survival. A calibration curve was made by incubating known amounts of live and dead cells with the reagents Samples (with 100, 95, 90, 75, 50, 25, 10, 5 and 0 %) live cells were prepared with the remaining % made up of dead cells. Samples of live cells were incubated with Tween-20 (0.1 % v/v in PBS) for 10 minutes, centrifuged at 300 g for 5 minutes, the supernatant was then removed and (1 mL) of fresh media was added. The number of dead cells was determined with Trypan blue staining whereby 5 µL of Trypan blue was mixed with 5 µL of cell solution in media and the mixed solution was loaded onto a heamocytometer. Cells stained blue were counted as dead cells. Trypan blue staining was also performed for the sample of live cells. Samples were incubated with the reagents for 60 minutes at 37 °C in a 96 black coated well plate, then read on a plate reader at Excitation 405 nm/Emission 510 nm (live) and Excitation 485 nm/Emission 520 nm (dead).

1:1 (S:E) coated substrates were incubated with different amounts of CKII (0, 4, 10 and 20 Units/mL) for two days before cytotoxicity measurements. At this point the media was removed and samples were incubated with 100 µL of reagents with 400 µL of media. 100 µL was transferred after 60 minutes incubation to a black coated 96 well plate and fluorescence measurement was taken on the plate reader at Excitation 405 nm/Emission 510 nm (Live) and Excitation 485 nm/Emission 520 nm (Dead).

5.2.7 Microscopy

Nikon eclipse TS100 was used to view cells through culture and for brightfield imaging (Nikon Instruments UK). Fluorescent images were taken on the Leica DM IRB microscope (Leika UK). 5 images/sample were taken with minimum n=4 per sample, a representative image of the average/sample type has been shown in this chapter.

5.2.8 Analysis software

Image J

Fiji Is Just Image J win64 Java 8 was used to analyse the cell images. The fluorescence images were false coloured and overlaid. The cell counting was manually performed, cells on the edge of the images were counted as were round cells (as cells were counted at time 1 and 2 hours after seeding). The percentage surface coverage was determined using ROI manager and manually selecting the cell covered areas.

5.2.9 Graphpad

Graphpad Prism 7 was used to determine statistical significance using one way ANOVA, multiple comparison in cell proliferation, cell attachment and cell coverage measurements significance set at 95%. Linear regression was used for the calibration curves for Cell Titer blue, AP assay and Multiflox Fluor assay.

5.3 Results and discussion

5.3.1 Adhesion and proliferation

To test the modified surfaces as suitable supports for cell culture MPC's were seeded onto the substrates and washed at time 1 and 2 hours with PBS. The supernatant was removed and any cells that were in suspension were counted using a heamocytometre however the numbers were too low to be statistically significant (< 20 was the maximum counted). Microscopy images were taken of the substrates (Figure 5.2 (Images of Glass and TCP controls can be found in Figure A.19) and cell numbers were counted using imageJ software (Table 5.1). All images display the cells as rounded as they have undergone stress during the passage and seeding process. There are significantly more cells

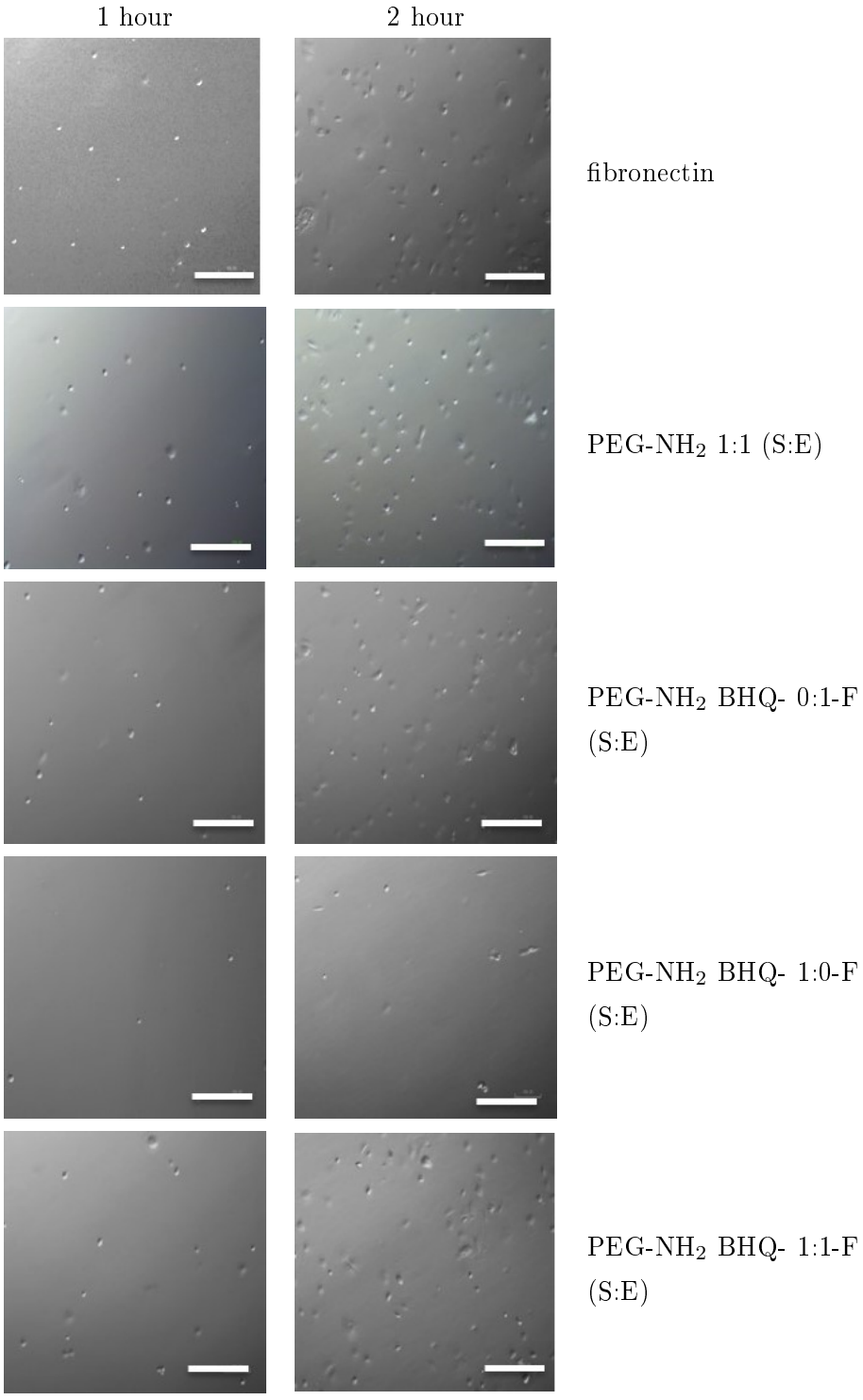


Figure 5.2: Brightfield images of MPC cells seeded on fibronectin coated surfaces as well as co and homopolymer modified surfaces of serine and glutamic acid at 10 X magnification, scale bar 100 µm (n=5)

Table 5.1: The number of MPC's adhered to control (fibronectin, glass and TCP) and polypeptide surface of varying composition after 1 and 2 hours incubation after seeding (n=5) .

	1 hour substrate	2 hour substrate
Fibronectin	14 ±3	53 ±11
Glass	121 ±15	115 ±23
TCP	17 ±4	46 ±8
PEG-NH_2 S:E 1:1	15 ±4	39 ±8
PEG-NH_2 BHQ- 0:1-F	16 ±5	53 ±16
PEG-NH_2 BHQ- 1:0-F	3 ±5	9±5
PEG-NH_2 BHQ- 1:1-F	13 ±6	67 ±17
PEG-NH_2 BHQ- 1p:1-F	17 ±7	68 ±18

present on the glass samples than the other substrates after 1 hour incubation, indicating the cells have better adherence on the glass coverslips than the modified samples. This observation persists after 2 hours, even though the number of cells on the glass samples did not increase significantly as opposed to all other samples were a marked increase in cell numbers was observed. One further exception was the serine homopolymer modified substrate that had a significantly lower number of cells adhered to the surface with no significant increase between time 1 and 2 hours. The other variation of copolymer samples exhibited similar cell adherence at both time points with no significance difference between themselves and between the controls Fibronectin and TCP.

MPCs cultured on the controls and substrates were monitored and imaged at day 1, 3 and 7 (Figure 5.3) Glass and TCP control images can be found in Figure A.20 . The elongation of the cells and increased surface coverage over time is an indicator that the substrates are effective at supporting MPC culture. There is no qualitative difference between the 1:1 (S:E) substrates with and without the introduction of the BHQ and fluorophor nor with the phosphorylated samples with close to 100% surface coverage and elongated cell morphologies at day 7. Homopolyserine substrate has very low cell surface coverage with predominantly rounded cells, glutamic acid homopolymer has lower surface coverage than the copolymers, with some elongation of cells, however some rounded cells are also present on the surfaces. These images indicate that the homopolymer substrates are less suited to supporting MPC culture than the controls and the copolymers. The WCA of the substrates is not significantly different to the copolymers so it is unlikely this is a contributing factor. It is possible the thickness, polymer chain length and density on the surface are contributing factors to these effects.

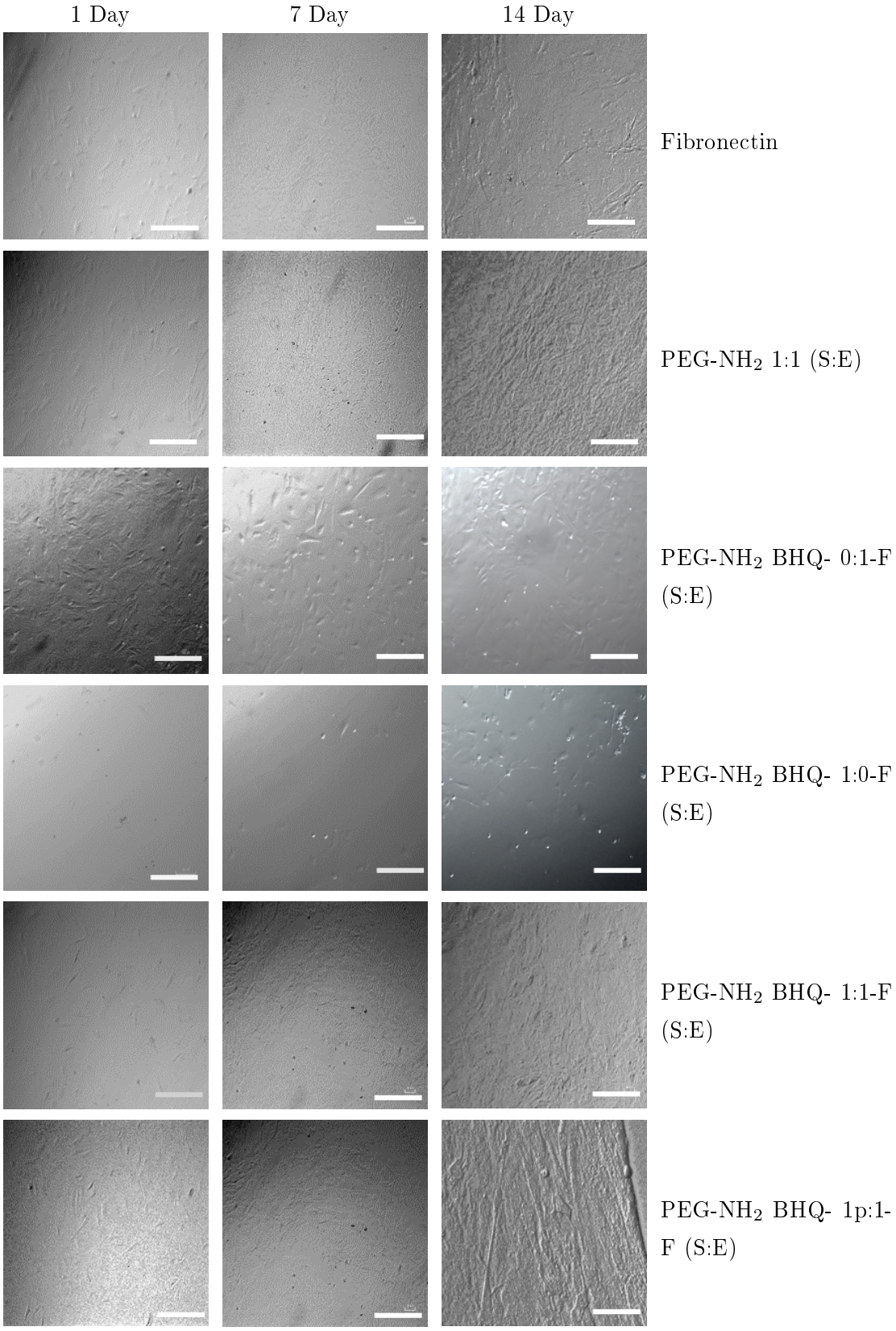


Figure 5.3: Brightfield images of MPC cells seeded on control substrates as well as co and homopolymer modified surfaces of serine and glutamic acid at 10 X magnification, scale bar 100 µm (n=5) at day 1, 7 and 14.

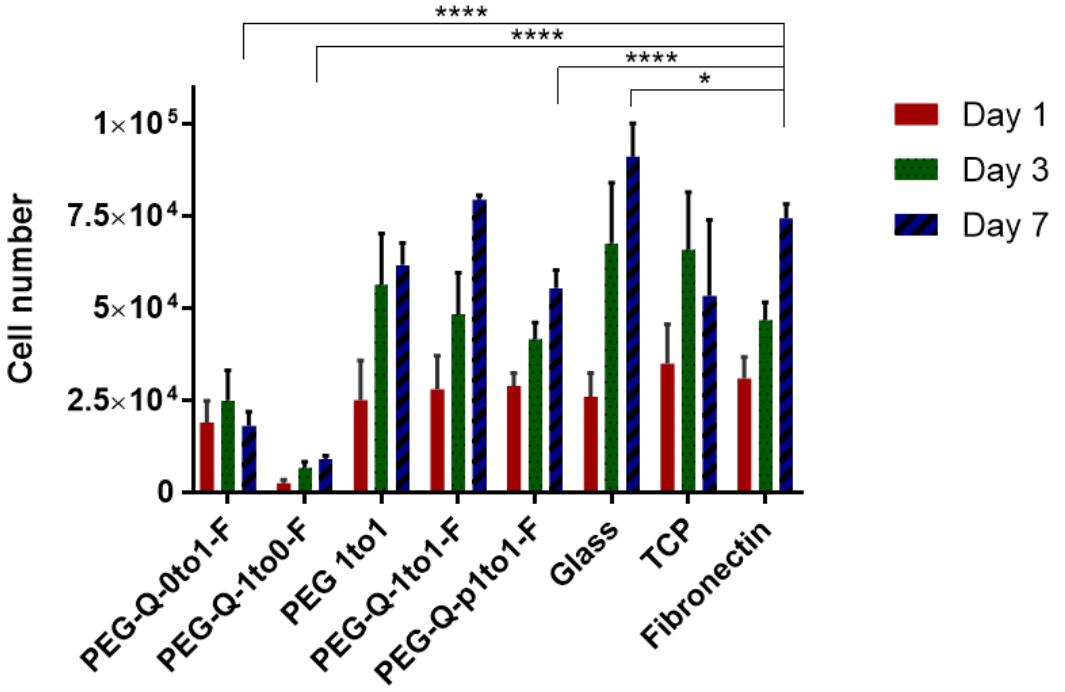


Figure 5.4: Cell number as determined using resazurin assay on different controls and polypeptide substrates at time 1, 3 and 7 days. One way ANOVA carried out to determine significance compared to the fibronectin control sample (*<0.05, ****<0.00005) error bar=SD (n=5)

5.3.2 Cell proliferation assay

The ability of MPC cells to proliferate on the modified surfaces and controls has been monitored over time (up to day 7) using a resazurin based colorimetric assay. This is an indicator as to how suitable the surfaces are to support cell culture. Resazurin is reduced to resofurin by $NADH/H^+$ to yield a pink product that fluoresces at Exc_{560}/Em_{590} nm. It is a measure of cell metabolism, which is an indicator of the number of cells present; however, it cannot distinguish between bacterial and mammalian cells. The assay works by comparing intensity values in cell culture populations with a calibration curve prepared with known cell numbers (Figure 5.4). The cells used for the calibration curve were cultured for 4 hours (the point at which cell spreading was observed) before any reagents were added. This was to reduce any variations in cell metabolism introduced due to the stressed state of the cell after passaging.

The cell number correlates to the images in Figure 5.3 with the two homopolymers having significantly lower number of cells than the controls ($p<0.0001$ ****). The copolymer and control surfaces show an increase in cell number with time indicating cells are proliferating on the substrates. At day 7 the number of cells on the copolymer substrates was much lower on PEG 1:1 and PEG-Q-1:1-F surfaces compared to Fibronectin samples however the phosphorylated samples do have significantly lower numbers of cells compared to the controls and the equivalent non-phosphorylated sample.Importantly, these

results indicate that the change in surface properties upon phosphorylation are sufficient to induce a noticeable change in the proliferation of MPCs. A One Way ANOVA analysis of the three copolymer substrates yields a significantly higher number of cells on the PEG-Q-1:1-F compared to PEG 1:1 and PEG-Q-p1to1-F, however no significant difference was observed between PEG 1:1 and PEG-Q-p1:1-F.

5.3.3 Osteogenic markers

Runt related transcription factor (RUNX2)

The aim of this work is to be able monitor conformational changes on the surface optically in situ by cell secreted enzyme AP in the presence of CKII. It is therefore integral that the cells secrete AP, in MPCs this will occur when the cells undergo osteogenesis. RUNX2 is an early osteogenic marker that is a transcription factor, essential for osteoblastic differentitation [208]. Immunohistochemical staining was used to stain the samples for RUNX2 expression which were imaged under a fluorescent microscope. Figure 5.5 shows MPCs cultured on control and polypeptide substrates. A nucleus stain Hoescht (blue) marks the distribution of the cells, Alexafluor546 tagged secondary antibody provides visual marker of RUNX2 expression in the cells (red) . These images have been overlapped. Glass and TCP control images can be found in Figure A.21.

RUNX2 is detected on cells cultured on all substrates. An early indicator that the cells on all substrates were undergoing osteogenesis. As the cells are cultured in osteogenic media, it is likely any surface effects would be dampened by the effect of the media.

Alkaline phosphatase secretion

AP is an osteogenic marker, found in intra and extracellular environments. It is one of the target enzymes in the enzyme reversible system developed in chapter 3 and 4, therefore monitoring the amount of AP secreted at different time points by the cells is important in order to determine the optimum time to test the reversibility of the polypeptide surfaces in the presence of cells. Comparing the amount of AP secreted by the cells with the minimum amount that has been added by an operator (in Chapter 4) for dephosphorylation is also important to ascertain whether concentrations of cell secreted AP by cells will be sufficient to induce a similar material response. The controls and polypeptide modified surfaces seeded with MPC cells were incubated in buffer containing pnpp at days 1, 7 and 14 for 1 hour. The conversion of p-npp to p-np by AP was measured on a plate reader at 405 nm (Figure 5.6).

AP activity in the cells supernatant after 1 hour incubation is shown in Figure 5.6. The controls and the copolymers with the FRET pair on the substrate have the maximum amount of AP secreted at day 14, this is consistent with data in the literature whereby AP secretion increase from day 7 and peaks at day 14. The copolymer with the FRET

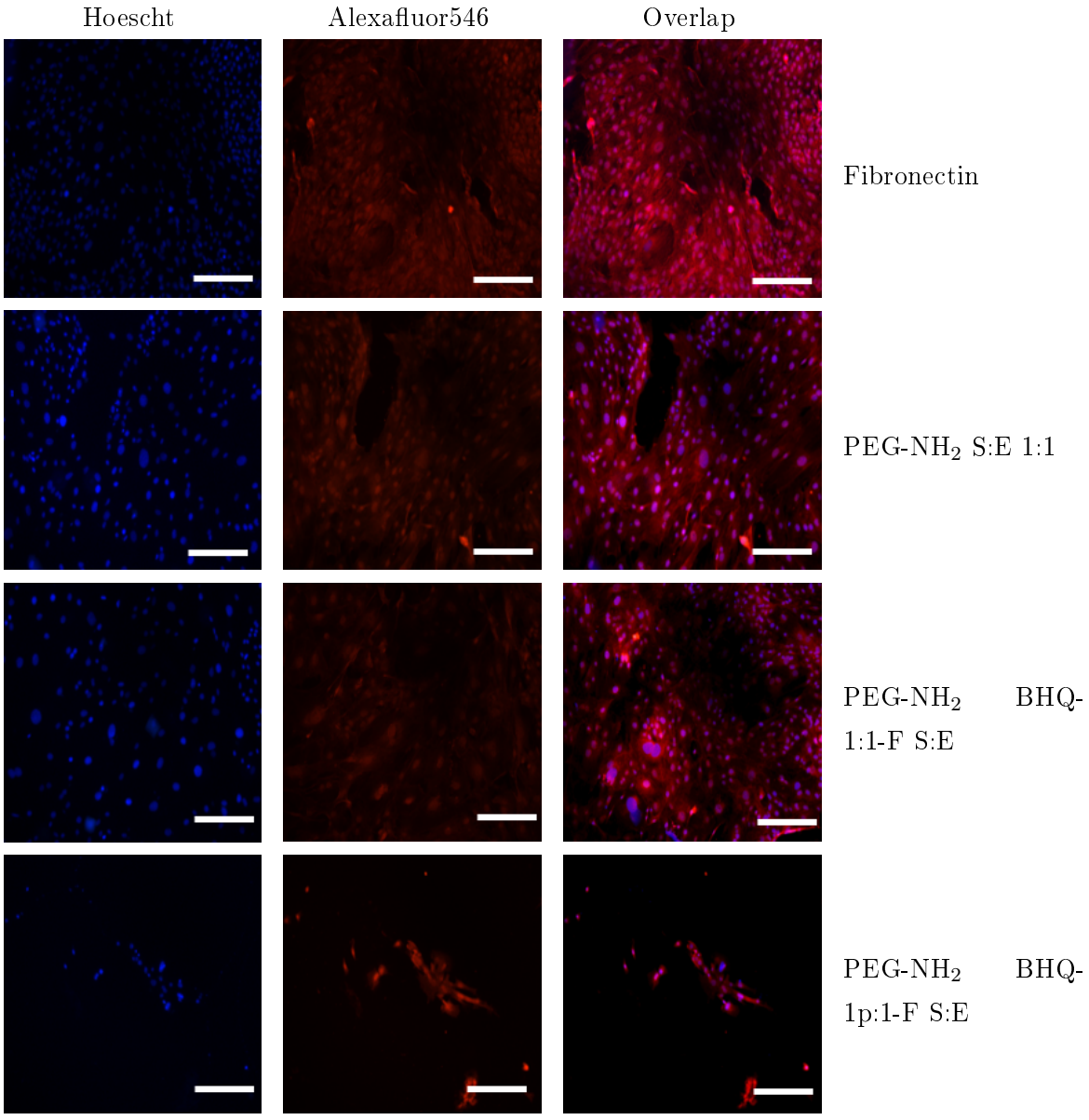


Figure 5.5: Images of cells stained with Hoechst (nucleus stain) and Goat anti-rat secondary antibody-Alexafluor546 (RUNX2 stain) seeded on copolypeptide of serine and glutamic acid in a 1:1 ratio and control surface at 10 x magnification (n=5) at day 3. scale bar = 100µm

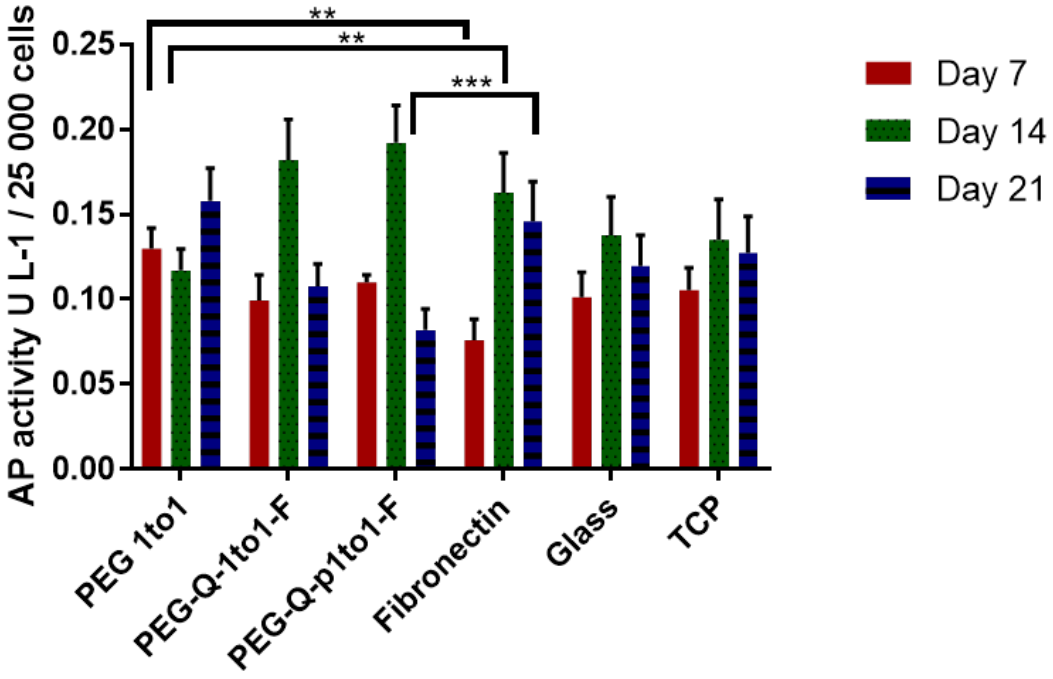


Figure 5.6: AP activity detected in supernatant after 60 minutes incubation with pnpp (0.5 mM) normalised to cell number (as determined with Cell Titer blue assay). One Way ANOVA compared to Fibronectin substrate with error bars=SD. A/V/T U = amount of enzyme to generate 1 µM of pnp in 1 min in 1 mL (n=4)

pair shows no significant difference between the phosphorylated and unphosphorylated samples indicating phosphorlyation of these samples has no effect on AP secretion by the MPCs. AP secretion is significantly lower between these samples and fibronectin at day 21 ($P<0.0005$). There is no difference between the three controls. Day 14 is therefore the best time point to measure any conformational changes as a result of phosphorylation/dephosphorylation on action of AP.

The maximum AP active units of enzyme secreted by the MPCs 300 U/mL/sample is higher than the units that have been required for dephosphorylating the phosphoserines on the surface, 24 U/mL (Chapter 3). Therefore the activity present in the supernantant should be sufficient to dephosphorylate the substrates.

5.3.4 Cell viability in the presence of CKII

Casein Kinase II is an intracellular enzyme, therefore within this system will need to be added into the supernatant to observe any reversible enzymatic mediated interactions with the substrate. It was investigated as to whether the cells were affected by the addition of different amounts of CKII and to find any threshold, if appropriate. The amount of CKII used was based on units used in chapter 4 which induced surface phosphorylation. MPCs were incubate for 2 days with the enzyme and cell morphology and number

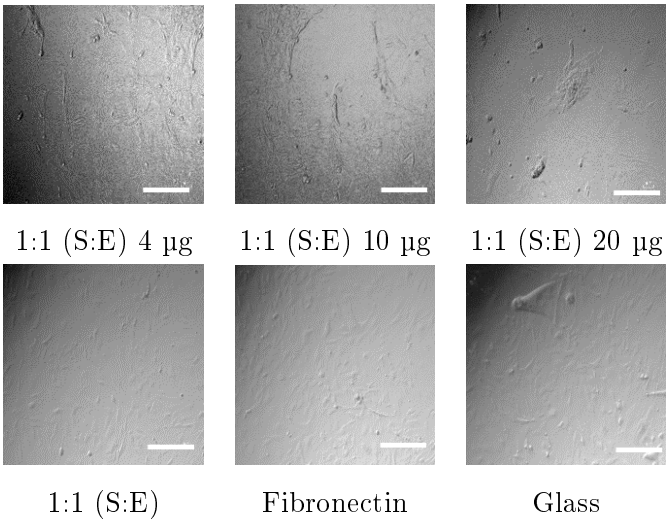


Figure 5.7: Brightfield images of cells incubated with different amounts of CKII for 2 days on copolymer modified surfaces and controls of fibronectin and glass (n=4). Scale bar = 100µm

was monitored by microscopy. Resazurin assay, viability assay and osteogenic ability were determined.

In the brightfield images shown in Figure 5.8, the cells in the two concentrations 4 and 10 U/ mL are elongated and there is good surface coverage like with the controls whereas for the 20 U/mL sample the cells are rounded and there is lower surface coverage indicating the cells are undergoing stress.

The Resazurin assay is in agreement with the images, with the substrate incubated with 20 U/mL having significantly lower cell number than the other samples. Indicating cell survival is negatively affected by the addition of 20 U/mL of CKII, whereas there is no difference measured between the 4 and 10 U/mL samples.

A Cell viability assay which can directly measure the number of live and dead cells was used to determine the toxic effects if any of MPC culture in the presence of different amounts of CKII. The number of live and dead cells is determined using a fluorescence assay with two fluorescent probes that are added into the cell culture together GF-AFC and Bis-AAF-R110. Firstly the cell permeable probe glycyl-phenylalanylamino fluorocoumarin (GF-AFC) fluoresces only after an intracellular protease cleaves the GF from the AFC which then fluoresces at Excitation 400 nm/Emission 505nm. This is an indicator for live cells. Simultaneously a non cell permeable compound, bisalanyl-alanyl-phenylalanyl-rhodamine 110 (Bis-AAF-R110) can be cleaved by a dead cell protease to release R110 that fluoresces at Excitation 485 nm/ Emission 520 nm.

Sensitivity of MPC's to the assay was determined and a calibration curve was made by incubating the reagents with known amounts of live and dead cells (Figure A.16 and Figure A.17). This was used to quantitatively determine the number of live and dead

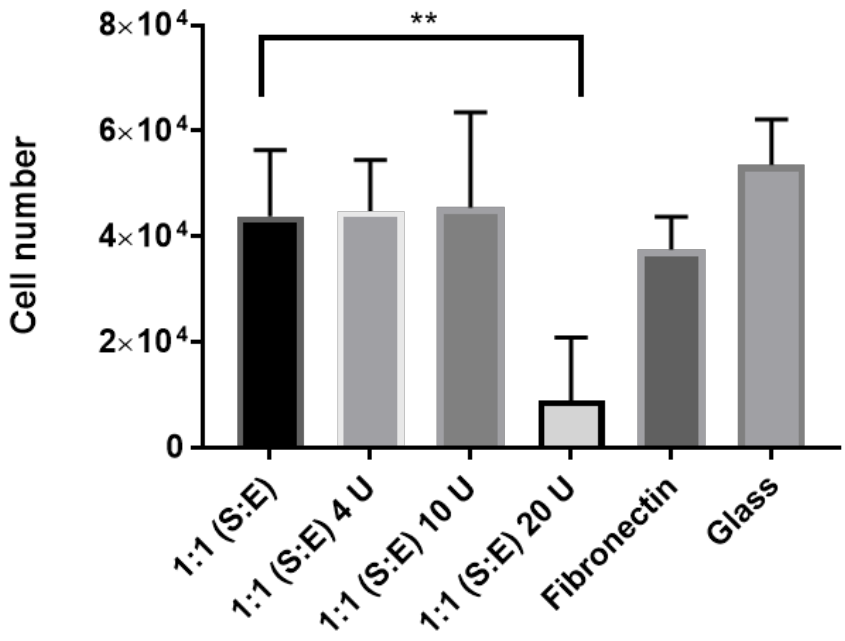


Figure 5.8: Cell number as determined using resazurin assay on different substrates after 2 days incubation with CKII in different concentrations. One way ANOVA test carried out to determine significance compared to control, 1:1 no enzyme. (n=5)

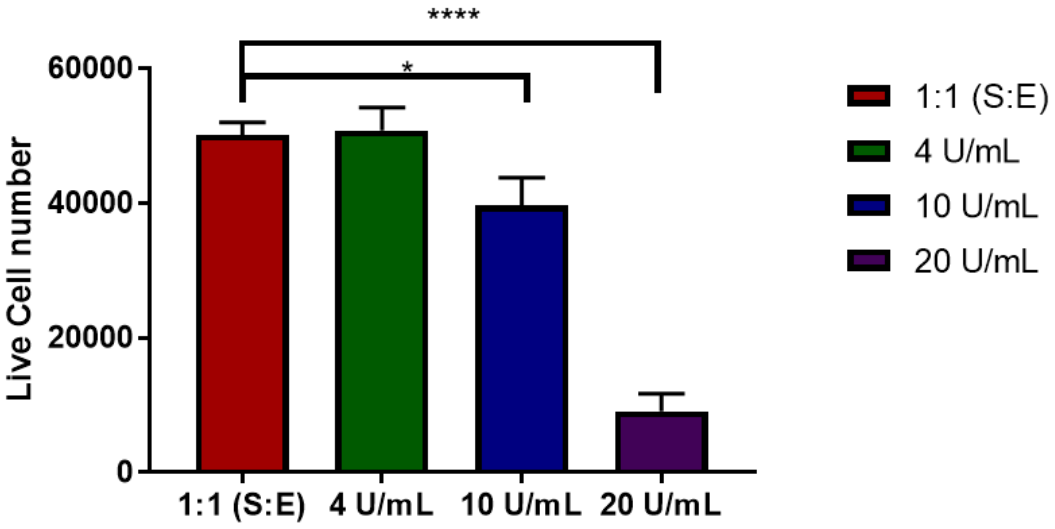


Figure 5.9: Live cell detected at Excitation 400 nm/ Emission 505 nm for detection of AFC fluorescence for MPCs seeded onto copolymer substrates incubated with different amounts of CKII. Statistics used: One way ANOVA, multiple comparison to 1:1 (S:E) error bars=SD of n=4

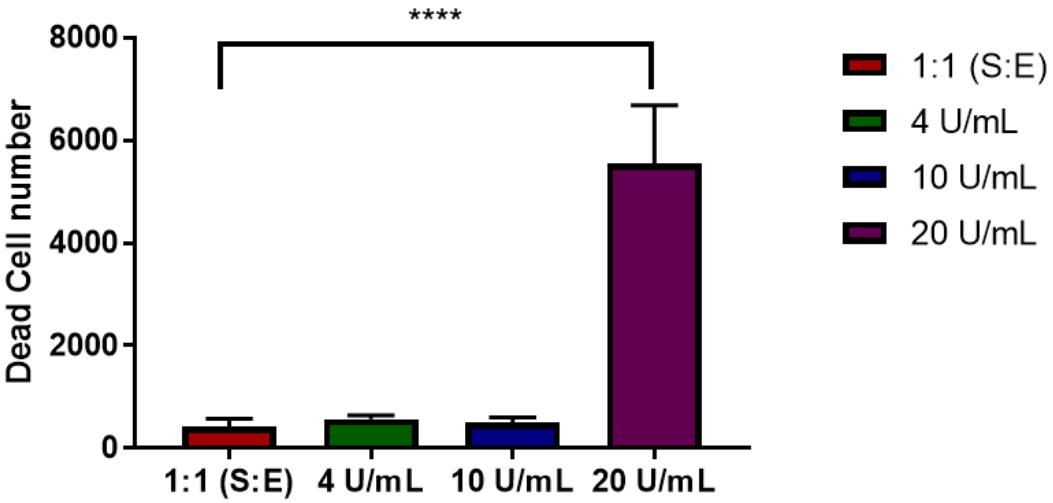


Figure 5.10: Dead cells detected atExcitation 400 nm/ Emission 505 nm for detection of R11O fluorescence for MPC's seeded onto copolymer substrates incubated with different amounts of CKII. Statistics used: One way ANOVA, multiple comparison to 1:1 (S:E) error bars=SD of n=4

cells in the culture. Firstly Figure 5.9 shows the number of live cells detected. CKII concentration of 4 U/mL has no effect on cell viability compared to controls whereas there is a significant difference between the copolymer substrate incubated with 20 U/mL of CKII ($p<0.00005$) and the 10 U/mL ($p<0.05$) when compared with the control sample with no enzyme. Significance is only detected in the 20 U/mL samples when measuring the dead cell fluorescence probe (Figure 5.10). The negative effect on cell viability at 20 U/mL is consistently apparent between the three different techniques (imaging, cell titer blue and viability asssay). Whereas at 10 U/mL it is only the live cell probe data that indicates a significant difference between the copolymer with and without presence of 10 U/mL of enzyme. This is not observed for the dead cell probe nor on the cell proliferation assay. This indicates at this concentration there is a negative effect on cell viability however this is a weak effect, especially when compared to the effects of 20 U/mL. The total number of dead and live cells detected for the 20 U/mL sample is lower than the initial seeded number, this can be accounted for by the change in media to add in the detection reagents. It is likely some of the dead cells will have come away from the surface and have been removed in this step.

5.4 Conclusion

MPCs ability to adhere to the substrates was assessed first. The cells were equally able to adhere to the copolymer substrates as the controls, whereas the cells did not adhere well to the serine homopolymer. The cells were able to proliferate equally on the copolymer substrates as the controls and in keeping with the poor adhesion exhibited after 1 and

2 hours of seeding, the serine homopolymer had significantly lower number of cells on the surface. The cells were unable to proliferate on the homoglutamic acid substrate, even though it showed no difference in the initial adhesion tests when compared to the copolymers and controls indicating that the homopolymers were poor substrates for the culture of MPCs.

The cells cultured on all substrates expressed RUNX2 the early osteogenic marker, the amount of AP secreted was determined and the maximum was reached at day 14 with no significant difference determined between copolymers with FRET molecules on the substrate and the controls at this time point. Indicating the copolymer substrates were able to support MPC osteogenesis and the amount of AP secreted was sufficient to induce dephosphorylation based on work in chapter 4.

Cell viability was determined in the presence and absence of the enzyme CKII at different concentrations. Incubation with 20 U/mL caused a significant reduction in both cell number and viable cells. 4 U/mL showed no toxic effects whereas the samples incubated with 10 U/mL showed some mild toxicity in one of the assays but not consistantly so. This indicates tha 10 U/mL (the amount used in the enzyme experiments in Chapter 3) is the absolute limit and that lower amounts should be investigated for phosphorylation in future work to eliminate any potential toxic effects.

In conclusion the copolymer substrates, with and without the BHQ and fluorphor, can support MPC culture. MPCs cultured on these substrates undergo osteogenesis and secret AP and are able to proliferate and survive in the presence of CKII up to 10 U/mL. This is necessary preliminary data that can be used in future work to determine whether the substrate can undergo conformational changes on the surface in the presence of cells and with cell secreted AP.

Chapter 6

Conclusions and Outlook

The aim of this work was to develop a reversible stimuli responsive surface that can undergo reversible conformational changes on the action of enzymes. This was achieved by targeting enzymes Casein kinase II and Alkaline phosphatase that activate the phosphorylation and dephosphorylation of polypeptides containing a specific recognition sequence. We successfully designed polypeptides that respond to these enzymes. NCA-ROP in solution was an effective method to synthesise polymers containing serine and glutamic acid in different ratios. Full benzyl deprotection of the polymers was unsuccessful in solution so protected polymers were analysed. Good control over polymer conformation was achieved by monomer feed composition. The monomers were shown to favour reactivity with one another rather than themselves inferring an alternating copolymer was likely to be synthesised with a monomer feed ratio of 1:1 (S:E). This is an ideal situation for the enzyme responsive systems and provides us with the information required to decide on conditions for the translation onto surfaces.

The work in solution was translated onto a surface whereby the grafting from by NCA ROP was adopted to modify the surfaces. Surface functionalisation with an amine initiator was achieved in three different ways by silanisation with APTMS, with GOPTS followed by PEG diamine coupling and by coupling BHQ-1-Lysine to the PEG-amine. The three types of functionalised surfaces were able to initiate polymerisation from the surface for co and homo polymers of glutamic acid and serine by NCA-ROP. This was determined by significant changes to surface wettability (WCA), the presence of ion fragments on the surface attributed to S and E (ToF SIMS) and the change in the % contribution of C and N elements and the change in carbon environments on the surface (XPS). Unlike in solution, full benzyl deprotection was achieved as determined by significant reduction in the WCA and by the loss of ions attributed to benzyl group (ToF SIMS). Unfortunately, attempts to determine polymer conformation on the surface were unsuccessful by FTIR due to a poor signal to noise ratio.

It was determined whether the modified surfaces could support the culture of mouse primary calvarial cells (MPC)'s. There was no significant difference between cell ad-

hesion and proliferation for the copolymers and the control samples as determined by resazurin based cell proliferation assay and cell counting of microscopy images. The addition of the FRET pair inferred no obvious effect on cell survival and proliferation. No significant difference in osteogenic potential of the cells cultured on the polymer modified surfaces was determined between the control and copolymer samples. This was determined by immunohistochemical staining with RUNX2 and by detection of AP secretion (p-npp colorimetric assay). No cytotoxic effects were detected with cells cultured with $<$10 U/mL of CKII, whereas reduced cell viability, cell numbers and surface coverage was detected at a CKII concentration of 20 U/mL.

The suitability of the copolymer surfaces to undergo phosphorylation with CKII was measured. ToF SIMS (for presence of phosphate) and a luminescent assay following ATP consumption confirmed that surfaces were phosphorylated. It was determined in Chapter two that the alternating copolymer composition was likely present in polymers synthesised in solution, the fact that the enzyme acts on the polymer brush, infers that the required amino acid sequence S-x-x-E structure is present in the polymer chains formed on the surface. Dephosphorylation was confirmed after subsequent incubation of phosphorylated samples with AP by ToF SIMS (loss of phosphate) and a colorimetric assay that detected phosphate in the supernatant. We have developed the first reversible enzyme responsive surface.

Knowing we had developed a reversible enzyme responsive surface we then investigated as to whether the phosphorylation and dephosphorylation was repeatable over a number of incubation cycles. The process is repeatable up to three times, after which it deteriorates. There is also some variability between the samples in terms of the number of cycles that the process can be repeated. This is likely due to batch to batch variation of polymer density and chain length which can affect the availability of the motif to the enzymes. Some variability was demonstrated between batches with Tof SIMS measurements with variation in ion intensities attributed to serine, glutamic acid and PEG as well as some inhomogenous distribution of the ions across the surface.

The incorporation of the BHQ-1-Lysine and fluorescein in the copolymer chain was successful, in progress towards a non-invasive method to monitor surface changes on interaction of the enzymes. Detection of ion fragments that can be attributed to the molecules was observed on the surface (Tof SIMS analysis). The introduction of the probes had no obvious influence on cell behaviour with the parametres measured. Fluorescence was detected on the surface using a plate reader. An increase in fluorescence intensity was observed after sample incubation with CKII and a decrease was observed on subsequent incubation with AP. Comparable to the observations by techniques ToF SIMS and the solution assays, this effect was not consistently repeatable over a number of cycles. This infers that after a number of cycles the availability of the polypeptide to the enzymes is restricted, inhibiting any further interactions.

Even though there is variability, this is likely due to sample behaviour; the analytical tools are appropriate and, importantly, the fluorescence method is suitable to follow surface changes. Further investigations are required to determine the cause of this variability, this will be discussed in the next section.

To conclude, this is the first report of a reversible enzyme responsive surface. Polymerising from the surface by NCA ROP to develop an enzyme responsive surface is an important step in advancing the applications for this polymerisation method as well as contributing to the field of enzyme responsive biomaterials.

6.1 Future work

Given the time constraints of a PhD there remains some interesting questions and avenues to explore to gain further insight into this system and for it's continued development.

We know our system can undergo reversible enzyme responsive behaviour, however there is variability in our system. It was apparent from the ToF SIMS data that variability arose between the different batches of samples, however this technique was used to only characterise the very surface due to it's limitations in penetration, therefore it would be interesting to use other surface characterisation techniques to further explore these inconsistencies. This could help in directing any improvements to improve the reproducibility of the samples between different batches which may in-turn reduce the inconsistency observed with the repeatability of enzyme interactions.

Other surface techniques such as quartz cystal microbalance (QCM), ellipsometry and surface plasmon resonance (SPR) could be interesting tools to further characterise the samples. Ellipsometry and SPR enable thickness of the polyemr layer on the surface to be determined and QCM enables mass depositions to be measured. This further characterisation could measure other variants in the surfaces and potentially be used as a tool to measure changes on action of the two enzymes (change in thickness and mass).

Unfortunately, direct measurement of conformation and orientation of the polymers on the surface was not achieved during this work. FTIR and circular dichroism have been reported as methods to observe both. Modifiying an IR crystal and measuring the wavelength of absorbance of IR can provide information on the secondary structure and orientation of polymer. The effects of interactions of enzymes on these parametres could also be measured. This could provide information on the action of enzymes and provide insight into variabilities in the system.

The FRET system developed on the surface was successful at measuring changes in fluorescence on action of enzymes. It would be interesting if these changes were also observable by fluorescence microscopy, however challenges such as over exposure and photo bleaching would need to be addressed.

We have developed a reversible enzyme responsive surface that can support cell culture. To be a truly autonomous system ideally the stimuli will be provided by the

biological environment rather than added by an operator (as in the case of this work). Therefore it would be of great interest to monitor surface conformation changes using FRET, in the presence of cells as a result of cell secreted AP. Surface properties have been investigated as influencing cell behaviour. Any cell behavioural changes as a result of surface phosphorylation and dephosphorylation would be interesting to measure and investigate potentially providing ideas for future applications of this system.

Furthermore this work has demonstrated the potential of NCA ROP as a method to modify surfaces for interactions with enzymes that require a specific peptide sequence to operate. It would be interesting to investigate other amino acid combinations that could lead to a peptide sequence capable of interacting with other reversible enzyme systems.

The broader aim of this work is to develop more biomimetic materials for medical implants and tissue engineered biomaterials. It would be interesting to investigate coatings on biomaterials of NCA-ROP derived peptide sequences that can interact with native enzymes and to measure the effects on biocompatibility and the acceptance or rejection of biomedical implants. This could have wide implications in the future for the design of medical devices.

Appendix A

A.1 Chapter 2

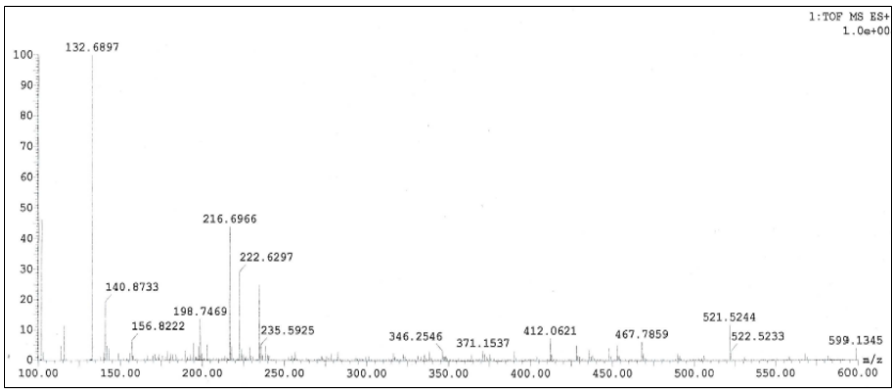


Figure A.1: Mass spectra for NCA-Ser (Bn)

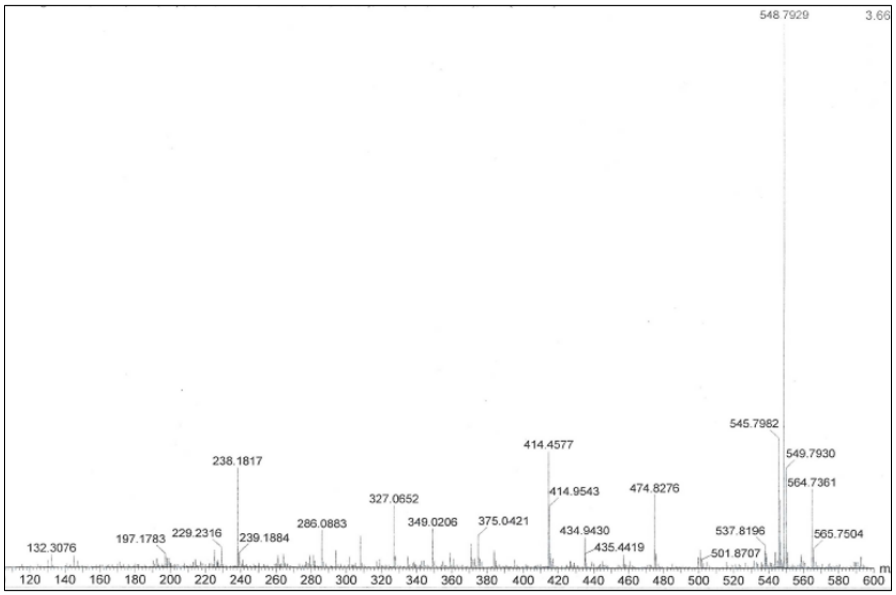


Figure A.2: Mass spectra for NCA-Glu (Bn)

A.1.1 Kinetic studies

Finemann-Ross

$$\frac{f\,(F-1)}{F} = \left(\frac{f^2}{F}\right) r_{Ser} - r_{Glu} \tag{A.1}$$

With

$$f = \frac{n_{Ser}}{n_{Glu}} \tag{A.2}$$

And

$$F = \frac{N_{Ser}}{N_{Glu}} \tag{A.3}$$

with n_{Ser} and n_{Glu} being the mole-fractions of Glu(Bn)-NCA and Ser(Bn)-NCA in the feed and N_{Glu} and N_{Ser} the mole-fractions of Glu(Bn) and Ser(Bn) n the ploymer.

A linear regression of the plot of $f(F-1)/F$ vs f^2/F yields r_{Glu} and r_{Ser} as the slope and the intercept, respectively.

Kelen-Tüdös

$$\eta = \xi\left(r_{Ser} + \frac{r_{Glu}}{\alpha}\right) - \frac{r_{Glu}}{\alpha} \tag{A.4}$$

With

$$\eta = \frac{f\,(F-1)}{F\left(\alpha + \frac{f^2}{F}\right)} \tag{A.5}$$

$$\xi = -\frac{\left(\frac{f^2}{F}\right)}{\alpha + \left(\frac{f^2}{F}\right)} \tag{A.6}$$

And

$$\alpha = \left(\left(\frac{f^2}{F}\right)_{max} \times \left(\frac{f^2}{F}\right)_{max}\right)^{\frac{1}{2}} \tag{A.7}$$

This equation equally yields a linea plot of η vs ξ for which slope and intercept can be determined. r_{Glu} can be determined when $\xi = 0$, which allows rearrangement of equation B.7 to:

$$r_{Glu} = -\eta_{\xi=0} \times \alpha = -d\alpha \tag{A.8}$$

If $\xi = 1$. $r_{Ser} = \eta$ which can be calculated from the equation of the linear regression according with k and d being the slope and the intercept of the linear regression, respectively.

$$r_{Ser} = \eta_{\xi=0} = k + d \tag{A.9}$$

Definition of parametres

$$r_{Ser} = \frac{k_{Ser}k_{Ser}}{k_{Ser}k_{Glu}} \tag{A.10}$$

$$r_{Glu} = \frac{k_{Glu}k_{Glu}}{k_{Glu}k_{Ser}} \tag{A.11}$$

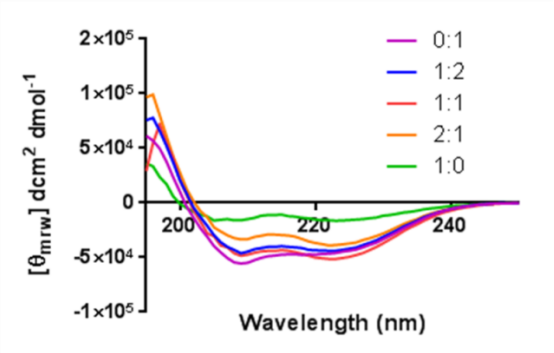


Figure A.3: Molar ellipticity of the copolypeptides at different ratios as determined by CD in HFIP.

A.2 Chapter 3

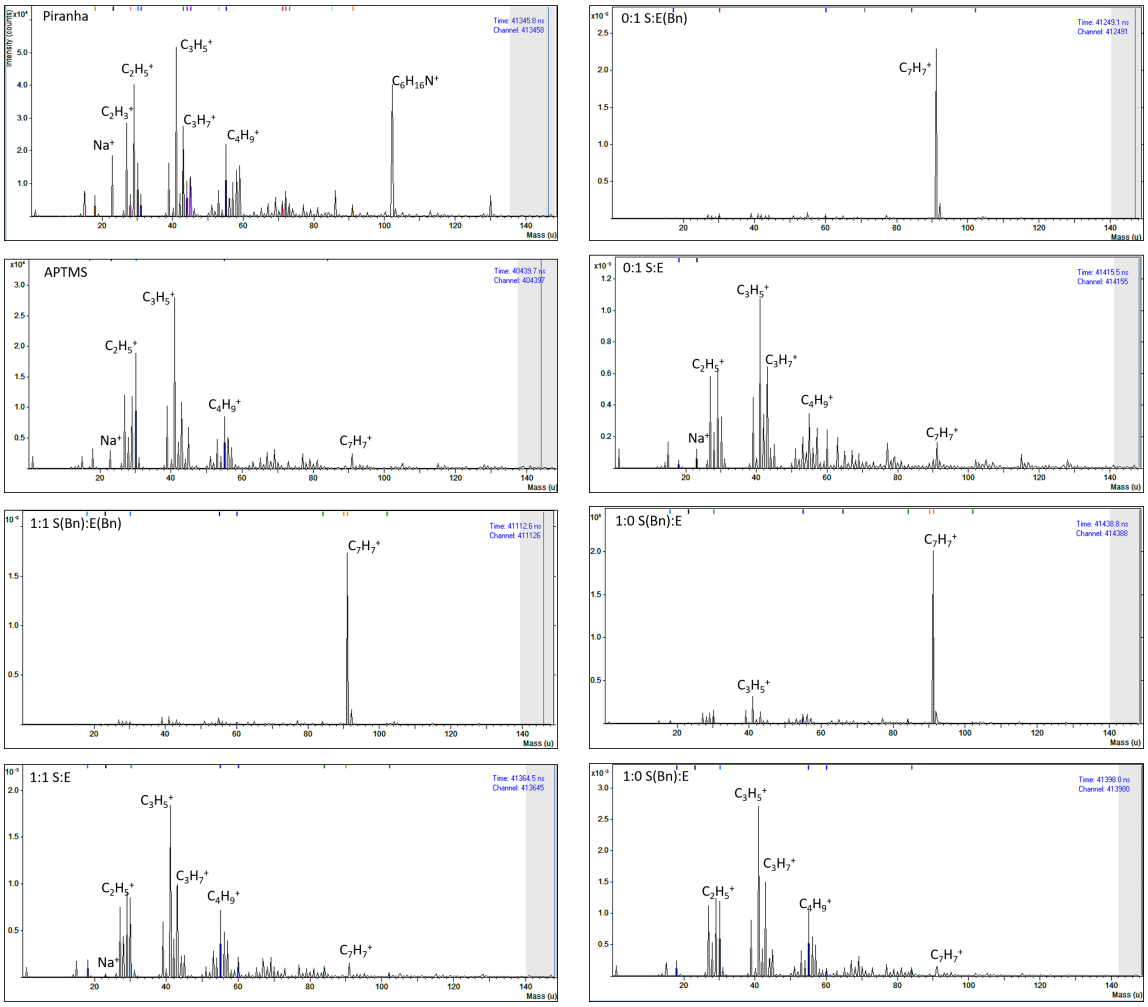


Figure A.4: Full ion spectra for substrates silanised with APTMS and polymerised with Serine and Glutamic acid in homo and copolymers. Most prominent ions have been labelled.

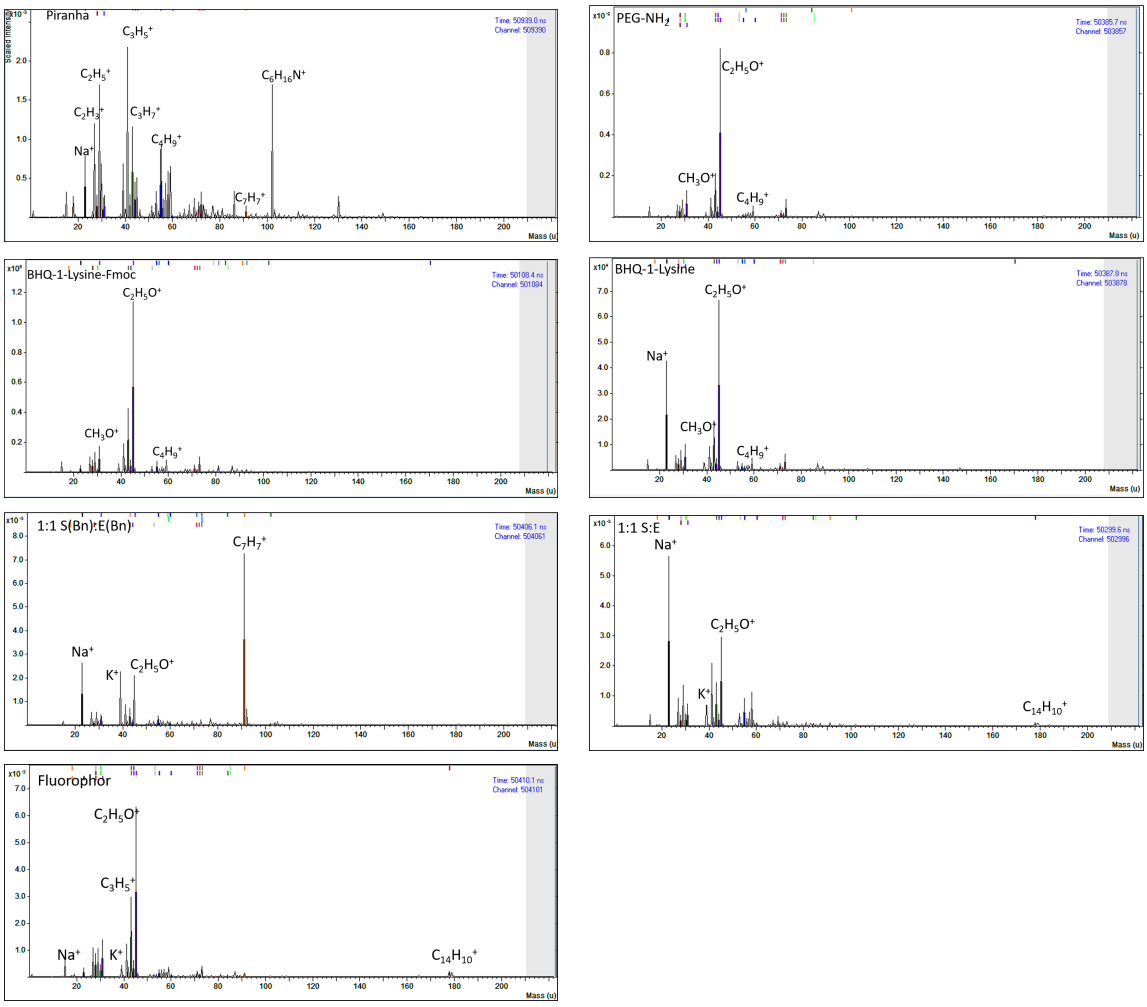


Figure A.5: Full ion spectra for substrates silanised with GOPTS, and polymerised with serine and glutamic acid from the BHQ-Lysine. Most prominent ions have been labelled.

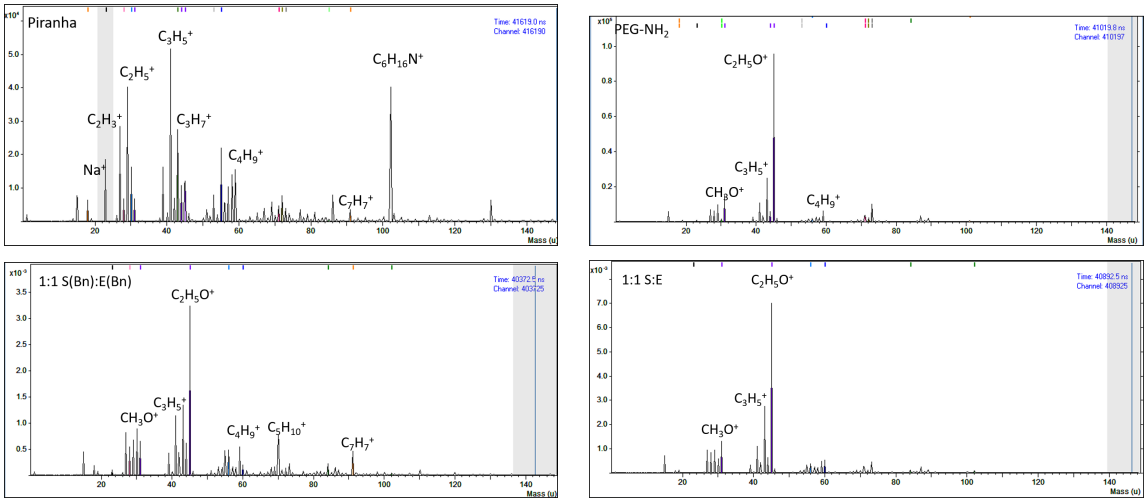


Figure A.6: Full ion spectra for substrates silanised with GOPTS, and polymerised with serine and glutamic acid from the PEG-diamine. Most prominent ions have been labelled.

Table A.1: ToF SIMS ion count for fragments of interest normalised to total ion count for samples initiated from BHQ. n=4 for 1.5 x1.5mm areas

	Piranha	PEG NH_2	BHQ-1 FMOC	BHQ-1	S(Bn):E(Bn)	S:E	Fluorescein
Na+	1.75E-02±1.10E-03	1.82E-03±6.33E-04	3.78E-02 ±1.05E-02	1.03E-01 ±3.61E-02	5.46E-02 ±1.46E-02	1.03E-01 ±1.67E-02	6.66E-03 ±1.69E-04
Si+	7.15E-03 ±1.42E-03	1.11E-05 ±1.42E-03	3.78E-02 ±3.42E-05	4.32E-04 ±2.07E-04	6.89E-05 ±1.91E-05	9.25E-04 ±4.93E-04	1.17E-03 ±2.21E-04
CH_3O+	8.16E-03 ±8.81E-05	4.63E-02 ±4.02E-04	3.25E-02 ±7.84E-04	3.16E-02 ±2.91E-03	1.05E-02 ±2.37E-03	1.40E-02 ±5.99E-03	4.11E-02 ±1.30E-04
C_2H_5O+	1.69E-02 ±3.90E-04	2.24E-01 ±4.73E-02	1.17E-01 ±1.40E-02	1.20E-01 ±2.11E-02	3.95E-02 ±1.64E-02	4.46E-02 ±1.43E-02	1.32E-01 ±6.46E-02
C_3H_3O+	3.33E-04 ±4.51E-04	3.86E-03 ±9.23E-04	2.37E-03 ±4.49E-05	3.59E-03 ±7.75E-04	9.76E-03 ±1.06E-03	5.87E-03 ±1.95E-03	7.96E-03 ±8.66E-06
C_2H_6NO+	1.07E-03 ±8.99E-05	1.22E-03 ±6.58E-05	0.00E+00 ±0.00E+00	9.45E-04 ±9.67E-05	5.04E-03 ±5.43E-04	3.81E-03 ±3.40E-04	4.07E-03 ±3.46E-05
C_4H_6NO+	0.00E+00 ±0.00E+00	8.97E-04 ±2.93E-04	4.81E-04 ±2.41E-04	1.10E-03 ±3.70E-04	3.68E-03 ±2.40E-04	2.38E-03 ±1.50E-04	2.70E-03 ±8.66E-05
$C_4H_8NO_2$+	0.00E+00 ±0.00E+00	0.00E+00 ±0.00E+00	0.00E+00 ±0.00E+00	6.58E-04 ±7.32E-05	3.01E-03 ±2.51E-04	2.51E-03 ±1.35E-04	1.73E-03 ±2.60E-05
C_7H_7+	8.74E-03 ±1.72E-04	2.53E-04 ±1.64E-04	2.10E-03 ±1.72E-04	1.48E-03 ±2.66E-04	2.09E-01 ±1.12E-02	2.79E-03 ±2.09E-04	2.96E-03 ±2.04E-04
$C_{14}H_{10}$+	±0.00E+00 ±0.00E+00	0.00E+00 ±0.00E+00	1.39E-02 ±6.18E-04	0.00E+00 ±0.00E+00	0.00E+00 ±0.00E+00	3.76E-03 ±4.27E-04	1.18E-02 ±4.33E-05

A.3 Chapter 4

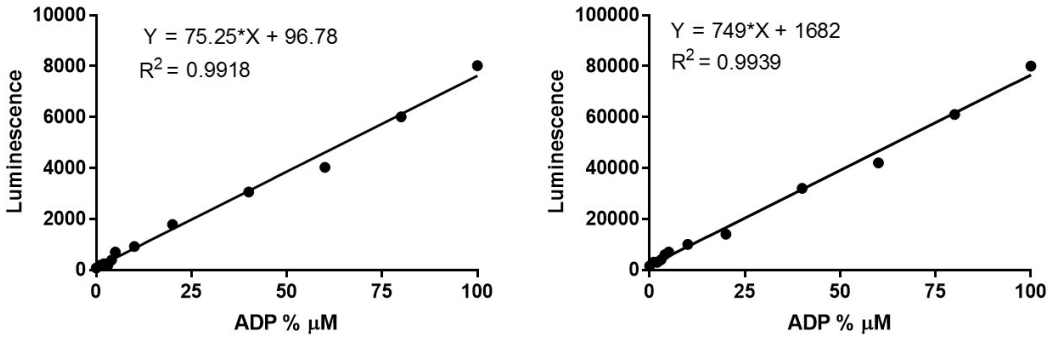


Figure A.7: Calibration curve for 1 (left)and 10 (right) µM ATP concentration

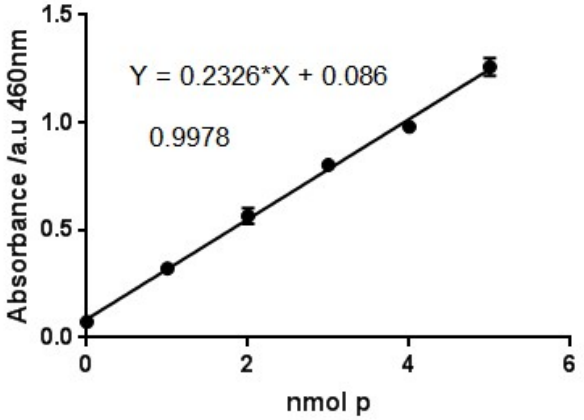


Figure A.8: Phosphate calibration curve

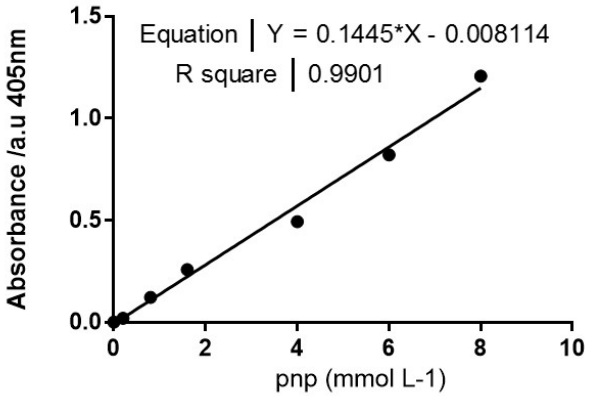


Figure A.9: AP calibration curve

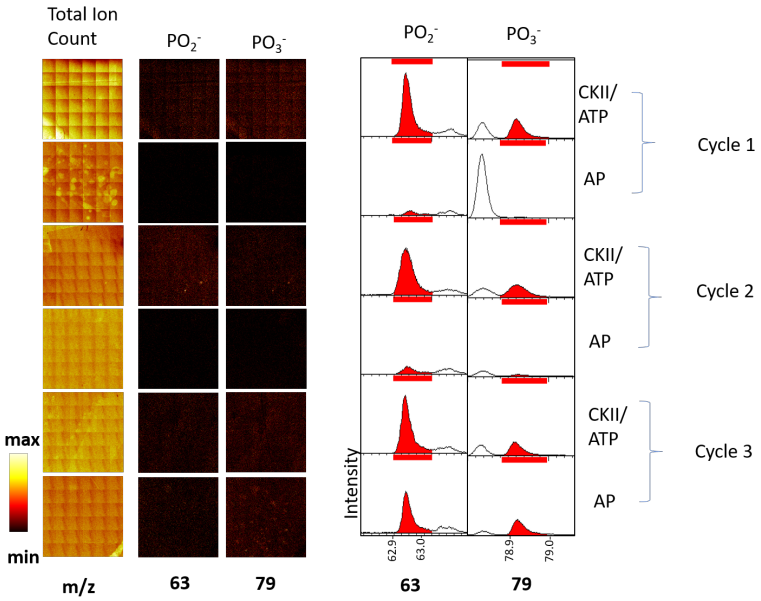


Figure A.10: ToF SIMS of samples initiated from PEG-NH_2 of three incubation cycles with CKII/ATP followed by AP. Left:Raster images of 3 x 3mm areas, Right: Spectra with peaks attributed to phosphate normalised to total ion count

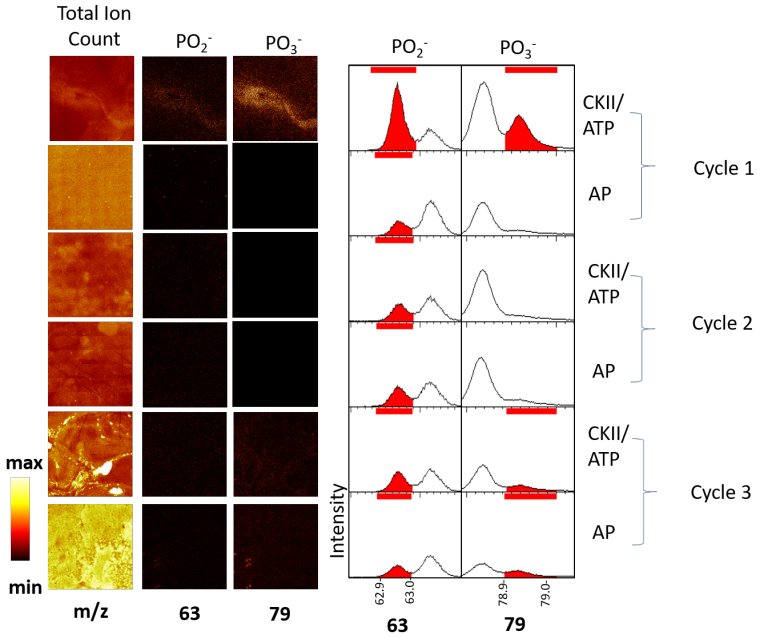


Figure A.11: ToF SIMS of samples initiated from BHQ-1-Lysine of three incubation cycles with CKII/ATP followed by AP. Left:Raster images of 3 x 3mm areas, Right: Spectra with peaks attributed to phosphate normalised to total ion count

A.4 Chapter 5

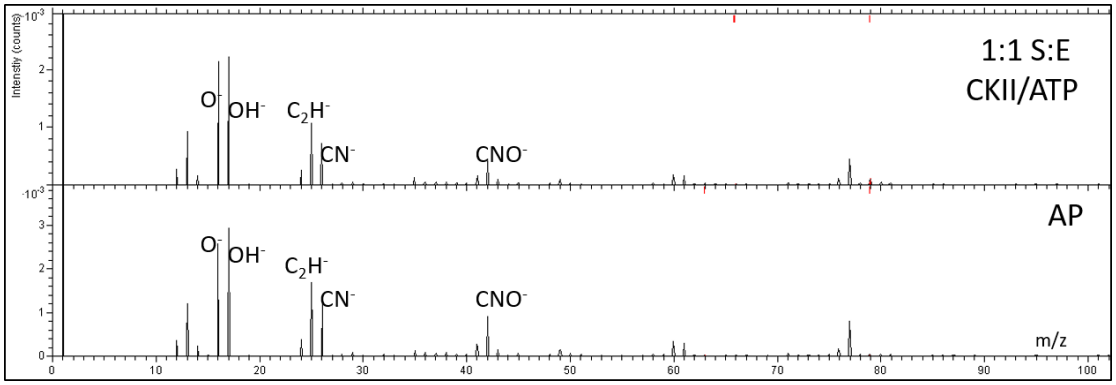


Figure A.12: Full mass spectra for negative polarity ToF SIMS. Surfaces polymerised from APTMS exposed to CKII/ATP and AP

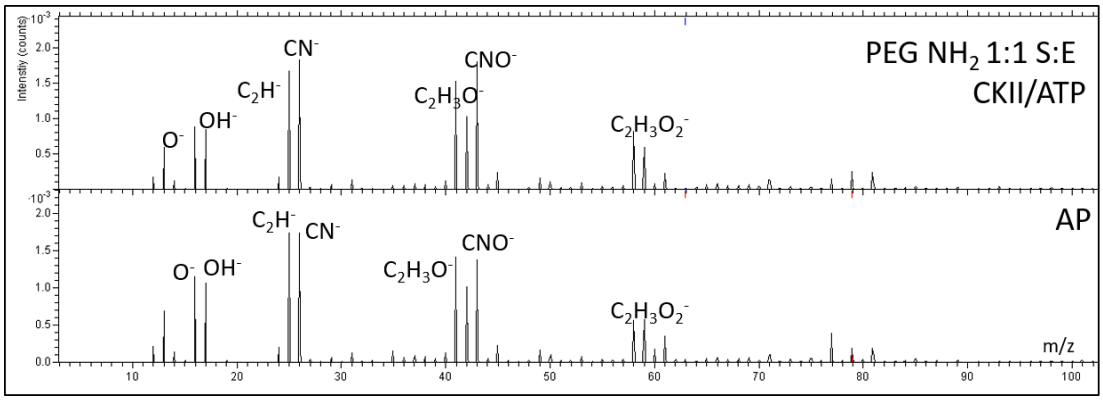


Figure A.13: Full mass spectra for negative polarity ToF SIMS. Surfaces polymerised from PEG diamine exposed to CKII/ATP and AP

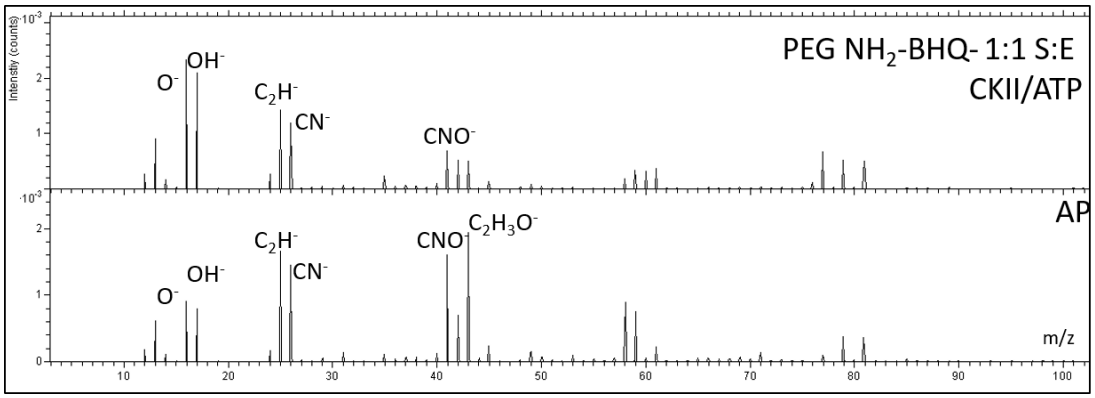


Figure A.14: Full mass spectra for negative polarity ToF SIMS. Surfaces polymerised from BHQ-1-Lysine exposed to CKII/ATP and AP

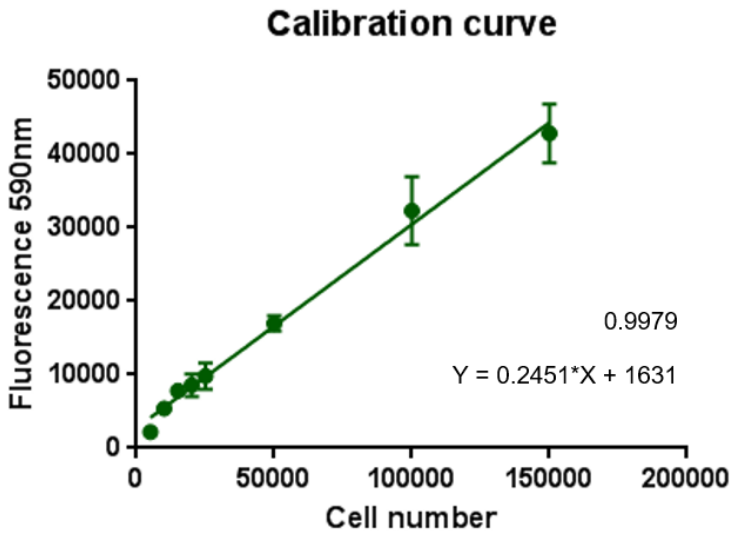


Figure A.15: CellTiter blue calibration curve

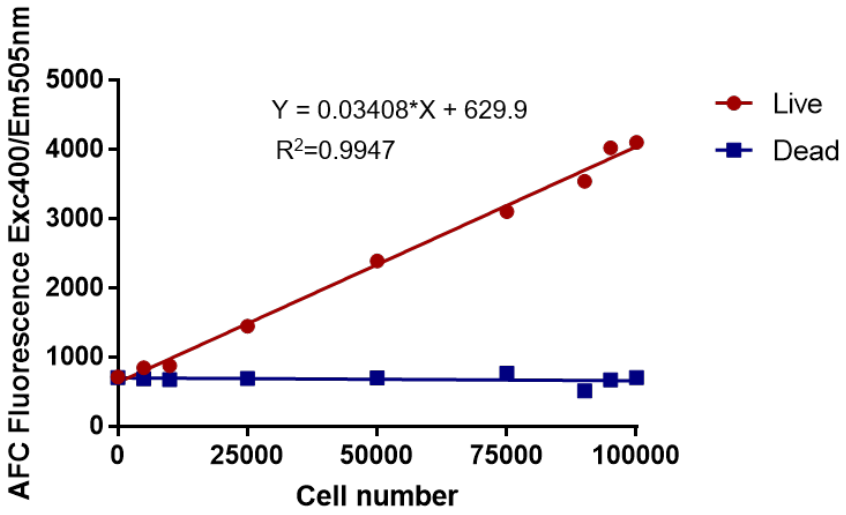


Figure A.16: Live cell calibration curve Excitation 400 nm/ Emission 505 nm for detection of AFC fluorescence

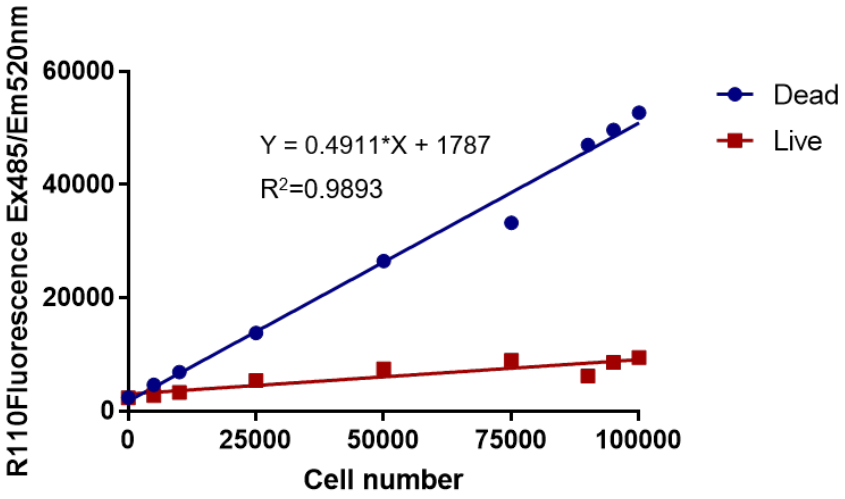


Figure A.17: Dead cell calibration curve Excitation 485 nm/ Emission 520 nm for detection of R11O fluorescence

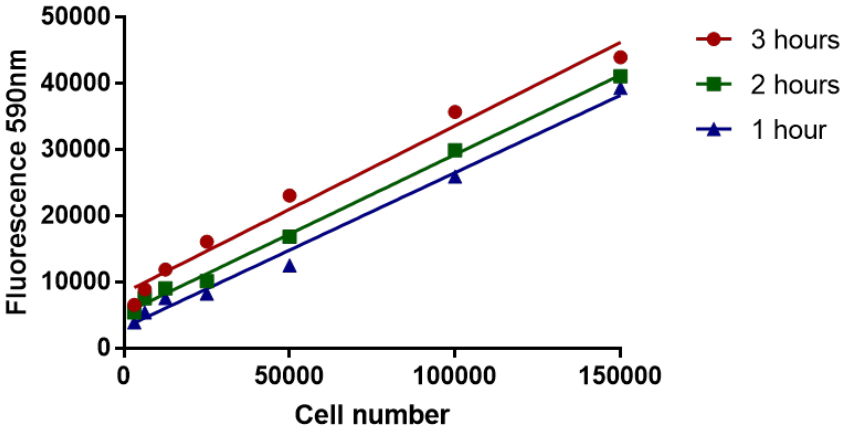


Figure A.18: Cell Titer calibration curve with known number of cells at different incubation times: 1 hour(R^2 = 0.9900), 2 hours (R^2 = 0.9967) and 3 hours (R^2 = 0.9802). Excitation 560nm/ emission 590 nm

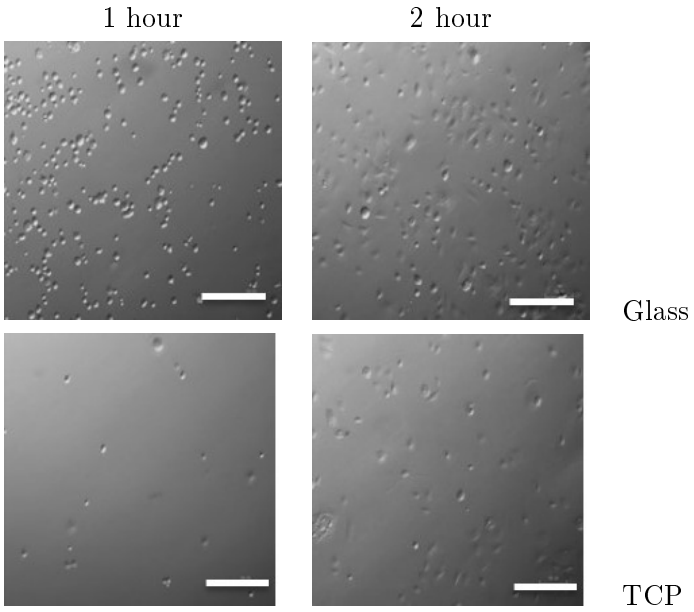


Figure A.19: Images of MPC cells cultured on controls glass and fibronectin after 1 and 2 hours incubation. Scale bar = 100µm

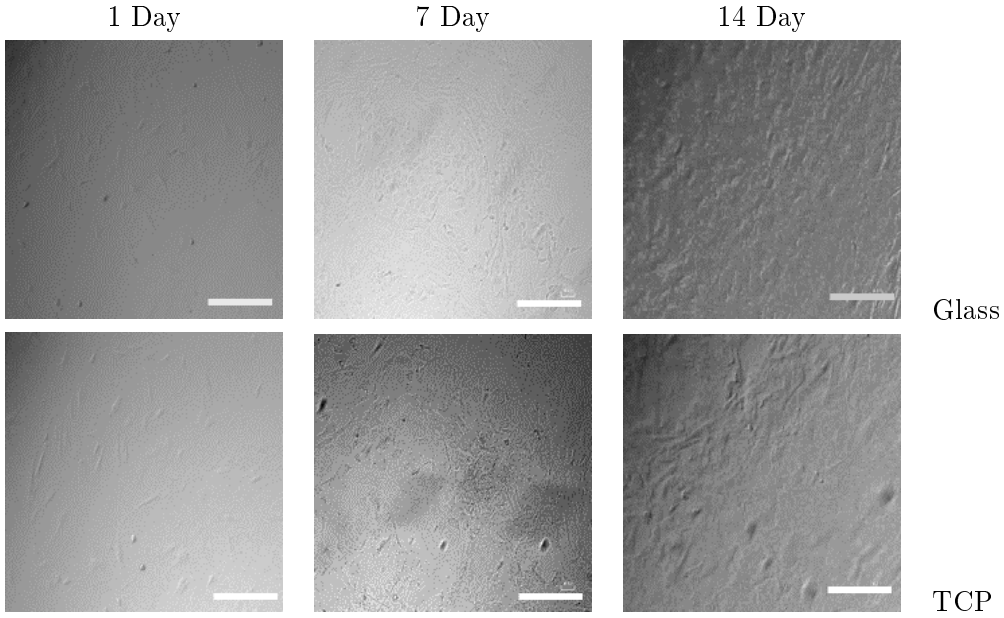


Figure A.20: Brightfield images of MPC cells seeded on control substrates glass and TCP at 10 X magnification, scale bar 100 µm (n=5) at day 1, 7 and 14.

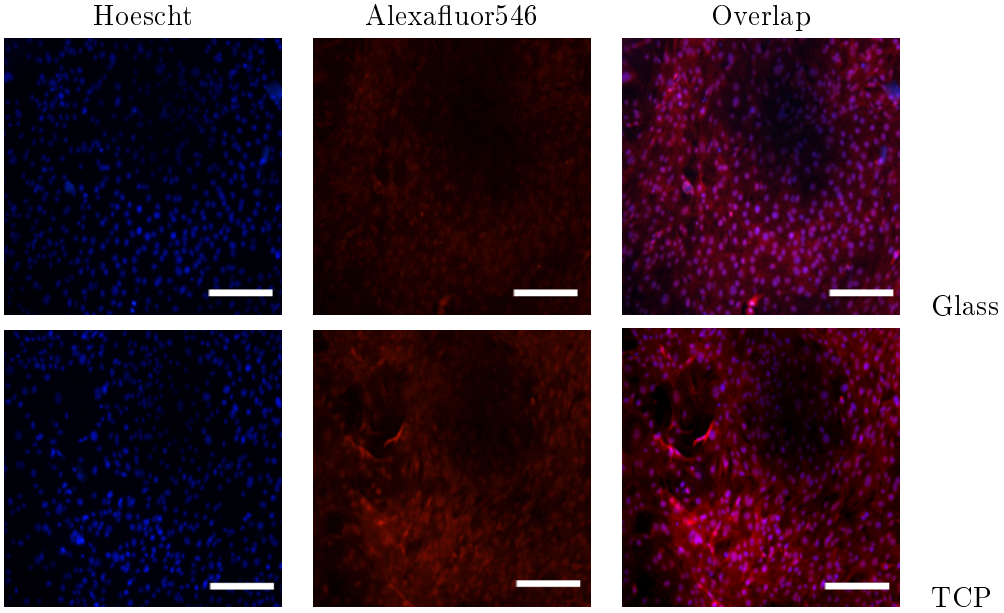


Figure A.21: Images of cells stained with Hoechst (nucleus stain) and Goat anti-rat secondary antibody-Alexafluor546 (RUNX2 stain) seeded on control surfaces at 10 x magnification (n=5) at day 3. scale bar = 100µm

Bibliography

[1] K M. Holtz and E R. Kantrowitz. The mechanism of the alkaline phosphatase reaction: Insights from NMR, crystallography and site-specific mutagenesis. *FEBS Letters*, 462(1-2):7–11, 1999.

[2] F Berthiaume, T J. Maguire, and M L. Yarmush. Tissue Engineering and Regenerative Medicine: History, Progress, and Challenges. *Annual Review of Chemical and Biomolecular Engineering*, 2(1):403–430, 2011.

[3] T Gaj, C A. Gersbach, and C F. Barbas. ZFN, TALEN, and CRISPR/Cas-based methods for genome engineering. *Trends in Biotechnology*, 31(7):397–405, 2013.

[4] C S. Hinrichs and S A. Rosenberg. Exploiting the curative potential of adoptive T-cell therapy for cancer. *Immunological Reviews*, 257(1):56–71, 2014.

[5] K Takahashi and S Yamanaka. Induction of pluripotent stem cells from mouse embryonic and adult fibroblast cultures by defined factors. *Cell*, 126(4):663–76, aug 2006.

[6] J U Paredes, P Alessandro, and W Chrzanowski. Protein-based Biointerfaces to Control Stem Cell Differentiation. In *Biointerfaces: Where material meets biology*, pages 1 –29. 2014.

[7] W. Chrzanowski, A. Kondyurin, J H Lee, M S Lord, M M M Bilek, and H W Kim. Biointerface: Protein enhanced stem cells binding to implant surface. *Journal of Materials Science: Materials in Medicine*, 23(9):2203–2215, 2012.

[8] B. D. Ratner and S. J. Bryant. Biomaterials: Where We Have Been and Where We Are Going. *Annual Review of Biomedical Engineering*, 6(1):41–75, 2004.

[9] L Liu, G Chen, T Chao, B D. Ratner, E. H Sage, and S & Jiang. Reduced foreign body reaction to implanted biomaterials by surface treatment with oriented osteopontin. *Journal of Biomaterials Science, Polymer Edition*, 19(6):821–835, 2012.

[10] B D Gomperts, I M Kramer, and P Tatham. Chapter 13: Signal Transduction to and from adhesion molecules. In *Signal Transduction (Second addition)*, pages 375–416. 2009.

[11] S Dedhar. Integrins and signal transduction. *current opinion in hemotology*, 1(6):37–43, 1999.

[12] S Johansson, G Svineng, K Wennerberg, A Armulik, and L Lohikangas. Fibronectin-integrin interactions. *Frontiers in bioscience : a journal and virtual library*, 2(11):d126–46, 1997.

[13] J. A. Askari, P. A. Buckley, A. P. Mould, and M. J. Humphries. Linking integrin conformation to function. *Journal of Cell Science*, 122(2):165–170, 2009.

[14] B H Luo and T A. Springer. Integrin structures and conformational signaling. *Current Opinion in Cell Biology*, 18(5):579–586, 2006.

[15] J W Cassidy, J N Roberts, C-A Smith, M Robertson, K White, M J Biggs, R O C Oreffo, and M J Dalby. Osteogenic lineage restriction by osteoprogenitors cultured on nanometric grooved surfaces: the role of focal adhesion maturation. *Acta biomaterialia*, 10(2):651–60, mar 2014.

[16] R J McMurray, N Gadegaard, P M Tsimbouri, K V Burgess, L E McNamara, R Tare, K Murawski, E Kingham, R O C Oreffo, and M J Dalby. Nanoscale surfaces for the long-term maintenance of mesenchymal stem cell phenotype and multipotency. *Nature materials*, 10(8):637–44, aug 2011.

[17] M Halai, A Ker, R D Meek, D Nadeem, T Sjostrom, B Su, L E McNamara, M J Dalby, and P S Young. Scanning electron microscopical observation of an osteoblast/osteoclast co-culture on micropatterned orthopaedic ceramics. *Journal of tissue engineering*, 5:2041731414552114, jan 2014.

[18] P M Mendes. Cellular nanotechnology: making biological interfaces smarter. *Chemical Society reviews*, 42(24):9207–18, dec 2013.

[19] S Even-Ram, V Artym, and K M Yamada. Matrix control of stem cell fate. *Cell*, 126(4):645–7, aug 2006.

[20] M Yaseen, X Zhao, A Freund, A M. Seifalian, and J R. Lu. Surface structural conformations of fibrinogen polypeptides for improved biocompatibility. *Biomaterials*, 31(14):3781–3792, 2010.

[21] M P Lutolf, P M Gilbert, and H M Blau. Designing materials to direct stem-cell fate. *Nature*, 462(7272):433–41, nov 2009.

[22] A Blau. Cell adhesion promotion strategies for signal transduction enhancement in microelectrode array in vitro electrophysiology: An introductory overview and critical discussion. *Current Opinion in Colloid & Interface Science*, 18(5):481–492, oct 2013.

[23] S F Badylak, D O Freytes, and T W Gilbert. Extracellular matrix as a biological scaffold material: Structure and function. *Acta biomaterialia*, 5(1):1–13, jan 2009.

[24] J Fan, H Park, S Tan, and M Lee. Enhanced osteogenesis of adipose derived stem cells with Noggin suppression and delivery of BMP-2. *PloS one*, 8(8):e72474, jan 2013.

[25] Y-K Wang, X Yu, D M Cohen, M Wozniak, M T Yang, L Gao, J Eyckmans, and C S Chen. Bone morphogenetic protein-2-induced signaling and osteogenesis is regulated by cell shape, RhoA/ROCK, and cytoskeletal tension. *Stem cells and development*, 21(7):1176–86, may 2012.

[26] L Yang, F Cheng, T Liu, J R Lu, K Song, L Jiang, S Wu, and W Guo. Comparison of mesenchymal stem cells released from poly(N-isopropylacrylamide) copolymer film and by trypsinization. *Biomedical materials (Bristol, England)*, 7(3):035003, jun 2012.

[27] Z Huang, P-G Ren, T Ma, R L Smith, and S B Goodman. Modulating osteogenesis of mesenchymal stem cells by modifying growth factor availability. *Cytokine*, 51(3):305–10, sep 2010.

[28] M Kamudzandu, Y Yang, P Roach, and R Fricker. Efficient alignment of primary CNS neurites using structurally engineered surfaces and biochemical cues. *RSC Adv.*, 5(28):22053–22059, 2015.

[29] D P. Dowling, I S. Miller, M Ardhaoui, and W M. Gallagher. Effect of Surface Wettability and Topography on the Adhesion of Osteosarcoma Cells on Plasma-modified Polystyrene. *Journal of Biomaterials Applications*, 26(3):327–347, 2011.

[30] B G. Keselowsky, D M. Collard, and A J. García. Surface chemistry modulates fibronectin conformation and directs integrin binding and specificity to control cell adhesion. *Journal of Biomedical Materials Research Part A*, 66A(2):247–259, 2003.

[31] F J. O'Brien. Biomaterials & scaffolds for tissue engineering. *Materials Today*, 14(3):88–95, 2011.

[32] R K Woo, D D. Jenkins, and R S Greco. Biomaterials: Historical Overview and Current directions. In *Nanoscale Technology in Biological Systems*, pages 1–21. 2005.

[33] L L Hench. The story of Bioglass. *Journal of materials science. Materials in medicine*, 17(11):967–78, nov 2006.

[34] J R Jones. Review of bioactive glass: from Hench to hybrids. *Acta biomaterialia*, 9(1):4457–86, jan 2013.

[35] R Langer and J.P. Vacanti. Tissue Engineering. *Science*, 260(May):920–926, 1993.

[36] A S Hoffman. Stimuli-responsive polymers: biomedical applications and challenges for clinical translation. *Advanced drug delivery reviews*, 65(1):10–6, jan 2013.

[37] M C Stuart, W T S Huck, J Genzer, M Müller, C Ober, M Stamm, G B Sukhorukov, I Szleifer, V V Tsukruk, M Urban, F Winnik, S Zauscher, I Luzinov, and S Minko. Emerging applications of stimuli-responsive polymer materials. *Nature materials*, 9(2):101–13, feb 2010.

[38] R J. Mart, R D. Osborne, M M. Stevens, and R V. Ulijn. Peptide-based stimuli-responsive biomaterials. *Soft Matter*, 2(10):822, 2006.

[39] P Theato, B S. Sumerlin, R K. O'Reilly, and T H. Epps. Stimuli responsive materials. *Chemical Society Reviews*, 42(17):7055, 2013.

[40] D Roy, J N. Cambre, and B S. Sumerlin. Future perspectives and recent advances in stimuli-responsive materials. *Progress in Polymer Science (Oxford)*, 35(1-2):278–301, 2010.

[41] A.K. Teotia, H. Sami, and A. Kumar. Thermo-responsive polymers: structure and design of smart materials. In *Switchable and Responsive Surfaces and Materials for Biomedical Applications*, pages 3–43. 2015.

[42] M E. Nash, D Healy, W M. Carroll, C Elvira, and Y Rochev. Cell and cell sheet recovery from pNIPAm coatings; motivation and history to present day approaches. *Journal of Materials Chemistry*, 22(37):19376, 2012.

[43] G. Kocak, C. Tuncer, and V. Bütün. pH-Responsive polymers. *Polym. Chem.*, 8(1):144–176, 2017.

[44] L. Jiang and L. Wen. *Photonic sensitive switchable materials*. Elsevier Inc., 2015.

[45] S. Y. Cheng, I. Constantinidis, and A. Sambanis. Use of glucose-responsive material to regulate insulin release from constitutively secreting cells. *Biotechnology and Bioengineering*, 93(6):1079–1088, 2006.

[46] M F Maitz, U Freudenberg, M V Tsurkan, M Fischer, T Beyrich, and C Werner. Bio-responsive polymer hydrogels homeostatically regulate blood coagulation. *Nature Commun*, 4:2168, 2013.

[47] S S Satav and S. Bhat, S and Thayumanavan. Feedback Regulated Drug Delivery Vehicles: Carbon Dioxide Responsive Cationic Hydrogels for Antidote Release. *Biomacromolecules*, 11(7):1735–40, 2010.

[48] R. R. Yocum, J. R. Rasmussen, and J. L. Strominger. The mechanism of action of penicillin. Penicillin acylates the active site of Bacillus stearothermophilus D-alanine carboxypeptidase. *Journal of Biological Chemistry*, 255(9):3977–3986, 1980.

[49] M Zelzer, S J. Todd, A R. Hirst, T O. McDonald, and R V. Ulijn. Enzyme responsive materials: design strategies and future developments. *Biomaterials Science*, 1(1):11, 2013.

[50] Miao-Ping Chien, Matthew P Thompson, Christopher V Barback, Ti-Hsuan Ku, David J Hall, and Nathan C Gianneschi. Enzyme-directed assembly of a nanoparticle probe in tumor tissue. *Advanced materials (Deerfield Beach, Fla.)*, 25(26):3599–604, jul 2013.

[51] Ti-hsuan Ku, Miao-ping Chien, Matthew P Thompson, Robert S Sinkovits, Norman H Olson, Timothy S Baker, and Nathan C Gianneschi. Controlling and Switching the Morphology of Micellar Nanoparticles with Enzymes. *Journal of American Chemical Society*, 133:8392–8395, 2011.

[52] M-P Chien, A M Rush, M P Thompson, and N C Gianneschi. Programmable shape-shifting micelles. *Angewandte Chemie (International ed. in English)*, 49(30):5076–80, jul 2010.

[53] M Mortato, S Argentiere, G L De Gregorio, G Gigli, and L Blasi. Enzyme-responsive multifunctional surfaces for controlled uptake/release of (bio)molecules. *Colloids and surfaces. B, Biointerfaces*, 123:89–95, nov 2014.

[54] JuJM Lee, B B R Choi, J-H Choi, G-C Kim, D-S Hwang, M C Chang, J-H Byun, and U-K Kim. Osteoblastic response to the hydroxyapatite/gelatin nanocomposite and bio-calcium phosphate cement. *Tissue Engineering and Regenerative Medicine*, 10(2):47–52, apr 2013.

[55] J Zhang, J Gao, M Chen, and Z Yang. Using phosphatases to generate self-assembled nanostructures and their applications. *Antioxidants & redox signaling*, 20(14):2179–90, may 2014.

[56] R. V. Ulijn. Enzyme-responsive materials: a new class of smart biomaterials. *Journal of Materials Chemistry*, 16(23):2217, 2006.

[57] X Li, H-C Kuang, Y Lin, and X Gao, J S, and Bing. Supramolecular Nanofibers and Hydrogels of Nucleopeptides. *Angewandte Chemie (International ed. in English)*, 50(40):9365–9369, 2012.

[58] S Wang, Y Zhang, H Wang, and Z Dong. Preparation, characterization and biocompatibility of electrospinning heparin-modified silk fibroin nanofibers. *International journal of biological macromolecules*, 48(2):345–53, mar 2011.

[59] Y-Q Yang, Y-Y Tan, R Wong, A Wenden, L-K Zhang, and B M Rabie. The role of vascular endothelial growth factor in ossification. *International journal of oral science*, 4(2):64–8, jun 2012.

[60] M Zelzer, L E. McNamara, D J. Scurr, M R. Alexander, M J. Dalby, and R V. Ulijn. Phosphatase responsive peptide surfaces. *Journal of Materials Chemistry*, 22(24):12229, 2012.

[61] J Ubersax and J E Ferrell. Mechanisms of specificity in protein phosphorylation. *Nature reviews. Molecular cell biology*, 8(7):530–41, jul 2007.

[62] D R Knighton, J Zheng, L Eyck, V A Ashford, N-H Xuong, S S Taylor, and J M Sowadski. Crystal Structure of the Catalytic Subunit of Cyclic Adenosine Monophosphate-Dependent Protein Kina. *Science*, 253(5018):407–414, 1991.

[63] G M. Hathaway and J A. Traugh. Casein Kinase II. In *Methods in Enzymology*, pages 317–313. 1984.

[64] C-S Goh, D Milburn, and M Gerstein. Conformational changes associated with proteinâĂŞprotein interactions. *Current Opinion in Structural Biology*, 14(1):104–109, 2004.

[65] A Onufriev, D Bashford, and D A. Case. Exploring Protein Native States and Large-Scale Conformational Changes with a Modified Generalized Born Model. *Proteins: Structure, Function and Genetics*, 55(2):383–394, 2004.

[66] P Roach, D Farrar, and C C. Perry. Interpretation of protein adsorption: Surface-induced conformational changes. *Journal of the American Chemical Society*, 127(22):8168–8173, 2005.

[67] H-C Cheng, R Z. Qi, H Paudel, and H-J Zhu. Regulation and Function of Protein Kinases and Phosphatases. *Enzyme Research*, 2011:1–3, 2011.

[68] S M Keyse. Protein phosphatases and the regulation of MAP kinase activity. *Cell & Developmental Biology*, 9:143–152, 1998.

[69] F. A. Barr, P. R. Elliott, and U. Gruneberg. Protein phosphatases and the regulation of mitosis. *Journal of Cell Science*, 124(14):2323–2334, 2011.

[70] S. V. Khlyntseva, Ya. R. Bazel', a. B. Vishnikin, and V. Andruch. Methods for the determination of adenosine triphosphate and other adenine nucleotides. *Journal of Analytical Chemistry*, 64(7):657–673, jun 2009.

[71] A S Dhillon, S Hagan, O Rath, and W Kolch. MAP kinase signalling pathways in cancer. *Oncogene*, 26(22):3279–3290, 2007.

[72] S Sprio and A Tampieri. *Bio-inspired Regenerative medicine*. Pan Stanford publishing, 2016.

[73] S Eskandari, T Guerin, I Toth, and R J. Stephenson. Recent advances in self-assembled peptides: Implications for targeted drug delivery and vaccine engineering. *Advanced Drug Delivery Reviews*, 110-111:169–187, 2017.

[74] H Acar, S Srivastava, E Ji Chung, M R. Schnorenberg, J C. Barrett, J L. LaBelle, and M Tirrell. Self-assembling peptide-based building blocks in medical applications. *Advanced Drug Delivery Reviews*, 110-111:65–79, 2017.

[75] H Lu, J Wang, Z Song, L Yin, Y Zhang, H Tang, C Tu, Y Lin, and J Cheng. Recent advances in amino acid N-carboxyanhydrides and synthetic polypeptides: chemistry, self-assembly and biological applications. *Chemical communications (Cambridge, England)*, 50(2):139–55, jan 2014.

[76] Yi Chen and Chang-Ming Pang, Xiao-Hui and Dong. Dual Stimuli-Responsive Supramolecular Polypepti de-Based Hydrogel and Reverse Micellar HydrogelMediated by HostâĂŞGuest Chemistry. *Advanced functional materials*, 20:579–586, 2010.

[77] C-J Carling, M L Viger, V A N Huu, A V Garcia, and A Almutairi. In Vivo Visible Light-Triggered Drug Release From an Implanted Depot. *Chemical science (Royal Society of Chemistry : 2010)*, 6(1):335–341, jan 2015.

[78] S Surjith Kumar, J-F Allard, D Morris, Y L. Dory, and Y Lepage, M and Zhao. Near-infrared light sensitive polypeptide block copolymer micelles for drug delivery. *Journal of Materials Chemistry*, 22:7252–7257, 2012.

[79] S Toledano, R J. Williams, and R V. Jayawarna, V , and Ulijn. Enzyme-Triggered Self-Assembly of Peptide Hydrogels via Reversed Hydrolysis. *American Chemical society*, 4(128):1070–1071, 2006.

[80] Y Qi and A Chilkoti. Growing polymers from peptides and proteins: a biomedical perspective. *Polymer Chemistry*, 5(2):266, 2014.

[81] H R Kricheldorf. Polypeptides and 100 years of chemistry of alpha-amino acid N-carboxyanhydrides. *Angewandte Chemie (International ed. in English)*, 45(35):5752–84, sep 2006.

[82] G L Rosano and E A Ceccarelli. Recombinant protein expression in Escherichia coli: advances and challenges. *Frontiers in microbiology*, 5(April):172, jan 2014.

[83] H Leuchs. Ueber die Glycin-carbonsäure. *Berichte der deutschen chemischen Gesellschaft*, 39(1):857–861, 1906.

[84] H Leuchs and W Manasse. Über die Isomerie der Carbäthoxyl-glycyl glycinester. *Ber. Dtsch. Chem. Ges*, 40:3235–3249, 1907.

[85] R Wilder and S Mobashery. The use of triphosgene in preparation of N-carboxy a-amino acid anhydrides. *J. Org. Chem.*, 57(9):2755–2756, 1992.

[86] F. Corneille, J.L. Copier, J.P. Senet, and Y. Robin. Procédé de Préparation des N-carboxyanhydrides, 2002.

[87] O Nuyken and S Pask. Ring-Opening Polymerization-An Introductory Review. *Polymers*, 5(2):361–403, apr 2013.

[88] J Cheng and T J Deming. Synthesis of polypeptides by ring-opening polymerization of α-amino acid N-carboxyanhydrides. *Topics in current chemistry*, 310:1–26, jan 2012.

[89] D L. Pickel, N Politakos, A Avgeropoulos, and J M. Messman. A Mechanistic Study of α-(Amino acid)- N -carboxyanhydride Polymerization: Comparing Initiation and Termination Events in High-Vacuum and Traditional Polymerization Techniques. *Macromolecules*, 42(20):7781–7788, oct 2009.

[90] H. Iatrou T. Aliferis and N. Hadjichristidis. Nanodomain-induced chain folding in poly(gamma-benzyl-L-glutamate)-b-polyglycine diblock copolymers. *Biomacromolecules*, 5(29):1653, 2004.

[91] T J. Deming. Facile synthesis of block copolypeptides of defined architecture. *Nature*, 390(November):5–8, 1997.

[92] W Zhao, Y Gnanou, and N Hadjichristidis. From competition to cooperation: a highly efficient strategy towards well-defined (co)polypeptides. *Chemical communications (Cambridge, England)*, 51(17):3663–3666, 2015.

[93] C D. Vacogne and H Schlaad. Primary ammonium/tertiary amine-mediated controlled ring opening polymerisation of amino acid N-carboxyanhydrides. *Chem. Commun.*, 51(86):15645–15648, 2015.

[94] V Dmitrovic, G J.M. Habraken, M M.R.M. Hendrix, W J.E.M. Habraken, A Heise, G de With, and N Sommerdijk. Random Poly(Amino Acid)s Synthesized by Ring Opening Polymerization as Additives in the Biomimetic Mineralization of CaCO3. *Polymers*, 4(4):1195–1210, may 2012.

[95] G J. M. Habraken, M Peeters, C H. J. T. Dietz, C E. Koning, and A Heise. How controlled and versatile is N-carboxy anhydride (NCA) polymerization at 0 C? Effect of temperature on homo-, block- and graft (co)polymerization. *Polymer Chemistry*, 1(4):514, 2010.

[96] Gijs J. M. Habraken, Karel H. R. M. Wilsens, Cor E. Koning, and Andreas Heise. Optimization of N-carboxyanhydride (NCA) polymerization by variation of reaction temperature and pressure. *Polymer Chemistry*, 2(6):1322, 2011.

[97] G J M Habraken, A Heise, and P D Thornton. Block Copolypeptides Prepared by N - Carboxyanhydride Ring-Opening Polymerization. *Macromolecular rapid communications*, 33:272–286, 2012.

[98] C Howard and H. A. Scheraga Cardinaux, F. Block Copolymers of Amino Acids. 11. Physicochemical Data on Copolymers Containing L-Alanine or L-Phenylalanine. *Biopolymers*, 16:2029–2051, 1977.

[99] R Rengifo, L Chen, C Grigoras, J Ju, and J T Koberstein. Click-Functional Block Copolymers Provide Precise Surface Functionality via Spin Coating. *Langmuir*, 24(20):7450–7456, 2008.

[100] A Harada, S Cammas, and K Kataoka. Stabilized R-Helix Structure of Poly (L - lysine) -block-poly (ethylene glycol) in Aqueous Medium through Supramolecular Assembly. *Macromolecules*, 29(96):6183–6188, 1996.

[101] A Harada and K Kataoka. Novel polyion complex micelles entrapping enzyme molecules in the core: Preparation of narrowly-distributed micelles from lysozyme and poly(ethylene glycol)-poly(aspartic acid) block copolymer in aqueous medium. *Macromolecules*, 31(2):288–294, 1998.

[102] S Hehir and N R Cameron. Recent advances in drug delivery systems based on polypeptides prepared from N -carboxyanhydrides. *Polymer International*, 63(6):943–954, jun 2014.

[103] D Teitelbaum, A Meshorer, T Hirshfeld, R Arnon, and M Sela. Suppression of experimental allergic encephalomyelitis by a synthetic polypeptide. *Eur. J. Immunol.*, 1:242–248, 1971.

[104] M Zelzer and A Heise. Terpolymerization kinetics of amino acid N-carboxy anhydrides. *Journal of Polymer Science Part A: Polymer Chemistry*, 52(9):1228–1236, may 2014.

[105] H R. Kricheldorf. *α-Aminoacid-N-Carboxy-Anhydrides and Related Heterocycles.* 1987.

[106] P. Bilalis, L.-A. Tziveleka, S. Varlas, and H. Iatrou. pH-Sensitive nanogates based on poly(l-histidine) for controlled drug release from mesoporous silica nanoparticles. *Polymer Chemistry*, 7(7):1475–1485, 2016.

[107] Y Jiang, S Wang, X Zhang, Y Tao, and X Wang. Controlled metal-free polymerization toward well-defined thermoresponsive polypeptides by polymerization at low temperature. *Journal of Polymer Science, Part A: Polymer Chemistry*, 54(16):2618–2624, 2016.

[108] Y Shen, X Fu, W Fu, and Z Li. Biodegradable stimuli-responsive polypeptide materials prepared by ring opening polymerization. *Chemical Society reviews*, 44(3):612–22, feb 2015.

[109] T J. Deming. Synthesis of Side-Chain Modified Polypeptides. *Chemical Reviews*, 116(3):786–808, 2016.

[110] M Byrne, P D. Thornton, S Cryan, and A Heise. Star polypeptides by NCA polymerisation from dendritic initiators: synthesis and enzyme controlled payload release. *Polymer Chemistry*, 3(10):2825, 2012.

[111] M Khuphe, A Kazlauciunas, M Huscroft, and P D. Thornton. The formation of biodegradable micelles from a therapeutic initiator for enzyme-mediated drug delivery. *Chem. Commun.*, 51(8):1520–1523, 2015.

[112] M. Khuphe, C.S. Mahon, and P.D. Thornton. Glucose-bearing biodegradable poly(amino acid) and poly(amino acid)-poly(ester) conjugates for controlled payload release. *Biomaterials Science*, 4(12):1792–1801, 2016.

[113] P D. Thornton, R J. Mart, S J. Webb, and R V. Ulijn. Enzyme-responsive hydrogel particles for the controlled release of proteins: designing peptide actuators to match payload. *Soft Matter*, 4(4):821, 2008.

[114] J.H. Hotchkiss and JM Goddard. Polymer surface modification for the attachment of bioactive compounds. *Progress in Polymer Science*, 32(7):698–725, 2007.

[115] H Donnelly, M J. Dalby, M Salmeron-Sanchez, and P E. Sweeten. Current approaches for modulation of the nanoscale interface in the regulation of cell behavior. *Nanomedicine: Nanotechnology, Biology, and Medicine*, pages 1–10, 2016.

[116] R Williams. *Surface Modification of Biomaterials -Methods, analysis and applications.* 2010.

[117] T Sun, G Qing, B Su, and L Jiang. Functional biointerface materials inspired from nature. *Chemical Society reviews*, 40(5):2909–21, may 2011.

[118] J F. Mano. Stimuli-responsive polymeric systems for biomedical applications. *Advanced Engineering Materials*, 10(6):515–527, 2008.

[119] M Lashkor, F J. Rawson, A Stephenson-Brown, J A. Preece, and P M. Mendes. Electrically-driven modulation of surface-grafted RGD peptides for manipulation of cell adhesion. *Chem. Commun.*, 50(98):15589–15592, 2014.

[120] M Kikuchi, T Ikoma, S Itoh, H N Matsumoto, Y Koyama, K Takakuda, Kenichi Shinomiya, and Junzo Tanaka. Biomimetic synthesis of bone-like nanocomposites using the self-organization mechanism of hydroxyapatite and collagen. *Composites Science and Technology*, 64(6):819–825, may 2004.

[121] A. S. de León, A. del Campo, J. Rodríguez-Hernández, and A. Muñoz-Bonilla. Switchable and pH responsive porous surfaces based on polypeptide-based block copolymers. *Materials and Design*, 131(June):121–126, 2017.

[122] Y H Gong, C Li, J Yang, H Y Wang, R X Zhuo, and X Z Zhang. Photoresponsive "smart template" via Host-Guest interaction for reversible cell adhesion. *Macromolecules*, 44(19):7499–7502, 2011.

[123] C Holmes and M Tabrizian. Chapter 14 - Surface Functionalization of Biomaterials. In *Stem Cell Biology and Tissue Engineering in Dental Sciences*, pages 187–206. 2015.

[124] C R.Vistas, A C.P.Águas, and G N.M.Ferreira. Silanization of glass chips-A factorial approach for optimization. *Applied Surface Science*, 286:314–318, 2013.

[125] J A. Howarter and J P. Youngblood. Optimization of silica silanization by 3-aminopropyltriethoxysilane. *Langmuir*, 22(26):11142–11147, 2006.

[126] Y Yao, W Li, S Wang, D Yan, and X Chen. Polypeptide Modification of Multiwalled Carbon Nanotubes by a Graft-From Approach. *Macromolecular Rapid Communications*, 27(23):2019–2025, dec 2006.

[127] B Zdyrko and I Luzinov. Polymer brushes by the "grafting to" method. *Macromolecular rapid communications*, 32(12):859–69, jun 2011.

[128] N Hadjichristidis, H Iatrou, M Pitsikalis, and G Sakellariou. Synthesis of well-defined polypeptide based materials via the ring opening polymerization of alpha amino acid N carboxyanhydrides. *Chemical reviews*, 109(11):5528–78, nov 2009.

[129] T Borase, M Iacono, S I. Ali, P D. Thornton, and A Heise. Polypeptide core-shell silica nanoparticles with high grafting density by N-carboxyanhydride (NCA) ring opening polymerization as responsive materials and for bioconjugation. *Polymer Chemistry*, 3(5):1267, 2012.

[130] J Rainer. *Surface-Initiated Polymerization I.* 2006.

[131] R C. Dvincula, W J. Brittain, K C. Caster, and J Rühe. *Polymer brushes.* 2004.

[132] S Minko. Grafting on Solid Surfaces Grafting to and Grafting from Methods. In *Polymer surfaces and interfaces*, pages 215–234. 2008.

[133] J K Whitesell and H K Chang. Directionally aligned helical peptides on surfaces. *Science*, 261(5117):73–76, 1993.

[134] H Duran, B Yameen, H U Khan, R Förch, and W Knoll. Surface-initiated ring opening polymerization of N-carboxy anhydride of benzyl-l-glutamate monomers on soft flexible substrates. *Reactive and Functional Polymers*, 73(3):606–612, mar 2013.

[135] Jin Huang and Andreas Heise. Stimuli responsive synthetic polypeptides derived from N-carboxyanhydride (NCA) polymerisation. *Chemical Society reviews*, 42(17):7373–90, 2013.

[136] S H Wibowo, A Sulistio, E H H Wong, A Blencowe, and G G Qiao. Polypeptide films via N-carboxyanhydride ring-opening polymerization (NCA-ROP): past, present and future. *Chemical communications (Cambridge, England)*, 50(39):4971–88, may 2014.

[137] B J Sparks, J G Ray, D Savin, C M Stafford, and D L Patton. Synthesis of thiol-clickable and block copolypeptide brushes via nickel-mediated surface initiated polymerization of α-amino acid N-carboxyanhydrides (NCAs). *Chemical communications (Cambridge, England)*, 47(22):6245–7, 2011.

[138] M Nitschke. Plasma Modification of Polymer Surfaces and Plasma Polymerization. In *Polymer surfaces and interfaces*, pages 203–214. 2008.

[139] C Chan and C V Hanser. *Polymer surface modification and characterization.* 1995.

[140] S Kwangseok, K Minyoung, and H K Do. Re-derivation of Young's Equation, Wenzel Equation, and Cassie-Baxter Equation Based on Energy Minimization. In *Surface Energy.* 2015.

[141] J C. Vickerman and I S. Gilmore. *Surface analysis the principal techniques, 2nd edition.* 2009.

[142] T Ha. Single-Molecule Fluorescence Resonance Energy Transfer. *Methods*, 25(1):78–86, 2001.

[143] R. M. Clegg. Fluorescence resonance energy transfer. *Current Opinion in Biotechnology*, 6(1):103–110, 1995.

[144] K. E. Sapsford, L. Berti, and I. L. Medintz. Materials for Fluorescence Resonance Energy Transfer Analysis: Beyond Traditional Donor-Acceptor Combinations. *Angewandte Chemie (International ed. in English)*, 45:4562–4589, 2006.

[145] C A Royer. Fluorescence spectroscopy. *Methods in molecular biology (Clifton, N.J.)*, 40:65–89, 1995.

[146] A Ogunleye, A Bhat, V U. Irorere, D Hill, C Williams, and I Radecka. Poly-glutamic acid: production, properties and applications. *Microbiology (Reading, England)*, 161(2015):1–17, 2015.

[147] C O Silva, B Sarmento, and C P Reis. Oral Delivery of Biopharmaceuticals. In *Mucosal Delivery of Biopharmaceuticals*, pages 125–147. 2014.

[148] T Kurosaki, T Kitahara, T Nakamura, K Nishida, S Fumoto, Y Kodama, H Nakagawa, N Higuchi, and H Sasaki. Development of effective cancer vaccine using targeting system of antigen protein to APCs. *Pharmaceutical Research*, 29(2):483–489, 2012.

[149] I Bajaj and R Singhal. Poly (glutamic acid)–an emerging biopolymer of commercial interest. *Bioresource technology*, 102(10):5551–61, may 2011.

[150] S Chung, C Gentilini, A Callanan, M Hedegaard, S Hassing, and M M. Stevens. Responsive poly (γ-glutamic acid) fibres for biomedical applications. *Journal of Materials Chemistry B*, 1(10):1397, 2013.

[151] P D. Thornton, R Brannigan, J Podporska, B Quilty, and A Heise. The generation of hydrophilic polypeptide-siloxane conjugates via n-carboxyanhydride polymerisation. *Journal of Materials Science: Materials in Medicine*, 23(1):37–45, 2012.

[152] Haoyu Tang and Donghui Zhang. General route toward side-chain-functionalized alpha-helical polypeptides. *Biomacromolecules*, 11(6):1585–1592, 2010.

[153] JX Ding, XL Zhuang, CS Xiao, YL Cheng, L Zhao, CL He, ZH Tang, and XS Chen. Preparation of photo-cross-linked pH-responsive polypeptide nanogels as potential carriers for controlled drug delivery. *Journal of Materials Chemistry*, 21:11383–91, 2011.

[154] S Matsumura, A R. Hlil, C Lepiller, J Gaudet, D Guay, Z Shi, S Holdcroft, and A S. Hay. Ionomers for proton exchange membrane fuel cells with sulfonic acid groups on the end-groups: Novel branched poly(ether-ketone)s. *American Chemical Society, Polymer Preprints, Division of Polymer Chemistry*, 49(1):511–512, 2008.

[155] I Yakovlev and T J Deming. Controlled synthesis of phosphorylcholine derivatives of poly(serine) and poly(homoserine). *Journal of the American Chemical Society*, 137(12):4078–81, apr 2015.

[156] D J. Price, M Khuphe, R P. W. Davies, J R. McLaughlan, N Ingram, and P D. Thornton. Poly(amino acid)-polyester graft copolymer nanoparticles for the acid-mediated release of doxorubicin. *Chem. Commun.*, 53:8687–8690, 2017.

[157] L. J Hughes, R. H Andreatta, and and Scheraga H. A. Helix-Coil Stability Constants for the Naturally Occurring Amino Acids in Water. V. Serine Parameters from Random Poly (hydroxybutylglutamine-co-L-serine). *Macromolecules*, 5(2):187–197, 1972.

[158] Eric M Norstrom and J A Mastrianni. The charge structure of helix 1 in the prion protein regulates conversion to pathogenic PrPSc. *Journal of virology*, 80(17):8521–9, sep 2006.

[159] D Lama, S T Quah, C S Verma, R Lakshminarayanan, R W Beuerman, D P Lane, and C J Brown. Rational optimization of conformational effects induced by hydrocarbon staples in peptides and their binding interfaces. *Scientific reports*, 3(figure 1):3451, jan 2013.

[160] Vladimir Uversky, Alexey V Uversky. *Amino acids, peptides and proteins.* 2014.

[161] A G. Jamieson, N Boutard, D Sabatino, and W D. Lubell. Peptide Scanning for Studying Structure-ActivityRelationships in Drug Discovery. *Chemical biological drug design*, 81:148–165, 2013.

[162] B Ciani, E G Hutchinson, R B Sessions, and D N Woolfson. A designed system for assessing how sequence affects alpha to beta conformational transitions in proteins. *The Journal of biological chemistry*, 277(12):10150–5, mar 2002.

[163] N E Kamber, W Jeong, R M Waymouth, R C Pratt, B G G Lohmeijer, and J L Hedrick. Organocatalytic Ring-Opening Polymerization. *Chemical reviews*, (107):5813–5840, 2007.

[164] C Krejtschi and K Hauser. Stability and folding dynamics of polyglutamic acid. *European biophysics journal : EBJ*, 40(5):673–85, may 2011.

[165] M Zelzer and A Heise. Determination of copolymerisation characteristics in the N-carboxy anhydride polymerisation of two amino acids. *Polymer Chemistry*, 4(13):3896, 2013.

[166] W. E Hanby, S. G Waley, and J Watson. Synthetic polypeptides. Part II. Polyglutamic acid. *Journal of the Chemical society (resumed)*, pages 3239–3249, 1950.

[167] J D Han, J X Ding, Z C Wang, S F Yan, X L Zhuang, X S Chen, and J B Yin. The synthesis, deprotection and properties of poly(γ-benzyl-l-glutamate). *Science China Chemistry*, 56(6):729–738, feb 2013.

[168] M Finemann and S D. Ross. Linear method for determining monomer reactivity ratios in copolymerization. *Journal of Polymer Science*, 5(2), 1950.

[169] T Kelen, F Tüdös, and T Béla. Confidence intervals for copolymerization reactivity ratios determined by the Kelen-Tüdös method. *Polymer bulletin*, 2(1):71–76, 1980.

[170] S M Kelly and N C Price. The use of circular dichroism in the investigation of protein structure and function. *Current protein & peptide science*, 1(4):349–84, dec 2000.

[171] S Heino and M D Byler. *Methods in enzymology: Resolution-enhanced fourier transform infrared spectroscopy of enzymes.* 1986.

[172] Y Shen, Z Li, and H A Klok. Polypeptide brushes grown via surface-initiated ring-opening polymerization of α-amino acid N-carboxyanhydrides. *Chinese Journal of Polymer Science (English Edition)*, 33(7):931–946, 2015.

[173] R. H. Wieringa, E. A. Siesling, P. J. Werkman, E. J. Vorenkamp, and A. J. Schouten. Surface grafting of poly(L-glutamates). 3: Block copolymerization. *Langmuir*, 17(21):6491–6495, 2001.

[174] B. J. Tyler, C. Bruening, S. Rangaranjan, and H. F. Arlinghaus. TOF-SIMS imaging of adsorbed proteins on topographically complex surfaces with Bi 3+ primary ions. *Biointerphases*, 6(3):135–141, 2011.

[175] S Todd, D J Scurr, J E. J Gough, and R V. Morgan, A R. and Ulijn. Enzyme Activated RGD Ligands on Functionalized Poly(ethylene glycol) Monolayers Surface Analysis and Cellular Response. *Langmuir*, 25(13):7533–7539, 2009.

[176] E J Vorenkamp, V Erb, M Stamm, and A J Schouten. Surface Grafting of Poly (L -glutamates). 1 . Synthesis and Characterization. *Langmuir*, 17(21):6477–6484, 2001.

[177] P Cohen. The regulation of protein function by multisite phosphorylation a 25 year update. In *Trends in Biochemical Sciences*, pages 596 – 601. 2000.

[178] A Venerando, M Ruzzene, and L A Pinna. Casein kinase the triple meaning of a misnomer. *Biochemical Journal*, 460(2):141–156, 2014.

[179] F Meggio, A P. Boulton, F Marchiori, G Borin, D P.W. Lennon, A Calderan, and L A. Pinna. Substrate-specificity determinants for a membrane-bound casein kinase of lactating mammary gland. A study with synthetic peptides. *European Journal of Biochemistry*, 177(2):281–284, 1988.

[180] F Meggio, J W. Perich, H E. Meyer, E Hoffman-Poroske, D P.W. Lennon, R. Basil Johns, and L A. Pinna. Synthetic fragments of β-casein as model substrates for liver and mammary gland casein kinases. *European Journal of Biochemistry*, 186(3):459–464, 1989.

[181] D. W Litchfield. Protein kinase CK2: structure, regulation and role in cellular decisions of life and death. *The Biochemical journal*, 369(Pt 1):1–15, 2003.

[182] J P. Turowec, N A. St. Denis, and D W. Litchfield. Casein Kinase II. In *Encyclopedia of signalling molecules*, pages 234–242. 2012.

[183] J. H. Trembley, G. Wang, G. Unger, J. Slaton, and K. Ahmed. CK2: A key player in cancer biology. *Cellular and Molecular Life Sciences*, 66(11-12):1858–1867, 2009.

[184] D S. Iimoto, E Masliah, R DeTeresa, R D. Terry, and T Saitoh. Aberrant casein kinase II in Alzheimer's disease. *Brain Research*, 507(2):273–280, 1990.

[185] E A Kuenzel, J A Mulligan, J Sommercorn, and E G Krebs. Substrate specificity determinants for casein kinase II as deduced from studies with synthetic peptides. *The Journal of biological chemistry*, 262(19):9136–9140, 1987.

[186] D Bossemeyer. Protein kinases–structure and function. *FEBS letters*, 369(1):57–61, 1995.

[187] L. N. Johnson, E. D. Lowe, M. E. M. Noble, and D. J. Owen. The structural basis for substrate recognition and control by protein kinases. *FEBS Letters*, 430(1-2):1–11, 1998.

[188] M J Maunders. Alkaline Phosphatase (EC 3.1.3.1). *Methods in Molecular Biology*, 16:331–341, 1993.

[189] E E Kim and W Harold. Reaction mechanism of alkaline phosphatase based on crystal structures: Two-metal ion catalysis. *Journal of Molecular Biology*, 218(2):449–464, 1991.

[190] E. Hove, C. A. Elvehjem, and E. B Hart. Effect of Zinc on Phosphatases. *Journal of Biological Chemistry*, pages 425–442, 1940.

[191] M J Weiss, P S Henthorn, M a Lafferty, C Slaughter, M Raducha, and H Harris. Isolation and characterization of a cDNA encoding a human liver/bone/kidney-type alkaline phosphatase. *Proceedings of the National Academy of Sciences of the United States of America*, 83(19):7182–7186, 1986.

[192] J Bilski, A Mazur-Bialy, D Wojcik, J Zahradnik-Bilska, B Brzozowski, M Magierowski, T Mach, K Magierowska, and T Brzozowski. The Role of Intestinal Alkaline Phosphatase in Inflammatory Disorders of Gastrointestinal Tract. *Mediators of Inflammation*, 2017:1–9, 2017.

[193] K P Lu, Y Liou, and X Z Zhou. Pinning down phosphorylation signaling. 12(4):164–172, 2002.

[194] I.B Wilson and J Dayan. *Biochemistry 4*. 1965.

[195] WE Hull, SE Halford, H Gutfreund, and BD. Sykes. 31P nuclear magnetic resonance study of alkaline phosphatase: the role of inorganic phosphate in limiting the enzyme turnover rate at alkaline pH. *Biochemistry*, 6(7):1547–1561, 1976.

[196] P. Gettins, M. Metzler, and J. E. Coleman. Alkaline phosphatase. 31P NMR probes of the mechanism. *Journal of Biological Chemistry*, 260(5):2875–2883, 1985.

[197] H Kühnle and H G Börner. Biotransformation on polymer-peptide conjugates: a versatile tool to trigger microstructure formation. *Angewandte Chemie (International ed. in English)*, 48(35):6431–4, jan 2009.

[198] J H Kim, S Lee, K Park, H Y Nam, S Y Jang, I Youn, K Kim, H Jeon, R W Park, I S Kim, K Choi, and I C Kwon. Protein-phosphorylation-responsive polymeric nanoparticles for imaging protein kinase activities in single living cells. *Angewandte Chemie (International ed. in English)*, 46(30):5779–82, 2007.

[199] P F Caponi, X P Qiu, F Vilela, F M. Winnik, R Ulijn, and V. Phosphatase/temperature responsive poly(2-isopropyl-2-oxazoline). *Polym. Chem.*, 2(2):306–308, 2011.

[200] R J Amir, S Zhong, D J Pochan, and C J Hawker. Enzymatically Triggered Self-assembly of Block Copolymers. *Journal of American Chemical Society*, pages 2–12, 2009.

[201] J Hu, G Zhang, and S Liu. Enzyme-responsive polymeric assemblies, nanoparticles and hydrogels. *Chemical Society reviews*, 41(18):5933–49, sep 2012.

[202] J Yang, M Yamato, K Nishida, T Ohki, M Kanzaki, H Sekine, T Shimizu, and T Okano. Cell delivery in regenerative medicine: the cell sheet engineering approach. *Journal of controlled release : official journal of the Controlled Release Society*, 116(2):193–203, nov 2006.

[203] J. K. Sahoo, M. S. Sirimuthu, N, A. Canning, M. Zelzer, D. Graham, and R. V. Ulijn. Analysis of enzyme-responsive peptide surfaces by Raman spectroscopy. *Chem. Commun.*, 52(25):4698–4701, 2016.

[204] R S Siffert. The role of alkaline phosphatase in osteogenesis. *The Journal of experimental medicine*, 93(5):415–26, 1951.

[205] S. L Dallas and L. F Bonewald. Author Manuscript Dynamics of the Transition from Osteoblast to Osteocyte. (816):437–443, 2011.

[206] J M Walker. *TGF-β Signaling IN Series Editor*. Human Press, 2016.

[207] J. Regis O'Keefe and Jennifer H. Jonathan. Isolation and Culture of Neonatal Mouse Calvarial Osteoblasts. In *Skeletal Development and Repair. Methods in Molecular Biology*, pages 295–305. 2014.

[208] M T Valenti, P Serafini, G Innamorati, A Gili, S Cheri, C Bassi, and L D Carbonare. Runx2 expression: A mesenchymal stem marker for cancer. *Oncology Letters*, 12(5):4167–4172, 2016.